University of Kent

Nanocarriers for the Targeted Delivery of Non-Steroidal Anti-Inflammatory Drugs (NSAIDs) to Tumours

by

Mhd Saeed Akkad

A thesis submitted to the University of Kent in partial fulfillment of the requirements for the degree of Doctor of Philosophy

October 2020

Abstract

A growing body of evidence suggests that the regular use of non-steroidal anti-inflammatory drugs (NSAIDs), especially aspirin, is associated with a reduced risk of many types of cancer including colorectal, breast, and prostate malignancies. It has also been shown that they might be beneficial in reducing metastasis and lengthening remission periods. However, the prolonged exposure to this class of drugs does not come without a cost as it carries with it the risk of augmenting the serious side effects of NSAIDs. These include haemorrhages, increased bleeding time, peptic ulcers, and hypersensitivity, to name a few.

This work aimed at employing the principles of nanotherapy to maximise the benefits of NSAIDs and minimise the risks of their harmful side effects. By exploiting the enhanced permeability and retention effect (EPR) unique to inflammatory tissues, NSAID-loaded nanocarriers could delivery high concentrations of the drugs to cancer tissue, compared to conventional therapy, while reducing the systemic exposure to their effects.

Block copolymers from a polymeric pro-drug, polysalicylate, and polyethylene glycol were synthesised and self-assembled into nanoparticles of a desirable size range. The polysalicylate at the core of the particles comprised solely of the active molecule, salicylic acid, and showed a good release profile in accelerated conditions, which suggests a possible sustained release in tumour tissue.

The cytotoxic activity of the nanoparticles and polysalicylate was tested against triple-negative cancer cell lines and neuroblastoma cell lines in vitro and was compared to conventional cytotoxic drugs. A modest biological response was observed with the low concentration at which the particles could be prepared, indicating that the accumulation of the nanoparticles in targeted tissue could produce the desired outcomes.

Developing other polyphosphoester-based polymeric nanocarriers as well as lipid nanocarriers was attempted. Possible factors that affected the synthesis of such carriers were discussed.

Declaration

I declare that the work presented herein is my own and that the thesis was written in my own words. I certify that it has not been submitted for the purposes of a qualification at any other institution or for any other degree.

Mhd Saeed Akkad

October 2020

Acknowledgement

First and foremost, I would like to express my deepest gratitude to my supervisor Dr Christopher Serpell for giving me the opportunity to work on this project in his lab. His brilliance, dedication to his work, and compassionate mentorship were a great inspiration, academically as well as personally. It is to his patience and eagerness to provide guidance, support, and encouragement that I owe the valuable skills and knowledge that I have acquired over the past few years.

My utmost gratitude also goes to the University of Kent and the Council for At-Risk Academics (Cara) whose funding and support made this work a reality. The lifeline that Cara provided me in collaboration with the University of Kent not only saved my life but also allowed me to grow on many levels. For that, I am eternally indebted to both.

I would also like to thank the academics and staff of the School of Physical Sciences for always providing feedback and advice. Further thanks go to Dr Andrew Morell for his help and with the HPLC analysis. I am also very grateful to Dr Martin Michaelis at the School of Biosciences for, very kindly and generously, receiving me in his lab for my biological studies. I thank everyone in the Michaelis/Garrett lab for everything they taught me. I especially thank Eithaar Al-Barwani and Edith Blackburn for their valuable help.

It would not have been quite the journey without the people with whom I shared the excitements, laughs, and woes. This is why I was fortunate to have known all the great people in the Serpell group, especially Emerald and Nadeema whom I have known the longest. I am genuinely grateful for the kindness that they have shown all along the way.

I would not have made it of course without the love and encouragement of my caring family that, even though I have been parted from them for years, have never failed to show me how much they believed in me. Mum, Ahmad, Ghaidaa, and Abdulrahman. I am humbled by your resilience and heartened by your love. No words can say how also grateful I am to my wonderful uncle, Ghazi, who has gone far and beyond in showing his love and support.

Last and by no means least, it goes without saying that without you by my side, I could have never done it. To the love of my life, I owe it all to you.

To my father, the greatest man I have ever known…

You still inspire me in your absence just as much as you did when you were around.

Dissemination

Peer-reviewed publication

S. Akkad and C. J. Serpell, Degradable Polymers and Nanoparticles Built from Salicylic Acid, Macromol. Rapid Commun., 2018, **39**, 1800182.

Poster presentations

"Nanocarriers for the delivery of non-steroidal anti-inflammatory drugs (NSAIDs) to targeted cancer tissues."
The 4th annual early-career researcher's meeting of the British Society of Nanomedicine (August 2018).

"Nanocarriers for the delivery of non-steroidal anti-inflammatory drugs (NSAIDs) to targeted cancer tissues."
The 4th Keele Nanopharmaceutics Symposium (June 2018).

"Polymeric nanocarriers for the delievery of Nanocarriers for the delivery of non-steroidal anti-inflammatory drugs (NSAIDs)."
The 3rd London Polyer Symposium (Apr 2017).

Table of Contents

Abstract i

Declaration ii

Acknowledgement iii

Dissemination v

Table of Contents vi

List of Abbreviations ix

List of Figures xiii

List of Tables xvii

Preface 1

Chapter 1. NSAIDs, cancer, and magic bullets 5

1.1. NSAIDs and cancer: clinical evidence 6
1.1.1. Colorectal cancers 6
1.1.2. Prostate Cancer 9
1.1.3. Breast cancer 11
1.1.4. Kidney cancer 13
1.1.5. Other cancers and metastasis 13
1.2. The pharmacological mechanisms of NSAIDs in cancer 14
1.2.1. The COX-dependent pathway. 14
1.2.2. COX-independent pathways 17
1.2.3. The side effects of NSAIDs 18
1.3. Nanotherapy and its prospects in cancer 20
1.3.1. The definition of nanomedicine and nanotherapeutics. 20
1.3.2. Tumour microenvironment 22
1.3.3. Types of targeting in nanotherapy 25
1.3.3.1. Passive targeting 25
1.3.3.2. Active targeting 27
1.3.3.3. Stimuli-responsive (triggered) targeting 28
1.3.3.3.1. Internal stimuli. 28
1.3.3.3.2. External stimuli 29
1.3.4. Design considerations and biological barriers 30
1.3.4.1. Particle size. 31
1.3.4.2. Particle shape 31
1.3.4.3. Particle surface charge 32
1.3.4.4. Mononuclear phagocytic system (MPS) 32
1.3.4.5. Other barriers 33

Table of Contents (cont.)

1.3.5. Types of nanotherapeutics 33
1.3.5.1. Polymer-based nanocarriers 33
1.3.5.1.1. Polymeric micelles 34
1.3.5.1.2. Polymeric nanoparticles 34
1.3.5.1.3. Dendrimers 35
1.3.5.2. Lipid-based nanocarriers 35
1.3.5.2.1. Liposomes 36
1.3.5.2.2. Lipid nanocarriers (LNs) 36
1.3.5.3. Carbon-based nanocarriers 37
1.3.5.4. Inorganic nanocarriers 37
1.3.6. NSAID-based nanocarriers 38
1.4. Conclusion 39
1.5. References 40

Chapter 2. NSAID-based polymeric prodrugs 56

2.1. Salicylic acid-pased polymer (polysalicylate)* 57
2.1.1. Introduction 57
2.1.2. Materials and instrumentation 61
2.1.3. Experimental 63
2.1.3.1. Salicylic acid polymer (polysalicylates) 63
2.1.3.2. Polysalicylate-block-methoxy polyethylene glycol (PSA-b-mPEG) 63
2.1.3.3. PSA-b-mPEG self-assembly 64
2.1.3.3.1. Stability of vesicles 64
2.1.3.4. Degradation of PSA 64
2.1.4. Discussion of results 65
2.1.4.1. Polysalicylate (PSA) 66
2.1.4.2. PSA-mPEG BCP 71
2.1.4.3. Self-assembly 77
2.1.4.4. Degradation studies 85
2.2. Polyphosphoesters (PPEs) 90
2.2.1. Introduction 90
2.2.2. Materials and instrumentation 94
2.2.3. Experimental 95
2.2.3.1. Ibuprofen-solketal ester 95
2.2.3.2. Deprotection (glyceryl ibuprofen) 95
2.2.3.3. Cyclic phosphate-ibuprofen ester monomer 95
2.2.3.4. ROP of the cyclic monomer 96
2.2.4. Results and discussion 96
2.2.4.1. Ibuprofen-solketal ester 96
2.2.4.2. Deprotection (glyceryl ibuprofen) 98
2.2.4.3. Cyclic phosphoester monomer 100
2.2.4.4. Ring-opening polymerisation (ROP) 102
2.3. Conclusion 104
2.4. References 105

Table of Contents (cont.)

Chapter 3. Liposomes as salicylic acid nanocarriers 111

3.1. Introduction **112**
3.2. Materials and methods **117**
3.3. Experimental **118**
3.3.1. PC liposomes by direct loading (freeze/thawing) 118
3.3.2. PC liposomes by direct loading (sonication) 118
3.3.3. DPPC liposomes by direct loading 119
3.3.4. DPPC liposomes by remote loading 119
3.3.5. Sample preparation for HPLC analysis 120
3.4. Results and discussion **120**
3.4.1. Liposomes prepared via the direct (passive) loading method 122
3.4.2. Liposomes prepared via the remote (active) loading method 129
3.5. Conclusion **134**
3.6. References **136**

Chapter 4. Preliminary *in vitro* studies 142

4.1. Introduction **143**
4.2. Materials and instrumentation **147**
4.3. Experimental **147**
4.3.1. Maintenance of cell lines 147
4.3.2. Cell counting 148
4.3.3. Cell viability assay 148
4.3.3.1. Determination of the half-maximal inhibitory concentrations (IC50) . 148
4.3.3.2. Drug comparison against different cell lines 149
4.3.4. Preparation of self-assembled PSA-b-mPEG NPs for the *in vitro* study 149
4.4. Results and discussion **149**
4.5. Conclusion **162**
4.6. References **163**

Chapter 5. Summary and future outlook 168

List of Abbreviations

AA	arachidonic acid
ADC	antibody-drug conjugate
ADP	adenosine diphosphate
AERD	aspirin-exacerbated respiratory disease
AIA	aspirin-induced asthma
ANOVA	analysis of variance
ASA	acetylsalicylic acid, aspirin
ATP	adenosine triphosphate
ATRP	atom transfer radical polymerisation
BCP	block co-polymer
BHT	butylated hydroxytoluene
CAF	cancer-associated fibroblast
$CDCl_3$	deuterated chloroform
cGMP	cyclic guanosine monophosphate
CI	confidence interval
CMC	critical micellar concentration
CME	clathrin-mediated endocytosis
CNS	central nervous system
CNT	carbon nanotube
COX	cyclooxygenase, *also* PTGS
CPM	cyclic phosphoester polymer
CRC	colorectal cancer
CV	cardiovascular
CvME	caveolae-mediated endocytosis
CWC	critical water content
DBU	1,8-diazabicyclo[5.4.0]undec-7-ene
DCM	dichloromethane
DIPEA	N, N-diisopropylethylamine
DLS	dynamic light scattering
DMAP	4-dimethylaminopyridine

DMF	dimethylformamide
DMSO	dimethyl sulfoxide
DMWD	differential molecular weight distribution
DNA	deoxyribonucleic acid
DOX	doxorubicin
DP	degree of polymerisation
DPPC	1,2-dipalmitoyl-sn-glycero-3-phosphocholine
DSC	rifferential scanning calorimetry
ECM	extracellular matrix
EDC	1-(3-Dimethylaminopropyl)-3-ethylcarbodiimide
EDTA	ethylenediaminetetraacetic acid
EE	encapsulation efficiency
EGF	epidermal growth factor
EGFR	epidermal growth factor receptor
EMT	epithelial-to-mesenchymal transition
EPR	enhanced permeability and retention
ER	oestrogen receptor
FBS	foetal bovine serum
FDA	food and Drug Administration
FGF	fibroblast growth factor
FTIR	Fourier transform infrared
GPC	gel permeation chromatography
GSH	glutathione
HER2	human epidermal growth factor receptor 2
HPLC	high-performance liquid chromatography
HR	hazard ratio
IBU	ibuprofen
IC_{50}	half-maximal inhibitory concentration
IFP	interstitial fluid pressure
IL	interleukin
IMDM	Iscove Modified Dulbecco Medium
LC	loading capacity
LN	lipid nanocarrier
LT	leukotriene
LUV	large unilamellar vesicle
MLV	multilamellar vesicle

MMP	matrix metalloprotease
MPPC	monopalmitoyl-phosphatidylcholine
MPS	mononuclear phagocytic system
MRI	magnetic resonance imaging
MTT	3-(4,5-dimethylthiazol-2-yl)-2,5-diphenyltetrazolium bromide
NK	natural killer
NLC	nanostructured lipid carrier
NMR	nuclear magnetic resonance
NP	nanoparticle
NSAID	non-steroidal anti-inflammatory drug
OR	odds ratio
OTC	over-the-counter
PAX	paclitaxel
PBS	phosphate-buffered saline
PC	phosphatidylcholine
PCL	poly(ε-caprolactone)
PDE	phosphodiesterase
PDGF	platelet-derived growth factor
PEEP	poly(ethyl ethylene phosphate)
PEG	polyethylene glycol
PEI	polyethylenimine
PG	prostaglandin
PGA	polyglycolic acid
PGE_2	since prostaglandin E_2
PGI_2	PGI_2, prostacyclin
PL	phospholipid
PLA	poly(D,L-lactic acid)
PLE	porcine liver esterase
PLGA	poly(D,L-lactic-co-glycolic acid)
PPE	polyphosphoester
PR	progesterone receptor
PSA	polysalicylate
PTGS	prostaglandin-endoperoxide synthases , *also* COX
PTL	parental
PVP	poly(vinyl alcohol)
QD	quantum dot

RCT	randomised controlled trial
RES	reticuloendothelial system
RI	refractory index
RNA	ribonucleic acid
ROMP	ring-opening metathesis polymerisation
ROP	ring-opening polymerisation
ROS	reactive oxygen species
RR	relative risk
SA	salicylic acid
SDS	sodium dodecyl sulphate
SLN	solid lipid nanoparticle
SPION	superparamagnetic iron oxide nanoparticle
SUV	small unilamellar vesicle
TAM	tumour-associated macrophage
TEM	transmission electron microscopy
TGA	thermogravimetric analysis
THF	tetrahydrofuran
TLC	thin-layer chromatography
TME	tumour microenvironment
TNBC	triple-negative breast cancer
TXA_2	thromboxane A_2
VEGF	vascular endothelial growth factor

List of Figures

Chapter 1

Figure no.	Description	Page no.
Fig 1.1.	The chemical classification of non-steroidal anti-inflammatory drugs (NSAIDs) with example of common drugs from each family	7
Fig 1.2.	The pyramid of evidence-based medicine	8
Fig 1.3.	The cyclooxygenase pathway	16
Fig 1.4.	A scale bar showing the size of nanotherapeutics in comparison to biological systems	21
Fig 1.5.	A schematic demonstrating the differences between healthy and tumourous tissues, especially in regards to the enhanced permeability and retention (EPR)	25
Fig 1.6.	Examples from the literature of NSAID-loaded polymers intended for targeted delievery	39

Chapter 2

Figure no.	Description	Page no.
Fig 2.1.	Aspirin metabolites	58
Fig 2.2.	Examples of salicylic acid-based polymers from the literature	60
Fig 2.3.	The proposed structure of polysalicylate (PSA)	66
Fig 2.4.	The proposed products of the polymerisation reaction of salicylic acid	67
Fig 2.5.	The proposed mechanism for the anhydride-ester rearrangement	68
Fig 2.6.	The ^{1}H-NMR spectrum of polysalicylate	69
Fig 2.7.	Reaction scheme for making the BCP	72
Fig 2.8.	Differntial molecular weight distributions (DMWDs) of polysalicylate (PSA), methoxy polyethylene glycol (mPEG), and the block co-polymer (BCP)	73
Fig 2.9.	The ^{1}H-NMR spectrum of the BCP	73
Fig 2.10.	FTIR spectra of PSA and PSA-mPEG	74
Fig 2.11.	Thermal analysis (DSC and TGA) of PSA and the BCP	75
Fig 2.12.	DMWDs for some of the BCPs synthesised with different PEG chains	76
Fig 2.13.	^{13}C- and ^{1}H-NMR spectra of a possible cyclic PSA	77

List of Figures (cont.)

Chapter 2 (cont.)

Figure no.	Description	Page no.
Fig 2.14.	DLS size distribution of the four preparations and their corresponding correlograms	78
Fig 2.15.	TEM images of self-assembled morphologies in THF/water	79
Fig 2.16.	TEM images of self-assembled morphologies in acetone/water	80
Fig 2.17.	Packing parameter (p) and its effect on the self-assembly behaviour	81
Fig 2.18.	Some deformations observed on the vesicles	84
Fig 2.19.	zeta-potential measurement of vesicles prepared from THF/water, and their size distribution change over time as a function of intensity	85
Fig 2.20.	PSA degradation in different media at 40 °C	86
Fig 2.21.	PSA degradation in different media at 70 °C	87
Fig 2.22.	PSA degradation in different media at 90 °C	89
Fig 2.23.	Prevalent natural PPEs that are essential for biological functions	91
Fig 2.24.	Some examples from the literature of PPEs in therapeutics	93
Fig 2.25.	Reaction scheme for making the ibuprofen-solketal ester	97
Fig 2.26.	^{1}H-NMR ($CDCl_3$) spectrum of the solketal-ibuprofen ester	98
Fig 2.27.	^{13}C-NMR ($CDCl_3$) spectrum of the solketal-ibuprofen ester	98
Fig 2.28.	Reaction scheme for making the ibuprofen-solketal ester	99
Fig 2.29.	^{1}H-NMR ($CDCl_3$) spectrum of glyceryl ibuprofen	99
Fig 2.30.	^{13}C-NMR ($CDCl_3$) spectrum of glyceryl ibuprofen	100
Fig 2.31.	Reaction scheme for making the cyclic phospate monomer	101
Fig 2.32.	^{1}H-NMR ($CDCl_3$) spectrum of the cyclic phosphate monomer	101
Fig 2.33.	^{13}C-NMR ($CDCl_3$) spectrum of the cyclic phosphate monomer	102
Fig 2.34.	^{31}P{^{1}H}-NMR ($CDCl_3$) spectrum of the cyclic phosphate monomer	102
Fig 2.35.	Reaction scheme for the ROP	103

List of Figures (cont.)

Chapter 3

Figure no.	Description	Page no.
Fig 3.1.	The basic anatomy of a liposome	112
Fig 3.2.	Some of the different types of liposomes that has been developed.	113
Fig 3.3.	Layout of Liposofast, the small-volume extruder used to homogenise liposomes.	120
Fig 3.4.	Size distribution of liposomes after extrusion as determined by DLS.	122
Fig 3.5.	HPLC chromatograms of SA at different stages of preparing egg PC liposomes	125
Fig 3.6.	HPLC chromatograms of SA at different stages of preparing DPPC:Chol (70:30%) liposomes	126
Fig 3.7.	HPLC chromatograms of freshly prepared standard samples of salicylcic acid and aspirin	128
Fig 3.8.	A summary of the remote loading (acetate gradient) method	130
Fig 3.9.	Washing liposomes with centrifugal filters	131
Fig 3.10.	The hydrolysis products of DPPC	132

Chapter 4

Figure no.	Description	Page no.
Fig 4.1.	A summary of the endocytotic process via different pathways. Numbers indicate pH levels in endosomes	145
Fig 4.2.	Reduction of MTT dye	149
Fig 4.3.	Normalised log(dose)-response curves of aspirin (ASA) and salicylic acid (SA) against the chemo-naïve (HCC1806 PTL) and the paclitaxil-resistant (HCC1806 PAX) breast cancer cell lines	150
Fig 4.4.	Normalised and non-normalised log(dose)-response curves of polysalicylate (PSA) against the chemo-naïve (HCC1806 PTL) and the paclitaxil-resistant (HCC1806 PAX) breast cancer cell lines	153
Fig 4.5.	Size distribution of the PSA-PEG NPs used for the cell viability assay	154
Fig 4.6.	Normalised and non-normalised log(dose)-response curves of PSA-PEG nanoparticles against the chemo-naïve (HCC1806 PTL) and the paclitaxil-resistant (HCC1806 PAX) breast cancer cell lines	155
Fig 4.7.	Log(dose)-response curves of methoxy polyethylene glycol ($mPEG_{1900}$) against the chemo-naïve (HCC1806 PTL) and the paclitaxil-resistant (HCC1806 PAX) breast cancer cell lines	156

List of Figures (cont.)

Chapter 4 (cont.)

Figure no.	Description	Page no.
Fig 4.8.	Normalised log(dose)-response curves of bleomycin and mitomycin against the chemo-naïve (HCC1806 PTL) and the paclitaxil-resistant (HCC1806 PAX) breast cancer cell lines	157
Fig 4.9.	comparison of cytotoxicity of different treatments, individually and in combinations, against the two breast cancer cell lines	158
Fig 4.10.	Normalised log(dose)-response curves of aspirin (ASA) and salicylic acid (SA) against the UKF-NB-3 neuroblastoma cell line	159
Fig 4.11.	Log(dose)-response curve of PSA against the UKF-NB-3 neuroblastoma cell line	160
Fig 4.12.	The normalised and non-normalised log(dose)-response curves of PSA-PEG NPs against the UKF-NB-3 cell line	160
Fig 4.13.	Normalised log(dose)-response curve of ibuprofen against HCC1806 PTL, HCC1806 PAX, and UKF-NB-3	161

List of Tables

Chapter 2		
Table no.	Description	Page no.
Table 2.1.	Different polymers obtained by varying reaction temperatures at both stages of the polymerisation reaction	70
Table 2.2.	Summery of size distribution data from DLS for the four self-assembly preparations	79
Chapter 3		
Table no.	Description	Page no.
Table 3.1.	Summary of the different salicylic acid liposomal preperation	133

Preface

Cancer has always been the immortal enemy of mankind. Even before Hippocrates encountered an abnormal growth with its veins spreading out in every direction and called it *"karkinos"* (i.e. crab) because it reminded him of the crustacean, the writer of a 5000-year-old papyrus from ancient Egypt described a bulging tumour of the breast as a grave disease that has no treatment.[1]

With all of today's medical advancements, cancer is still the second cause of death worldwide after cardiovascular diseases.[2] In 2018 alone, over 18 million new cases of cancer were reported and over 9.5 million cancer-related deaths were recorded globally, and projections to 2040 show an increase of incidence rate by about 63%.[3,4] In the UK, cancer accounts for more than a quarter (28%) of all deaths with an average of around 1000 newly-diagnosed cases and around 450 cancer-related deaths every day.[5]

Cancer has also a huge economic impact as it costs the world more than any other disease. It is estimated that about $895 is spent on cancer each year between diagnosis, treatment, and end-of-life care.[6] The journey of developing a new drug for cancer treatment, from discovery to development and then to clinical trials and drug approval, is estimated to cost about £1.15 billion and takes and average of 12.5 years to complete.[6]

It is for these reasons that researchers have always strived to develop treatments that are not only efficacious against cancer, but that are also cost-effective in terms of development, implementation, and the reduction of the frequency of hospitalisation that might arise from the need for repeated administration of treatment, failure of therapy, or unwanted adverse reactions.

One strategy for developing such treatments entails revisiting old therapeutics that have proven their efficacy for the management of other illnesses, understand how their mechanisms of action relate to cancer and what their advantages might be, and then design new approaches by which these drugs can be used effectively and safely in cancer therapy.

This work is part of the efforts to build on pre-existing knowledge about the effectiveness of safe, cheap, conventional drugs and reutilising them in innovative formulations that maximises their benefits, reduce their side effects, and enhances the overall quality of life of patients.

Aspirin and other nonsteroidal anti-inflammatory drugs (NSAIDs) have shown some promising potential for the treatment and prevention of certain types of cancer, both clinically and *in vitro*.[7–9] However, even though they are often considered to be safe for the management of common pain and inflammatory conditions, they are not free of side effects and can cause so much harm especially with prolonged exposure or in susceptible patients.[10]

The current work aims at maximising the therapeutic benefits of NISADs in cancer and reducing the risks of unwanted adverse effects by formulating these drugs in novel nanoscale delivery systems that take advantage of the uniqueness of the solid tumours' microenvironment to concentrate their cargo in targeted cancer tissues and diminish the systemic distribution of the drugs.[11]

In Chapter 1, the clinical evidence around the role of NSAIDs in the prevention and treatment of different types of cancer is reviewed, followed by a discussion about the potential mechanisms by which NSAIDs suppress tumours. Then an overview of nanotherapy is presented where the pathophysiology of the tumour microenvironment and how it relates to targeted therapy is discussed. The types of targeting are then reviewed along with examples of the different types of nanocarriers that have been developed for the purposes of targeting tumours.

Chapter 2 presents the work that has been carried to create polymer-based nanoparticles for the delivery of NSAIDs. A salicylic acid polymer is first synthesised and characterised and then its release profile investigated. The polymer is then conjugated with polyethylene glycol to create an amphiphilic block co-polymer that could self-assemble in aqueous solutions. The self-assembled nanoparticles are analysed and studied.

The chapter also introduces an attempt to synthesise a biodegradable and biocompatible polyphosphoester for the delivery of another NSAID, ibuprofen. The steps towards the making of the polymer are presented.

In Chapter 3, another type of nanocarriers, liposomes, is prepared with salicylic acid as cargo. The chapter exhibits the different methods carried out to synthesise the liposomes and discusses the challenges associated with the preparation and stability of these nanocarriers.

The *in vitro* studies of the developed nanoparticles are presented in Chapter 4. The Cytotoxicity of the nanoparticles is measures against two cancer cell lines and is compared with cytotoxicity of the monomer. Combination treatments with other established chemotherapeutic agents is also studied and compared to individual agents.

References

1 S. I. Hajdu, *Cancer*, 2011, **117**, 1097–1102.

2 H. Ritchie, Causes of Death, https://ourworldindata.org/causes-of-death, (accessed 30 September 2020).

3 World Health Organisation, Cancer fact sheets, https://gco.iarc.fr/today/fact-sheets-cancers, (accessed 30 September 2020).

4 World Health Organisation, Cancer tomorrow, https://gco.iarc.fr/tomorrow/home, (accessed 30 September 2020).

5 Cancer Research UK, Cancer Statistics for the UK, https://www.cancerresearchuk.org/health-professional/cancer-statistics-for-the-uk, (accessed 30 September 2020).

6 Cancer Research UK, Health economics: the cancer drugs cost conundrum, https://www.cancerresearchuk.org/funding-for-researchers/research-features/2016-08-10-health-economics-the-cancer-drugs-cost-conundrum, (accessed 30 September 2020).

7 P. C. Elwood, A. M. Gallagher, G. G. Duthie, L. A. Mur and G. Morgan, *Lancet*, 2009, **373**, 1301–1309.

8 J. Cuzick, M. A. Thorat, C. Bosetti, P. H. Brown, J. Burn, N. R. Cook, L. G. Ford, E. J. Jacobs, J. A. Jankowski, C. La Vecchia, M. Law, F. Meyskens, P. M. Rothwell, H. J. Senn and A. Umar, *Ann. Oncol.*, 2015, **26**, 47–57.

9 A. I. J. Bashir, C. S. Kankipati, S. Jones, R. M. Newman, S. T. Safrany, C. J. Perry and I. D. Nicholl, *Int. J. Oncol.*, 2019, **54**, 1256–1270.

10 A. Davis and J. Robson, *Br. J. Gen. Pract.*, 2016, **66**, 172–173.

11 C. Fernandes, D. Suares and M. C. Yergeri, *Front. Pharmacol.*, 2018, **9**, 1230.

Chapter 1

NSAIDs, cancer, and magic bullets

1.1. NSAIDs and cancer: clinical evidence

The use of aspirin as a potential therapeutic agent in cancer has been contemplated for decades, with colorectal cancers (CRCs) being the most extensively studied target. In the early 1970s, it was noted that cancer metastasis was associated with platelet aggregation both *in vivo* and *in vitro* and that thrombocytopenia (the deficiency of blood platelets), which results in the lack of blood clotting, caused suppression of metastatic malignancies.[1–3] The potential usefulness of aspirin in CRC was further supported when the concentration of the prostaglandins responsible for platelet aggregation, and whose synthesis can be inhibited with aspirin, was proved to be elevated in the colorectal tumour tissues.[4,5]

Some of the first clinical evidence of the potential effectiveness of aspirin and possibly other non-steroidal anti-inflammatory drugs (NSAIDs) (Figure 1.1) might have been inferred from early trials like the Finnish study[6] that was investigating the link between certain types of cancer and rheumatoid arthritis. The study found a lower incidence rate of digestive tract tumours in female patients with rheumatoid arthritis, and although no direct interpretation could be made, it was later speculated that those patients were prone to taking NSAIDs frequently and for prolonged periods of time.

1.1.1. Colorectal cancers

The aforementioned speculation came from Thun *et al.*[7] who were among the first to investigate this effect on a large scale through a longitudinal prospective cohort study in the late 80s and the early 90s of the past century. In contrast to a few case-control[8,9] and cohort[10,11] studies and small-scale randomised controlled trials (RCTs)[12,13] that were published earlier and had relatively a small number of patients producing contradicting results, Thun's study[7] evaluated the effects of the frequent use of aspirin on death rates from colon cancer in over 660 thousand patients. After following participants over a period of 6 years, it was found that death rates related to colon cancer in patients taking aspirin for more than 16 times a week for at least a year decreased by 40% in men (relative risk [RR]: 0.6, 95% confidence interval [CI]: 0.40-0.89) and by 42% in women (RR: 0.58, 95% CI: 0.37-0.90). The research group later published further multivariate statistical analyses[14] of the same cohort to investigate other types of cancer and concluded that the frequent use of aspirin

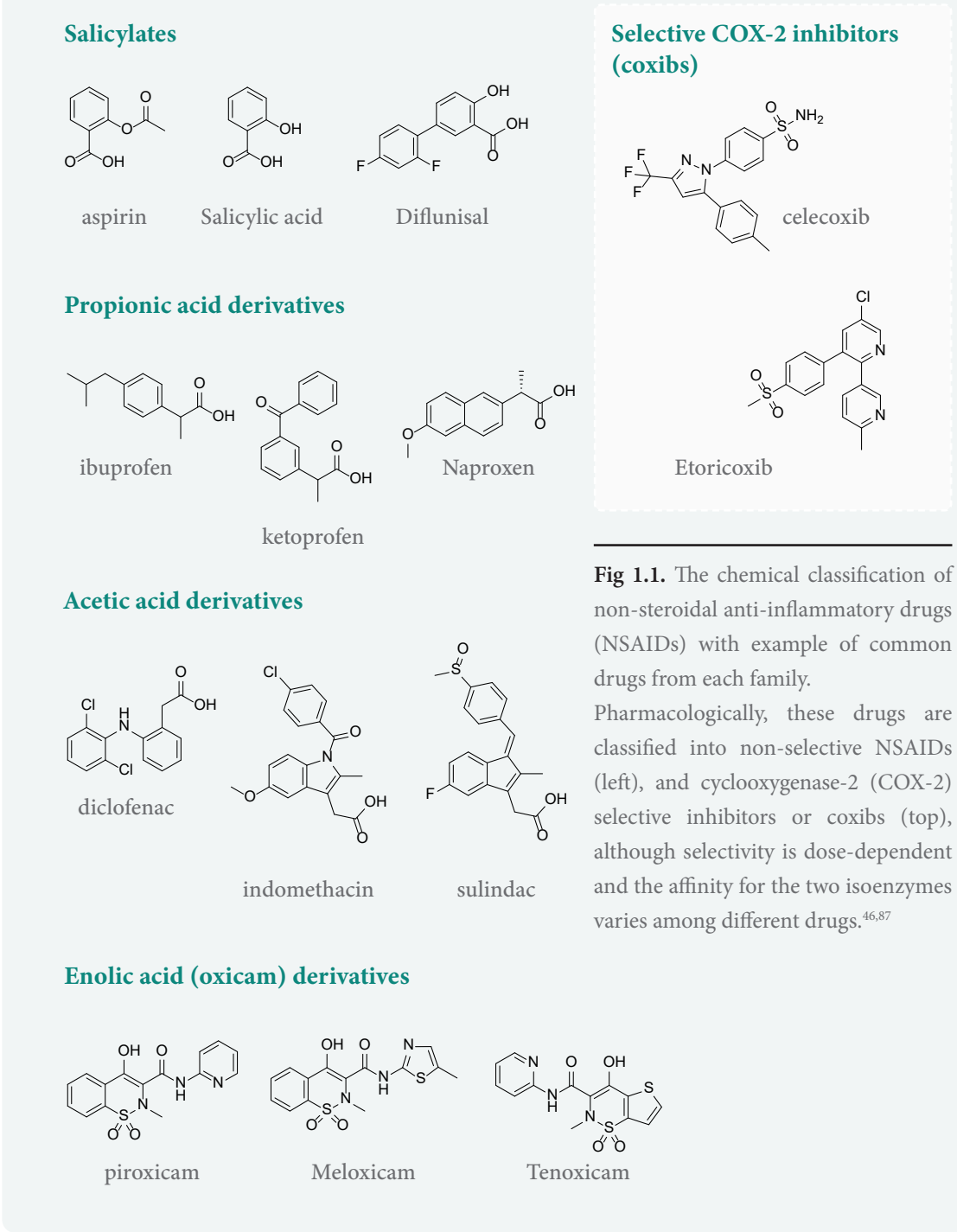

Fig 1.1. The chemical classification of non-steroidal anti-inflammatory drugs (NSAIDs) with example of common drugs from each family.
Pharmacologically, these drugs are classified into non-selective NSAIDs (left), and cyclooxygenase-2 (COX-2) selective inhibitors or coxibs (top), although selectivity is dose-dependent and the affinity for the two isoenzymes varies among different drugs.[46,87]

might have a positive effect on other types of cancer such as oesophageal (RR: 0.59, 95% CI, 0.34-1.03, *P*=0.054), gastric (total adjusted RR: 0.53, 95% CI: 0.34-0.81, *P*<0.0001), colon (RR: 0.58, 95% CI: 0.45-0.74, *P*<0.0001), and rectal (RR: 0.46, 95% CI: 0.25-0.82, *P*<0.0001) cancers. This study had a few shortcomings such as relying on a short self-administered questionnaire to collect data on NSAID use and performed the analysis based on cancer mortality rather than incidence rates as well as having a relatively short follow-up period. It was also proposed by the authors that the

study might have suffered a "detection bias" where gastrointestinal bleeding that developed from taking the aspirin could have resulted in patients receiving more extensive medical examination and subsequently an earlier detection of polyps (which are the precursor to most colorectal cancers)[15] and early-stage tumours thus enhancing survival.

Since stronger clinical evidence would come from randomised controlled trials (RCTs),[16] where biases are minimised (Figure 1.2), yet it would be ethically controversial to deprive control groups of the potential benefits of the treatment, early analyses examined the data from the already-existing trials in which aspirin was being investigated for its cardiovascular effects. Some of the earliest studies nested within two of the largest RCTs of aspirin could not provide proof of the drug's ability to curb the growth of tumours. A cohort study by Gann *et al.*[17] nested within the US Physicians' Health Study (ClinicalTrials.gov identifier: NCT00000500), in which 22071 participants were randomised between treatment group that took 325 mg of aspirin every other day and a placebo group and were followed up for five years, found that aspirin provided no reduction in the incidence of CRCs (RR: 1.15, 95% CI: 0.80-1.65).

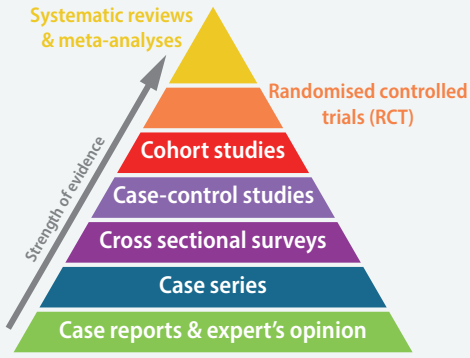

Fig 1.2. The pyramid of evidence-based medicine, adapted from [16]. Strongest evidence that shape clinical guidelines comes from randomised controlled trials (RCTs), systematic reviews, and meta-analyses.

The Women's Health Study (ClinicalTrials.gov identifier: NCT00000479) was another large RCT in the US that had about 40,000 women randomised between a group using 100 mg every other day and a placebo group and followed up patients for a median of 10 years for cardiovascular-related effects. A study by Cook *et al.*[18] nested within this trial found no significant effect of aspirin on the risk of colorectal cancer (RR: 0.97, 95% CI: 0.77-1.24, P=0.83), although a later analysis by the same research group[19] after an extended median follow-up period of 18 years of the same study found a reduction of CRC incidence by 20% (hazard ratio [HR]: 0.80, 95% CI: 0.67-0.97, P=0.021) with a post-trial reduction by 42% (HR:0.58, 95% CI: 0.42-0.80, P<0.001).

In the UK, similar RCTs that studied the cardiovascular effects of aspirin also investigated the potential chemopreventive actions. Among the most noticeable are the British Doctors Aspirin Trial (BDAT),[20] in which 5139 male doctors were allocated between an aspirin group taking 500 mg of aspirin a day and a control group (match ratio 2:1) for five years, and the United Kingdom transient ischaemic attack (UK-TIA),[21] in which 2437 participants were divided into three equal groups of 300 mg aspirin per day, 600 mg aspirin per day, and a placebo control group for periods between 1-7 years. Rothwell *et al.*[22] investigated the effect of aspirin in these studies at the incidence of cancer with a follow-up period of 20 years and found a 26% reduction in colorectal cancer incidence. These findings, however, were only statistically significant with a latency of 10 years or more (HR for years 0-9: 0.92, 95% CI: 0.56-1.49, P=0.73, HR for years 10-19: 0.60, 95% CI: 0.42-0.87, P=0.007). The effect of the follow-up period on the statistical significance of all the above studies could be explained by the fact that colorectal polyps take 10-15 years to develop into cancerous tissue[23,24] thus there would be no significance between the aspirin and the non-aspirin groups if the follow-up was less than ten years.

A later meta-analysis[25] by Rothwell *et al.* of the BDAT and UK-TIA trials alongside three other RCTs[26–28] with a median follow-up period of 18.3 years found that taking aspirin for five or more years was associated with the greatest reduction of cancer incidence and mortality of proximal colon that reached about 70% (incidence HR: 0.35, 95% CI: 0.20–0.63, mortality HR: 0.24, 95% CI: 0.11–0.52, both P<0.0001) and rectal cancers of about 50% (incidence HR: 0.58, 95% CI: 0.36–0.02, P=0.02, mortality HR: 0.47, 95% CI: 0.26–0.87, P=0.01), providing more reliable evidence of the effectiveness of the long-term use of aspirin in reducing the incidence of colorectal cancers and its consequences.

1.1.2. Prostate Cancer

Prostate cancer (PC) is the most prevalent cancer in males worldwide.[29] In the UK alone, it is estimated that there are about 47,740 new cases annually, which accounts for about 130 new cases every single day.[30] Given that the risk factors of PC cannot be attenuated through lifestyle modifications,[31] the prospect of having a preventative measure such as a low-risk protective daily dose of aspirin offers a compelling option to reduce the risk of PC.

However, the evidence of NSAIDs effectiveness in reducing the incidence rate of PC is inconsistent. Two meta-analyses that were conducted around the same time in 2014 came to different conclusions. Wang *et al.*[32] (15 cohort studies and 14 case-control studies) found that the use of aspirin had very little effect on the incidence of PC (odds ratio [OR]: 0.95, 95% CI: 0.93-0.98) and the same was true for non-aspirin (OR: 0.94, 95% CI: 0.90-0.98), while analysing data for all-NSAID intake found that it was positively correlated with the incidence rate of PC (OR: 1.18, 95% CI: 1.15-1.22). Nonetheless, this analysis showed a significantly statistical heterogeneity (I^2 = 92.4%, P<0.001 for aspirin, I^2 = 60.7%, P<0.001 for non-aspirin NSAIDs, and I^2 = 55.9%, P<0.01 for all-NSAID use). Liu *et al.*[33] in their analysis (19 cohort studies and 20 case-control studies) concluded similarly when they found that the use of aspirin slightly reduced the incidence risk of total PC (OR: 0.92, 95% CI: 0.87-0.97, I^2 = 66.2%, P<0.001) and advanced PC (OR: 0.81, 95%CI: 0.73-0.89, I^2 = 23.9%, P=0.20). It also slightly reduced the mortality risk of both total (HR: 0.86, 95% CI: 0.78-0.96, I^2 = 39.2%, P=0.145) and advanced (OR: 0.81, 95% CI: 0.71-0.92) PC. The pooled analysis for all-NSAID use however found no significantly statistical correlation between treatment and incidence risk of total (OR: 0.9, 95% CI: 0.75-1.07, I^2 = 93.5%, P<0.001) or advanced (OR: 0.86, 95% CI: 0.52-1.40, I^2 = 94.2%, P<0.001).

In 2018, Shang *et al.*[34] included more recent large-scale studies in their meta-analysis (a total of 43 observational studies). The analysis concluded that the regular use of any NSAID reduced the risk of PC by about 11% (pooled RR:0.89, 95% CI: 0.81–0.98, I^2 = 94%, P<0.001) and that further reduction is even noticeable if the use was ≥ 5 years rather than ≥ 4 years (pooled RR:0.882, 95% CI: 0.785–0.991, I^2 = 27.4%, P=0.248). It also found that the use of aspirin was associated with a modest reduction in PC (pooled RR:0.93, 95% CI: 0.89–0.96, I^2 = 79.5%, P<0.001) and that this reduction was more pronounced (pooled RR:0.875, 95% CI: 0.792–0.967, I^2 = 28.4%) with the daily use of aspirin (1 or more pill per day) rather than the prolonged overall use (≥ 4 years of any use). The pooled analysis of non-aspirin NSAID use, however, showed no statistically significant reduction in PC risk.

As presented above, evidence regarding the role of NSAIDs in reducing the risk of PC is indecisive with a high degree of heterogeneity in some cases. This can be attributed to multiple factors. Firstly and more importantly, all of the analyses were of observational and case-control studies

which can involve many factors that can complicate the analysis, and there is a lack of RCTs that can provide stronger evidence, reduce biases, and adjust for confounders. Secondly, most of the analysed studies depended on questionnaires and interviews in which patients were asked about their NSAID consumption history, which can be prone to recall bias where patients over- or underestimate their consumption habits. This can be further complicated by the fact that many NSAIDs are available over-the-counter (OTC) and there might not be accurate records of their use, and thus recall bias is exaggerated even further.

Thirdly, the regular consumption of NSAIDs has shown to lower the serum levels of prostate-specific antigen (PSA) although it is unclear whether this is a result of a protective or a masking effect.[35,36] Since PSA assay is regularly used for screening purposes of PC, false low PSA resulting from NSAID use could have complicated the results of the analyses. For example, PC incidence could have been underestimated in patients taking NSAIDs for an extended period of time, or the stratification of patients between early-stage and advanced PC (in which PSA levels are much higher) could have been influenced by misinterpretation of PSA levels leading to selection bias in some studies.

Nonetheless, these meta-analyses still provided some evidence on the protective role of NSAIDs in prostate cancer, although further well-designed RCTs are necessary to provide more conclusive evidence.

1.1.3. Breast cancer

As with prostate cancer, there is a lack of high-grade evidence regarding the chemopreventive effects of NSAIDs in breast cancer since data comes mostly from cohort and case-control studies rather than large-scale RCTs. Two meta-analyses that analysed data from existing studies, however, found an inverse association between the use of NSAIDs and breast cancer incidence. Takkouche *et al.*[37] conducted a meta-analysis in 2008 on 38 studies that spanned over 42 years preceding the analysis and included over 2.7 women. The analysis found a 12% reduction in breast cancer risk with any-NSAID use (RR: 0.88, 95% CI: 0.84-0.93) with a risk reduction of 13% associated with aspirin use (RR: 0.87, 95% CI: 0.82-0.92) and 21% with ibuprofen use (RR: 0.79, 95% CI: 0.64-0.97). Zhao *et al.*[38] conducted a similar meta-analysis around the same time and found similar results and, just as with Takkouche's analysis, they reported high levels of heterogeneity (I^2 = 92%,

P=0.04). Huang *et al.*[39] concluded in a more recent meta-analysis that included one RCT that NSAID use is associated with enhanced survival and decreased breast-cancer-related mortality, although the analysis was not statistically significant and had high levels of heterogeneity which were attributed to the presence of confounding factors such as the age and race of the participants as well as to the hormone receptor status and the subtype of the cancer (i.e. oestrogen-receptor [ER], progesterone-receptor [PR], human epidermal-growth-factor-receptor-2 [HER2] statuses), although no further details were provided in any of the three analyses in this regards. This could be of relevance since prostaglandin E_2 (PGE_2), whose synthesis is catalysed by cyclooxygenase-2 (COX-2), is thought to be responsible of the local production of oestrogen and thus promoting the development of ER+ breast cancer[40] although there is also some evidence suggesting that COX-2 might also play a role in the development of ER- and HER2- breast cancers.[41]

A few studies have investigated the correlation between the tumour hormone status and the effect of NSAID use found different responses depending on the cancer subtype; The Spanish Multi-Case-Control Study[42] found a reduction in risk of hormone-positive (ER+ and/or PR+) breast cancer (OR: 0.72, 95% CI: 0.60=0.88, *P*<0.001) and HER+ breast cancer (OR: 0.63, 95% CI: 0.45-0.88, *P*=0.007) but not with triple-negative breast cancer (OR: 0.87, 95% CI: 0.58=1.33, *P*=0.49) with all NSAID use. When analysing data for specific NSAID subgroups, however, the risk reduction was only statistically significant for global NSAID use, with acetic acid derivatives (e.g. diclofenac and indomethacin), propionic acid derivatives (e.g. ibuprofen, ketoprofen, naproxen), and COXIBs (i.e. selective COX-2 inhibitors), but not with aspirin. The Sister Study, a cohort study of over 50,000 women who had a sister(s) with breast cancer by Sangmi *et al.*[43] found no statistical significance of the breast cancer risk reduction associated with NSAID use by cancer subtype. Its conclusion, however, was that the risk of breast cancer in premenopausal women was significantly reduced by the prolonged use of NSAIDs (HR_{4vs1}: 0.66, 95% CI: 0.50-0.87, *P*=0.025) and especially aspirin (HR_{4vs1}: 0.57, 95% CI: 0.33-0.98, *P*=0.038) while it was insignificant with all other NSAID (HR_{4vs1}: 0.73, 95% CI: 0.53-1.01, *P*=0.182). It is also worth noting that in Brasky *et al.*'s case-control study[44] it was found that aspirin had a reducing effect on breast cancer risk regardless of the subtype of cancer and, more interestingly, that ibuprofen was associated with an increased risk with many of the subtypes although that most of the analysis in both cases had no statistical significance.

As with prostate cancer, there is a lack of well-designed RCTs that focus on investigating the effects of prolonged exposure to NSAIDs on breast cancer to minimise the impact of confounding factors on the evidence. Cook *et al.* in their study[18] within the Women's Health Study RCT and their follow-up analysis[19] however, found no statistically significant risk reduction of breast cancer with the long-term use of low-dose aspirin (alternate-day 100 mg). In the light of COX-2's potential involvement in breast cancer development, this might be explained by the fact that aspirin is about 160 times more selective to COX-1 than COX-2 at low doses (75-100 mg) and requires higher doses (≥1200 mg) to suppress COX-2 and produce the anti-inflammatory effect.[45,46]

1.1.4. Kidney cancer

Renal cell carcinoma is perhaps the only type of cancer that has shown evidence of being positively correlated with the prolonged use of some NSAIDs. A meta-analysis by Choueiri *et al.*[47] of 18 case-control and cohort studies found that the use of non-aspirin NSAIDs was correlated with an increased risk of renal cell carcinoma (RR: 1.25, 95% CI: 1.06–1.46) but did not find that association with the use of aspirin (RR: 1.10, 95% CI: 0.95–1.28) except when the five non-US studies were pooled together (RR: 1.17, 95% CI: 1.04–1.33). Cho *et al.*'s analysis[48] of the large prospective Nurses' Health Study[49] (about 127,000 subjects with a follow-up period of 20 years) arrived at a similar conclusion of an increased risk of kidney cancer with the use of non-aspirin NSAIDs (RR: 1.51, 95% CI: 1.12-2.04).

Although neither analysis could provide an explanation for this finding, it might be related to the effects of NSAIDs on the renal homeostasis and kidney function[50] that will be discussed more in detail later, although this does not explain why this is observed with non-aspirin NSAIDs but not with aspirin.

1.1.5. Other cancers and metastasis

A meta-analysis by Wang *et al.*[51] that mostly included case-control studies on the effect of NSAID use on gastric cancer incidence found that aspirin users had a lower risk of non-cardia gastric cancer (OR: 0.73, 95% CI: 0.63-0.86) as did non-aspirin NSAID users (OR: 0.74, 95% CI: 0.55-1.00). When stratifying patients into regular vs irregular users, the risk reduction was found to be statistically significant with the regular NSAID use (OR: 0.57, 95% CI: 0.44-0.74) as opposed to irregular use (OR: 0.84, 95% CI: 0.66-1.07).

An analysis of 12 case-control studies by Trabert *et al.*[52] also found that the regular use of aspirin inversely correlated with ovarian cancer risk (OR: 0.91, 95% CI: 0.84-0.99, I^2 = 5.2%) but was statistically insignificant with non-aspirin NSAIDs (OR: 0.90, 95% CI: 0.77-1.05, I^2 = 73.2%).

As for metastasis, a meta-analysis by Zhao *et al.*[53] of related reports in the literature found that patients who were exposed to NSAIDs had a lower risk of distant metastasis whether this exposure was pre-diagnostic (RR 0.708, 95% CI 0.586–0.856) or post-diagnostic (RR: 0.484, 95% CI: 0.393–0.595), and that this reduction was significant for prostatic cancer (pre-diagnosis 22.6%, post-diagnostic 51.8%), and breast cancer (pre-diagnosis 33.6%, post-diagnostic 52.5%) but less pronounced (only 5.1%) with pre-diagnostic use in lymph node metastasis.

Despite all the promising evidence, regulatory bodies and practitioners are still reluctant to make strong recommendations regarding the use of NSAIDs for the prevention of cancer. For example, the highly-regarded U.S. Preventive Services Task Force, who provides evidence-based clinical guidelines on preventative medicine that are followed by practitioners in the US and worldwide, cautiously advised in its latest recommendations[54] to prescribe aspirin as a chemopreventative against CRCs only in patients beyond a certain age who are at a low risk of bleeding and who are willing to take low-dose aspirin daily for at least 10 years.

Clinical guidelines, in general, are based on balancing the risks and benefits of any particular treatment. The same pharmacological effects through which therapeutic benefits manifest in the body can determine the potential side effects that can be induced by the treatment and the pre-existing contra-indications that can prevent from using it. Below we discuss the pharmacological actions exerted by NSAIDs that could potentially explain their chemotherapeutic effects as well as their common adverse reactions.

1.2. The pharmacological mechanisms of NSAIDs in cancer

There are multiple proposed pathways in which NSAIDs exert their chemotherapeutic activity; what follows is an overview of these pathways:

1.2.1. The COX-dependent pathway

Many physiological processes are moderated by prostaglandins (PGs), a subgroup of bioactive,

hormone-like lipids called eicosanoids. They exist in most human tissues and are responsible for a wide array of biological regulatory processes such as maintaining homeostasis and mediating inflammatory responses.[55] It has been long proposed that many PGs might be responsible for promoting cancer growth and metastasis.[56,57] The pro-inflammatory prostaglandin E_2 (PGE_2), in particular, has been found to be overexpressed locally in many tumours such as colon,[58] breast,[59] lung,[60] and head and neck[61] cancers and is suspected of playing a role in tumour growth, angiogenesis, cell adhesion, and metastasis.[56] These findings encouraged researchers to suggest that suppressing PGE_2 might carry a tremendous chemotherapeutic value.

Prostaglandins are synthesised *in vivo* from a 20-carbon chain fatty acid called arachidonic acid (AA) which is freed from the phospholipid layer of the plasma membrane by phospholipase A_2 and then further metabolised into prostaglandins by cyclooxygenases (COXs, also known as prostaglandin-endoperoxide synthases or PTGSs). The COX enzymes comprise of 2 isoforms; COX-1 which mediates the synthesis of the "housekeeping" PGs (i.e. PGs responsible for blood clotting, stomach epithelial cytoprotection, and homeostasis), and COX-2 which mediates the synthesis of the inflammatory and proliferative prostaglandins, including PGE_2.[55,57] The overexpression of PGE_2 is thought to promote the proliferation of colon cancer by activating the RAS-ERK signalling pathway[62] as it does in lung cancer.[63] It is also believed to upregulate the aromatase production and the subsequent synthesis of oestrogen in the adipose stroma surrounding breast cancer tissue, thus promoting its growth.[64] Figure 1.3 illustrates the COX synthesis pathway and the effects of the major prostaglandins.

NSAIDs exert their anti-inflammatory effects through the inhibition of COX enzymes, although they vary in terms of the extent and selectivity of this inhibition. While aspirin is the only NSAID capable of irreversibly deactivating both isoenzymes through modifying their structure by acetylation, thus requiring the synthesis of new molecules to restore their activity, all other NSAIDs reversibly bind to the COX enzymes. Furthermore, aspirin is more selective to COX-1 at low doses and it becomes non-selective at higher doses. In contrast, other NSAIDs such as ibuprofen are inherently non-selective, and others like celecoxib are entirely selective to COX-2 (hence collectively called COX-2 selective inhibitors or COXIBs).[45,46,65] PGE_2 synthesis, among other PGs, is mediated through COX-2 and the inhibition of the latter and hence the subsequent

production of PGE_2 is believed to be the main mechanism by which NSAIDs produce their anti-tumour activity.[57] It has also been suggested that COX-1 might promote the progression of some cancers since it has been found to be overexpressed in ovarian cancer.[66]

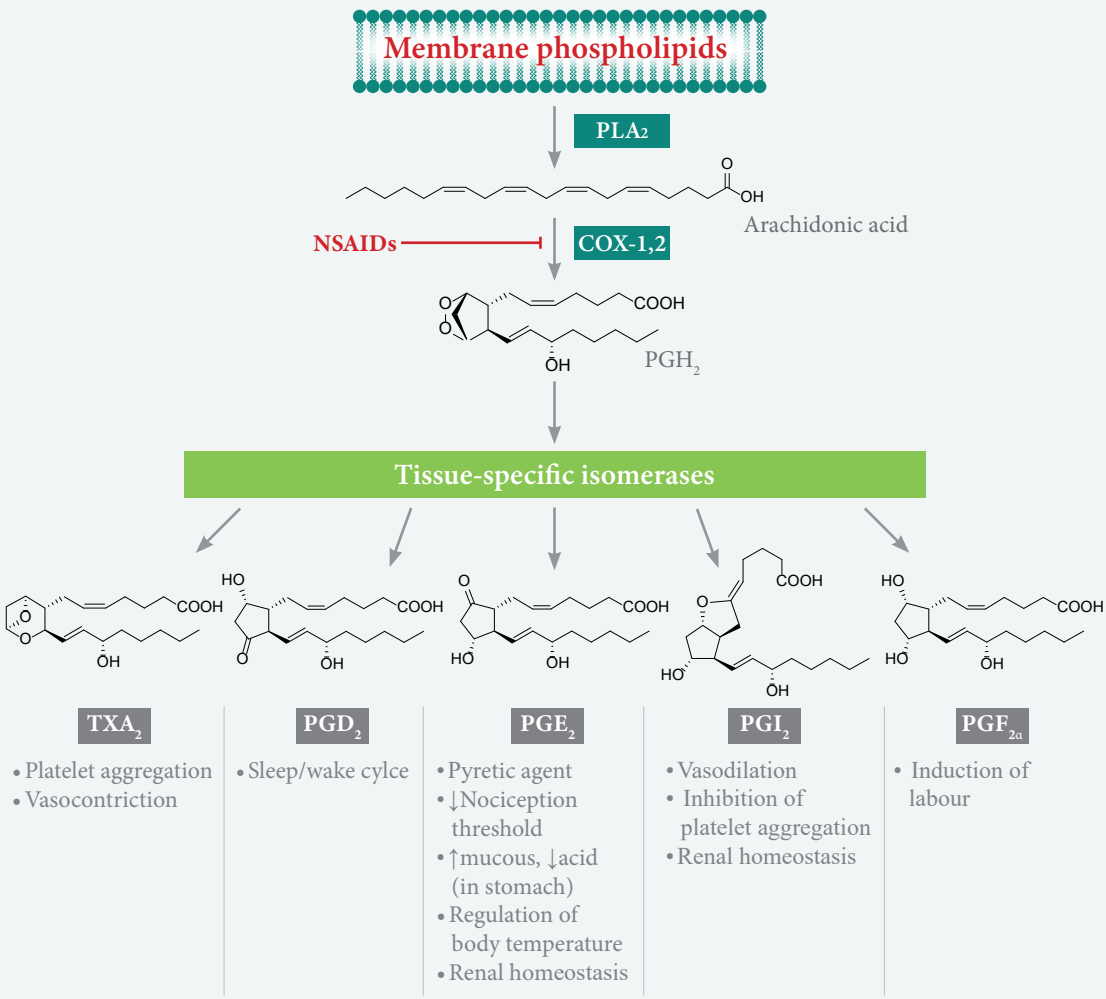

Fig 1.3. The cyclooxygenase pathway adapted from [55]. **COX:** cyclooxygenase, **NSAIDs:** non-steroidal anti-inflammatory drugs **PLA2:** phospholypase A2, **PG:** prostaglandin, **TXA2:** thromboxane A2.

The antiplatelet effect of aspirin, which is achieved through the irreversible suppression of COX-1 and the subsequent inhibition of the production of the eicosanoid thromboxane A_2 (TXA_2) that is responsible for platelet aggregation,[67] is also believed to play a role in the growth and spread of tumours. It has been speculated that activating platelet aggregation might facilitate the metastasis of cancer cells while reducing aggregation could reduce the tumour burden, at least in animal tumour models.[68,69] Aspirin also could possess the capability not only to suppress platelet aggregation but also to change the profile of many proteins secreted from platelets upon their activation (collectively known as the platelet releasate), such as interleukin 7 (IL-7), vascular

endothelial growth factor (VEGF), angioprotein-1, and fibroblast growth factor (FGF) among others,[70,71] all of which are pro-inflammatory factors and are suspected of playing a part in the promotion of angiogenesis and metastasis.[72] It has also been suggested that some component of releasate, especially VEGF and FGF, induce COX-2 production and the subsequent rise in the production of PGE_2 and other COX-2-mediated inflammatory factors.[73] Finally, TXA_2 itself is a suspect of possessing a supportive role in inducing the production of local COX-2 and in the angiogenesis and metastasis processes, and suppressing its synthesis by aspirin might prove to be beneficial.[74,75]

1.2.2. COX-independent pathways

Although the COX-dependent mechanisms of NSAIDs as chemopreventive are the most prominent and the most studied, there are other suggested mechanisms by which NSAIDs exert such effects.

Eluding apoptosis (i.e. the naturally-programmed cell death) is a hallmark of cancerous cells, and reactivating the kill switch in these cells is the target for many anti-tumour drugs.[76] NSAIDs are believed to induce apoptosis through modulating the effects of Bcl-2, a family of genes responsible for encoding the proteins that either inhibit or induce apoptosis mainly through controlling cell membrane potential and its permeability for apoptotic elements.[77] Aspirin was found to decrease the expression of the anti-apoptotic Bcl-2 gene and increase the expression of the pro-apoptotic Bax gene in lung and ovarian cancer cells.[78] Naproxen and sulindac showed similar effects in bladder[79] and colon[80] cancer cells, respectively, while celecoxib is believed to amplify the expression of p53 anti-tumour proteins in colorectal cancer cells.[81]

Aspirin has also been found to increase the production of intracellular reactive oxygen species (ROS) that induces cell apoptosis through increased oxidative stress, as well as disrupt the activity of mitochondrial respiratory enzymes and the related energy production, subsequently promoting cell death in liver cancer.[82]

Other mechanisms by which NSAIDs potentially induce apoptosis include:

- the inhibition of cyclic guanosine monophosphate phosphodiesterases (cGMP PDEs) that inactivates cGMP which is otherwise responsible for normal apoptosis.[83]
- Modulating peroxisome proliferator-activated receptors (PPAR) α, γ, and δ.[84,85]

- Inhibition of the transcriptional signalling of nuclear factor NF-κB which mediates several anti-apoptotic and cell survival-promoting pathways.[86]

In addition to promoting apoptosis, the inhibitory role of NSAIDs of other tumour-related activities, i.e. angiogenesis and metastasis, might also be explained through COX-independent pathways. Since cGMP plays an active role in tumour angiogenesis, it might be possible that this process is inhibited by NISADs via the suppression of cGMP PDEs as well as the previously discussed COX-mediated suppression of VEGF.[87] Matrix metalloproteases (MMPs), a family of proteinases that exist in most solid tumours and are responsible for the degradation of the extracellular matrix (ECM) thus facilitating metastasis, are also thought to be inhibited by NSAIDs, more specifically, MMP2 and MMP9.[88]

1.2.3. The side effects of NSAIDs

Even though NSAIDs have a wide therapeutic window and many of them are available over-the-counter (OTC), they are still not free of side effects that can be serious in some cases. Those side effects are generally linked to the pharmacological effects, mainly the ones related to the COX pathways discussed above.

As previously mentioned, many of the prostaglandins whose synthesis is catalysed by the COX isoenzymes have homeostatic effects throughout the body. Some prostaglandins, especially PGE_2 and PGI_2 (also known as prostacyclin), for example, mediate the gastric acid and mucus secretions. These prostaglandins maintain the balance between gastric acid production and inducing the secretion of the stomach mucosal layer, hence maintaining the integrity of the stomach lining and protecting it from being digested by its acidic content.[89] Non-selective NSAIDs suppress PGI_2 resulting in the most prominent side effect to these NSAIDs, i.e. peptic and duodenal ulcers.[90] In the presence of risk factors, such as old age or prolonged use of NSAIDs, these ulcers can develop into bleeding lesions leading to anaemia, or even perforate the stomach into the abdominal cavity leading yet to more serious complications.[91,92] This bleeding complication is observed mainly with aspirin due to its irreversible antiplatelet effect that lessens the body's ability to produce thrombosis in the bleeding gastric tissue.[93] This irreversible antiplatelet effect is also the reason why the prolonged use of aspirin is associated with an increased risk of intracranial bleeding and haemorrhagic strokes.[94]

Although COXIBs, by being inherently selective to COX-2, help reduce the production of the COX-2-mediated pain and inflammation PGs while being far less harmful to the stomach, this does not come without a price. COXIBs inhibit the production of prostacyclin, a dominant vasodilator, in blood vessels while leaving the constrictive and pro-aggregation effects of the COX-1-mediated TXA_2 unopposed. This pro-thrombotic imbalance carries the risk of serious cardiovascular (CV) events (such as angina pectoris or myocardial infarction) should any predisposing risk factors exist.[95,96]

In a similar fashion, by suppressing prostacyclin synthesis in the renal afferent arteriole, both selective and non-selective NSAIDs affect the renal function and can lead to reversible acute renal failure that can develop to a chronic state if the injury was prolonged. In brief, suppressing the vasodilating effect of prostacyclin causes a constricted renal arteriole to let less blood into the kidney leading to poor renal perfusion and a subsequent reduction in glomerular filtration rate and renal ischemia might eventually develop. This effect could also lead to an elevation of blood pressure and the formation of oedemas, which pose an added risk to patients with hypertension and heart failure.[97,98]

Prostaglandins, especially PGE_2, play a significant role in maintaining the muscle tone of the respiratory system. PGE_2 controls the tone of the bronchi through binding to different subtypes of receptors, mainly EP_1 receptors that promote bronchoconstriction and EP_2 that causes bronchodilation. Suppressing the production of PGE_2 causes imbalance in this system leading to bronchospasm.[99] PGE_2 is also believed to be a major stabiliser of mast cells, the immune cells whose activation is responsible for the release of histamine and other pro-inflammatory and broncho-constricting agents from the leukotriene (LT) family. It is through the inhibition of the PGE_2 synthesis and the subsequent destabilisation of mast cells and the release of inflammatory LTs that aspirin and other NSAIDs cause aspirin-exacerbated respiratory disease (AERD) or aspirin-induced asthma (AIA) in susceptible patients and making this class of drugs altogether contra-indicated in asthma patients.[100]

From what has been discussed above, it is clear how the mechanisms by which NSAIDs produce their response immensely affect the delicate risks/benefits balance and can vary largely from one patient to another furtherly complicating the clinical practitioner's decision and either robbing a

potential candidate from the NSAIDs' chemotherapeutic gains or causing harmful, and sometimes lethal, effects to another. This has led us to consider exploiting a concept that has been extensively studied, and, to a lesser extent, commercially used to maximise the therapeutic benefits while minimising the risks, namely, *nano-scale delivery systems*.

1.3. Nanotherapy and its prospects in cancer

Since the beginning of the twentieth century when the German physician, scientist, and Nobel Laureate Paul Ehrlich envisioned a "magic bullet"[101] that would target only pathogens, scientists have been trying to tailor therapeutics in a manner that would concentrate treatment in ailed organs while sparing healthy ones potential toxicity, and many advances have been made in this regard especially in the field of immunology. Targeted therapy started taking form in the 1980s primarily as antibody-drug conjugates (ADCs) where specific antibodies are linked to drug molecules which would only exert their pharmacological effect upon cells that have a corresponding antigen to the conjugated antibody.[102] However, around the early 1990s, other targeted strategies were evolving from the emergent nanotechnology field that was conceptualised by pioneers like Richard Feynman a little over 30 years prior.[103] The idea of building minute systems that can deliver high drug payloads only to the cite of action was quite appealing, and the field of nanomedicine started to take shape.

1.3.1. The definition of nanomedicine and nanotherapeutics

As the name suggests, the term *nanomedicine* came to be when nanotechnology converged with medicine. The prefix "nano-" (from the Greek word "nanos", meaning "dwarf") pertains objects and processes that are happening on the nanometre scale, i.e. one billionth of a metre.[104] Because the size factor can be unfairly limiting to the definition of the vast discipline of nanomedicine in which chemistry, biology, physics, and engineering are involved, the National Institute of Health (NIH) gave a broader definition[105] to the practices involved in nanomedicine as:

1. studies that use nanotechnology tools and concepts to study biology;
2. the engineering of biological molecules toward functions very different from those they have in nature; or

3. manipulation of biological systems by methods more precise than can be done by standard molecular biological, synthetic chemical or biochemical approaches.

Based on this definition, the term *nanodrugs* can be applied to particles on the nanoscale that can be used for the diagnosis, prevention, and treatment of disease, yet variations in nomenclature can be used to further identify *nanotherapeutics* whose primary purpose is the prevention and treatment and *nanotheranostics* which can also aid in diagnosing diseases. Although these names entail that the described entities can fall somewhere between 1 nm and 1000 nm, in the biomedical and pharmaceutical contexts, it is particles that are mainly under 200 nm that might be more clinically-relevant.[104] Figure 1.4 compares the size of nanotherapeutics to biological components.

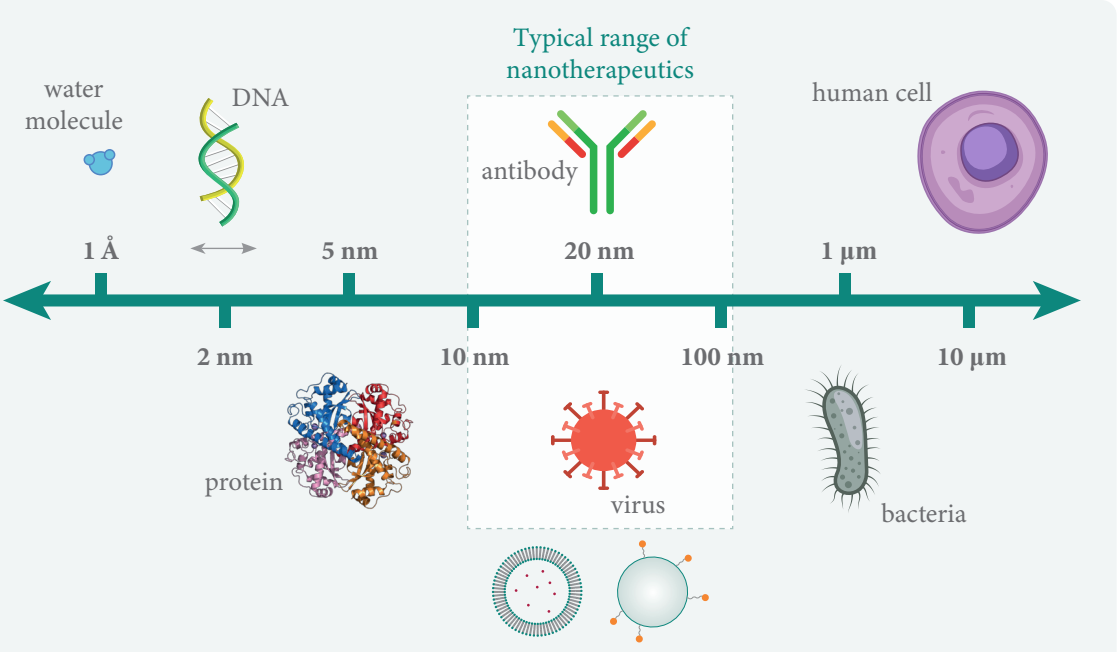

Fig 1.4. A scale bar showing the size of nanotherapeutics in comparison to biological systems.

Nanotherapeutics have offered a promising alternative to conventional therapy. In the case of cancer, for example, cytotoxic drugs that are used conventionally to suppress the abnormal proliferation of cancer cells can also inhibit normal cells which have rapid growth rates such as those in hair follicles, bone marrow, and gastrointestinal tract giving rise to the common side effects associated with those drugs.[106] The unique physicochemical characteristics of nanocarriers can help reduce the systemic effects of cytotoxic drugs by delivering them almost exclusively to the targeted sites and at the same time accumulate higher payloads at those sites in a way that conventional therapy cannot achieve. Moreover, nanocarriers provide another advantage over conventional therapy and

other forms of targeted therapy related to the antibodies and antibody-drug conjugates (ADCs) and that is enhancing the pharmacokinetic profile of the drug payload. Nanocarriers can prevent or slow down the degradation of their payload by blood enzymes as well as reduce its renal clearance resulting in prolonging the drug half-life and enhancing its bioavailability. Thus formulating drugs into nanocarriers can also resolve issues related to drug solubility as well as allow control over their release kinetics for added therapeutic benefits.[106–108]

Although nanotherapeutics has many potential clinical applications including cancer, pain management, and the treatment of infectious disease,[109] we will look at the mechanisms, advantages, and utilisation from the cancer perspective, as it is the one related to the work at hand as well as being the one most-extensively researched.

1.3.2. Tumour microenvironment

In his "seed and soil" hypothesis, Stephen Paget proposed in the late 19th century that cancer "seeds" (that we now call metastases) can only grow when embedded in a suitable "soil" that provides protection and nutrients.[110] Clinical and experimental studies in the past decades have confirmed that the "soil" concept applies to the cellular environment in which solid tumours grow, proliferate, and from which they metastasise. The non-malignant components of a tumour are collectively termed the tumour microenvironment (TME), and it is the exploitation of its uniqueness and contrast with healthy tissues that constitutes the most important aspect of targeted nanotherapy.[111]

TME is majorly composed of a (a) stromal scaffold that consists mainly of cancer-associated fibroblasts (CAFs), (b) the extracellular matrix (ECM) which is a conglomerate of macromolecules such as collagen and proteoglycans, (c) immune cells and other bone marrow-derived cells, and (d) a chaotic network of blood vasculature, each having a part in cancer growth and metastasis.[112]

CAFs are previously normal fibroblasts, cells that normally promote wound healing, that have been activated through various carcinogenic conditions and turned into perpetually-activated immortal cells that resist apoptosis and boost tumorigenic activity.[113] Upon their activation, CAFs form the framework that supports solid cancer cells. They also help generate the ECM that further define the physical characteristics of the tumour.[114] CAFs also induces the epithelial-to-mesenchymal transition (EMT) process which gives rise to mesenchymal cells that do not provide the tumour

with the same structural integrity that epithelial cell layers have in normal tissues thus encouraging cancer cell invasion and metastasis.[115,116] CAFs are also implicated in releasing multiple growth factors such as the vascular endothelial growth factor (VEGF), fibroblast growth factor (FGF), and platelet-derived growth factor (PDGF), all of which aid in tumoural angiogenesis and the growth and proliferation of cancer cells.[115]

The ECM also has a supportive role in the physical structure of solid tumours. It consists of the non-cellular components of the microenvironment, mainly the fibrous proteins like collagen, elastin, and fibronectin as well as the proteoglycans chondroitin sulphate, heparin sulphate, keratin sulphate, and hyaluronic acid, all of which help define the mechanical characteristics such as stiffness and deformability of solid tumours and help guide cancer cell invasion and metastasis.[117,118] Collagen, in particular, is responsible for the stiffness of the tumour mass. While the stiffness of normal stroma is typically around 150 Pa, the presence of high levels of crosslinked collagen in the ECM of tumours causes the stiffness of tumour stroma to be about 400 Pa.[119] It is also suspected of making structural conduits that aid in cancer cell migration.[120]

In addition to the supportive role, the proteoglycan components of the ECM, especially heparin and heparan sulphate, are also suspected of facilitating tumour growth and metastasis by binding growth factors such as VEGF, PDGF, and EGF (epidermal growth factor) and acting as reservoirs that release those factors upon activation via growth signalling.[121] It is also worth noting that hyaluronic acid raises the interstitial fluid pressure in the tumour mass causing an outward movement of fluids that prevent drugs in the main bloodstream from diffusing into the tumour.[120,122]

Other major components of the TME are immune cells that have been recruited into the location of cancer as a response to the inflammatory process. These cells include mast cells, neutrophils, natural killer (NK) cells, and most importantly, macrophages.[112] Macrophages found in solid tumours, doped tumour-associated macrophages (TAMs), are the most prominent immune cells found in tumours and they can be distinguished into two phenotypes; M1 macrophages that are part of the normal inflammatory response of the host to the tumour, i.e. the destruction and phagocytosis of cancer cells, and M2 macrophages that are involved in pro-tumourigenic processes that encourage angiogenesis and metastasis.[112,122] In invasive cancer, there is a high polarisation of

M1 to M2 TAMs, and it is the latter that produces growth factors and inflammatory cytokines such as IL-10 and prostaglandin E_2 (PGE_2).[112] It is also believed that those cells might be involved in promoting the development of the premetastatic niches thus priming the "soil" for the migrating cancer cells invade and form new metastatic foci.[123]

From all discussed above, it can be clear that growth factors are excessively produced by many components of the TME. This is due to the fact that those factors, among others, mediate the regulation of the processes that vascularise tumour tissues.[112] The rapidly-growing tumour mass possesses a high oxygen demand that the existing vasculature continuously fails to fulfil and, as a result, chronic hypoxia ensues especially in the deep layers of the tumour where the oxygen concentration is believed to be in the range of 1-2% as opposed to 3-6% in normal tissues.[122] This leads to the activation of signalling pathways that promote angiogenesis (i.e. the formation of new blood vessels through branching out from pre-existing ones) and vasculogenesis (i.e. the formation of new blood vessels through recruiting circulating endothelial cells).[124] However, due to the high metabolism rate of cancer cells, the resulting branching is often chaotic leading to an uneven lumen and a highly-fenestrated, thus leaky, endothelium causing irregular blood flow and a further increase in the interstitial fluid pressure (IFP) which can be 10-40 folds of that of normal tissues.[125] All of this worsens the hypoxia and promotes the tumour development.[111,126] Figure 1.5 illustrates the composition of a solid cancer tissue.

It is also noteworthy that, due to this hypoxic state, the abnormally metabolic cancer cells depend on oxygen-independent glycolysis (known as the Warburg effect) to obtain energy as opposed to the oxidative phosphorylation that happens in normal cells. This causes the excessive production of lactate and carbon dioxide and the subsequent increase in proton ions concentration. The result is an acidic extracellular pH in the tumour (pH_e = 6.5-6.9) compared to the normal physiological pH (7.2-7.4).[127,128]

These unique characteristics of the TME separate it from normal tissues, and exploiting this uniqueness has been an appealing catalyst for creating more effective and safer therapies. However, while many targeted therapy strategies fall within the field of molecular biology, i.e. the development and use of monoclonal antibodies that target specific components of the TME such as those that target growth factors, TAMs, or any of the factors that modulate the signalling pathways involved

in tumourigenic activities,[112] we will focus on the approach related to the project at hand, namely, targeted nanotherapy. This approach entails formulating existing conventional therapeutic agents into nanocarriers that take advantage of some of the unique characteristics of the TME discussed above to maximise the delivery of those therapeutics to cancer foci while sparing healthy tissues the potential toxicities associated with conventional therapies.

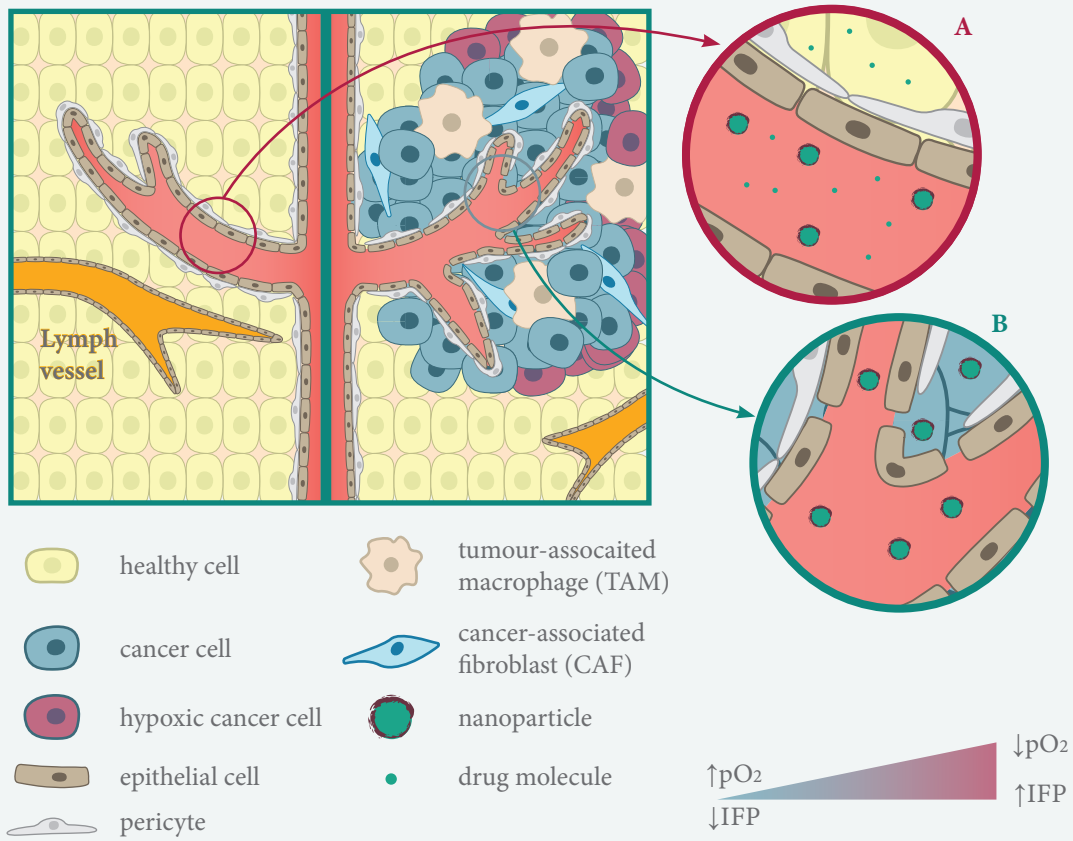

Fig 1.5. A schematic demonstrating the differences between healthy and tumourous tissues, especially in regards to the enhanced permeability and retention (EPR) by which nanoparticles are able to extravasate into tumour tissues (B) mainly due to the fenestrations and gaps in vasculature, unlike healthy tissues (A) where the tight junctions between epithelial cells allow only small molecules to pass through.
IFP: interstitial fluid pressure. pO_2: partial pressure of oxygen.

1.3.3. Types of targeting in nanotherapy

1.3.3.1. Passive targeting

As discussed earlier, the tumour vasculature can be contrasted with that of healthy tissue in the rate and manner of formation. Normally, when new capillary blood vessels form through controlled angiogenesis in tissues like muscles, skin, lung, heart, and the central nervous system (CNS) the resulting lumen wall is lined with tightly-packed endothelial cells. Those cells are held together

by junction proteins and thus help maintain the integrity of the epithelial walls while the tight junctions allow only small molecules to bypass into the surrounding tissues.[129] However, the chaotic angiogenesis process in tumours along with the absence of the junction proteins in the tumour's periphery result in large gaps within the epithelial walls that usually range in size between 380-780 nm[130] but can reach up to 1.5 μm.[129] The tumour epithelial cells also noticeably have intercellular fenestrae (pores) that can reach up to 0.5 μm in diameters, and although some organs like the endocrine glands and the kidney peritubular plexus do have fenestrae within their epithelial cells (60-80 nm), they are still sealed by a non-membranous diaphragm (basal membrane) that regulates the movement of fluids and solutes without allowing big molecules to pass through, whereas a similar seal is lacking in the epithelial cells of tumours.[129] This leakiness of the epithelial walls within the TME allows particles that are smaller than the gaps and fenestrae within the walls to permeate into the cancer tissue, and because of their size, nanocarriers circulating through the bloodstream can inherently escape through these openings.

Moreover, the lymphatic system that is normally responsible for clearing large particles from the interstitial space is also functionally impaired in the tumour microenvironment allowing the infiltrating nanocarriers to linger further within the tumour tissue. The combined phenomena of leaky vasculature and poor lymphatic drainage are termed the "*enhanced permeability and retention" (EPR) effect*.[131] This effect is what gives nanoparticles their preference to accumulate in tumours minimising penetration to normal tissues, and it constitutes the golden standard when designing nanocarriers for targeted cancer therapy and, because it depends solely on the pathophysiological properties of the TME, this type of targeting is considered as "passive" by nature.[131–133]

It should be noted, nonetheless, that there is significant heterogeneity in the EPR effect within and between tumours, since there are differences in the pore dimensions and the structure of the vasculature depending on the type of the tumour and its location (primary vs metastases).[134] Furthermore, heterogeneity in the density of ECM and the different cellular components as well as in the coagulation and clotting in tumour vessels are some of the factors that limit the ability to effectively translate the EPR effect, and nanomedicine in general into the clinic.[135] Some have even suggested that the entry of nanoparticles to solid tumours happens via active trans-endothelial pathways rather than through the inter-endothelial gaps.[136]

1.3.3.2. Active targeting

Since all nanocarriers have some degree of passive EPR effect, active targeting cannot be separated from the passive targeting aspects but provides an added advantage that enhances the chances of nanotherapeutics to be successful in their selective targeting to cancer tissue. This can be achieved by using targeting ligands such as antibodies or peptides that can be recognised by cancer tissue cells, thus increasing their binding to and uptake by those cells.[137] Two types of active targeting can be recognised:

1. Active targeting to cancer cells: in this type, nanoparticles can be conjugated with ligands that are over-expressed on cancer cells themselves. This is especially useful to enhance the internalisation of therapeutics into cancer cell rather than increasing the accumulation of nanoparticles in the tumour tissue.[133] Multiple potential targets exist for this purpose, the most important of which are:
    a) Transferrin receptors. Transferrin is a glycoprotein responsible for binding and transporting iron and plays an essential role in cell growth. The expression of its receptors in cancer cells are up to a hundred-fold higher than that of normal cells, thus conjugating transferrin to drug-loaded nanoparticles can boost their uptake into cancer cells by to a great extent.[132]
    b) Folate receptors. Folate (vitamin B_9) is essential for the synthesis of nucleotide bases and the subsequent synthesis and replication of DNA. Since this is crucial for cell growth and proliferation, folate receptors are overly expressed in most cancer cells, and thus folate has been widely used as a conjugate to nanocarriers to enhance their targeting capabilities.[106]
    c) Epidermal growth factor receptors (EGFR). EGFR has a crucial role in angiogenesis and the growth, proliferation, and metastasis of tumours. Antibodies that can selectively bind to its receptors are attractive candidates for use in the active targeting of tumours.[132]
    d) Other specific targets. Via the use of aptamers, which are short single-stranded DNA or RNA sequences that can bind to specific corresponding targets on the surface of cancer cells.[137]
2. Active targeting to tumour endothelium: Nanocarriers can encounter some barriers between the epithelium of the blood microvessels and the deep layers of tumour cells, such as the presence of pericytes, smooth muscle cells or simply multiple layers of cancer cells. Conjugating

these nanocarriers with ligands that correspond with target receptors on endothelial cells enhances their chances of being internalised by the tumour.[135] Not only can this increase the chances of nanocarriers reaching their target, but the nanoparticles can also be designed to release their drug load within the endothelial layer upon being taken up by its cells which can cause the released low-weight molecules to penetrate further within the tumour.[133] Some of the most prominent examples of this approach are ligands that bind to the VEGF receptors in the epithelial cells and those that bind to the matrix metalloproteinases (MMPs).[138]

1.3.3.3. Stimuli-responsive (triggered) targeting

Stimuli-responsive targeting adds more control over the delivery of therapeutics from loaded nanoparticles in either of their forms, the passively or actively targeted. This type of nanocarriers are designed to either take advantage of the unique internal features of TME like enzymatic composition or pH, or respond to an external stimulus like heat or a magnetic field.[139]

1.3.3.3.1. Internal stimuli

As mentioned before, because of the Warburg effect where excessive amounts of lactic acid are produced within the TME, the extracellular pH is more acidic (6.5-6.9) than normal tissues (7.2-7.4) which has led to designing many strategies that take advantage of this difference in pH. One strategy depends on the hydrophobic-hydrophilic transition of materials depending on their protonation state. Bae *et al.* used the pH-dependent reversible transition of poly-L-histidine (polyHis) and created stable micelles by mixing polyHis-b-PEG copolymer with poly(L-lactic acid)-b-PEG at a pH above 7.4 and proved that the micelles have destabilised gradually below a pH of 7.0.[140] Other strategies include the use of polymer-drug conjugates with acid-labile bonds,[141] and the fabrication of NPs with zwitterionic features.[142,143]

Another internal stimulus that can be exploited to trigger the release of therapeutics is the enzymatic composition of the TME, which shows high selectivity to specific substrates. For example, Mansour *et al.* developed an albumin-doxorubicin prodrug that is joined together with a sequence-specific peptide linker that can be cleaved by matrix metalloproteinase 2 (MMP2) that is overexpressed in most tumours.[144]

The redox potential can also be used as a trigger for drug release. The most researched in this area is glutathione (GSH), which is a tripeptide responsible for the reduction of disulfide linkages and has an intracellular concentration that is 100-1000 higher than that in the blood.[145] Furthermore, its concentration in cancer tissues is at least 4 times that of normal ones.[146] Ma *et al.*, for example, exploited this by creating doxorubicin-loaded micelles from an amphiphilic block copolymer that had a long side alkyl chain conjugated via a disulfide group. When the micelles reached the tumour, the high levels of GSH cleaved the disulfide group causing a hydrophobic to hydrophilic transition in one of the main-chain polymers which lead to the disassembly of the micelles and the release of the drug.[147]

1.3.3.3.2. External stimuli

Many therapeutics depend on external stimuli instead of internal ones to induce the change in the structure of the particles that prompt the release or activation of the loaded therapeutic molecules.

Temperature is the most typical example of such stimuli. Drug-loaded liposomes prepared using lipids that are rigid at normal body temperature and have higher solid-gel transition temperatures (usually, lipids such as dipalmitoylphosphatidylcholine that have a transition temperature of about 41 °C are preferred) can accumulate in the tumour after their injection into the body. Then an external clinically-controlled hyperthermia using water baths, electromagnets, or focused ultrasound is applied to the tumour site to induce the transition of the lipid bilayer and increase its permeation to the drug load prompting its release.[148,149] Another widely used example of temperature-responsive nanomaterials are conjugates of poly(N-isopropylacrylamide) (PNIPAM) which changes from the hydrophilic coil confirmation to the hydrophobic globule conformation when the temperature is raised above its lower critical solution temperature (LCST) causing the structure of the nanocarrier to be damaged and the drug released.[150]

Magnetically-sensitive materials have also been extensively studied as externally-stimulated delivery systems. Superparamagnetic iron oxide nanoparticles (SPIONs) are a family of tiny magnetic nanoparticles (about 10 nm in diameters) with good biocompatibility that can be used as contrast agents to increase the sensitivity of magnetic resonance imaging (MRI)[151] but can also be co-loaded into other drug nanoparticles to increase their concentration at the desired site using external magnetic guidance.[152] SPIONs can also be used with a focused alternating magnetic field

to create localised heat that would help induce apoptosis to eradicate the tumour, a process termed "magnetic thermal ablation."[153]

Light has also been used as an external trigger for the release of drugs from photo-sensitive nanomaterials. For example, azobenzene-incorporated DNA double strands have been used as switchable caps for the pores of drug-loaded mesoporous silica nanoparticles. The photoisomerisation of the azobenzene from *trans* to *cis* under UV and visible lights respectively causes the DNA double strands to hybridise/dehybridise, making the pores open and close on command.[154] Another example is the use of UV light-triggered spiropyran-merocyanine isomerisation in PEGylated lipid nanoparticles to shrink their size to more than a third of the original size in order to allow deeper tissue penetration.[155] However, these systems are limited by the poor skin penetration of short-wavelength light, and other systems that use near-IR with better penetration have been developed.[156,157]

1.3.4. Design considerations and biological barriers

From what has been discussed so far, it is clear that nanoparticle-based therapy offers a promising alternative to conventional therapy in terms of effectiveness and safety by exploiting the unique attributes of the TME and by the versatility of the tools that can be employed to take advantage of those attributes fully. Ideally, an effective nanocarrier should meet the following requirements:[158]

1. Formulation with biocompatible and/or biodegradable materials that in themselves and their by-products are harmless to the body.
2. Possess high loading capacity for the drug intended for delivery to maximise the exposure of the tumour and reduce the need for frequent administration.
3. Site-specific delivery mechanism of the loaded cargo to minimise normal tissue exposure.
4. Negligible or no premature release of the drug load.

Controlled release mechanism that allows precise control over the delivery of the drug to target tissues.Since biological systems are complex and their interaction with injected particles involves an array of factors that would complicate the efficacy and safety of the NPs, some considerations should be taken into account when designing NPs for theranostic purposes:

1.3.4.1. Particle size

The particle size plays a significant role in the fate of nanocarriers. While small NPs (<5 nm) get rapidly cleared from the bloodstream through the kidneys,[159] particles in the micrometre range (2-5 μm) readily accumulate in the pulmonary capillaries making them good candidates for the use in targeting metastatic tumours in the lungs.[107]

Moreover, While the majority of microcapillaries in the body are lined with a discrete layer of endothelial cells and a basal membrane that prevents the penetration of large particles as mentioned earlier, the liver and spleen are an exception. The blood capillaries in these two organs have sinusoidal gaps that allow the spleen to filter out blood cells and the liver to take up chylomicrons, the lipoproteins that transport nutritional fat.[129] These gaps measure about 200-500 nm in the former and about 0.1-1 μm in the latter,[160] which makes these two organs responsible for the nonspecific retention of particles that are >200 nm in size.

All together combined, it has been postulated that NPs with the average size of 100-200 nm could be good candidates as drug carriers to prolong its circulation half-life and enhance the chances of its accumulation in most solid tumours.[107,161]

1.3.4.2. Particle shape

Conventional nanocarriers used in clinical and pre-clinical settings are typically spherical, but the shape of NPs have been found to influence their uptake and accumulation in tumour tissues. It has been observed that discoid and rod-like particles are more likely to penetrate tumours,[107,125,162] and this might be determined by haemorheological factors and how NPs flow within blood vessels, mainly through what is known as margination dynamics. Margination is the lateral drift of particles towards the area (which is called the cell-free layer) near the vessel walls as opposed to the core of the blood vessel where red blood cells move. It is believed that spherical NPs have a poor lateral drift and thus have less contact with blood vessel walls and less chance to encounter the fenestration through which they can extravasate or encounter a vascular marker to which they would bind in case of active targeted NPs, unlike discoid or rod-like NPs that show a more complex movement that involves tumbling and rolling which causes their lateral drifting and increases the possibility of tumour penetration.[163]

The shape also massively affect the circulation half-life of NPs. Discher *et al.* demonstrated that filamentous polymer micelles (filomicelles) had circulation lifetimes of over one week compared to their spherical counterparts that could be detected in the blood for only 2-3 days, which was attributed to the tendency of filomicelles to align with blood flow.[164]

1.3.4.3. Particle surface charge

The surface charge of NPs is a double-edged sword. On the one hand, it was found that neutral and negative surface charges reduce the adsorption of serum proteins onto the particles, thus increasing their circulation half-life.[165] On the other hand, positively charged particles demonstrate better uptake by tumour endothelial cells when they come in close contact with their negatively charged membranes.[166,167]

This can be exploited through a charge-conversion strategy by making stimuli-responsive zwitterionic nanoparticles that would have prolonged circulation because of their net-zero charge, and that would shed the anionic component upon extravasating into the low-pH microenvironment resulting in an accelerated uptake by the endothelial cells. For example, some research groups developed polymer-based NPs with both amine and carboxylate surface groups that give the particle its overall zero-charge. However, the carboxylate groups are linked via acid-labile amide bonds that break in acidic conditions similar to that of the TME giving the NPs a positive charge that increases their interaction with the cell membrane and thus enhancing their cellular uptake.[142,143]

1.3.4.4. Mononuclear phagocytic system (MPS)

Also known as the reticuloendothelial system (RES), MPS is a collective term for the leukocytic cells responsible for the taking up (or "phagocytising") and clearance of large insoluble materials such as cellular debris, bacteria, or nanoparticles.[168] These phagocytes can be either tissue-resident macrophages in filtration organs such as the red pulp macrophages and Kupffer macrophages lining the endothelium of the spleen and the liver, respectively, or blood-circulating monocytes that can extravasate into any tissue and differentiate into macrophages.[169]

Macrophages are a significant hurdle for effective nanotherapy. When NPs enter the blood circulation, a wide array of plasma proteins including serum albumin, apolipoproteins, and

immunoglobulins (especially opsonins) adsorb on the surface of the NPs forming a protein "corona" that alters the physicochemical and biological characteristics of the particles and accelerates the opsonisation process;[170] Opsonins help phagocytes recognise the attached NPs which in turn get phagocytised and fused with lysosomes where they undergo degradation.[171]

The prevalent strategy used to overcome this issue is to "stealth" NPs via PEGylation where polyethylene glycol (PEG) is grafted on the surface of the particles so it would form a hydration layer in the blood that shields the NPs from the adsorption of proteins and the subsequent opsonisation.[172] Other common strategies involve coating the particles with CD47-derived 'self' peptides that act as a 'don't eat me' signal,[173] incorporating a coating derived from the membrane red blood cells,[174] or a leuko-like coating (derived from leukocyte membranes).[175]

1.3.4.5. Other barriers

Another factor that proves to be challenging is elevated IFP. In contrast to the EPR effect, high interstitial pressure drives fluids in an outward movement away from the tumour tissue reducing the ability of NPs to extravasate into it.[107] One possible strategy to overcome this obstacle was proposed by Jain *et al.* - the co-administration of the angiotensin II receptor antagonist losartan to enhance the accumulation of NPs in tumours by reducing the IFP via suppressing the production of collagen, owing to the anti-fibrotic properties of losartan.[176]

Another barrier worthy of note is the protein corona that forms around NPs in the bloodstream as it might mask targeting ligands thus reducing the efficacy of actively targeted NPs.[177]

1.3.5. Types of nanotherapeutics

Many nanocarriers used to target the delivery of cytotoxic drugs can be recognised both in clinical practice and preclinical studies. What follows is a quick overview of the most common types of nanocarriers that have potentials for clinical applications and their general characteristics.

1.3.5.1. Polymer-based nanocarriers

Polymer-based NPs are a versatile and highly-tuneable form of targeted nanoparticles. They often offer higher *in vivo* stability, bioavailability, loading capacities, and more control over their release profiles than other nanotherapeutics.[106]

1.3.5.1.1. Polymeric micelles

Polymeric micelles consist of amphiphilic block copolymers that self-assemble in aqueous solutions into structures comprising of a hydrophobic core and a hydrophilic shell. The hydrophobic core can be used to incorporate the poorly-soluble drugs while the outer shell improves the solubility of the micelles, thus enhancing the bioavailability of the drug and making it more suitable for intravenous injection.[178] Self-assembled micelles typically range in size between tens and a few hundred nanometres making them good candidates for the targeted delivery to tumours.[179] One of the most preferred and widely used hydrophilic polymers to form the outer shell (or the corona) is PEG. As well as its stealthing effect that hinders opsonisation by the MPS, PEG is highly tolerated by the body due to its high biocompatibility and hydrophilicity, although there has been some concerns regarding its possible immunogenicity in susceptible individuals.[180–182] Nonetheless, other polymers have also been studied such as poly(vinyl alcohol) (PVP), polyethylenimine (PEI), and poly(N-vinyl-2-pyrrolidone) (PVP) as the hydrophilic shell, as well as poly(D,L-lactic acid) (PLA), poly(D,L-lactic-co-glycolic acid) (PLGA), and poly(ε-caprolactone) (PCL) for making the hydrophobic core of the micelles.[181] Polysaccharides has also been of interest as stealthing agents because of their biocompatibility and the ease of chemical manipulation.[183]

In addition to that, polymeric micelles are very versatile systems the size and morphology of which are highly modifiable. Although the most common type is spherical micelles, different architectures, like filamentous (worm-like), rods, and disc-like micelles, can be produced depending on the number, ratios, and structure of the copolymers used and the method of micellisation.[184]

Polymeric micelles still have some drawbacks that limit their clinical applications, most prevalently, their instability and dissociation upon dilution.[185]

1.3.5.1.2. Polymeric nanoparticles

Polymeric NPs are biodegradable colloidal systems that can be either nanospheres where the drug intended for delivery is dispersed within the polymeric matrix, or nanocapsules where the drug is confined within a cavity surrounded by a polymeric membrane.[186] Depending on the intended purpose for the NPs different approaches can be considered in their design; (a) drug molecules can be attached to the polymer to get a polymer-drug conjugate that can increase the bioavailability and prolong the half-life of the drug, (b) the drug is dissolved in an aqueous or an oily medium

within the cavity of the nanocapsule to increase its solubility, or (c) the drug can be incorporated within the biodegradable polymer matrix of the nanosphere to achieve better control over its release.[187,188] Compared to other NPs such as polymeric micelles and liposomes, polymeric NPs provide better stability and more homogeneous size distribution as well as better control over the release profile especially in the case of nanospheres where the drug is released via diffusion through or the erosion of the polymeric matrix.[106,189] The FDA-approved polymers that have good biocompatibility and biodegradability include synthetic polymers such as polyglycolic acid (PGA), poly(D-L-lactide-co-glycolic) acid (PLGA), polyethylene glycol (PEG), polylactic acid (PLA), and polycaprolactine (PCL), and naturally-occurring polymers such as chitosan, collagen, heparin, alginate, heparin, albumin, and dextran.[190]

Abraxane® is an FDA-approved albumin-bound paclitaxel indicated for the treatment of breast, pancreatic, and non-small cell lung cancers. The 130 nm formulation improves the solubility of paclitaxel and enhances its delivery to tumours.[188]

1.3.5.1.3. Dendrimers

Dendrimers (from the Greek word *dendron* for "tree") are highly-branched macromolecules consisting of polymeric chains stemming from a central core and are synthesised in a stepwise manner allowing a high level of control over their molecular weight, size, shape, and physicochemical properties.[191] These particles can be used as drug carriers by either non-covalently entrapping the drug molecules or by chemically conjugating the drug to their structures during or after the synthesis of the dendrimers.[192] Small drug molecules are usually encapsulated within the dendrimer's void spaces while it is preferable to adsorb large molecules onto their surface.[193] dendrimers show high promise in nanotherapy because of their controlled, step-wise synthesis that results in uniformly distributed particles with low polydispersity and well-defined peripheral groups.[187] They are also highly tuneable which allows adding multifunctionality, such as incorporating different drug molecules, adding targeted moieties, or PEGylation to enhance solubility, dendrimers show high promise in nanotherapy.[193]

1.3.5.2. Lipid-based nanocarriers

These carriers consist mainly of lipids that are similar in composition to many physiological compounds, hence they are well-tolerated and very biocompatible, and they normally break down

to non-toxic components, which makes them very desirable means of targeted therapy.[194]

1.3.5.2.1. Liposomes

Liposomes have been described since the 1960s as nanovesicles consisting of at least one phospholipid bilayer entrapping an aqueous compartment.[195] The size of the vesicles is defined by the manufacturing process as is the number of lipid bilayers, forming either small unilamellar vesicles (SUV), large unilamellar vesicles (LUV), or concentrically arranged multilamellar vesicles (MLV).[196] Because of their biphasic nature, liposomes can be loaded with either hydrophilic drugs in their aqueous phase or hydrophobic drugs within their lipid lamellae, or both, offering better bioavailability for both sorts of drugs and showing high biodegradability and biocompatibility and practically no immunogenicity due to their similarity to cellular composition.[187] Liposomes can also be modified by integrating targeting ligands or PEG into their structures enhancing their targeting abilities and bioavailability even further.[188] The relatively easy manufacturing process and high modifiability made liposomes quickly find their way into clinical practice. A classic example is Doxil®, the first FDA-approved nanoparticle formulation in 1995 for the anticancer drug doxorubicin (DOX).[197] This PEGylated liposomal formulation of DOX has been found to reduce the cardiotoxicity of the free drug as well as enhancing its availability at the cancer site by 4-16 folds.[198]

1.3.5.2.2. Lipid nanocarriers (LNs)

Solid lipid nanocarriers (SLNs) were the first generation developed of LNs. They are comprised of glycerides that have high melting points and are rigid at both room and body temperatures, and because they mimic those that are naturally found in the body, they are highly biocompatible and biodegradable.[199] They are considered good carriers for drugs that are highly lipophilic to enhance their bioavailability and, because of their rigidity they offer better control over drug release.[200] They do, however, have a low drug loading capacity and they might show drug expulsion from the carrier during storage due to the polymorphic transformation of the lipids over time which is more pronounced with pure lipids as opposed to lipid mixtures which leads to instability of the particles and the loss of the release control advantage.[201]

The second generation of LNs was developed to overcome these limitations. Nanostructured lipid carriers (NLCs) are made of a mixture of solid and liquid lipids to create controlled structures.

The imperfections between the two lipids provide a space for accommodating the drug instead of the rigid matrix of the SLNs, which maximises the loading capacity.[202]

1.3.5.3. Carbon-based nanocarriers

Carbon nanotubes (CNT) are single- or multi-walled tubular networks of carbon atoms that can be only a few nanometres in diameters and reach up to 100 μm in length.[203] CNTs are considered a versatile medium for biomedical applications such as drug delivery, imaging, and stimuli-responsive therapy because of their structural, mechanical, electrical, and optical properties and their extensive surface area.[204] CNTs can both carry the drug load in the entrapped volume within their walls, and they can have their surfaces functionalised for various purposes and, biologically, they can be taken up into cells either by endocytosis or needle-like penetration of membranes.[205] Nonetheless, because of their insolubility, they have raised toxicity concerns as they have been found to accumulate in the liver, spleen, and lungs of test animals.[206]

Carbon dots (CDs) in contrast, potentially have lower toxicity as they are less than 10 nm in all dimensions and thus are quickly filtered out of the blood by the kidneys and excreted into urine and show very little accumulation in the lungs and liver,[207] and they are more biocompatible than conventional semiconductor quantum dots (QDs) that are based on heavy metals.[208] CDs show potential for having applications in biosensing, imaging, and drug delivery.[209]

1.3.5.4. Inorganic nanocarriers

As well as QDs that are limited by their toxicity, this category includes gold-based nanocarriers whose plasmonic characteristics can be used for the purposes of biosensing and imaging.[210] However, even though gold was used in the past for the treatment of arthritis, there are no gold-based NPs currently approved for clinical practice because toxicity is still an issue.[188]

Other particles include silica-based NPs such as Cornell dots (C-dots) are undergoing clinical trials as potential theranostic tools.[211] Nanothem™, a formulation of superparamagnetic iron oxide nanoparticles (SPION) discussed elsewhere, is also undergoing clinical trials to investigate its efficacy and safety in the magnetic hyperthermia therapy of glioblastoma.[212]

1.3.6. NSAID-based nanocarriers

Many of the NSAID-based nanocarriers that exist in the literature focus on the making of lipid-based formulations to enhance the skin penetration of topical NSAIDs for the management of pain and other inflammatory disorders.[213,214] However, there are other formulations that involve developing NSAID nanocarrier for systemic administration, some of which are aimed at the management of inflammatory diseases but other also focused on cancer.

Of these systemic formulations, lipid nanocarriers are the most common. For example, Lopes-de-Araújo *et al.* created oxaprozin-loaded NLCs intended for oral administration for the management of inflammation. The particles were also functionalised with folic acid for enhanced uptake.[215] B. Lee *et al.* synthesised nano-emulsions of the NSAID flufenamic acid that produced an inhibitory effects on human glioma cells.[216] The ketoprofen-loaded liposomes prepared by Tarţaŭ *et al.* produced a longer analgesic effect in mice than free ketoprofen, indicating that a liposomal drug might produce a more sustained release of the drug.[217]

The versatility of polymeric NPs has also allowed for the creation of different kinds of NSAID-loaded carrier. For instance, S. Lee *et al.* produced a naproxen-loaded dextran NPs. In this drug-polymer conjugate, naproxen was loaded on dextran via a boronic ester linker that is sensitive to the reactive oxygen species (ROS) similar to those found in inflammatory tissues.[218] Zeng *et al.* used atom transfer radical polymerisation (ATRP) to build a pH-responsive amphiphilic co-polymer in which mPEG was the hydrophilic chain while the hydrophobic chain carried ibuprofen molecules via ester bonds. During self-assembly, the cytotoxic drug doxorubicin was loaded in the core of the micelles. These NPs showed an inhibitory effect against a melanoma cell line *in vitro* comparable to free doxorubicin, and prevented also prevented metastasis to the lung *in vivo*.[219] Shehata *et al.* also developed a norbornene-derived PEG-Ibuprofen copolymers via ring-opening metathesis polymerisation (ROMP) for tumour targeting.[220] Figure 1.6 shows the structure of these three polymeric systems.

NSAID-loaded magnetic NPs have also been developed for a more controlled delivery of these drugs. Giannousi *et al.* functionalized aspirin, mefenamic acid, and naproxen on manganese ferrite NPs and obtained different release profiles from the 10-nm NPs via PEGylation.[221] Gronczewska *et al.* also used dextran-coated magnetic NPs to load ibuprofen and diclofenac.[222]

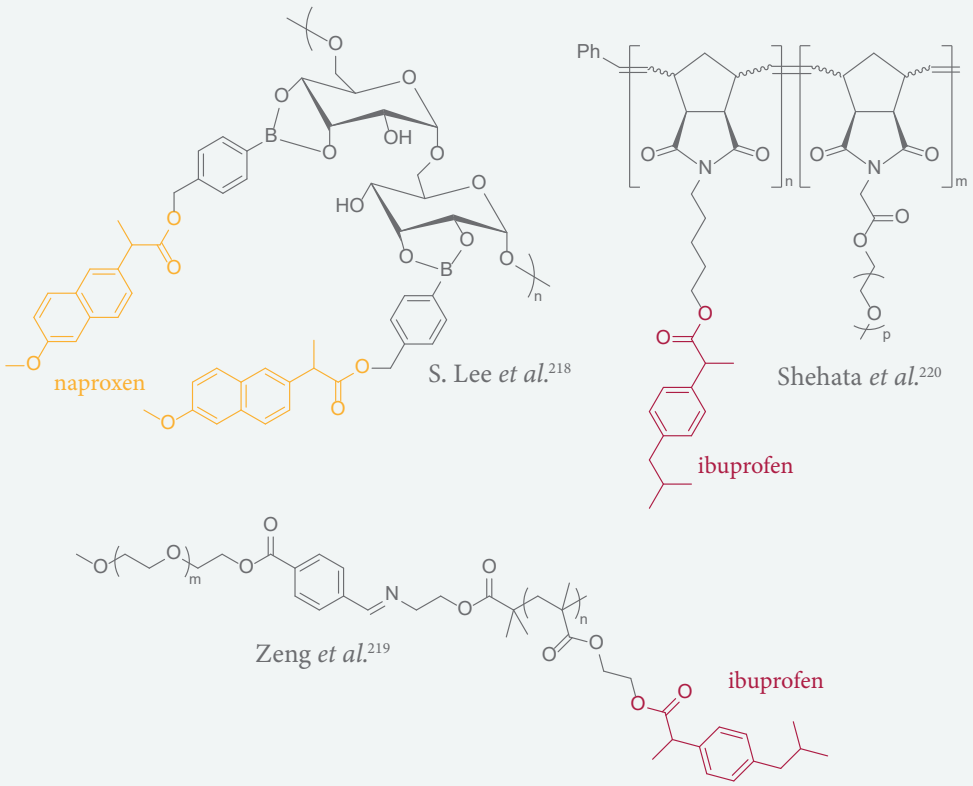

Fig 1.6. Examples from the literature of NSAID-loaded polymers intended for targeted delievery.

1.4. Conclusion

It can be clear that nanotherapeutics demonstrate great potentials to be versatile and dynamic systems that would serve as alternatives to conventional therapy not only to enhance the bioavailability of the hydrophobic drugs and concentrate higher doses at the target tissue but also to widen the therapeutic window of the cytotoxic drugs and make them more tolerable and less harmful to healthy tissues and organs. However, even though this concept has been around for decades, only a handful of nanoformulations are approved for clinical use, although many more are undergoing pre-clinical studies to determine their safety and pharmacokinetic/pharmacodynamic profiles.[223] An analysis done by Wilhelm *et al.* to determine the efficacy of NPs in published in literature found, after analysing 232 published data sets between 2005 and 2015, that only a median of 0.7% of the injected dose of NP preparations found its way to the tumour,[125] which shows that we still have a long way to go in order to understand how nanotherapeutics interact with the human body so we can learn how to accurately shoot those "magic bullets" and hit the bull's eye.

1.5. References

1 G. J. Gasic, T. B. Gasic and C. C. Stewart, *Proc. Natl. Acad. Sci. U. S. A.*, 1968, **61**, 46–52.

2 G. Gasic, T. Gasic and S. Murphy, *Lancet*, 1972, **300**, 932–933.

3 J. Kolenich, E. Mansour and A. Flynn, *Lancet*, 1972, **300**, 714.

4 B. M. Jaffe, *Prostaglandins*, 1974, **6**, 453–461.

5 B. A and D. T. M, *Gut*, 1975, **16**, 409.

6 H. A. Isomäki, T. Hakulinen and U. Joutsenlahti, *J. Chronic Dis.*, 1978, **31**, 691–696.

7 M. J. Thun, M. M. Namboodiri and C. W. Heath, *N. Engl. J. Med.*, 1991, **325**, 1593–1596.

8 G. A. Kune, S. Kune and L. F. Watson, *Int. J. Epidemiol.*, 2007, **36**, 951–957.

9 L. Rosenberg, J. R. Palmer, A. G. Zauber, M. E. Warshauer, P. D. Stolley and S. Shapiro, *J. Natl. Cancer Inst.*, 1991, **83**, 355–358.

10 A. Paganini-hill, G. Hsu, R. K. Ross and B. E. Henderson, *JNCI J. Natl. Cancer Inst.*, 1991, **83**, 1182–1183.

11 A. Paganini-Hill, A. Chao, R. K. Ross and B. E. Henderson, *Br. Med. J.*, 1989, **299**, 1247–1250.

12 D. Labayle, D. Fischer, P. Vielh, F. Drouhin, A. Pariente, C. Bories, O. Duhamel, M. Trousset and P. Attali, *Gastroenterology*, 1991, **101**, 635–9.

13 A. Lipton, S. Scialla, H. Harvey, R. Dixon, R. Gordon, R. Hamilton, H. Ramsey, M. Weltz, R. Heckard and D. White, *J. Med.*, 1982, **13**, 419–29.

14 M. J. Thun, M. M. Namboodiri, E. E. Calle, W. D. Flanders and C. W. Heath, *Cancer Res.*, 1993, **53**, 1322–7.

15 S. M. Powell, N. Zilz, Y. Beazer-Barclay, T. M. Bryan, S. R. Hamilton, S. N. Thibodeau, B. Vogelstein and K. W. Kinzler, *Nature*, 1992, **359**, 235–237.

16 C. Jones, *Evidence-based medicine research methods*, 2002, vol. 268.

17 P. H. Gann, J. E. Manson, R. J. Glynn, J. E. Buring and C. H. Hennekens, *J. Natl. Cancer Inst.*, 1993, **85**, 1220–1224.

18 N. R. Cook, I. M. Lee, J. M. Gaziano, D. Gordon, P. M. Ridker, J. A. E. Manson, C. H. Hennekens and J. E. Buring, *J. Am. Med. Assoc.*, 2005, **294**, 47–55.

19 N. R. Cook, I. Lee, S. M. Zhang, M. V. Moorthy and J. E. Buring, *Ann. Intern. Med.*, 2013, **159**, 77.

20 R. Peto, R. Gray, R. Collins, W. C. Warlow, B. Hafner and E. Thompson, *Br. Med. J.*, 1988, **296**, 313–316.

21 B. Farrell, J. Godwin, S. Richards and C. Warlow, *J. Neurol. Neurosurg. Psychiatry*, 1991, **54**, 1044–1054.

22 E. Flossmann and P. M. Rothwell, *Lancet*, 2007, **369**, 1603–1613.

23 S. Kozuka, M. Nogaki, T. Ozeki and S. Masumori, *Dis. Colon Rectum*, 1975, **18**, 494–500.

24 A. F. CASTRO, G. W. AULT and R. S. SMITH, *Surg. Gynecol. Obstet.*, 1951, **92**, 164–171.

25 P. M. Rothwell, M. Wilson, C. E. Elwin, B. Norrving, A. Algra, C. P. Warlow and T. W. Meade, *Lancet*, 2010, **376**, 1741–1750.

26 The Salt Collaborative Group, *Lancet*, 1991, **338**, 1345–1349.

27 T. W. Meade, H. C. Wilkes, C. C. Kelleher, P. J. Roderick, P. J. Brennan, C. W. Wilson, D. J. Howarth, Y. Stirling, K. Garrow, C. J. Dickinson, G. Rose, G. J. Miller, W. S. Peart, A. M. Breckenridge, D. G. Grahame-Smith, S. J. Pocock and S. R. Zuhrie, *Lancet*, 1998, **351**, 233–241.

28 S. Juul-Moller, N. Edvardsson, S. Sorensen, B. Jahnmatz, A. Rosén and R. Omblus, *Lancet*, 1992, **340**, 1421–1425.

29 F. Bray, J. Ferlay, I. Soerjomataram, R. L. Siegel, L. A. Torre and A. Jemal, *CA. Cancer J. Clin.*, 2018, **68**, 394–424.

30 Cancer Research UK, Prostate Cancer incidence statistics., https://www.cancerresearchuk.org/health-professional/cancer-statistics/statistics-by-cancer-type/prostate-cancer/incidence#ref-0, (accessed 13 December 2019).

31 D. G. Bostwick, H. B. Burke, D. Djakiew, S. Euling, S. M. Ho, J. Landolph, H. Morrison, B. Sonawane, T. Shifflett, D. J. Waters and B. Timms, *Cancer*, 2004, **101**, 2371–2490.

32 X. Wang, Y. Lin, J. Wu, Y. Zhu, X. Xu, X. Xu, Z. Liang, Z. Hu, S. Li, X. Zheng and L. Xie, *World J. Surg. Oncol.*, 2014, **12**, 304.

33 Y. Liu, J. Q. Chen, L. Xie, J. Wang, T. Li, Y. He, Y. Gao, X. Qin and S. Li, *BMC Med.*, 2014, **12**, 55.

34 Z. Shang, X. Wang, H. Yan, B. Cui, Q. Wang, J. Wu, X. Cui, J. Li, T. Ou and K. Yang, *Front. Oncol.*, 2018, **8:437**, 1–21.

35 E. A. Singer, G. S. Palapattu and E. van Wijngaarden, *Cancer*, 2008, **113**, 2053–2057.

36 S. L. Chang, L. C. Harshman and J. C. Presti, *J. Clin. Oncol.*, 2010, **28**, 3951–7.

37 B. Takkouche, C. Regueira-Mendez and M. Etminan, *JNCI J. Natl. Cancer Inst.*, 2008, **100**, 1439–1447.

38 Y.-S. Zhao, S. Zhu, X. Li, F. Wang, F. Hu, D. Li, W. Zhang and X. Li, *Breast Cancer Res. Treat.*, 2009, **117**, 141–150.

39 X. Z. Huang, P. Gao, J. X. Sun, Y. X. Song, C. C. Tsai, J. Liu, X. W. Chen, P. Chen, H. M. Xu and Z. N. Wang, *Cancer Causes Control*, 2015, **26**, 589–600.

40 K. Subbaramaiah, P. G. Morris, X. K. Zhou, M. Morrow, B. Du, D. Giri, L. Kopelovich, C. A. Hudis and A. J. Dannenberg, *Cancer Discov.*, 2012, **2**, 356–365.

41 S. A. Glynn, R. L. Prueitt, L. A. Ridnour, B. J. Boersma, T. M. Dorsey, D. A. Wink, J. E. Goodman, H. G. Yfantis, D. H. Lee and S. Ambs, *BMC Cancer*, 2010, **10**, 626.

42 T. Dierssen-Sotos, I. Gómez-Acebo, M. de Pedro, B. Pérez-Gómez, S. Servitja, V. Moreno, P. Amiano, T. Fernandez-Villa, A. Barricarte, A. Tardon, M. Diaz-Santos, R. Peiro-Perez, R. Marcos-Gragera, V. Lope, E. Gracia-Lavedan, M. H. Alonso, M. J. Michelena-Echeveste, A. Garcia-Palomo, M. Guevara, G. Castaño-Vinyals, N. Aragonés, M. Kogevinas, M. Pollán and J. Llorca, *BMC Cancer*, 2016, **16**, 660.

43 S. Kim, D. L. Shore, L. E. Wilson, E. I. Sanniez, J. H. Kim, J. A. Taylor and D. P. Sandler, *BMC Cancer*, 2015, **15**, 960.

44 T. M. Brasky, M. R. Bonner, K. B. Moysich, C. B. Ambrosone, J. Nie, M. H. Tao, S. B. Edge, B. V. S. Kallakury, C. Marian, D. S. Goerlitz, M. Trevisan, P. G. Shields and J. L. Freudenheim, *Cancer Causes Control*, 2011, **22**, 965–975.

45 J. A. Mitchell, P. Akarasereenont, C. Thiemermann, R. J. Flower and J. R. Vane, *Proc. Natl. Acad. Sci. U. S. A.*, 1993, **90**, 11693–11697.

46 A. Ornelas, N. Zacharias-Millward, D. G. Menter, J. S. Davis, L. Lichtenberger, D. Hawke, E. Hawk, E. Vilar, P. Bhattacharya and S. Millward, *Cancer Metastasis Rev.*, 2017, **36**, 289–303.

47 T. K. Choueiri, Y. Je and E. Cho, *Int. J. Cancer*, 2014, **134**, 384–396.

48 E. Cho, G. Curhan, S. E. Hankinson, P. Kantoff, M. B. Atkins, M. Stampfer and T. K. Choueiri, *Arch. Intern. Med.*, 2011, **171**, 1487–1493.

49 G. A. Colditz and S. E. Hankinson, *Nat. Rev. Cancer*, 2005, **5**, 388–396.

50 D. P. Sandler, *Ann. Intern. Med.*, 1991, **115**, 165.

51 W. H. Wang, *CancerSpectrum Knowl. Environ.*, 2003, **95**, 1784–1791.

52 B. Trabert, R. B. Ness, W. H. Lo-Ciganic, M. A. Murphy, E. L. Goode, E. M. Poole, L. A. Brinton, P. M. Webb, C. M. Nagle, S. J. Jordan, H. A. Risch, M. A. Rossing, J. A. Doherty, M. T. Goodman, G. Lurie, S. K. Kjær, E. Hogdall, A. Jensen, D. W. Cramer, K. L. Terry, A. Vitonis, E. V Bandera, S. Olson, M. G. King, U. Chandran, H. Anton-Culver, A. Ziogas, U.

Menon, S. A. Gayther, S. J. Ramus, A. Gentry-Maharaj, A. H. Wu, C. L. Pearce, M. C. Pike, A. Berchuck, J. M. Schildkraut and N. Wentzensen, *J. Natl. Cancer Inst.*, 2014, **106**, djt431–djt431.

53 X. Zhao, Z. Xu and H. Li, *Sci. Rep.*, 2017, **7**, 1875.

54 K. Bibbins-Domingo, *Ann. Intern. Med.*, 2016, **164**, 836.

55 E. Ricciotti and G. A. FitzGerald, *Arterioscler. Thromb. Vasc. Biol.*, 2011, **31**, 986–1000.

56 D. G. Menter and R. N. DuBois, *Int. J. Cell Biol.*, 2012, **2012**, 1–21.

57 D. Wang and R. N. Dubois, *Nat. Rev. Cancer*, 2010, **10**, 181–193.

58 B. Rigas, I. S. Goldman and L. Levine, *J. Lab. Clin. Med.*, 1993, **122**, 518–23.

59 D. Wang and R. N. DuBois, *Semin. Oncol.*, 2004, **31**, 64–73.

60 T. L. McLemore, W. C. Hubbard, C. L. Litterst, M. C. Liu, S. Miller, N. A. McMahon, J. C. Eggleston and M. R. Boyd, *Cancer Res.*, 1988, **48**, 3140–7.

61 M. Hambek, M. Baghi, J. Wagenblast, J. Schmitt, H. Baumann and R. Knecht, *Head Neck*, 2007, **29**, 244–248.

62 D. Wang, F. G. Buchanan, H. Wang, S. K. Dey and R. N. DuBois, *Cancer Res.*, 2005, **65**, 1822–1829.

63 K. Krysan, K. L. Reckamp, H. Dalwadi, S. Sharma, E. Rozengurt, M. Dohadwala and S. M. Dubinett, *Cancer Res.*, 2005, **65**, 6275–6281.

64 J. Zhou, B. Gurates, S. Yang, S. Sebastian and S. E. Bulun, *Cancer Res.*, 2001, **61**, 2328–2334.

65 N. Osafo, C. Agyare, D. D. Obiri and A. O. Antwi, in *Nonsteroidal Anti-Inflammatory Drugs*, InTech, 2017, vol. 16, pp. 509–527.

66 R. A. Gupta, L. V Tejada, B. J. Tong, S. K. Das, J. D. Morrow, S. K. Dey and R. N. DuBois, *Cancer Res.*, 2003, **63**, 906–11.

67 K. Schrör, *Semin. Thromb. Hemost.*, 1997, **23**, 349–356.

68 E. Camerer, A. A. Qazi, D. N. Duong, I. Cornelissen, R. Advincula and S. R. Coughlin, *Blood*, 2004, **104**, 397–401.

69 J. Palumbo, *Semin. Thromb. Hemost.*, 2008, **34**, 154–160.

70 J. M. Herter, J. Rossaint and A. Zarbock, *J. Thromb. Haemost.*, 2014, **12**, 1764–1775.

71 S. NADAR, A. BLANN and G. LIP, *Am. J. Hypertens.*, 2006, **19**, 970–977.

72 C. E. Holmes, J. Jasielec, J. E. Levis, J. Skelly and H. B. Muss, *Clin. Transl. Sci.*, 2013, **6**, 386–390.

73 R. Salcedo, X. Zhang, H. A. Young, N. Michael, K. Wasserman, W. H. Ma, M. Martins-Green, W. J. Murphy and J. J. Oppenheim, *Blood*, 2003, **102**, 1966–1977.

74 N. Nakahata, *Pharmacol. Ther.*, 2008, **118**, 18–35.

75 M. J. Thun, E. J. Jacobs and C. Patrono, *Nat. Rev. Clin. Oncol.*, 2012, **9**, 259–267.

76 R. S. Wong, *J. Exp. Clin. Cancer Res.*, 2011, **30**, 87.

77 Y. Tsujimoto, *Genes to Cells*, 1998, **3**, 697–707.

78 Z. Zhang, F. Chen and L. Shang, *Cancer Manag. Res.*, 2018, **Volume 10**, 4631–4640.

79 M. S. Kim, J. E. Kim, D. Y. Lim, Z. Huang, H. Chen, A. Langfald, R. A. Lubet, C. J. Grubbs, Z. Dong and A. M. Bode, *Cancer Prev. Res.*, 2014, **7**, 236–245.

80 A. Bank, J. Yu and L. Zhang, *Nutr. Cancer*, 2008, **60**, 98–103.

81 H.-F. Liu, P.-W. Hsiao and J.-I. Chao, *Chem. Biol. Interact.*, 2008, **176**, 48–57.

82 H. Raza, A. John and S. Benedict, *Eur. J. Pharmacol.*, 2011, **668**, 15–24.

83 G. A. Piazza, W. J. Thompson, R. Pamukcu, H. W. Alila, C. M. Whitehead, L. Liu, J. R. Fetter, W. E. Gresh, A. J. Klein-Szanto, D. R. Farnell, I. Eto and C. J. Grubbs, *Cancer Res.*, 2001, **61**, 3961–8.

84 J. M. Lehmann, J. M. Lenhard, B. B. Oliver, G. M. Ringold and S. A. Kliewer, *J. Biol. Chem.*, 1997, **272**, 3406–3410.

85 T. C. He, T. A. Chan, B. Vogelstein and K. W. Kinzler, *Cell*, 1999, **99**, 335–345.

86 Y. Yamamoto, M. J. Yin, K. M. Lin and R. B. Gaynor, *J. Biol. Chem.*, 1999, **274**, 27307–27314.

87 E. Gurpinar, W. E. Grizzle and G. A. Piazza, *Front. Oncol.*, 2013, **3**, 1–18.

88 H. C. Lee, I. C. Park, M. J. Park, S. An, S. H. Woo, H. O. Jin, H. Y. Chung, S. J. Lee, H. S. Gwak, Y. J. Hong, D. H. Yoo, C. H. Rhee and S. Il Hong, *J. Cell. Biochem.*, 2005, **94**, 597–610.

89 B. J. R. Whittle, *Brain Res. Bull.*, 1980, **5**, 7–14.

90 J. L. Wallace, *Physiol. Rev.*, 2008, **88**, 1547–1565.

91 S. E. Gabriel, *Ann. Intern. Med.*, 1991, **115**, 787.

92 M. C. Allison, A. G. Howatson, C. J. Torrance, F. D. Lee and R. I. Russell, *N. Engl. J. Med.*, 1992, **327**, 749–754.

93 J. Cuzick, M. A. Thorat, C. Bosetti, P. H. Brown, J. Burn, N. R. Cook, L. G. Ford, E. J. Jacobs, J. A. Jankowski, C. La Vecchia, M. Law, F. Meyskens, P. M. Rothwell, H. J. Senn and A. Umar, *Ann. Oncol.*, 2015, **26**, 47–57.

94 W. Y. Huang, J. L. Saver, Y. L. Wu, C. J. Lin, M. Lee and B. Ovbiagele, *JAMA Neurol.*, 2019, **76**, 906–914.

95 I. L. Meek, M. A. F. J. van de Laar and H. E. Vonkeman, *Pharmaceuticals*, 2010, **3**, 2146–2162.

96 C. J. Hawkey, *Best Pract. Res. Clin. Gastroenterol.*, 2001, **15**, 801–820.

97 G. N. C. Lucas, A. C. C. Leitão, R. L. Alencar, R. M. F. Xavier, E. D. F. Daher and G. B. da Silva Junior, *J. Bras. Nefrol.*, 2019, **41**, 124–130.

98 C. Huerta, J. Castellsague, C. Varas-Lorenzo and L. A. García Rodríguez, *Am. J. Kidney Dis.*, 2005, **45**, 531–539.

99 J. Säfholm, S. E. Dahlén, I. Delin, K. Maxey, K. Stark, L. O. Cardell and M. Adner, *Br. J. Pharmacol.*, 2013, **168**, 794–806.

100 D. D. Stevenson and A. Szczeklik, *J. Allergy Clin. Immunol.*, 2006, **118**, 773–786.

101 S. Y. Tan and S. Grimes, *Singapore Med. J.*, 2010, **51**, 842–3.

102 C. H. Chau, P. S. Steeg and W. D. Figg, *Lancet (London, England)*, 2019, **394**, 793–804.

103 R. Feynman, *Eng. Sci. Mag.*, 1960, **23**, 22–36.

104 C. L. Ventola, *P T*, 2012, **37**, 512–25.

105 R. Seigneuric, L. Markey, D. S.A. Nuyten, C. Dubernet, C. T.A. Evelo, E. Finot and C. Garrido, *Curr. Mol. Med.*, 2010, **10**, 640–652.

106 E. Pérez-Herrero and A. Fernández-Medarde, *Eur. J. Pharm. Biopharm.*, 2015, **93**, 52–79.

107 E. Blanco, H. Shen and M. Ferrari, *Nat. Biotechnol.*, 2015, **33**, 941–951.

108 M. Prasad, U. P. Lambe, B. Brar, I. Shah, M. J, K. Ranjan, R. Rao, S. Kumar, S. Mahant, S. K. Khurana, H. M. N. Iqbal, K. Dhama, J. Misri and G. Prasad, *Biomed. Pharmacother.*, 2018, **97**, 1521–1537.

109 R. A. Petros and J. M. Desimone, *Nat. Rev. Drug Discov.*, 2010, **9**, 615–627.

110 R. R. Langley and I. J. Fidler, *Int. J. Cancer*, 2011, **128**, 2527–2535.

111 L. Hui and Y. Chen, *Cancer Lett.*, 2015, **368**, 7–13.

112 C. Belli, D. Trapani, G. Viale, P. D'Amico, B. A. Duso, P. Della Vigna, F. Orsi and G. Curigliano, *Cancer Treat. Rev.*, 2018, **65**, 22–32.

113 R. Kalluri and M. Zeisberg, *Nat. Rev. Cancer*, 2006, **6**, 392–401.

114 J. J. Tomasek, G. Gabbiani, B. Hinz, C. Chaponnier and R. A. Brown, *Nat. Rev. Mol. Cell Biol.*, 2002, **3**, 349–363.

115 K. Lee and C. M. Nelson, in *International Review of Cell and Molecular Biology*, Elsevier Inc., 1st edn., 2012, vol. 294, pp. 171–221.

116 B. G. Cuiffo and A. E. Karnoub, *Cell Adhes. Migr.*, 2012, 6, 220–230.

117 C. Frantz, K. M. Stewart and V. M. Weaver, *J. Cell Sci.*, 2010, **123**, 4195–4200.

118 O. Trédan, C. M. Galmarini, K. Patel and I. F. Tannock, *J. Natl. Cancer Inst.*, 2007, **99**, 1441–54.

119 T. R. Cox and J. T. Erler, *Dis. Model. Mech.*, 2011, **4**, 165–178.

120 E. L. Siegler, Y. J. Kim and P. Wang, *J. Cell. Immunother.*, 2016, **2**, 69–78.

121 R. O. Hynes, *Science (80-.).*, 2009, **326**, 1216–1219.

122 C. Fernandes, D. Suares and M. C. Yergeri, *Front. Pharmacol.*, 2018, **9**, 1230.

123 B. Psaila and D. Lyden, *Nat. Rev. Cancer*, 2009, **9**, 285–293.

124 J. M. Brown, *Br. J. Radiol.*, 2014, **87**, 20130686.

125 S. Wilhelm, A. J. Tavares, Q. Dai, S. Ohta, J. Audet, H. F. Dvorak and W. C. W. Chan, *Nat. Rev. Mater.*, 2016, **1**, 16014.

126 P. Carmeliet and R. K. Jain, *Nature*, 2011, **473**, 298–307.

127 V. Estrella, T. Chen, M. Lloyd, J. Wojtkowiak, H. H. Cornnell, A. Ibrahim-Hashim, K. Bailey, Y. Balagurunathan, J. M. Rothberg, B. F. Sloane, J. Johnson, R. A. Gatenby and R. J. Gillies, *Cancer Res.*, 2013, **73**, 1524–1535.

128 V. P. Chauhan and R. K. Jain, *Nat. Mater.*, 2013, **12**, 958–62.

129 M. I. Setyawati, C. Y. Tay, D. Docter, R. H. Stauber and D. T. Leong, *Chem. Soc. Rev.*, 2015, **44**, 8174–99.

130 S. K. Hobbs, W. L. Monsky, F. Yuan, W. G. Roberts, L. Griffith, V. P. Torchilin and R. K. Jain, *Proc. Natl. Acad. Sci. U. S. A.*, 1998, **95**, 4607–12.

131 J. Fang, H. Nakamura and H. Maeda, *Adv. Drug Deliv. Rev.*, 2011, **63**, 136–151.

132 F. Danhier, O. Feron and V. Préat, *J. Control. Release*, 2010, **148**, 135–46.

133 T. Lammers, F. Kiessling, W. E. Hennink and G. Storm, *J. Control. Release*, 2012, **161**, 175–187.

134 U. Prabhakar, H. Maeda, R. K. Jain, E. M. Sevick-Muraca, W. Zamboni, O. C. Farokhzad, S. T. Barry, A. Gabizon, P. Grodzinski and D. C. Blakey, *Cancer Res.*, 2013, **73**, 2412–2417.

135 F. Danhier, *J. Control. Release*, 2016, **244**, 108–121.

136 S. Sindhwani, A. M. Syed, J. Ngai, B. R. Kingston, L. Maiorino, J. Rothschild, P. MacMillan, Y. Zhang, N. U. Rajesh, T. Hoang, J. L. Y. Wu, S. Wilhelm, A. Zilman, S. Gadde, A. Sulaiman, B. Ouyang, Z. Lin, L. Wang, M. Egeblad and W. C. W. Chan, *Nat. Mater.*, 2020, **19**, 566–575.

137 N. Muhamad, T. Plengsuriyakarn and K. Na-Bangchang, *Int. J. Nanomedicine*, 2018, **13**, 3921–3935.

138 J. D. Byrne, T. Betancourt and L. Brannon-Peppas, *Adv. Drug Deliv. Rev.*, 2008, **60**, 1615–1626.

139 J. Du, L. A. Lane and S. Nie, *J. Control. Release*, 2015, **219**, 205–214.

140 H. Yin, E. S. Lee, D. Kim, K. H. Lee, K. T. Oh and Y. H. Bae, *J. Control. Release*, 2008, **126**, 130–138.

141 M. Dalela, T. G. Shrivastav, S. Kharbanda and H. Singh, *ACS Appl. Mater. Interfaces*, 2015, **7**, 26530–26548.

142 J. Z. Du, T. M. Sun, W. J. Song, J. Wu and J. Wang, *Angew. Chemie - Int. Ed.*, 2010, **49**, 3621–3626.

143 Y. Y. Yuan, C. Q. Mao, X. J. Du, J. Z. Du, F. Wang and J. Wang, *Adv. Mater.*, 2012, **24**, 5476–5480.

144 A. M. Mansour, J. Drevs, N. Esser, F. M. Hamada, O. A. Badary, C. Unger, I. Fichtner and F. Kratz, *Cancer Res.*, 2003, **63**, 4062–4066.

145 X. Zhang, L. Han, M. Liu, K. Wang, L. Tao, Q. Wan and Y. Wei, *Mater. Chem. Front.*, 2017, **1**, 807–822.

146 N. V. Rao, H. Ko, J. Lee and J. H. Park, *Front. Bioeng. Biotechnol.*, 2018, **6**, 1–15.

147 Y. C. Ma, J. X. Wang, W. Tao, C. Y. Sun, Y. C. Wang, D. D. Li, F. Fan, H. S. Qian and X. Z. Yang, *ACS Appl. Mater. Interfaces*, 2015, **7**, 26315–26325.

148 L. Zhu and V. P. Torchilin, *Integr. Biol. (United Kingdom)*, 2013, **5**, 96–107.

149 D. Needham, J. Y. Park, A. M. Wright and J. Tong, *Faraday Discuss.*, 2012, **161**, 515–534.

150 E. S. Gil and S. M. Hudson, *Prog. Polym. Sci.*, 2004, **29**, 1173–1222.

151 M. Mahmoudi, A. Simchi, M. Imani, M. A. Shokrgozar, A. S. Milani, U. O. Häfeli and P. Stroeve, *Colloids Surfaces B Biointerfaces*, 2010, **75**, 300–309.

152 L. Zhu, Z. Huo, L. Wang, X. Tong, Y. Xiao and K. Ni, *Int. J. Pharm.*, 2009, **370**, 136–143.

153 Y. Ling, X. Tang, F. Wang, X. Zhou, R. Wang, L. Deng, T. Shang, B. Liang, P. Li, H. Ran, Z. Wang, B. Hu, C. Li, G. Zuo and Y. Zheng, *RSC Adv.*, 2017, **7**, 2913–2918.

154 Q. Yuan, Y. Zhang, T. Chen, D. Lu, Z. Zhao, X. Zhang, Z. Li, C. H. Yan and W. Tan, *ACS Nano*, 2012, **6**, 6337–6344.

155 R. Tong, H. D. Hemmati, R. Langer and D. S. Kohane, *J. Am. Chem. Soc.*, 2012, **134**, 8848–8855.

156 G. Yang, J. Liu, Y. Wu, L. Feng and Z. Liu, *Coord. Chem. Rev.*, 2016, **320**–**321**, 100–117.

157 A. Raza, U. Hayat, T. Rasheed, M. Bilal and H. M. N. Iqbal, *J. Mater. Res. Technol.*, 2019, **8**, 1497–1509.

158 C. Marianecci, L. Di Marzio, F. Rinaldi, C. Celia, D. Paolino, F. Alhaique, S. Esposito and M. Carafa, *Adv. Colloid Interface Sci.*, 2014, **205**, 187–206.

159 H. Soo Choi, W. Liu, P. Misra, E. Tanaka, J. P. Zimmer, B. Itty Ipe, M. G. Bawendi and J. V. Frangioni, *Nat. Biotechnol.*, 2007, **25**, 1165–1170.

160 E. Wisse, *J. Ultrasructure Res.*, 1970, **31**, 125–150.

161 S.-Y. Qin, A.-Q. Zhang and X.-Z. Zhang, *Small*, 2018, **14**, 1802417.

162 R. Agarwal, V. Singh, P. Jurney, L. Shi, S. V. Sreenivasan and K. Roy, *Proc. Natl. Acad. Sci. U. S. A.*, 2013, **110**, 17247–17252.

163 P. Decuzzi, R. Pasqualini, W. Arap and M. Ferrari, *Pharm. Res.*, 2009, **26**, 235–243.

164 Y. Geng, P. Dalhaimer, S. Cai, R. Tsai, M. Tewari, T. Minko and D. E. Discher, *Nat. Nanotechnol.*, 2007, **2**, 249–255.

165 F. Alexis, E. Pridgen, L. K. Molnar and O. C. Farokhzad, *Mol. Pharm.*, 2008, **5**, 505–515.

166 D. Hühn, K. Kantner, C. Geidel, S. Brandholt, I. De Cock, S. J. H. Soenen, P. Rivera_Gil, J.-M. Montenegro, K. Braeckmans, K. Müllen, G. U. Nienhaus, M. Klapper and W. J. Parak, *ACS Nano*, 2013, **7**, 3253–3263.

167 G. Thurston, J. W. McLean, M. Rizen, P. Baluk, A. Haskell, T. J. Murphy, D. Hanahan and D. M. McDonald, *J. Clin. Invest.*, 1998, **101**, 1401–13.

168 H. H. Gustafson, D. Holt-Casper, D. W. Grainger and H. Ghandehari, *Nano Today*, 2015, **10**, 487–510.

169 S. Epelman, K. J. Lavine and G. J. Randolph, *Immunity*, 2014, **41**, 21–35.

170 S. Tenzer, D. Docter, J. Kuharev, A. Musyanovych, V. Fetz, R. Hecht, F. Schlenk, D. Fischer, K. Kiouptsi, C. Reinhardt, K. Landfester, H. Schild, M. Maskos, S. K. Knauer and R. H. Stauber, *Nat. Nanotechnol.*, 2013, **8**, 772–81.

171 G. Sahay, D. Y. Alakhova and A. V. Kabanov, *J. Control. Release*, 2010, **145**, 182–195.

172 J. Milton Harris and R. B. Chess, *Nat. Rev. Drug Discov.*, 2003, **2**, 214–221.

173 P. L. Rodriguez, T. Harada, D. A. Christian, D. A. Pantano, R. K. Tsai and D. E. Discher, *Science*, 2013, **339**, 971–5.

174 C. M. J. Hu, L. Zhang, S. Aryal, C. Cheung, R. H. Fang and L. Zhang, *Proc. Natl. Acad. Sci. U. S. A.*, 2011, **108**, 10980–10985.

175 A. Parodi, N. Quattrocchi, A. L. Van De Ven, C. Chiappini, M. Evangelopoulos, J. O. Martinez, B. S. Brown, S. Z. Khaled, I. K. Yazdi, M. V. Enzo, L. Isenhart, M. Ferrari and E. Tasciotti, *Nat. Nanotechnol.*, 2013, **8**, 61–8.

176 B. Diop-Frimpong, V. P. Chauhan, S. Krane, Y. Boucher and R. K. Jain, *Proc. Natl. Acad. Sci. U. S. A.*, 2011, **108**, 2909–2914.

177 A. Salvati, A. S. Pitek, M. P. Monopoli, K. Prapainop, F. B. Bombelli, D. R. Hristov, P. M. Kelly, C. Åberg, E. Mahon and K. A. Dawson, *Nat. Nanotechnol.*, 2013, **8**, 137–43.

178 Z. L. Tyrrell, Y. Shen and M. Radosz, *Prog. Polym. Sci.*, 2010, **35**, 1128–1143.

179 K. Kataoka, A. Harada and Y. Nagasaki, *Adv. Drug Deliv. Rev.*, 2001, **47**, 113–131.

180 C. W. Perrault SD, Walkey C, Jennings T, Fischer HC, *Nano Lett*, 2009, **9**, 1909–15.

181 A. S. Deshmukh, P. N. Chauhan, M. N. Noolvi, K. Chaturvedi, K. Ganguly, S. S. Shukla, M. N. Nadagouda and T. M. Aminabhavi, *Int. J. Pharm.*, 2017, **532**, 249–268.

182 H. Parhiz, M. Khoshnejad, J. W. Myerson, E. Hood, P. N. Patel, J. S. Brenner and V. R. Muzykantov, *Adv. Drug Deliv. Rev.*, 2018, **130**, 90–112.

183 M. N. V. R. Kumar, R. A. A. Muzzarelli, C. Muzzarelli, H. Sashiwa and A. J. Domb, *Chem. Rev.*, 2004, **104**, 6017–6084.

184 S. S. Kulthe, Y. M. Choudhari, N. N. Inamdar and V. Mourya, *Des. Monomers Polym.*, 2012, **15**, 465–521.

185 W. Lin, Y. He, J. Zhang, L. Wang, Z. Wang, F. Ji and S. Chen, *Colloids Surfaces B Biointerfaces*, 2014, **115**, 384–390.

186 S. K. Sahoo and V. Labhasetwar, *Drug Discov. Today*, 2003, **8**, 1112–20.

187 M. Estanqueiro, M. H. Amaral, J. Conceição and J. M. Sousa Lobo, *Colloids Surfaces B Biointerfaces*, 2015, **126**, 631–648.

188 D. Bobo, K. J. Robinson, J. Islam, K. J. Thurecht and S. R. Corrie, *Pharm. Res.*, 2016, **33**, 2373–2387.

189 C. M. J. Hu, S. Aryal and L. Zhang, *Ther. Deliv.*, 2010, **1**, 323–334.

190 X. Wang, Y. Wang, Z. G. Chen and D. M. Shin, *Cancer Res. Treat.*, 2009, **41**, 1.

191 Y. Cheng, Z. Xu, M. Ma and T. Xu, *J. Pharm. Sci.*, 2008, **97**, 123–143.

192 K. Thanki, R. P. Gangwal, A. T. Sangamwar and S. Jain, *J. Control. Release*, 2013, **170**, 15–40.

193 S. Svenson, *Eur. J. Pharm. Biopharm.*, 2009, **71**, 445–462.

194 M. Rawat, D. Singh, S. Saraf and S. Saraf, *Biol. Pharm. Bull.*, 2006, **29**, 1790–1798.

195 T. M. Allen, *Drugs*, 1997, **54**, 8–14.

196 S. Vemuri and C. T. Rhodes, *Pharm. Acta Helv.*, 1995, **70**, 95–111.

197 Y. Barenholz, *J. Control. Release*, 2012, **160**, 117–134.

198 A. Gabizon, R. Catane, B. Uziely, B. Kaufman, T. Safra, R. Cohen, F. Martin, A. Huang and Y. Barenholz, *Cancer Res.*, 1994, **54**, 987–92.

199 S. Vyas, S. Rai, R. Paliwal, P. Gupta, K. Khatri, A. Goyal and B. Vaidya, *Curr. Nanosci.*, 2008, **4**, 30–44.

200 G. Chen, I. Roy, C. Yang and P. N. Prasad, *Chem. Rev.*, 2016, **116**, 2826–2885.

201 J. Pardeike, A. Hommoss and R. H. Müller, *Int. J. Pharm.*, 2009, **366**, 170–184.

202 Y. Darwis, A. Ali Khan, J. Mudassir and N. Mohtar, *Int. J. Nanomedicine*, 2013, **8**, 2733.

203 H. Nagai, Y. Okazaki, S. H. Chew, N. Misawa, Y. Yamashita, S. Akatsuka, T. Ishihara, K. Yamashita, Y. Yoshikawa, H. Yasui, L. Jiang, H. Ohara, T. Takahashi, G. Ichihara, K. Kostarelos, Y. Miyata, H. Shinohara and S. Toyokuni, *Proc. Natl. Acad. Sci.*, 2011, **108**, E1330–E1338.

204 C.-M. Tîlmaciu and M. C. Morris, *Front. Chem.*, 2015, **3**, 59.

205 K. Kostarelos, L. Lacerda, G. Pastorin, W. Wu, S. Wieckowski, J. Luangsivilay, S. Godefroy, D. Pantarotto, J. P. Briand, S. Muller, M. Prato and A. Bianco, *Nat. Nanotechnol.*, 2007, **2**, 108–113.

206 V. Amenta and K. Aschberger, *Wiley Interdiscip. Rev. Nanomedicine Nanobiotechnology*, 2015, **7**, 371–386.

207 X. Huang, F. Zhang, L. Zhu, K. Y. Choi, N. Guo, J. Guo, K. Tackett, P. Anilkumar, G. Liu, Q. Quan, H. S. Choi, G. Niu, Y. P. Sun, S. Lee and X. Chen, *ACS Nano*, 2013, **7**, 5684–5693.

208 H. Ding, L. W. Cheng, Y. Y. Ma, J. L. Kong and H. M. Xiong, *New J. Chem.*, 2013, **37**, 2515–2520.

209 M. L. Liu, B. Bin Chen, C. M. Li and C. Z. Huang, *Green Chem.*, 2019, **21**, 449–471.

210 S. Zeng, X. Yu, W. C. Law, Y. Zhang, R. Hu, X. Q. Dinh, H. P. Ho and K. T. Yong, *Sensors Actuators, B Chem.*, 2013, **176**, 1128–1133.

211 E. Phillips, O. Penate-Medina, P. B. Zanzonico, R. D. Carvajal, P. Mohan, Y. Ye, J. Humm, M. Gönen, H. Kalaigian, H. Schöder, H. W. Strauss, S. M. Larson, U. Wiesner and M. S. Bradbury, *Sci. Transl. Med.*, 2014, **6**, 260ra149.

212 K. Mahmoudi, A. Bouras, D. Bozec, R. Ivkov and C. Hadjipanayis, *Int. J. Hyperth.*, 2018, **34**, 1316–1328.

213 W. Badri, K. Miladi, S. Robin, C. Viennet, Q. A. Nazari, G. Agusti, H. Fessi and A. Elaissari, *Pharm. Res.*, 2017, **34**, 1773–1783.

214 G. Cevc and G. Blume, *Biochim. Biophys. Acta - Biomembr.*, 2001, **1514**, 191–205.

215 J. Lopes-De-Araújo, A. R. Neves, V. M. Gouveia, C. C. Moura, C. Nunes and S. Reis, *Pharm. Res.*, 2016, **33**, 301–314.

216 B.-S. Lee, C. W. Yoon, A. Osipov, N. Moghavem, D. Nwachokor, R. Amatya, R. Na, J. L. Pantoja, M. D. Pham, K. L. Black and J. S. Yu, *J. Drug Deliv.*, 2011, **2011**, 1–13.

217 L. Tarţău, A. Cazacu and V. Melnig, *J. Mater. Sci. Mater. Med.*, 2012, **23**, 2499–2507.

218 S. Lee, A. Stubelius, N. Hamelmann, V. Tran and A. Almutairi, *ACS Appl. Mater. Interfaces*, 2018, **10**, 40378–40387.

219 Z. Zeng, Z. Wei, L. Ma, Y. Xu, Z. Xing, H. Niu, H. Wang and W. Huang, *J. Mater. Chem. B*, 2017, **5**, 6860–6868.

220 S. Shehata, C. J. Serpell and S. C. G. Biagini, *Mater. Today Commun.*, 2020, **25**, 101562.

221 K. Giannousi, E. Koutroumpis, V. Georgiadou, V. Karagkounis and C. Dendrinou-Samara, *Eur. J. Inorg. Chem.*, 2019, **2019**, 1895–1903.

222 E. Gronczewska, A. Defort and J. J. Kozioł, *Pharm. Chem. J.*, 2019, **53**, 527–534.

223 Y. Min, J. M. Caster, M. J. Eblan and A. Z. Wang, *Chem. Rev.*, 2015, **115**, 11147–11190.

Chapter 2

NSAID-based polymeric prodrugs

2.1. Salicylic acid-pased polymer (polysalicylate)*

2.1.1. Introduction

In 1895, the German company Bayer tasked the young chemist Felix Hoffman with enhancing the efficacy and safety of the already successful salicylic acid (SA) that was being widely used as an analgesic and antipyretic. Hoffman, also driven by his concern for his father who could no longer take SA without feeling nauseous, put forth a method to acetylate the hydroxyl group on the molecule. Aspirin was hence born, and after two years of testing it was released to the public to become the most popular drug in the world.[1]

After its administration, aspirin is rapidly hydrolysed into acetate and salicylic acid. It is estimated that about 40% of an oral dose of aspirin is hydrolysed during the first-pass by hepatic carboxylesterases while the circulating aspirin is metabolised by the plasma cholinesterases and possess the half-life of about 13-20 minutes.[2–4]

The primary metabolite, salicylic acid, has a half-life of approximately 3-5 hours and is eliminated through urine and bile after being converted to its metabolites, mainly salicyluric acid (its glycine conjugate which constitutes about 75% of all metabolites), salicylphenolic glucuronide, salicylacyl glucuronide, and gentisic acid, while about 10% of salicylic acid is renally excreted without change.[5–7] Of all metabolites, gentisic acid is the only one that is pharmacologically active.[8] The half-life can, however, increase by up to three-folds as the plasma albumin that normally binds the free drug becomes saturated with repeated doses.[6,9] Figure 2.1 illustrates the main metabolites of aspirin after its hydrolysis to salicylic acid.

Even though the pharmacological effects of aspirin are mainly attributed to the transfer of its acetyl group to the serine residue in the active sites of COX enzymes, thus irreversibly inactivating them, its longer-circulating hydrolysis by-product, i.e. salicylic acid, still exhibits anti-inflammatory activity through COX-dependent and -independent pathways.[10,11] Moreover, it has been speculated that fruit, vegetable, spices and herbs that are naturally rich with salicylate might be responsible for the lower cancer rate in certain demographies.[12,13]

*Parts of this work were peer-reviwed and published in Macromolecular Rapid Communications.[31]

In addition to having therapeutic properties similar to those of its parent drug, salicylic acid is a simple molecule with two functional groups which makes it an attractive candidate for the design of polymeric prodrugs for the purpose of targeted therapy in a variety of ailments.

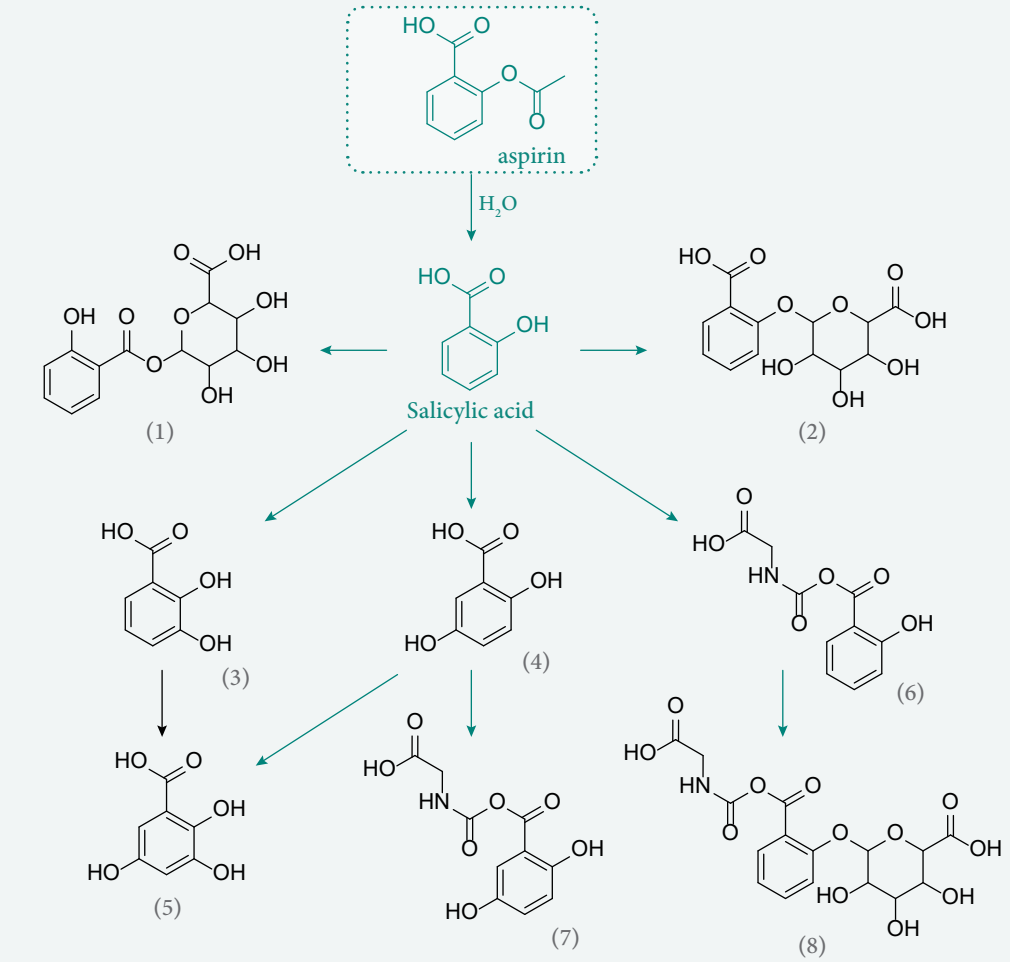

Fig 2.1. Aspirin metabolites. **(1)** Salicylacyl glucuronide, **(2)** Salicylphenol glucuronide, **(3)** 2,3-Dihydroxybenzoic acid, **(4)** Gentisic acid, **(5)** 2,3,5-Trihydroxybenzoic acid, **(6)** Salicyluric acid, **(7)** Gentisuric acid, **(8)** Salicyluric phenolic glucuronide. Adapted from [7]

Kathryn Uhrich and her group have developed biodegradable salicylic acid-derived poly(anhydride-esters). These polymers, collectively patented as PolyAspirin™ (Figure 2.2a), incorporated salicylic acid (SA) within their backbone and were intended to be polymeric prodrugs for the use with diseases such as inflammatory-bowl disease and with drug-releasing bone implants.[14,15] One of their earliest polymers was synthesised by melt condensation polymerisation of an SA-sebacic acid diester. The final polymer had a high loading capacity of the drug (62 wt%) and showed a slow *in vitro* degradation profile to salicylic acid and the biocompatible sebacic acid. The degradation rate varied depending on the pH of the medium used and took about 90 days to fully

degrade at pH=7 as opposed to 38 hours at pH=10 with insignificant degradation at pH=3.5.[16] Using solution polymerisation method instead of melt condensation yielded a polymer with similar characteristics.[17] This polymer [poly(1,10-bis(o-carboxyphenoxy)decanoate) or poly-CPD], however, had a transition temperature (T_g) of 27 °C making the polymer softer at body temperature and limiting its stability in biomedical devices. In order to solve this issue, the group co-polymerised poly-CPD with a similar one [poly(1,6-bis(p-carboxyphenoxy)hexane) or poly-*p*-CPH] at different ratios through melt condensation. The resulting copolymers had higher T_g values than the original homopolymers (33-38 °C) but significantly lower drug loading (6-31 wt% inversely correlated with T_g).[18] The group also experimented with changing the linker from sebacic acid to adipic and suberic acids and showed that it slightly affected the release profile of SA (100% release after 7, 6, and 10 days with sebacate, suberate, and adipate, respectively).[19] Microspheres (2 to 34 μm) prepared from similar polymers with different linkers in the polymer backbone showed release profiles that varied significantly. 100% of the SA was released in 20 days from microspheres of polymers with a linear aliphatic linker as opposed to 100% release in just 3 days with a heteroaromatic linker, while a branched aliphatic linker caused a lag period of 10 days after which only 20% of SA was released in 20 days.[20]

Chandorkar *et al.* synthesised a very similar polymer (Figure 2.2b) through the melt-condensation of the same SA-sebacic acid monomer but with mannitol molecules instead of the end acetyl groups. The mannitol served as a cross-linker and resulted in an even more prolonged release of SA. The non-cured polymer showed an *in vitro* release of about 30% after 4 months at a pH=7.4 and 37 °C while the cured version of the polymer showed a release of 3.5% in 4 months under the same conditions. Even though the potential application of the polymer in cancer therapy was suggested by the authors, only some cytocompatibility tests were conducted that proved that the polymer was compatible with certain murine myoblasts.[21]

The T_g of these polymers, however, was 1 °C and 17 °C for the non-cured and cured polymers, respectively (as a result of the difference in the degree of cross-linking). Because these temperatures are much lower than that of the body temperature, these polymers would have high chain mobility at the body temperature and therefore higher degradation rate. They would, however, have high elasticity at temperatures above T_g and could still be useful in the development of elastomeric

biomaterials.[22,23] Also, the addition of mannitol to the monomer decreased the loading capacity of the polymer almost by half (35 wt%). Nonetheless, the group has demonstrated that implants made of the cured polymer reduced the inflammatory response in mice over a period of 16 weeks.[24]

Dasgupta *et al.* developed a polymer similar to the last except that they used adipic acid instead of sebacic acid and they substituted mannitol with xylitol as the cross-linker (figure 2.2c). Using different ratios of the diacid and the cross-linker resulted in T_g values ranging between 17-33 °C and hydrolytic degradation rates ranging between 4-65% in 7 days. The release rate of SA was affected, however, by the curing of the polymer where the non-cured polymer exhibited a release rate of 35% of SA as opposed to 10% of the cured polymer in 7 days at 37 °C and pH=7.4. Nonetheless, the initial loading dose of SA was lower than the previous polymers (11-18%).[25]

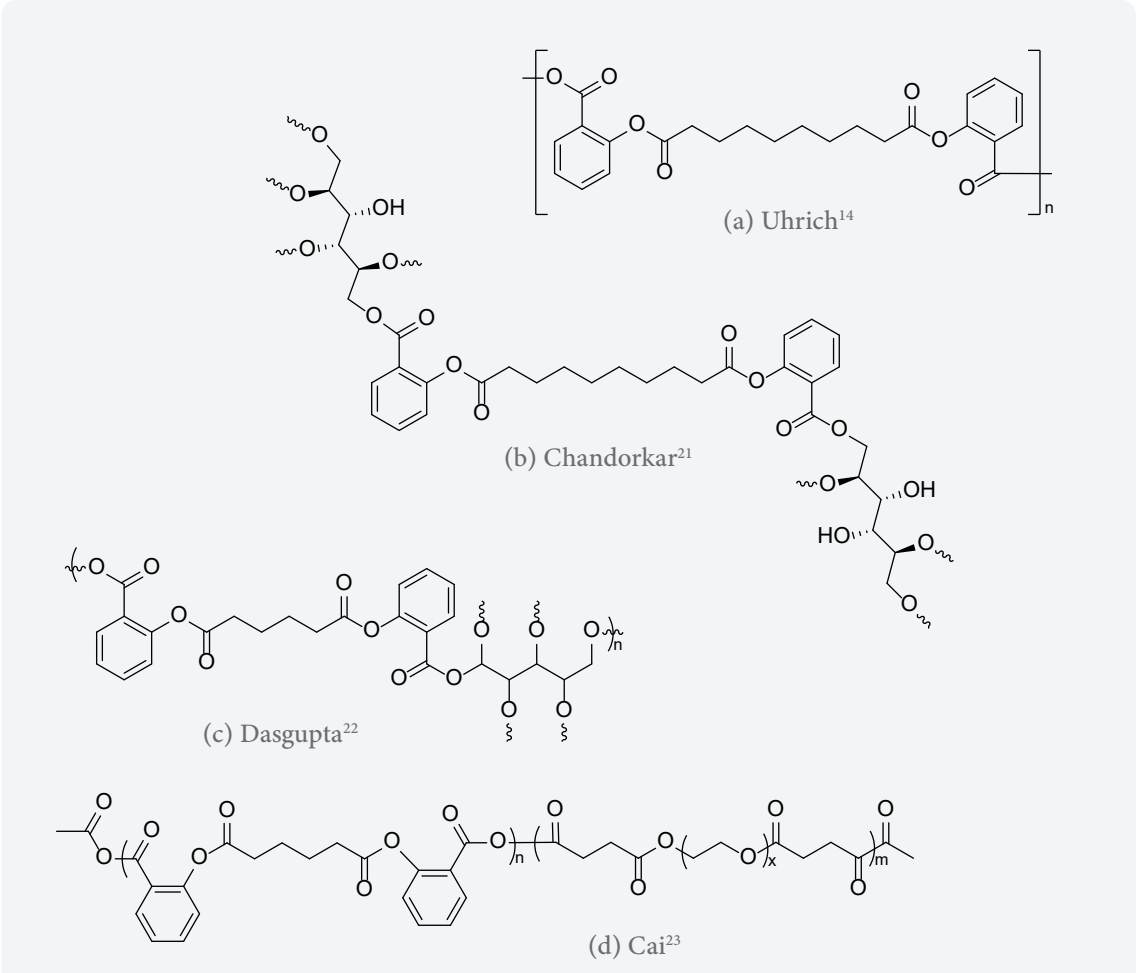

Fig 2.2. Examples of salicylic acid-based polymers from the literature

In contrast, Cai *et al.* wanted to develop a polymer that not only have a higher drug loading but that would also degrade at a faster rate in the distal intestinal conditions so it would be useful in the local delivery of SA to the colon (Figure 2.2d). Their poly[bi(o-carboxyphenyl)adipate-polyethylene glycol] anhydrides, or shortly P(BOCA-PEG), had a loading capacity ranging between 43.5-71.3% and exhibited an *in vitro* release rate of 15% in 21 hours in a medium that simulated the beginning of the large intestine, while less than 0.2% was released in 21 hours in simulated gastric conditions.[26]

Other attempts to create SA-based polymers for the localised and/or controlled delivery include incorporating SA into dendrimers,[27] and creating polymer-drug conjugates such as SA-poly(vinyl alcohol) ester.[28]

While all the previous work focused on creating SA-loaded polymers that can be used for elastomeric biomaterials such as drug-eluting stent coatings,[29] as anti-biofilm urological catheter coatings,[30] or for the localised delivery of SA in inflammatory bowel disease and colon cancer,[16] no systemically-administered, SA-based nanocarriers for the purpose of targeting solid tumours were identified in the literature.

This chapter presents the work[31] carried out to create amphiphilic copolymers with high payload and sustained release profile of SA that self-assemble into nanostructures. These nanoparticles (NPs) could potentially be administered intravenously as carriers for the delivery of SA into solid tumours, regardless of their location, by taking advantage of the uniqueness of the tumour microenvironment (TME) and the enhanced permeability and retention (EPR) effect as discussed in Chapter 1.

2.1.2. Materials and instrumentation

Polysalicylate (PSA) and PSA-*b*-mPEG. Salicylic acid, acetic anhydride, thionyl chloride, and N, N-diisopropylethylamine (DIPEA), were obtained from Acros Organics. Polyethylene glycol monomethyl ether was obtained from Alfa Aesar. 4-dimethylaminopyridine (DMAP) was obtained from Fluorochem.

NMR spectra were obtained on a Bruker AV2 400 MHz spectrometer and were calibrated to the centre of the set solvent peak and chemical shifts were reported in parts per million (ppm).

Gel permeation chromatography (GPC) was conducted using PL-GPC 50 Plus system by Varian Inc. The separation media consisted of two Agilent (300x 7.5 mm) 5µm MIXED-C columns in series in a 40 °C oven. Refractive index (RI) detection was used and THF, stabilised with 250 ppm BHT, was the eluent. The flow rate was set at 1 mL/min and the sample run time was 25 minutes.

TGA-DSC was carried out in a Netzsch STA 409 PC/PG. The samples were heated from 25 °C to 600 °C at 10 °C/min.

FTIR spectra were recorded on a Shimadzu IRAffinity-1S with and ATR gate. A sweep of 500-4000 cm^{-1} with a resolution of 2 cm^{-1} and 64 scans was performed.

Self-assembly. Visking dialysis tubing was obtained from Medicell Membranes Ltd.

Dynamic light scattering (DLS) measurements were performed using Zeta Sizer Nano-ZS by Malvern Instruments Limited. Measurements were conducted using a glass cuvette at 25 °C. The refractive index RI of the dispersant (water) was set to 1.33 with the viscosity of 0.8872 cP while the RI for the material measured was set to 1.45.

Zeta-potential measurements were performed in Litesizer 500 by Anton Paar GmbH using a zeta-potential cell at 25 °C.

Transmission electron microscopy (TEM) was performed on a Jeol 1230, operating at an accelerating voltage of 80 kV and the images were recorded with a Gatan Multiscan 790 digital camera.

Degradation. Gibco® phosphate-buffered saline and HyClone™ foetal bovine serum were obtained from Thermo Fisher Scientific. Lyophilised esterase from porcine liver was obtained from Sigma-Aldrich.

Degradation studies were carried out in Mastercycler™ Pro PCR System by Eppendorf.

UV- visible absorption spectra were recorded on NanoDrop One spectrophotometer by Thermo Fisher Scientific.

2.1.3. Experimental

2.1.3.1. Salicylic acid polymer (polysalicylates)

PSA was prepared in two steps. In the first step, SA was refluxed with 1.1-2 equivalents of acetic anhydride under nitrogen at temperatures ranging between 150-200 °C for varying durations of time (6-20 hours). In stage two, a distillation head was installed and the temperature was raised to 250-300 °C as vacuum was applied to remove the excess acetic anhydride and the acetic acid by-product over periods of time ranging between 1 and 36 hours. As the reaction vessel was left to cool down, a glassy amber solid formed and spontaneously cracked as it was reaching room temperature and was then extracted from the flask. The resulting polymer was soluble in dichloromethane (DCM), chloroform, tetrahydrofuran (THF), and dimethyl sulfoxide (DMSO). Long-chain forms of the PSA were partially soluble in acetone while the short-chain ones had a better solubility. PSA was practically insoluble in water, methanol (MeOH), ethanol (EtOH), dimethyl formamide, diethyl ether, and hexane.

To remove residual monomers and other reactants, the polymer was dissolved in DCM and was then precipitated in MeOH. The precipitate was centrifuged and washed three times with MeOH and then dissolved again in DCM and reduced to dryness again using the rotating evaporator under vacuum. Further drying was achieved using high vacuum overnight.

The pure products had an amorphous brittle cotton-candy-like structure that had a white to yellowish colour. Yields ranged between 72 and 87%.

^{1}H NMR (400 MHz, $CDCl_3$) δ (ppm): 8.13 (b, n1H, **ArH**), 7.29 (b, n1H, **ArH**), 7.03 (b, n2H, **ArH**), 2.17 (s, 3H, **CH_3**), where n corresponds with the degree of polymerisation.

2.1.3.2. Polysalicylate-block-methoxy polyethylene glycol (PSA-b-mPEG)

PSA with nine repeating units of the monomer (PSA_9) was conjugated with methoxy polyethylene glycol 1900 (mPEG-1900). An acyl chloride of PSA_9 (M_n = 668) was first obtained by refluxing the polymer with thionyl chloride at 65 °C overnight with a catalytic amount (5-10 mol%) of 4-dimethylaminopyridine (DMAP). The excess of thionyl chloride was removed using the rotary evaporator under vacuum. The polysalicyloyl chloride was then dissolved in DCM and 2 molar equivalents of *N,N*-diisopropylethylamine (DIPEA) and 3 molar equivalents of mPEG (nominal

M_n = 1900) were added. The reaction was then left stirring at room temperature overnight. The reaction mixture was then transferred to a separation funnel and washed with 10% solution of HCl to remove the DIPEA and DMAP, then three times with de-ionised water and once with brine. The organic layer was reduced to dryness and then re-dissolved in a 1:1.5 mixture of DCM/diethyl ether and washed multiple times with de-ionised water and brine to remove the excess mPEG. The purpose of the DCM/ether mixture is to make the mPEG less soluble in the organic layer, resulting in its partition to the aqueous phase. The organic layer was then dried over magnesium sulphate and the solvent evaporated. The resulting product was dried further under high vacuum overnight. The resulting product was an amorphous white solid and the yield was 61%.

^{1}H-NMR (400 MHz, $CDCl_3$) δ (ppm): 8.13 (b, 9H, **ArH**), 7.29 (b, 9H, **ArH**), 7.03 (b, 9H, **ArH**), 3.57 (b, 168H, $\mathbf{CH_2CH_2}$), 3.32 (s, 3H, $\mathbf{CH_3}$), 2.17 (s, 3H, $\mathbf{CH_3}$).

2.1.3.3. PSA-b-mPEG self-assembly

The co-solvent method was used for the self-assembly of NPs where two sets of solutions of the BCP in two common solvents (THF and acetone) were prepared with two concentrations each (1 and 10 wt%) in separate round-bottom flasks. As the solutions were being stirred, de-ionised water was added dropwise in a uniform manner using a micropipette until a tenfold dilution was achieved. Suspensions prepared from acetone were left stirring for a few hours to remove the solvent while the ones prepared from THF were dialysed using Visking dialysis membrane with a molecular weight cut-off of 12-14 kDa. Volumes were measured before and after removing the solvent to keep track of and adjust concentrations accordingly.

2.1.3.3.1. Stability of vesicles

Zeta-potential (ζ-potential) measurement for the vesicle preparation with the final concentration of 1 wt% was conducted at 25 °C.

DLS measurements of the same sample were taken at different time points over a month. Measurements at each time point were done in triplicates and then averaged.

2.1.3.4. Degradation of PSA

Five different media were prepared for the degradation studies; de-ionised water (pH =7-8), sodium hydroxide 2 $mol.dm^{-3}$ (pH ≈14), phosphate-buffered saline (PBS, pH ≈7.4), 10% foetal

bovine serum (FBS) in PBS (pH ≈7.4), and a 36 units.mL^{-1} solution of porcine liver esterase (PLE) in PBS (pH ≈7.4). Equal volumes of degradation media were added to Eppendorf vials containing accurately-weighed equal amounts of PSA_9. Five sets of vials were prepared in this manner for the five time points intended for measurement. Another five sets were also prepared but only contained the degradation media for blanks. This way each sample in a specific medium had a corresponding blank with the same medium and ran for the same amount of time. The vials were placed in the thermal cycler, and the temperature was fixed at 40 °C and was held at that point for the entirety of the experiment. At each predefined time point (2, 4, 8, 24, and 96 hours), a set was removed from the thermal cycler and the samples were analysed using UV spectroscopy in the wavelength range of 200-360 nm. Readings were carried out using the Nanodrop and each measurement was performed against its corresponding blank. The quantitative comparison was conducted by contrasting the absorbance value at the wavelength of 296 nm from the PSA samples with solutions of SA in the respective media corresponding to a 100% degradation of the polymer. The experiment was repeated at 70 and 90 °C.

2.1.4. Discussion of results

Given the potential benefits of aspirin for the chemoprevention and treatment of cancer as discussed in Chapter 1, the aim of this work was synthesising a polymeric prodrug based on the hydrolysis by-product of aspirin, salicylic acid, which also possesses similar anti-inflammatory properties and a much longer half-life.

The SA-based polymers for biomedical applications that are already existing in the literature mainly focus on the use of such polymers in biocompatible implants for the anti-inflammatory, analgesic, and antiseptic effects of SA. Hence, a polymer patented by White *et al.*[32] re-purposed to create a delivery system that has the following advantages over the existing polymers:

1- A higher capacity of SA, at least theoretically, since the polymer is made up entirely of the therapeutic molecule.
2- The ability to conjugate the polymer with another that is hydrophilic and biocompatible, such as PEG, to create an amphiphilic BCP which is capable of self-assembly into entities that could be useful for targeted therapy, especially for solid tumours.
3- A higher T_g that would delay biodegradation and provide a prolonged release of SA.

2.1.4.1. Polysalicylate (PSA)

The synthesis of polysalicylate (PSA) (Figure 2.3) was based on a patent by White *et al.*[32] that aimed at synthesising this polymer as a capping agent for other polymers, such as polyphenylene ethers, with side hydroxyl groups. The author proposed that extreme conditions, such as high temperature in the presence of oxygen, can cause discolouration and brittleness of these other polymers. Inactivating such groups using polymers with high glass transition temperatures can protect the polyethers and help preserve their physicochemical properties.

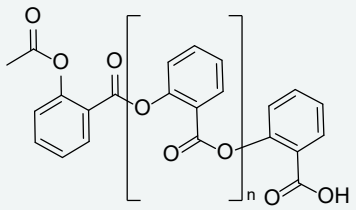

Fig 2.3. The proposed structure of polysalicylate (PSA).

Herein, PSA is re-purposed to be used in a nanoparticle-based formulation since this polymer was solely comprised of repeating units of salicylic acid (SA) thus eliminating the need for polymeric backbones that would otherwise occupy the bulk of the particle. This will eventually lead to an increase in the drug payload of the nanocarriers. Another advantage of this polymer would be that SA units are exclusively linked by ester bonds that are potentially hydrolytically and enzymatically biodegradable.[33] It is speculated that the slow hydrolytic degradation would offer relative long-term stability in an enzyme-free medium, i.e. during the storage of NPs, while it becomes accelerated by endogenous enzymes upon delivery to target tumours.

Even though the patent followed for making the PSA had adequate details about synthesis, the information about the structure is somewhat vague. The reaction mechanism is not discussed but it is indicated in the document that the specified conditions result mainly in linear polymers with one end acetyl group for each 15-50 repeating units of salicylate. Nonetheless, by comparison with similar polymers in the literature[16–18] the reaction mechanism can be speculated.

Figures 2.4 illustrates the possible reaction scheme. During the first stage of the reaction, refluxing salicylic acid with acetic anhydride at high temperatures yields acetylation on the hydroxyl and the carboxyl groups depending on the reaction stoichiometry. In the second stage, heating the

reaction mixture at temperatures above 200 °C under reduced atmospheric pressure initiates melt condensation polymerisation through anhydride elimination. If the acetic anhydride is used in excess during the first stage of the reaction, the yield would be mainly compound **(a)**, i.e. methyl o-acetoxybenzoate, and the resulting polymer **(c)** would have an acetyl group at both ends. However, because only 1.1 to 2 equivalents are used, the yield is likely to be a mixture of compounds **(b)**, i.e. aspirin, and **(a)** since acetylation happens favourably on the phenolic hydroxyl first. As a result, polymerisation of the two monomers is more likely to yield a polymer **(e)** that has acetyl on one terminal and a carboxyl on the other. It is also worth noting that very high temperatures can result in cyclic polymer species **(d)**.

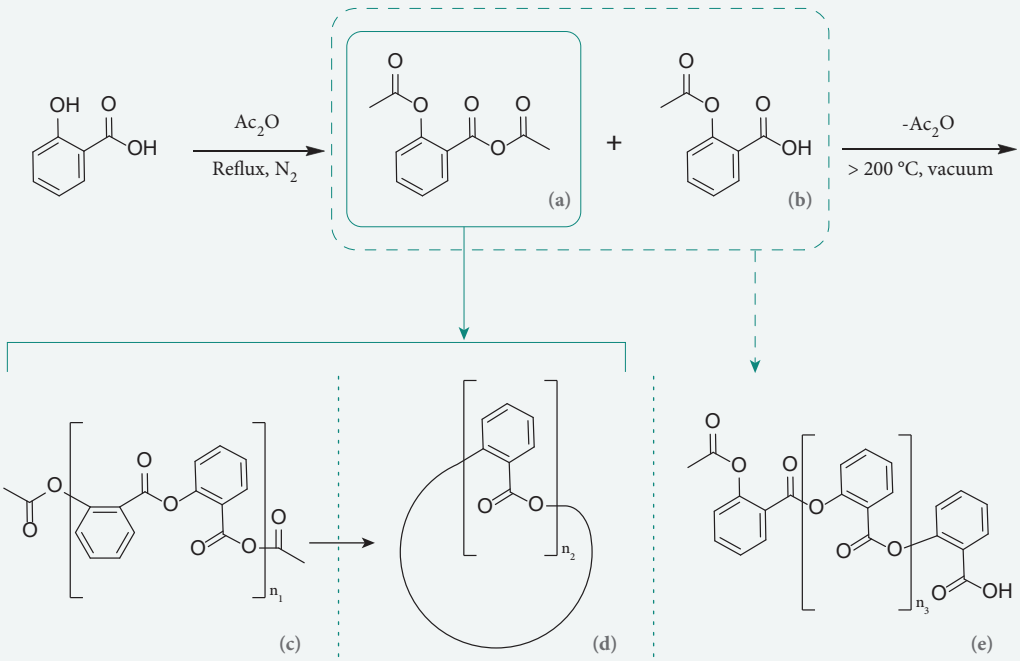

Fig 2.4. The proposed products of the polymerisation reaction of salicylic acid.

Moreover, the reaction may go through another pathway as the salicylate–anhydride **(f)** resulting from monomer **(b)** undergoes rearrangement driven by the energy from the high temperature to form a more thermodynamically-stable ester **(g)**.[17] Figure 2.5 illustrates the possible mechanism of the rearrangement.

It might also be worth mentioning that acetic anhydride is necessary for the production of monomer **(a)** and as a reaction medium. An attempt was made to polymerise aspirin by heating

it to high temperatures. Aspirin did not polymerise but instead it sublimed and condensed again at the neck of the flask.

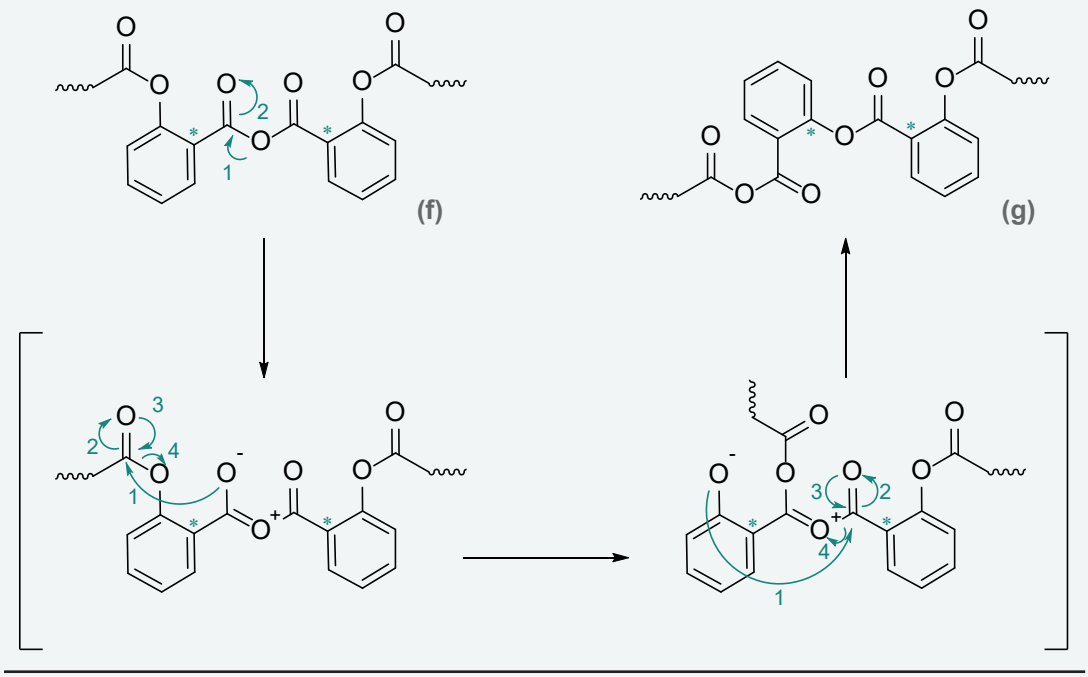

Fig 2.5. The proposed mechanism for the anhydride-ester rearrangement. Adapted from [17]

Gel permeation chromatography (GPC)/size exclusion chromatography (SEC) and ^{1}H-NMR were used to characterise the synthesised polymers.

The average molecular weights and the polydispersity values of the polymers were determined using GPC. Results were reported mainly using number average molecular weight (M_n), weight average molecular weight (M_w) and dispersity ($Đ$).[34]

M_n is defined as the sum of the molecular weight of all species by their mole fractions:

$$\overline{M}_n = \sum n_i \overline{M}_i$$

Where n_i is the mole fraction (or number of molecules) of the species *i* that has a molecular weight of M_i.

M_w is defined as the sum of the molecular weight of all species by their weight fractions:

$$\overline{M}_w = \sum w_i \overline{M}_i$$

Where w_i is the weight fraction of the species i that has a molecular weight of M_i.

Finally, $Đ$ is the dispersity which is calculated by dividing M_w by M_n:

$$Đ = \frac{\overline{M}_w}{\overline{M}_n}$$

^{1}H-NMR was also used to characterise the synthesised polymers. The spectra showed broadening of the peaks of the aromatic region (6.9-8.3 ppm) indicative of polymerisation. The integration of the peak centred at 8.13 ppm, belonging to the protons on the *ortho* position to the carboxyl group on the aromatic rings in the polymeric chain, with the protons of the end acetyl group at 2.17 ppm allowed for the calculation of the number of the salicylate units in the polymer chain (FIgure 2.6).

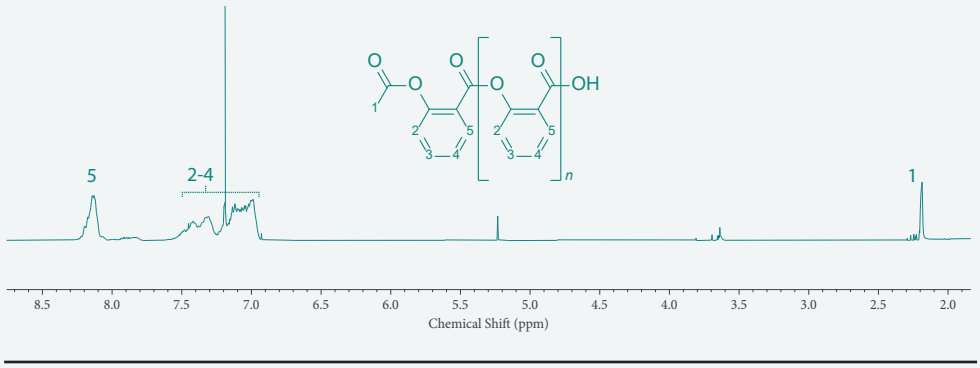

Fig 2.6. The ^{1}H-NMR spectrum of polysalicylate

Typically, two DP values can be obtained from GPC data; the number average DP ($DP_n = M_n/M_0$) and the weight average DP ($DP_w = M_w/M_0$) where M_0 is the molecular weight of the monomer. In contrast, ^{1}H-NMR can provide information only about M_n since the areas under the resonance peaks in the spectra are proportional to the molar concentration of the species in the analysed sample.[35] Table 2.1 exhibits some of the polymers obtained by varying reaction temperatures and summarises the data obtained from ^{1}H-NMR and GPC for each polymer.

Since GPC depends on separating polymer species based on their hydrodynamic volume rather than their molecular weight, and due to the difference in nature between the analysed polymers (PSA) and the standard polymers used for calibration (polystyrene), this method is prone to significant errors.[35] This can be seen in the differences in the reported degree of polymerisation between those obtained from GPC measurement and their counterparts that are calculated from ^{1}H-NMR integrals in Table 2.1. The trends, however, are still comparable, and while ^{1}H-NMR

integrations are better for calculating the average number molecular weight of the polymers, GPC remains the main tool for determining their dispersity.

#	PSA_n	Reaction temp	Mn	Mw	Đ	DP_n
1	PSA_9	140 °C – 3h 220 °C – 3h	668	1055	1.58	5
2	PSA_{17}	140 °C – 3h 220 °C – 6h	1767	2752	1.56	13
3	PSA_{22}	140 °C – 6h 250 °C – 36h	2344	3444	1.47	17
4	PSA_{11}	150 °C – 6h 250 °C – 18h	1063	1597	1.50	8
5	PSA_{29}	200 °C – 20h 250 °C – 26h	1962	3053	1.56	14
6	PSA_{15}	200 °C – 20h 250 °C – 24h	1876	2701	1.44	13
7	PSA_{18}	280 °C – 12h 280 °C – 1h	3339	4927	1.47	24
8	PSA_{19}	220 °C – 12h 220 °C – 1h	1504	2436	1.62	11

n: the number of SA units (degree of polymerisation) calculated via ^{1}H-NMR integrals.
DP_n: degree of polymerisation calculated from Mn obtained by GPC.

Table 2.1. Different polymers obtained by varying reaction temperatures at both stages of the polymerisation reaction.

Nonetheless, it should be noted that using NMR integration to calculate the degree of polymerisation of the desired PSA, has its drawback in the case of PSA since these calculations might be complicated by the formation of species other than the linear PSA with an acetyl group on one end and a carboxyl on the other, such as the bi-acetylated chains, cyclic chains, or even poly-anhydride (as opposed to the polyester) species.

The data in Table 2.1 demonstrate that the overall temperature and reaction time are directly correlated with the length of the resulting polymers (especially when looking at DPs calculated from NMR analyses which, as discussed above, is more representative of M_n and DP than data obtained from GPC). This is in agreement with the literature.[32] Additionally, a few observations can be made when comparing reaction conditions between phase A (the formation of acetylated

monomers) and phase 2 (polycondensation). At moderate temperatures (140-150 °C) in phase A, the polymer length appears to be mainly determined in phase B, such is the case with polymers **1**, **2**, and **3** where increasing the reaction time and temperature in phase B accelerated chain growth and resulted in longer polymer chains. However, increasing the reaction time and temperature of phase A to around 200-280 °C, produced long polymer chains regardless of reaction time in phase B, such as in the case of polymers **7** and **8**. This could be due to the fact that increasing reaction time and temperature in phase A produced more acetylated species (Figure 2.4 a and b) which expedited polycondensation in phase B.

The significant variation between DP obtained from ^{1}H-NMR and GPC for some of the synthesised polymers could be explained by the formation of species other than the target polymer. In polymer **5**, for example, the prolonged reaction times at high temperature might have produced more cyclic polymer species than the linear one which resulted in a weaker acetyl signal in the ^{1}H-NMR spectrum leading to false integration. On the other hand, the difference in DP between polymers **7** and **8** as determined by GPC despite the similarity in DP determined by ^{1}H-NMR could be a result of the presence of linear species with two end acetyl groups (one on each end), which causes a stronger acetyl signal in the ^{1}H-NMR spectrum and another false integration but in the opposite direction to the one from the previous example.

Finally, it is worth noting that very high temperatures do not only result in cyclic chains, but they can also cause reversible thermal depolymerisation.[17] This could explain the difficulty in attaining longer polymer chains even with prolonged reaction times, such as the case in polymers **3**, **5**, and **6**, for example.

2.1.4.2. PSA-mPEG BCP

Besides its function as the hydrophilic segment of the BCP that is essential for self-assembly, mPEG complements the assembled morphologies with added therapeutic advantages. The PEGylation of NPs enhances their pharmacokinetic profile by increasing their solubility, reducing their renal clearance due to the increase in size, and protecting them from being eliminated from the bloodstream via the reticuloendothelial system (RES).[36,37]

Since PEG is a non-biodegradable polyether, some issues have lately been raised concerning its safety. There are some concerns about the possible accumulation in cells and tissues upon repeated

administration of PEG-containing NPs and the possible immunogenicity in susceptible individuals, yet no clinical evidence is so far available to support such concerns.[38,39] However, PEG remains the gold standard for increasing the biocompatibility and half-life of nanopharmaceutics and it has been widely used in clinically-approved formulations since the early 1990s.[40] PEG clearance is mainly renal for PEGs that are less than 30 kDa, while higher chains primarily undergo biliary excretion.[41]

In this work, it was speculated that the presence of an end carboxyl group on the PSA would enable the production of PEGylated NPs without the need for a linker molecule. Conjugating mPEG with the PSA through esterification would create the amphiphilic chain necessary for self-assembly while connecting the therapeutic element with its shield via an ester bond that is cleavable by esterases that are widespread throughout the body.

To preserve the ester groups of the polymer, a mild approach for esterification was necessary for making the PSA-mPEG conjugate. Steglich esterification, a common method for making such esters using a carbodiimide, was first adopted but failed after many attempts. After some tweaking, the method that worked involved converting the carboxylic acid to its more reactive species, acyl chloride, and then using DIPEA as the hydrogen chloride scavenger to make the ester. Figure 2.7 summarises the reaction scheme for the preparation of the block copolymer (BCP).

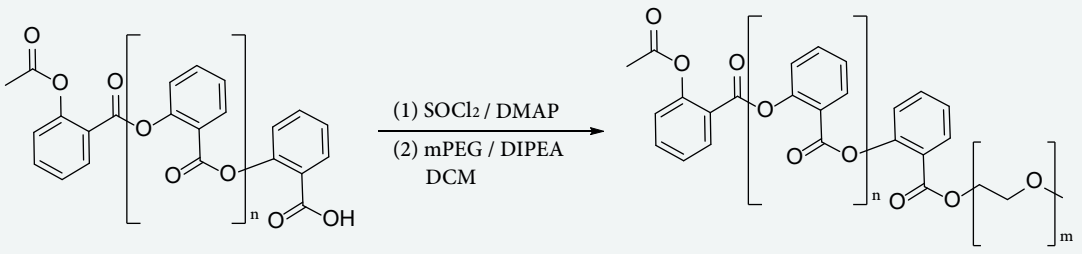

Fig 2.7. Reaction scheme for making the BCP. Step (1) involves making the acyl chloride. Step (2) is making the conjugate with mPEG catalysed by DIPEA.

The formation of the BCP was always first investigated using GPC via comparing the differential molecular weight distributions (DMWDs) of the BCP with those of the individual homopolymers. DMWD describes the contribution of different polymer species to the overall molecular weight of the polymer and is expressed by plotting the weight fractions ($dwt/dLogM_i$) of polymers having

the molecular weight of M_i (where i is the number of the repeating units in any given species) as a function of $LogM_i$.[42,43] Figure 2.8 illustrates the DMWD of PSA, mPEG, and the BCP.

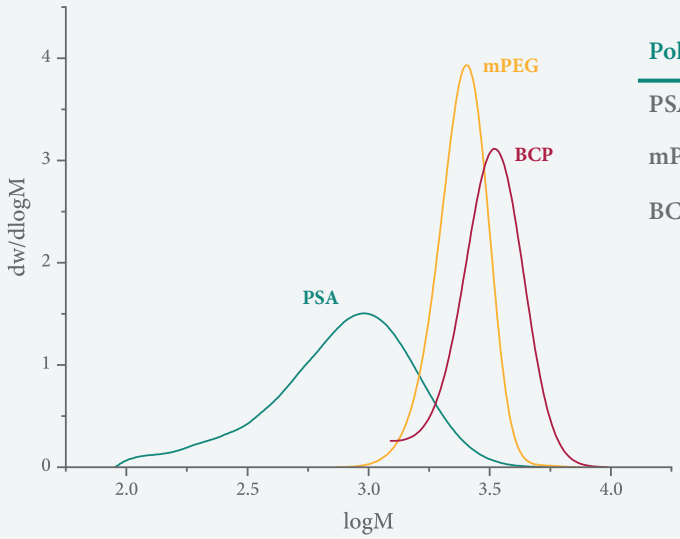

Polymer	Mn	Mw	Đ
PSA	668	1055	1.58
mPEG-1900	2344	2490	1.06
BCP	2998	3315	1.11

Fig 2.8. Differntial molecular weight distributions (DMWDs) of polysalicylate (PSA), methoxy polyethylene glycol (mPEG), and the block co-polymer (BCP).

When comparing the DMWDs of the BCP and the individual homopolymers a shift in the curve of the BCP on the *x* axis is noted due to the emergence of new polymer chains that are longer than those in both PSA and PEG, which indicates a successful copolymerisation. The M_n of the copolymer was 2998, M_w was 3315, and Đ was 1.11.

^{1}H-NMR was also used to characterise the BCP (Figure 2.9). Integrating peak 5 that belongs to the salicylate chain with the PEG peak yielded a ratio of 1:1.3 suggesting a successful PEGylation with some residual PEG that could not be removed from the final product with the washing mixture.

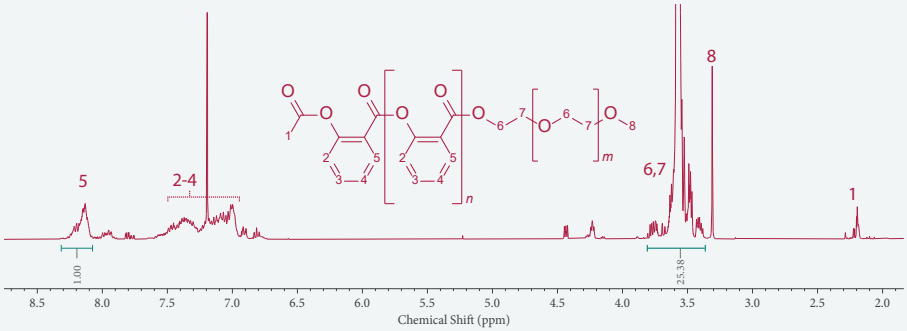

Fig 2.9. The ^{1}H-NMR spectrum of the BCP

Conjugation was also confirmed by comparing the FTIR spectra of the homopolymer and the BCP (Figure 2.10). The broad weak peak at ~3050 cm^{-1} corresponding to the carboxylic acid O-H stretch of PSA was replaced by the intense peak at ~2890 cm^{-1}, arising due to C-H stretches in the mPEG chain.

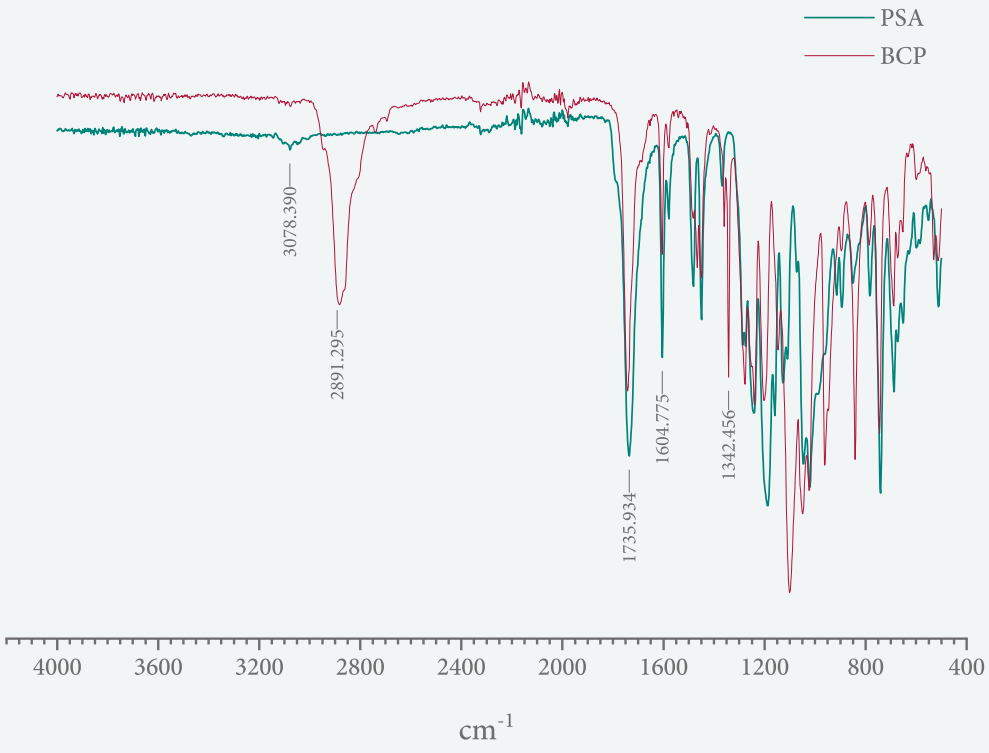

Fig 2.10. FTIR spectra of PSA and PSA-mPEG

Thermal analysis was also performed for the homopolymer and the BCP (Figure 2.11). The DSC calorigram of the PSA shows the glass transition temperature (T_g) at around 100 °C. The endothermic peak that follows indicates the melting temperature (T_m) to be around 225 °C and the exothermic peak of decomposition starting around 450 °C. For the BCP, an endothermic peak at the beginning of the calorigram indicated the melting point of the residual mPEG. T_g and T_m for the BCP were hard to identify because their peaks were complicated by the exothermic peak of cold crystallisation. An exothermic decomposition peak similar to that of the PSA could also be identified.

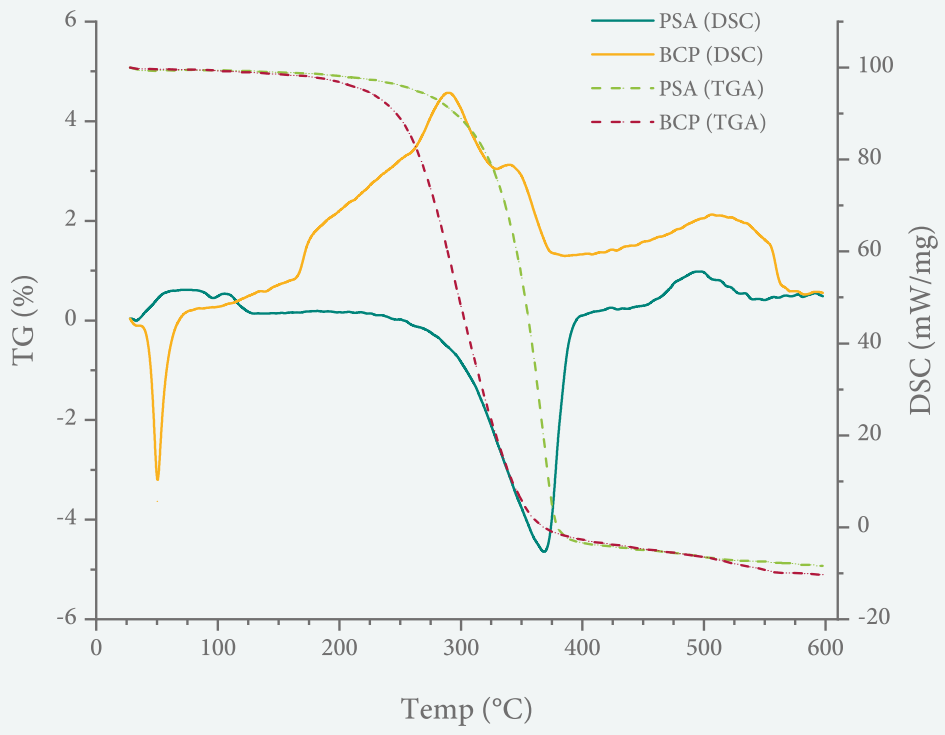

Fig 2.11. Thermal analysis (DSC and TGA) of PSA and the BCP

The drug loading capacity (LC) of the BCP is defined by the percentage of the drug in the polymer and can be calculated by the equation:[44]

$$LC\ (\%) = \frac{m_d}{m_{tot}}\ x\ 100$$

Where m_d is the mass of the drug in the polymer, and m_{tot} is the weight of the whole polymer.

As discussed before, the PSA used for the synthesis of the BCP consisted of 9 units with the molar mass of the monomer being 138.121 mg.mol^{-1}. The mass of the BCP calculated from its structure is about 3145 mg.mol^{-1}. Therefore, the approximate LC of SA of the synthesised BCP is:

$$LC\ (\%) = \frac{9\ x\ 138}{3145}\ x\ 100 = 39.5\%$$

Numerous attempts were made to create BCPs with higher SA payloads by using longer PSA chains and shorter PEGs (PEG-550 and PEG-750). The conjugation, however, was not always

straightforward regardless of the esterification and purification methods used. Figure 2.12 shows some of the attempts to make BCPs with higher loading of SA.

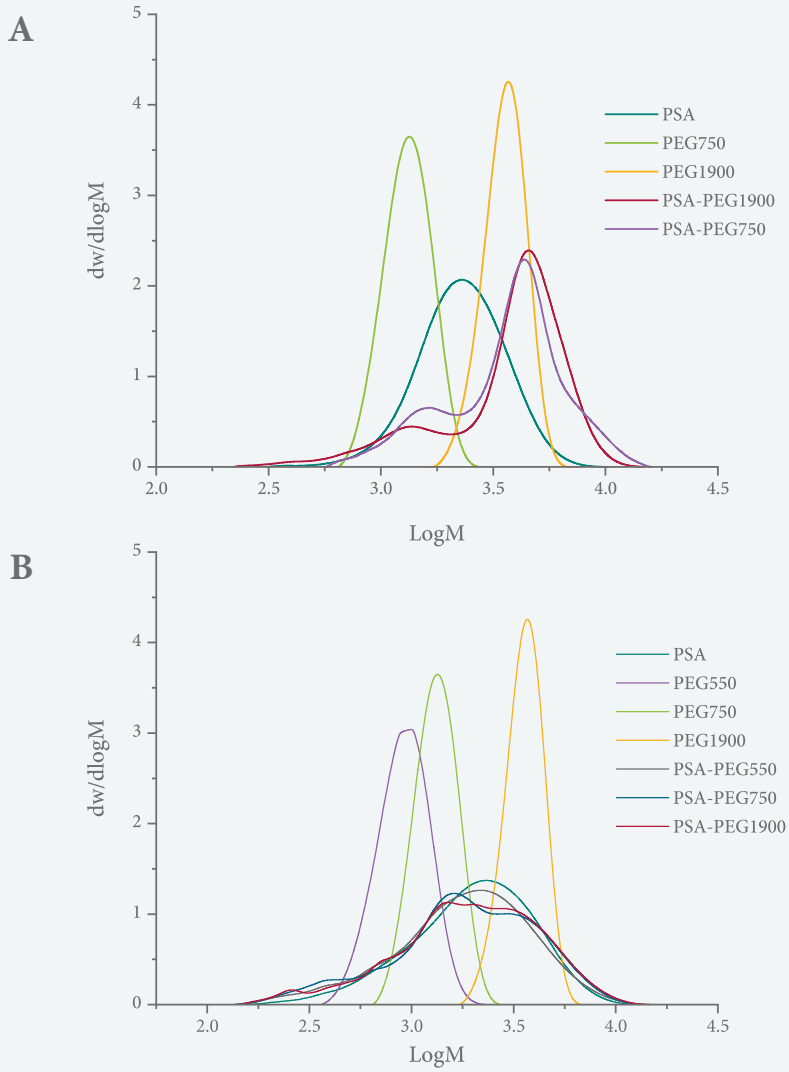

Fig 2.12. DMWDs for some of the BCPs synthesised with different PEG chains.

In Figure 2.12A, for instance, BCPs with either PEG-1900 or PEG-750 could be made, as shown by the shift in the DMWDs, but the shoulders on the peaks indicate that there is still some residual PSA that could not be esterified and neither could it be removed from the BCP using the conventional purification techniques. The presence of the homopolymer complicate self-assembly as it precipitates in aqueous solutions. Figure 2.12B shows a PSA sample that could hardly be esterified with any chain length of PEG in spite of long reaction times (days).

A possible explanation for the incomplete or unsuccessful copolymerisation is the steric hindrance to the carboxyl group by the bulk of the polymer, which was the reason for the use of the acyl chloride form of the polymer.

Another possible cause is that some of the prepared polymers are either cyclic or have their both ends capped by acetyl groups. In retrospect, by examining the ^{13}C-NMR spectrum of one PSA sample that failed to conjugate, it can be inferred that the used homopolymer was, in fact, a cyclic one (Figure 2.13).

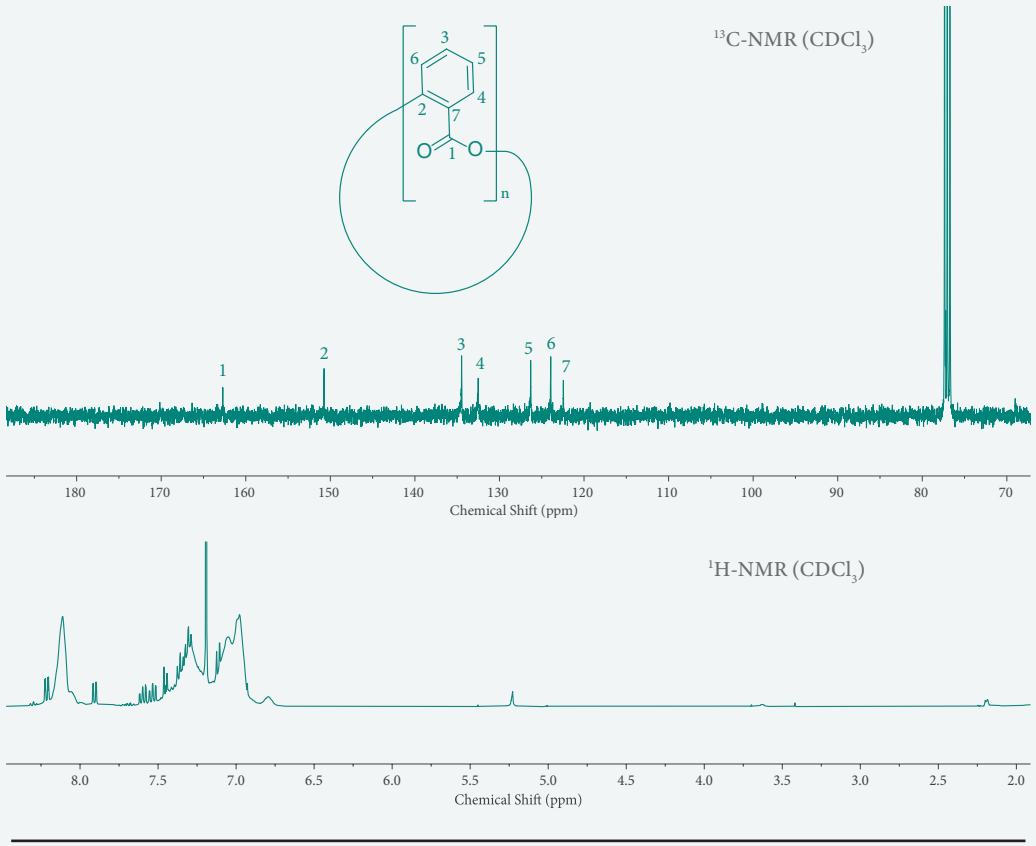

Fig 2.13. ^{13}C- and ^{1}H-NMR spectra of a possible cyclic PSA.

2.1.4.3. Self-assembly

Dynamic light scattering (DLS) was used for the size analysis of the self-assembled particles. Measurement was done in triplicate and then averaged. Samples prepared from the THF solutions showed a mean particle size ranging between 250-300 nm, while the ones prepared from the acetone solutions were about 25 nm in size. Figure 2.14 shows the size distribution of NPs in all four samples by intensity, number, and volume.

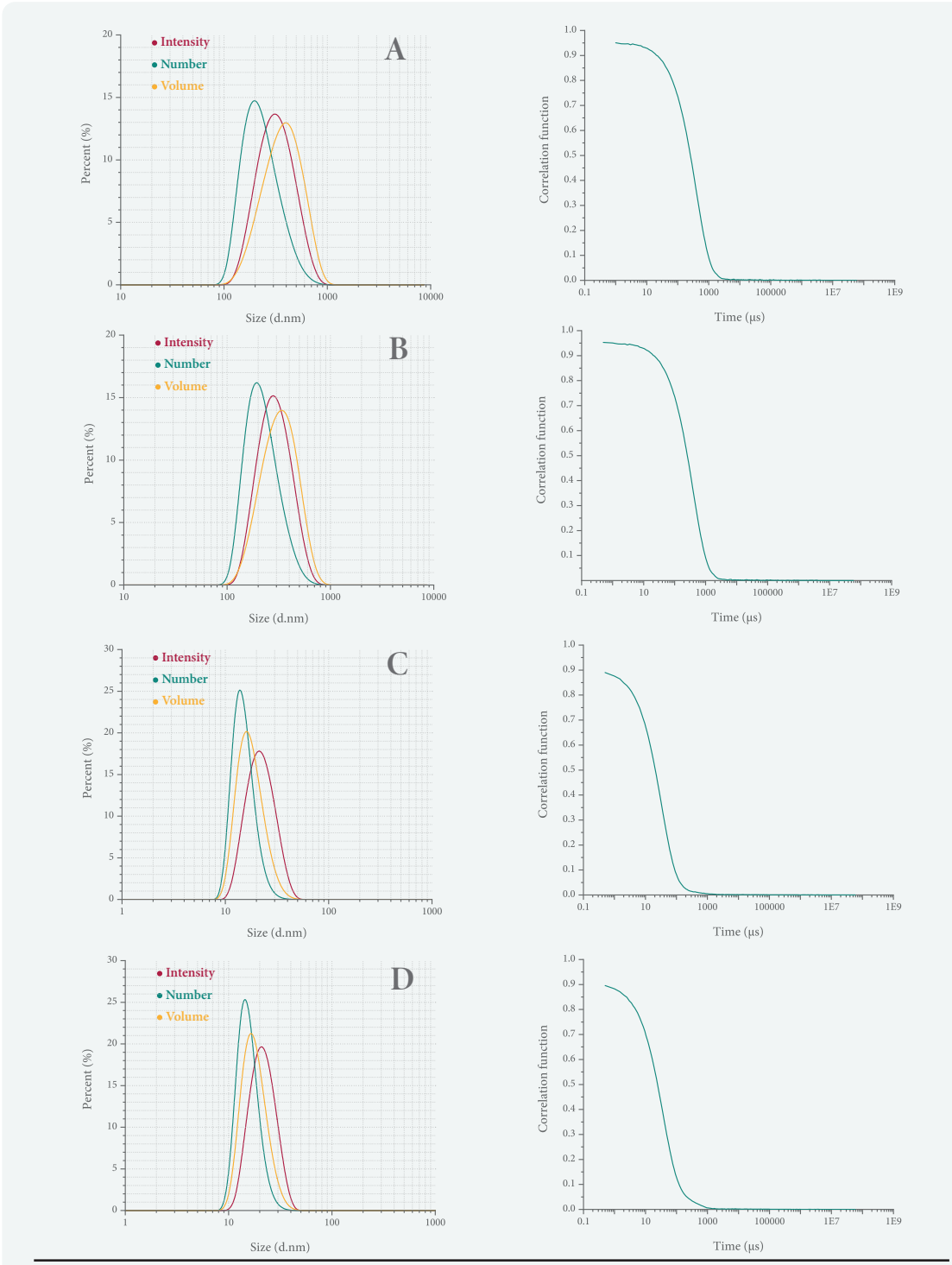

Fig 2.14. DLS size distribution of the four preparations and their corresponding correlograms **(A)** 1 wt% in THF. **(B)** 10 wt% in acetone. **(C)** 10 wt% in THF. **(D)** 10 wt% in acetone.

The concentrations used for both solvents had no apparent effect on the self-assembly. The results from the four samples can be summarised in Table 2.2.

Preparation	Z-average (d.nm)	PdI	Size distribution (d.nm)					
			Intensity	Std dev	Number	Std dev	Volume	Std dev
A	291.4	0.137	338.5	132.8	243.1	104.3	396.0	160.9
B	236.0	0.139	303.0	107.4	229.8	87.67	340.0	127.8
C	23.19	0.247	22.71	6.537	15.48	3.774	18.25	5.311
D	26.88	0.366	21.87	5.812	15.61	3.648	18.11	4.975

Table 2.2. Summery of size distribution data from DLS for the four self-assembly preparations.

Self-assembled morphologies were also examined using transmission electron microscopy (TEM). Samples were deposited on Formvar-coated copper grids and left to dry, and then they were negatively stained with 1% uranyl acetate for better contrasting. Figures 2.15 and 2.16 exhibit TEM images for the morphologies self-assembled in THF/water and acetone/water, respectively.

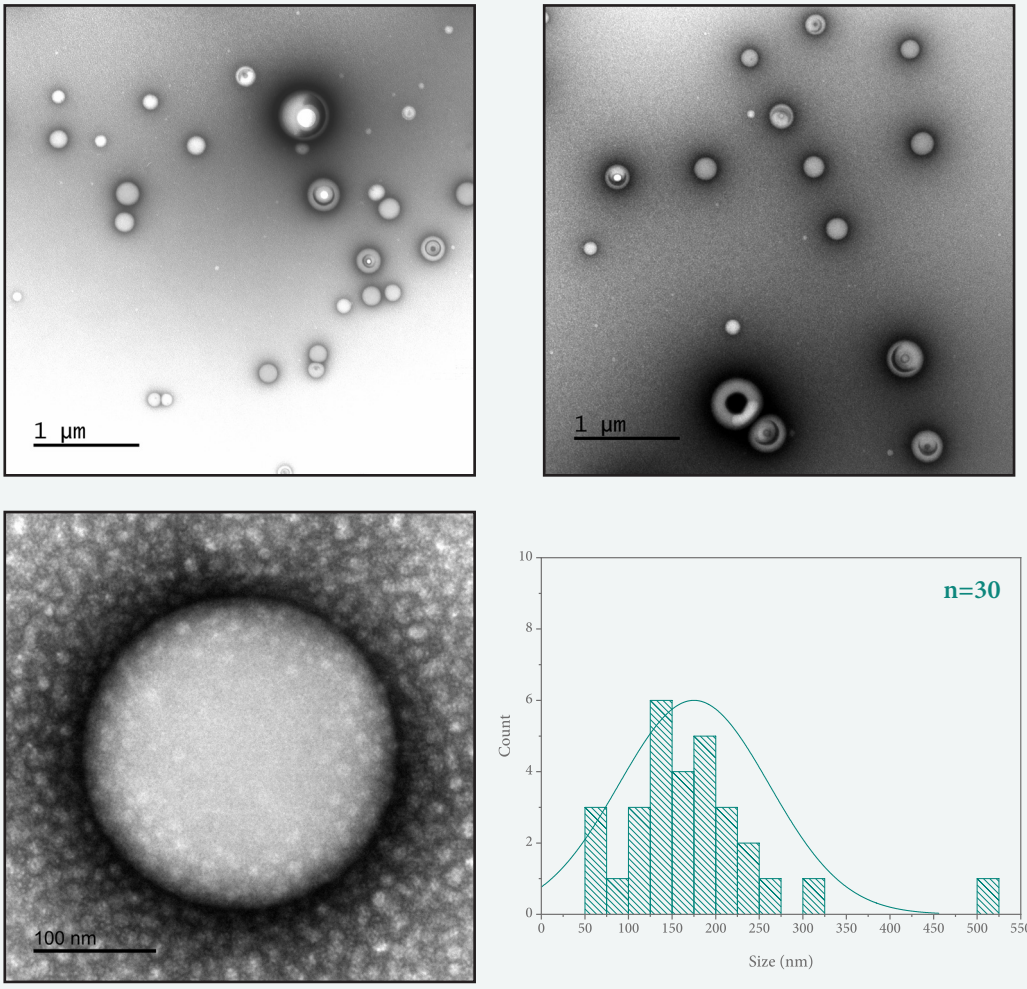

Fig 2.15. TEM images of self-assembled morphologies in THF/water.

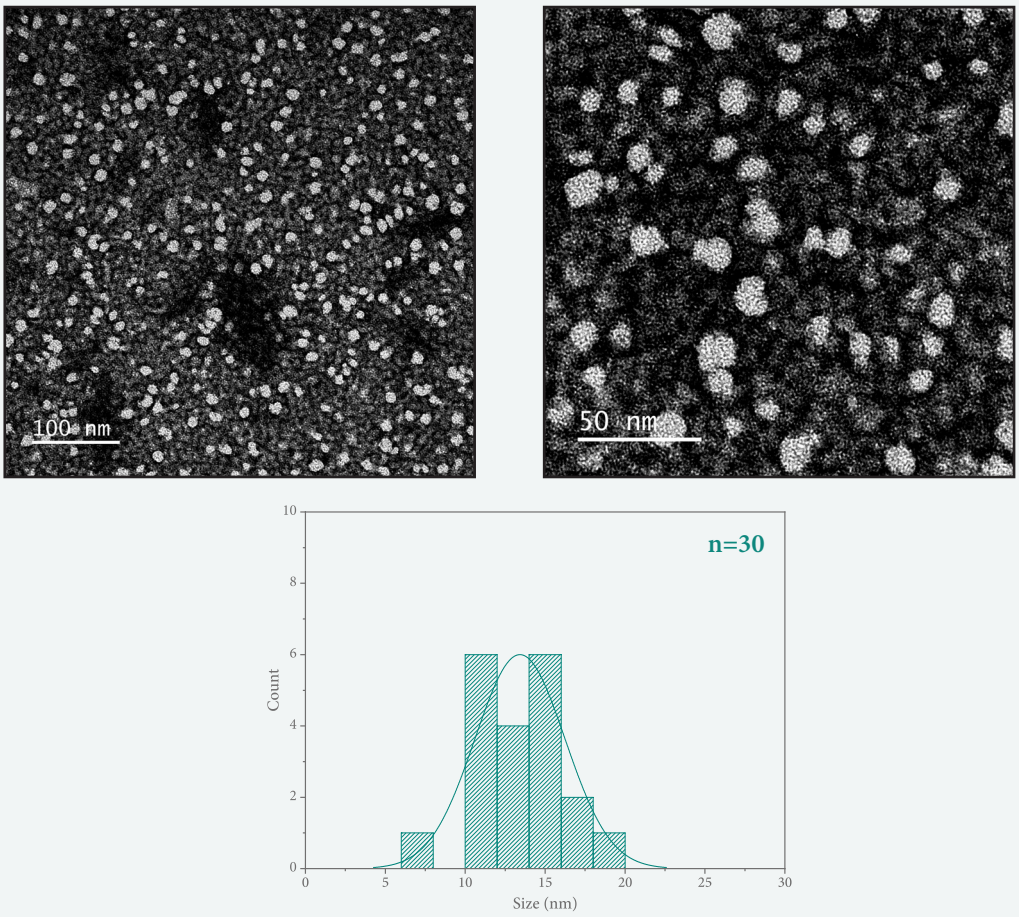

Fig 2.16. TEM images of self-assembled morphologies in acetone/water.

The morphologies resulting from the self-assembly of BCPs is theoretically governed by many factors, mainly the degree of polymerisation, Flory-Huggins interaction parameters (χ), and the volume fraction (*f*) of polymers relative to one another.[45,46]

Flory-Huggins parameter (χ) describes free energy and phase behaviour of polymer mixtures in the solutions and can be experimentally and mathematically calculated but its complexity increases as the number of the components in the system.[47] Self-assembly of (A-B) copolymer in a solvent-nonsolvent (S-N) mixture, for example, involves six χ parameters; χ_{AB}, χ_{AS}, χ_{AN}, χ_{BS}, χ_{BN}, and χ_{SN}, where each parameter determines the compatibility of one of the components with each of the other components in terms of solubility, miscibility, swelling, and molecular interactions. These, however, are challenging to measure and model.[45,47]

A more practical approach to explain the self-assembly behaviour is via the packing parameter (p). It is what primarily determines the morphologies resulting from self-assembly and is define by the equation:

$$p = \frac{v}{a_0 l_c}$$

where v is the volume of the hydrophobic chain, a_0 is the optimal area of the head group, and l_c is the length of the hydrophobic tail.[48] Adjusting the factors that affect p, such as the composition and concentration of the BCP, the common solvent, water content, and additives can result in different morphologies.[46] Figure (2.17) illustrates the morphological transition of self-assembled di-BCP in a solvent-nonsolvent system.

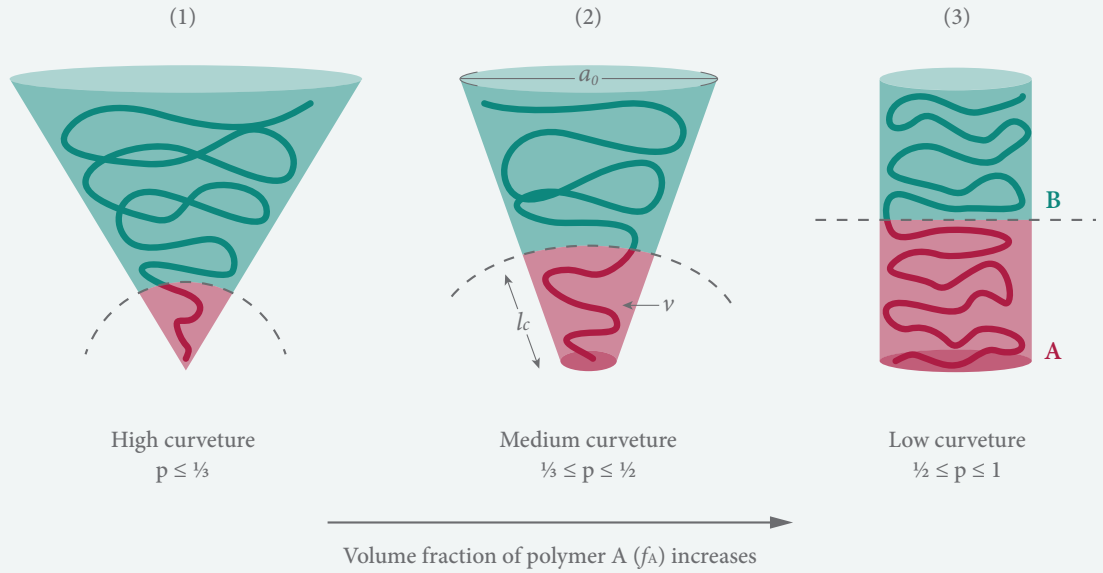

Fig 2.17. Packing parameter (p) and its effect on the self-assembly behaviour. Multiple factors affect the volume fraction of the core polymer A (f_A) and, subsequently, the packing paramater. Low values lead to sperical morphologies (1). As p value goes up, other morphologies like rods (2) then vesicles and lamellae (3) emerge. Adapted from [37].

In this work, self-assembly of the synthesised di-BCP was investigated in two solvent-nonsolvent systems, THF and acetone, each at two different concentrations, 1 and 10 wt%, of the BCP. The reasoning behind choosing these two common solvents is their differences in dissolving PSA (THF which was a good solvent for all chains versus acetone that dissolves only low chains) as well as having two different dielectric constants (ε = 7.5 for THF and 21 for acetone). It has also been demonstrated that these two solvents might produce different particle sizes on self-assembly of

BCPs depending on the chain length of each polymer.[49] In terms of concentrations used, the two points were chosen on the basis of preserving the potential therapeutic value of the NPs by not going below 0.1 wt% (after dilution during self-assembly) and avoiding high concentrations that would complicate self-assembly through possible precipitation.

While concentration did not have a role in the structure of the formed particles in the same solvent system, changing the common solvent resulted in a significant change in the size and morphology of the particles. DLS data shows a hydrodynamic diameter of around 25 nm for particles self-assembled in acetone/water versus 250-300 nm for those self-assembled in THF/water, both with Gaussian distribution. This was corroborated with TEM imaging with negative staining that showed spherical particles with similar diameters to those observed by DLS.

The differences in these morphologies can be explained in relation to the packing parameter (p) which is controlled by a force balance between three factors; the stretching of the hydrophobic polymer in the core, the surface tension between the core and the outside solvent, and the repulsion among the corona chains. Since the mPEG chains that constitute the corona of the particle are relatively long, its effect will be stronger than the other forces and it could be the main determinant of the morphology of the assembled particles.

In the case of the acetone/water system, acetone has a relatively high dielectric constant which causes the PEG chains to be relatively charged increasing the repulsion forces among these chains. This, in turn, increases the volume of the corona domain leading to more curvature upon self-assembly and the formation of spherical micelles (Figure 2.17). Since the corona chains are much longer than the core chains, the formed morphologies are "star-like" micelles as opposed to "crew-cut" micelles that would result from a configuration in which the hydrophobic chain is longer than the hydrophilic one.[50]

On the other hand, using a common solvent with a lower dielectric constant, like THF, reduces the inter-chain repulsion in the corona which decreases the effective volume of the corona and increases the volume fraction of the core polymer. The results in reducing curvature and causes the formation of bigger morphologies such as rods and, in this case, vesicles.[45]

Dissolution of the core polymer in the common solvent also plays a role in the morphologies resulting from self-assembly. During the addition of water, the solvent is still present in the hydrophobic domain, and if the core polymer has good solubility in this solvent, the core polymer chains will still have high mobility which leads to increased stretching and therefore and increased volume fraction of the core chains. Also, because of the high mobility of the chains in THF, the window between the critical water content (CWC, i.e. the amount of water corresponding with the critical micelle concentration, CMC), and the point at which morphologies become frozen is broad, which increases the chance for morphologies to change from spheres to rods and vesicles before the structures are frozen.[51] However, to better understand the relationship between the core polymer and the solvent and its effect on the self-assembly behaviour, the solubility parameter of PSA needs to be identified and compared in different solvents.

The vesicular nature of the morphologies formed in the THF/water system can be furtherly affirmed by the deformations that appear on some of the particles. In fact, it is common to encounter deformities such as slight indentations on the vesicles, or the vesicles appearing as stomatocytes or "kippah" structures. During preparation, the increase in water content, especially during quenching, causes an increase in water concentration outside the vesicles as opposed to their inside. This causes the diffusion of the solvent to the exterior of the vesicle and the water to its interior, but since the diffusion of the solvent through the hydrophobic portion of the wall is faster than that of the water, this creates a negative pressure inside the vesicle leading to indentations or the formation of stomatocytes. By the time the pressure has stabilised, the T_g of the hydrophobic part of the wall would have reached a level sufficient to preserve the vesicle in its deformed state.[52] Kippah deformations are especially encountered when vesicles are subjected to high vacuum without freezing, as the case in traditional TEM.[53] Figure 2.18 shows some of the deformations encountered with the synthesised vesicles.

Given their size and structure, the self-assembled vesicles seemed to be fitting for the main objective of the project for multiple reasons; firstly, the mean size of the vesicles is around the preferable size for particles that are intended for passive drug delivery to solid tumours through the EPR effect. Secondly, the particles have a PEG shell that would provide a hydration shield in biological fluids that would enhance the half-life of the particles. And finally, the internal phase of

the vesicles can be re-purposed to obtain added benefits from the particles such as entrapping the monomer in the internal phase to increase the payload of SA, loading another therapeutic agent as a combination therapy, adding a diagnostic agent so the NPs would serve a theranostic tool, or a combination of the above. This, of course, requires further investigation as any additional components in the solvent/nonsolvent system could influence the self-assembly process and produce different morphologies or affect the size of the vesicles.

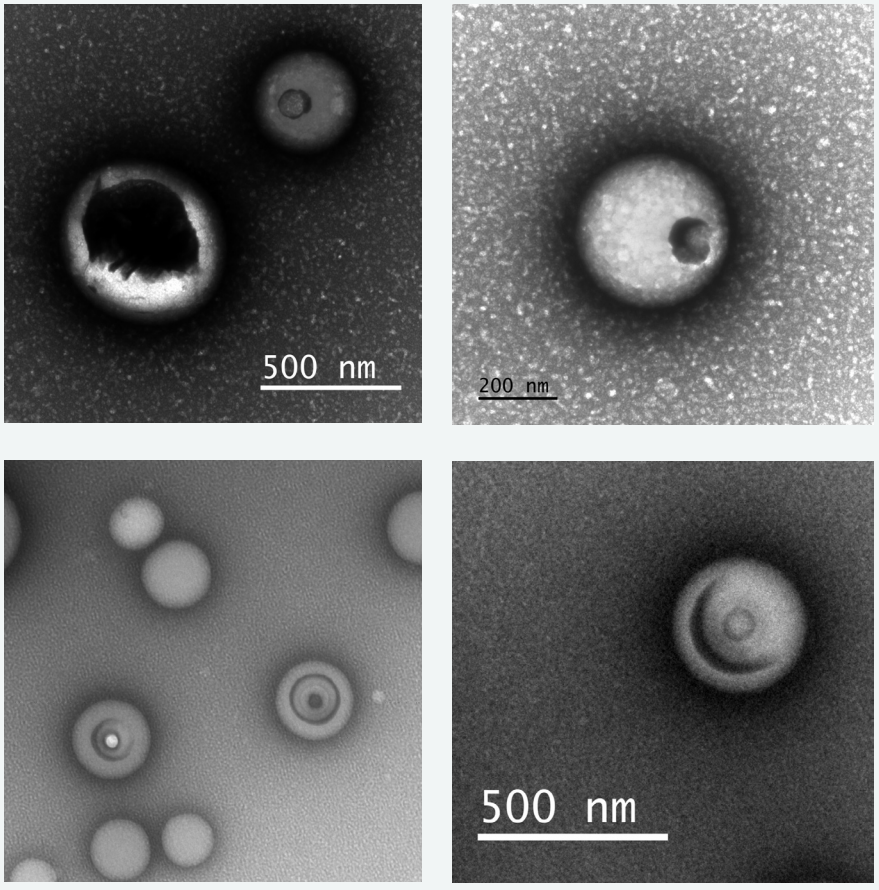

Fig 2.18. Some deformations observed on the vesicles. The images at the top showing indented and collapsed vesicles, while the images at the bottom show stomatocyte-like deformations.

Vesicles were hence the focus of the biological studies in Chapter 4, and for this reason, their stability was monitored over time. ζ-potential of the colloidal suspension was close to zero (-2.58 mV) which indicated poor colloidal stability.[54] The low charge in this buffer is expected since the outer shell of the corona consists manly of methoxy groups and the pH of the dispersant was close to 7. Nonetheless, DLS measurements of the same sample were consistent over the period of one month at room temperature and no change in size was recorded, which dismisses aggregation.

Only fine sedimentation was noted and simple reconstitution was all that was required before measurements. This could be explained by the robustness of the vesicular wall due to the high T_g of the PSA as well as the relatively high melting point of the mPEG used (52 °C) which helped preserve the structure of the particles. Figure 2.19 illustrate the ζ-potential of the vesicles and their size distribution change over time.

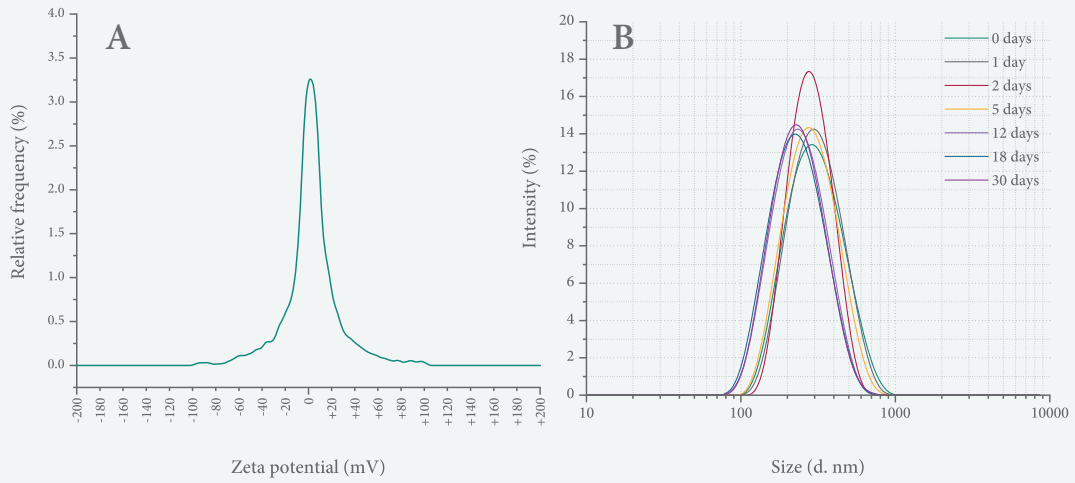

Fig 2.19. **(A)** zeta-potential measurement of vesicles prepared from THF/water. **(B)** Size distribution change over time as a function of intensity.

2.1.4.4. Degradation studies

Degradation of the PSA was investigated in biological and non-biological conditions. Water was used as a simple medium, 2 M NaOH as a strong alkaline hydrolysis agent, PBS as a simple buffer resembling that of biological fluids without their enzymatic components, FBS that mimics blood serum with its protein components, and PLE as a pure biological esterase.

Degradation was first investigated at 40 °C, close to normal average body temperature. In all media, except for NaOH, degradation was negligible. In the alkaline medium, SA release was noted in the early stages of the experiment with about 15%. More than half was released after 8 hours and degradation was complete after 24 hours. Figure 2.20 shows PSA degradation UV spectra in all media at 40° C.

To accelerate release from other media, the experiment was repeated at 70 °C. Degradation was again negligible in all media except for NaOH. This time, nearly half of SA was released after 2 hours and degradation was almost complete after 8 hours. Figure 2.21 shows PSA degradation UV spectra in all media at 70° C.

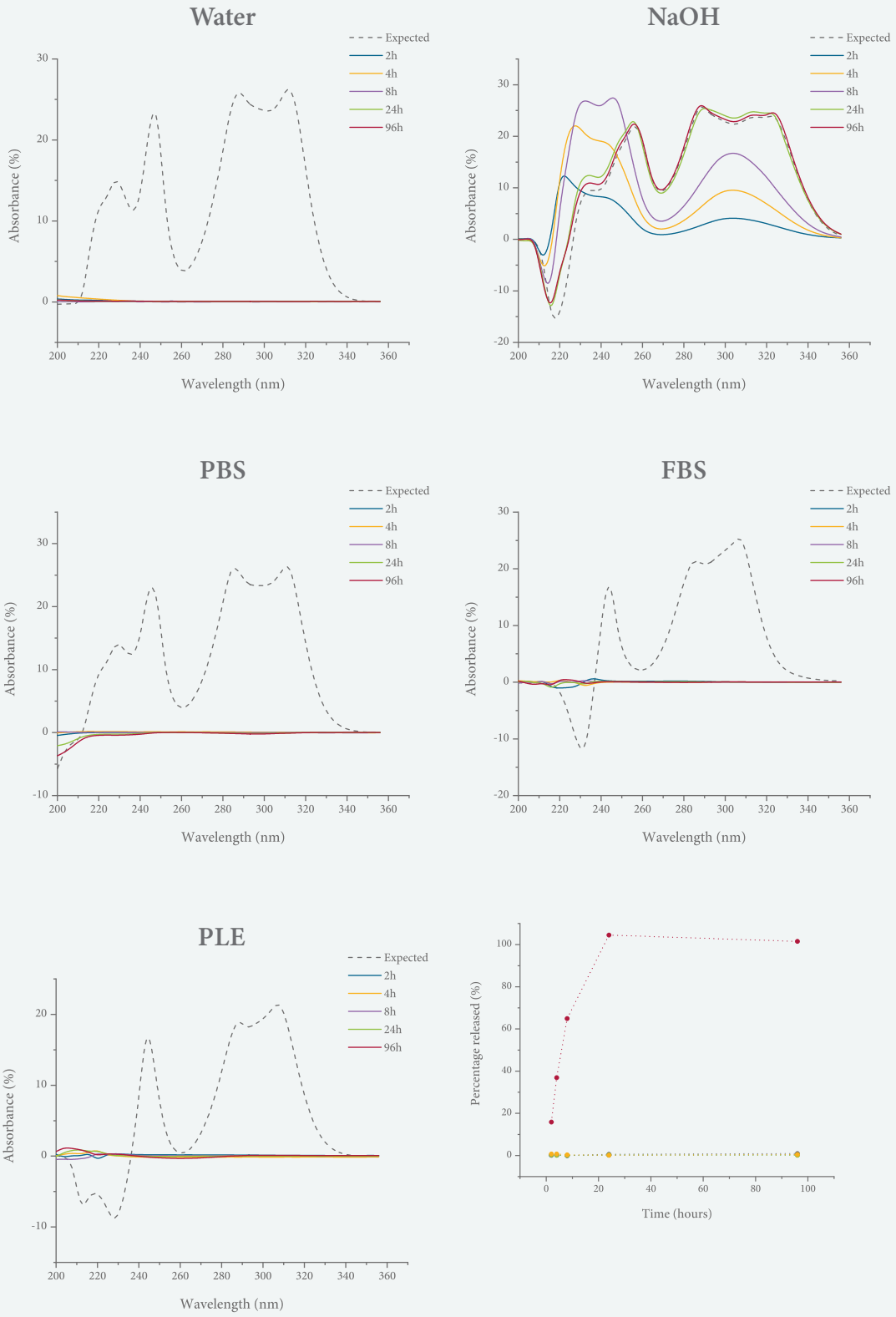

Fig 2.20. PSA degradation in different media at 40 °C. **PBS**: phosphate-buffered saline, **FBS**: foetal bovine serum, **PLE**: porcine liver esterase.

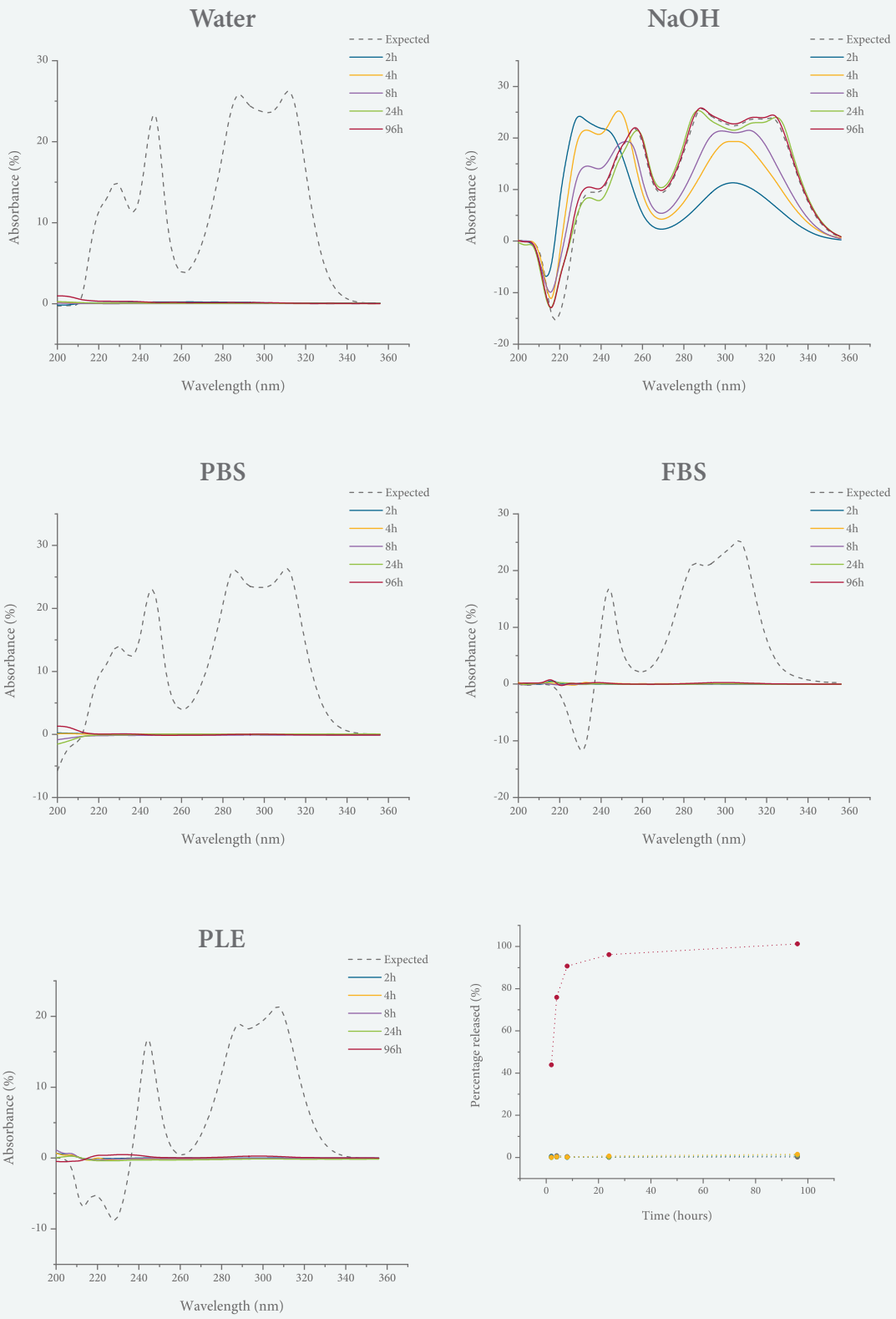

Fig 2.21. PSA degradation in different media at 70 °C. **PBS**: phosphate-buffered saline, **FBS**: foetal bovine serum, **PLE**: porcine liver esterase.

A third experiment was conducted at 90 °C. This time, a mediocre release of no more than 5% and 11% in water and PBS, respectively, was noted by the end of the experiment while the degradation was complete in NaOH after the first two hours. Figure 2.22 shows PSA degradation UV spectra in all media at 90° C.

What is worthy of note is that the polymer degraded by almost half in both FBS and PLE even though it would be expected that temperature would render hydrolytic enzymes inactive through denaturation. Nonetheless, it has been demonstrated that denaturing might have complicated pressure-dependent kinetics and that moderate pressure could prevent the inactivation of enzymes.[55] Since degradation experiments took place in the thermal cycler where there was a certain degree of increased pressure within the test vials, it is possible that similar kinetics preserved the enzymatic activity although it was not practically possible to measure it.

Furthermore, a possible explanation for why high temperature boosted the release of SA from the polymer is that polymers with high T_g have restricted chain mobility.[22] Increasing the temperature near to the T_g of PSA, which is around 100 °C, increased the chain mobility and accelerated the hydrolysis kinetics which promoted the release of SA.

Even though degradation was only possible in extreme conditions within the timeframe of the experiment, it might still be an indication that SA release could happen sustainably. This could be clinically beneficial if the PSA-loaded NPs were to reach solid tumours and be trapped within for prolonged periods of time through the EPR effect.

With the successful synthesis and characterisation of PSA-based NPs, this part of the project came to an end in order to allow time for the exploration of other possible polymeric nanodelivery systems; polyphosphoesters. Nonetheless, both PSA and the PSA-mPEG self-assembled NPs were tested later *in vitro* to investigate their biological effects on cancer cell lines, as presented in Chapter 4.

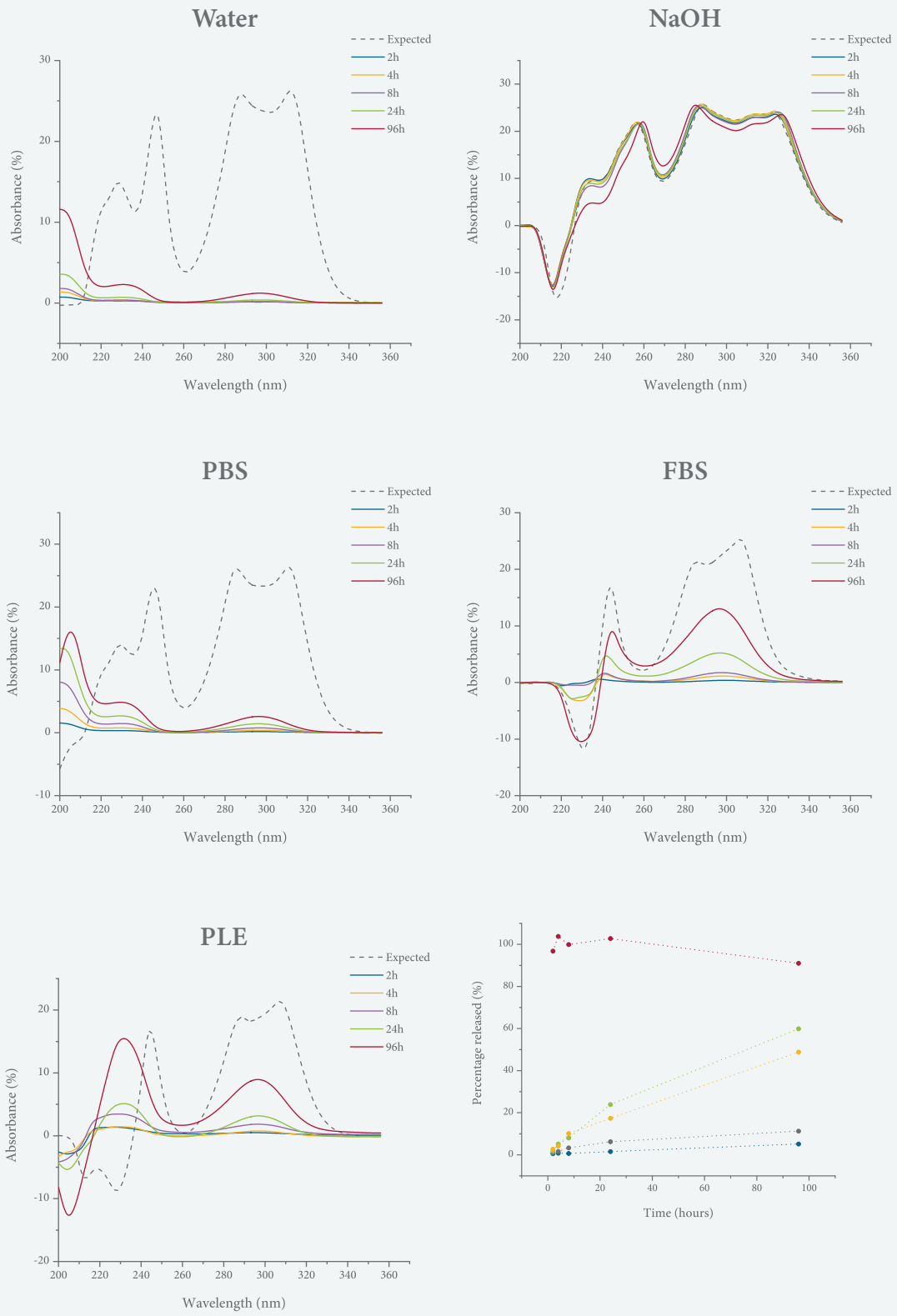

Fig 2.22. PSA degradation in different media at 90 °C. **PBS**: phosphate-buffered saline, **FBS**: foetal bovine serum, **PLE**: porcine liver esterase.

2.2. Polyphosphoesters (PPEs)

2.2.1. Introduction

Natural polyphosphoesters (PPEs) exist in all life forms since they constitute the structural backbone of the genetic material and they have a crucial role in the storage and release of energy in the biology.[56]

In contrast with other degradable linking groups, such as carboxylic acid esters, phosphoesters are the nature's selection when it comes to groups that are generally stable in physiological conditions yet degradable on demand. For example, genetic material needs to have stable enough linkage to preserve the genetic code throughout the life of the organism yet hydrolysable in a controlled manner when needed, and this is what is observed with phosphoester linker in living cells.[57] DNA and RNA, which are natural PPEs, owe their stability in their aqueous environment mainly to their phosphoester backbone. The negative charge of the phosphate groups makes the ester more resistant to hydrolysis.[58] The phosphate groups also help DNA bind to positively charged proteins called histones which stack together and ultimately coil into chromatin fibres. This process helps pack two metres of double-strand DNA inside the nucleus of the human cell.[59]

Natural phosphorus anhydrides are crucial for energy transfer and in metabolism. Adenosine triphosphate (ATP), a phosphorus anhydride conjugate, is considered the energy currency of the cell. Energy is reserved in the covalent bond between the phosphate groups, i.e. the pyrophosphate group, and is released when the bond is hydrolysed and ATP is converted to ADP, the diphosphate form. Likewise, the cell store energy by converting ADP to ATP.[60] Phosphate is also a part of the structure of the nicotinamide adenine dinucleotide (NAD^+/NADH) redox system that has an important role in metabolism.[61] Compared to carboxylic anhydrides, the negative charge on the phosphorus anhydrides gives them kinetic stability by slowing down the hydrolytic attack of water and other nucleophiles, yet they are thermodynamically unstable which, in the presence of proper catalysts (i.e. enzymes like phosphatases) drives chemical processes to completion.[58]

It is also worth mentioning that phosphate and its corresponding acids are an important part of the biological buffer system, and that inorganic polyphosphate is potentially involved in essential

blood coagulation and bone formation processes, hence phosphate is regarded as biologically benign, and in a degradable polymer system would be 'traceless'.[62,63] Figure 2.23 illustrates some of the important phosphorus-containing biomolecules.

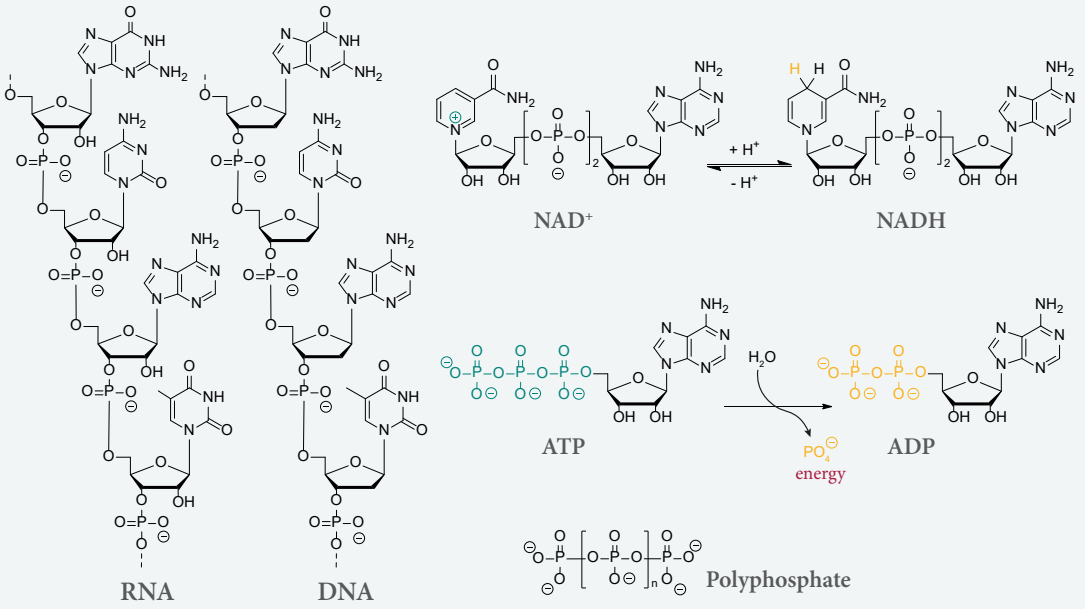

Fig 2.20. Prevalent natural PPEs that are essential for biological functions. RNA: ribonucleic acid; DNA: deoxyribonucleic acid, NADH/NAD⁺: nicotinamide adenine dinucleotide redox pair. ATP: adenosine triphosphate. ADP: adenosine diphosphate. Adapted from [57].

The prevalence of phosphate and its derivatives, phosphoric acid esters in particular, in humans gives synthetic PPEs a potential therapeutic value in terms of creating polymeric prodrugs that are biodegradable with low toxicity profile. Since phosphorous in phosphoric acid can form three stable divergent groups, it is possible to not only form stable polyesters but also functionalise the PPE with other moieties through side-chain modification. In this case, the moieties of interest are therapeutic agents.

Historically, PPEs are used as industrial flame-retardant additives to plastics but in recent years there has been an increasing academic interest in these polymers for biomedical applications. PPEs can be synthesised via multiple methods, the most important of which are:[56,57,64]

1- Polycondensation: The most widely used method to prepare general-purpose PPEs. It usually involves reacting phosphoric or phosphonic acid or their dihalide derivatives with a diol. However, the side reactions and the formation of cyclic polymers reduce the yield

and the molecular weight of the desired polymers. Incorporating functional groups post-polymerisation is also challenging.

2- Polyaddition: Typically, by reacting phosphoric acid dichlorides with bisepoxides or bisoxetans using onium salts as catalysts. This method results in PPEs with reactive chloromethyl pendant groups. However, the limitations of the starting materials make this method less popular compared to other methods.

3- Ring-opening polymerisation (ROP): Starting from a cyclic phosphate monomer, a catalysed ring-opening polymerisation can produce PPEs that differ in their hydrophilicity profiles depending on the pendant groups. The development of controlled (living) polymerisation mechanisms has allowed the production of not just linear, but branched, hyperbranched and cross-linked PPEs.

Because of their biocompatibility, degradability, and potentially-low toxicity, PPEs have been considered as a promising platform to overcome some of the challenges related to pharmacological therapy such as solubility, drug bioavailability, and targeted delivery. In fact, Wurm and his group demonstrated that nanocarriers coated with polyphosphoesters, specifically poly(ethyl ethylene phosphate) or PEEP, exhibit a stealth effect similar to that observed with PEG through the hydration shell that forms around the nanocarriers. This novel 'PPEylation' technique might prove superior to PEGylation in terms of safety since PPEs are degradable, unlike PEGs.[65,66]

The research regarding the synthesis of PPE-based therapeutics using the conventional polycondensation method is limited since, as discussed above, it could yield different side reaction and cyclic product. Conjugating drug molecules with the PPE backbone post-polymerisation is also difficult and requires certain conditions. Bogomilova *et al.* (Figure 2.24a), for example, managed to conjugate the anti-cancer drug melphalan to a PPE backbone under Atherton-Todd reaction conditions. The resulting PPE-melphalan conjugate had better water solubility and reduced toxicity while the drug's therapeutic efficacy was preserved.[67]

On the other hand, the literature is full of examples relating to ROP as it remains the preferred method in the synthesis of PPE-based biomaterials due to the ease of conjugating active moieties and the high structural control it allows as well as yielding polymers with high molecular weights and low polydispersities.[56]

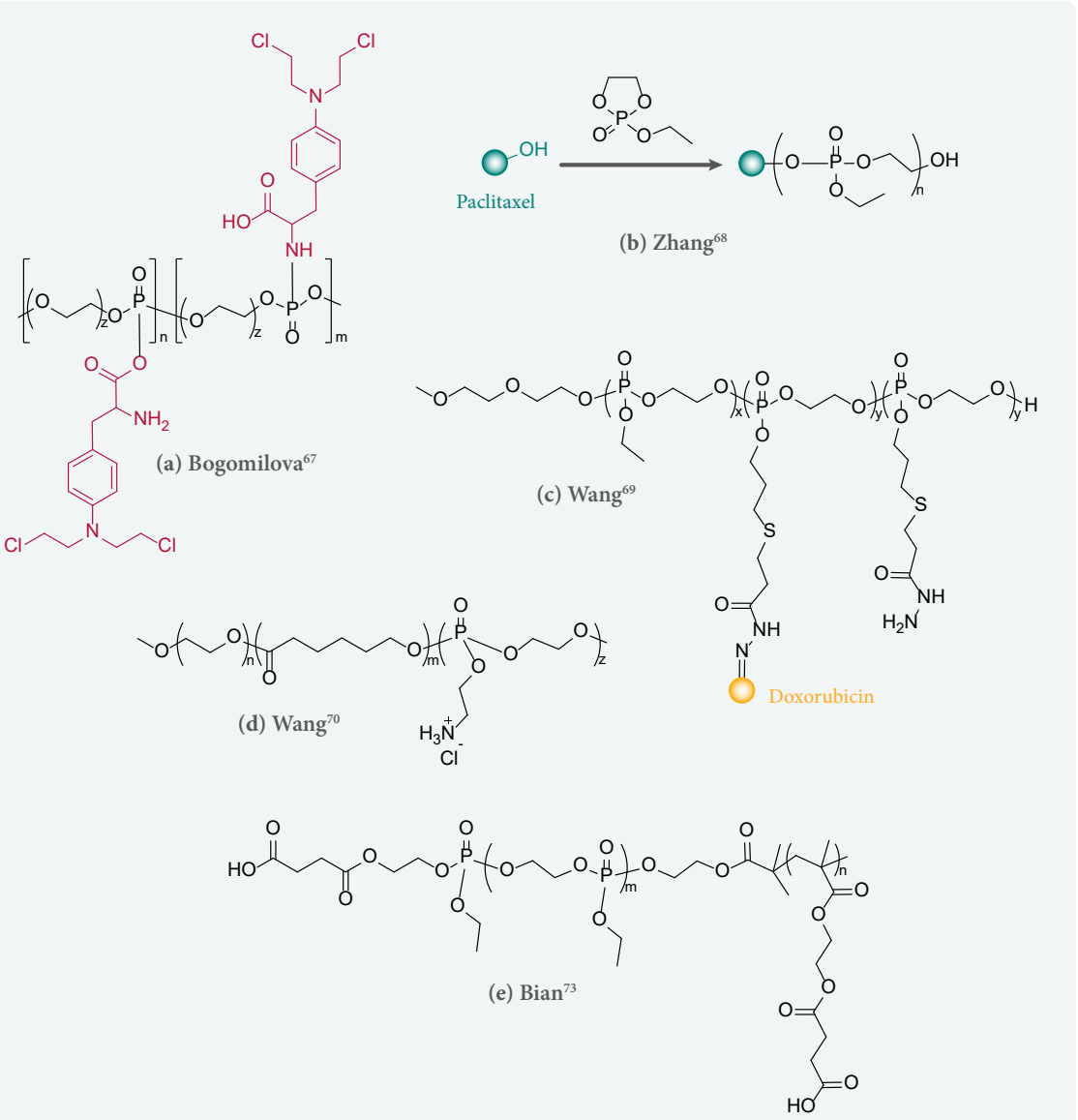

Fig 2.24. Some examples from the literature of PPEs in therapeutics. Only (a) is made via post-polymerisation modification and its purpose is to increase the solubility of the conjugated drug, melphalan. All the other examples are synthesised via ROP and they self-assemble to make NPs for the purposes of targeted therapy. In (b) and (c), the drug is part of the amphiphilic chain, while (d) and (e) are used for entrapping the drug on self-assembly.

Using this method, a wide array of drug-loaded NPs have been synthesised. For example, Zhang *et al.* (Figure 2.24b) used the anti-tumour drug, paclitaxel (PAX), as the initiator for the ROP reaction to create a PAX-PEEP conjugate that could then self-assemble into polymeric micelles with the drug being at the core of the micelles.[68] Wang and his group had different approaches in designing delivery systems for anti-cancer drugs. On the one hand, they created a PEG-PEEP copolymer via ROP then conjugated the cytotoxic drug, doxorubicin, on the pendant groups through labile hydrazone bonds (Figure 2.24c). The BCP was amphiphilic and could self-assemble into micelles.[69]

On the other hand, they also used ROP to make BCPs that did not have the therapeutic moiety in the polymer structure (Figure 2.24d). Instead, the BCPs comprised of poly(ethylene glycol)-b-poly(ε-caprolactone)-b-poly(2-aminoethyl ethylene phosphate). This PEG-PLC-PPEEA cationic amphiphilic triblock copolymer self-assembled into micelles that had a positive surface charge that could be used to load anti-cancer small interfering RNA (siRNA) after the self-assembly.[70] The group also used the same method to create multifunctional micelles that are capable of delivering both siRNA and PAX, the latter being loaded in the micelles' core during self-assembly.[71] ROP has also been used to create non-ionic, anionic, cationic, and zwitterionic micelles by manipulating the pendant groups on the phosphorus atom of the cyclic phospholane monomer precursor.[72]

The only example that could be found in the literature related to the use of PPE-based NPs for the delivery of NSAIDs was of a ROP-synthesised PPE amphiphilic copolymer that self-assembles in aqueous conditions into micelles that are used to encapsulate the NSAID naproxen (Figure 2.24e).[73]

In this section of the project, the prospect of using ROP to make a PPE that has ibuprofen (IBU) linked to it through pendant ester groups for the targeted delivery of the NSAID was explored.

2.2.2. Materials and instrumentation

4-Isobutyl-α-methylphenylacetic acid (ibuprofen), 1,8-diazabicyclo[5.4.0]undec-7-ene (DBU), and 1-(3-Dimethylaminopropyl)-3-ethylcarbodiimide hydrochloride (EDC HCl) were obtained from Alfa Aesar. Solketal, benzyl alcohol, and phosphorus oxychloride were obtained from Acros Organics. 4-dimethylaminopyridine (DMAP) was obtained from Fluorochem**.**

NMR spectra were obtained on a Bruker AV2 400 MHz spectrometer and were calibrated to the centre of the set solvent peak and chemical shifts were reported in parts per million (ppm).

Gel permeation chromatography (GPC) was conducted using PL-GPC 50 Plus system by Varian Inc. The separation media consisted of two Agilent (300x 7.5 mm) 5μm MIXED-C columns in series in a 40 °C oven. Refractive index was used for the detector and THF, stabilised with 250 ppm BHT, was the eluent. The flow rate was set at 1 mL/min and the sample run time was 25 minutes.

2.2.3. Experimental

2.2.3.1. Ibuprofen-solketal ester

2 equivalents EDC in dry DCM was added to a well-stirred solution of IBU in dry DCM in an ice bath. 2 equivalents of DMAP was added to the reaction mixture and then 3 equivalents of solketal was added as well. The reaction was left stirring overnight. The solvent was then removed and the mixture was re-dissolved in di-ethyl ether and washed with 2M HCl, then three times with water and once with brine. The organic layer was dried over magnesium sulphate, filtered, and dried *in vacuo* to leave a colourless viscous liquid (97% yield). ^{1}H NMR (400 MHz, $CDCl_3$) δ (ppm): 7.20 (d, J = 8.1 Hz, 2H), 7.09 (d, J = 8.4 Hz, 2H), 4.24 (m, 1H), 4.12 (m, 2H), 3.95 (m, 1H), 3.73 (qd, J = 7.2, 1.1 Hz, 1H), 3.63 (m, 1H), 2.44 (d, J = 7.2 Hz, 2H), 1.84 (dt, J = 13.5, 6.8 Hz, 1H), 1.50 (d, J = 7.2 Hz, 3H), 1.35 (d, J = 12.6 Hz, 6H), 0.89 (d, J = 6.6 Hz, 6H). ^{13}C NMR (100 MHz, $CDCl_3$) δ (ppm): 174.62, 140.75, 137.60, 129.46, 127.26, 109.81, 73.60, 66.30, 64.85, 45.12, 30.29, 26.71, 25.52, 22.48, 18.54.

2.2.3.2. Deprotection (glyceryl ibuprofen)

The product from the previous step was mixed with 30 mL of 80% acetic acid for 20 min. The formation of the diol was tracked using a TLC plate. After the conversion was complete, di-ethyl ether was added and the mixture was moved to a separation funnel. The organic layer was washed with saturated potassium carbonate solution, water, and brine. The organic layer was dried over magnesium sulphate, filtered, and dried *in vacuo* to leave a colourless viscous liquid (89.9% yield). ^{1}H NMR (400 MHz, $CDCl_3$) δ (ppm): 7.19 (d, J = 8.1 Hz, 2H), 7.10 (d, J = 8.2 Hz, 2H), 4.12 (m, 2H), 3.82 (m, 1H), 3.73 (q, J = 7.2 Hz, 1H), 3.55 (m, 1H), 3.43 (m, 1H), 2.51 (s, 2H), 2.44 (d, J = 7.2 Hz, 2H), 1.83 (dt, J = 13.5, 6.8 Hz, 1H), 1.49 (d, J = 7.2 Hz, 3H), 0.89 (d, J = 6.7 Hz, 6H). ^{13}C NMR (100 MHz, $CDCl_3$) δ (ppm): 175.24, 140.86, 137.41, 129.49, 127.10, 70.07, 65.41, 63.18, 45.03, 30.21, 22.39, 18.32.

2.2.3.3. Cyclic phosphate-ibuprofen ester monomer

In a flame-dried, three-neck round-bottom flask, 15 mL of dry toluene was stirred under an influx of nitrogen and the reaction flask was cooled to around -10 °C using an ice/salt bath. Glyceryl ibuprofen (1 mmol) in 5 mL of dry toluene was added slowly and simultaneously with phosphorus oxychloride (1 mmol) in 5 mL of dry toluene to the flask and was then left stirring for 4 hours. The

reaction was then quenched with about 50 mL of dry MeOH and stirred overnight. The solvent was then evaporated and the product was further dried *in vacuo* to leave a yellowish transparent viscous liquid. ^{1}H NMR (400 MHz, CDCl3) δ (ppm): 7.17 (m, 2H), 7.09 (m, 2H), 4.16 (m, 1H), 4.02 (m, 2H), 3.74 (m, 5H), 3.50 (m, 1H), 2.44 (m, 2H), 1.83 (dt, J = 13.4, 6.7, 3.1 Hz, 1H), 1.49 (m, 3H), 0.89 (m, 6H). ^{13}C NMR (100 MHz, CDCl3) δ (ppm): 175.34, 141.00, 137.54, 129.62, 127.26, 70.19, 65.58, 63.27, 54.57, 52.16, 45.12, 30.33, 22.50, 18.76. ^{31}P NMR (160 MHz, $CDCl_3$) δ (ppm): 2.48.

2.2.3.4. ROP of the cyclic monomer

In a flame-dried round-bottom flask, the cyclic monomer (280 mmol) was dissolved in 10 mL of dry DCM and stirred. The flask was cooled to 0 °C in an ice bath, and then benzyl alcohol (2.8 mmol) in dry DCM and DBU (4.2 mmol) in dry DCM were added to the flask and left to stir for 6 hours.

2.2.4. Results and discussion

2.2.4.1. Ibuprofen-solketal ester

The proposed polymer comprised of phosphoester polymer with IBU linked to the phosphate groups of the chain through pendant ester groups. Since ROP provides the possibility of attaching the therapeutic molecule to the monomer through the prospective pendant groups, it was logical to have this as a starting point rather than making the PPE then doing a post-polymerisation modification.

Two main things had to be considered towards the making of the monomer that will be used for polymerisation. Firstly, a simple diol carbon chain whose hydroxyl groups are separated by two or three carbons in order to make the five- or six-member cyclic phosphate needed for the ROP. Secondly, the chain must also have a functional group to attach the IBU through a bond cleavable in biological conditions. Since IBU has one functional group which is a carboxyl group, an ester linker was believed to be the most suitable for this purpose, especially that the ester group is inherently biocompatible and could degrade through hydrolysis to release the drug under certain biological conditions. Therefore, glycerol seemed to be the most appropriate choice for making the molecule that linked IBU to the cyclic phosphate. Glycerol is also naturally-occurring and is used

by many tissues for the biosynthesis of triglycerides (or triacylglycerols), the major energy storage form, and by the liver for the gluconeogenesis, i.e. the production of glucose.[74,75]

Hence, the final degradation products of the proposed polymer would be the drug and two benign components, phosphate and glycerol, which is optimal for a drug delivery system.

Since esterification was required on one hydroxy group while the other two were supposed to be preserved for making the cyclic phosphate, it was necessary to temporarily protect two of the groups before esterification. This was attempted by converting glycerol to solketal (2,2-dimethyl-4-hydroxymethyl-1,3-dioxolane) via the condensation of glycerol with the readily available acetone.

Glycerol was refluxed with an excess of acetone and p-toluenesulfonic acid was used as a catalyst. To push the reversible reaction towards the favourable direction, the reaction was done in toluene with a Dean-Stark apparatus attached to continuously remove water from the reaction medium. Purification was then attempted via fractional distillation (boiling points are 189 °C and 290 °C for solketal and glycerol, respectively) and multiple attempts failed to separate the solketal.

It was then found to be more efficient to use the commercially available solketal. Esterification of solketal with IBU was straightforward and it was achieved via Steglich esterification using EDC and DMAP (Figure 2.25).

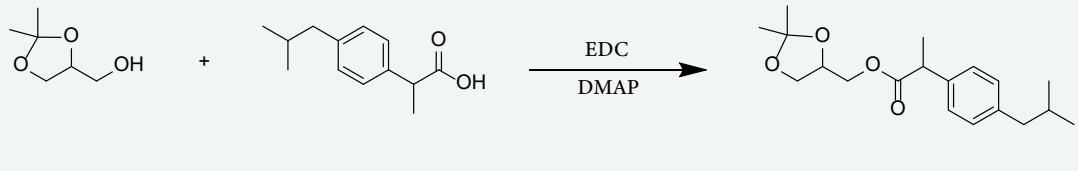

Fig 2.25. Reaction scheme for making the ibuprofen-solketal ester.

Esterification was investigated using ^{1}H-NMR of the final product after purification. Integrating the peak at 1.35 ppm belonging to the two methyl groups on the solketal end with either the side methyl at 1.49 ppm or end methyl groups at 0.89 ppm belonging to the ibuprofen showed an coupling of 1:1.05 indicative of a highly pure product. Figures 2.26 and 2.27 exhibit the ^{1}H-NMR and ^{13}C-NMR spectra of the ester, respectively.

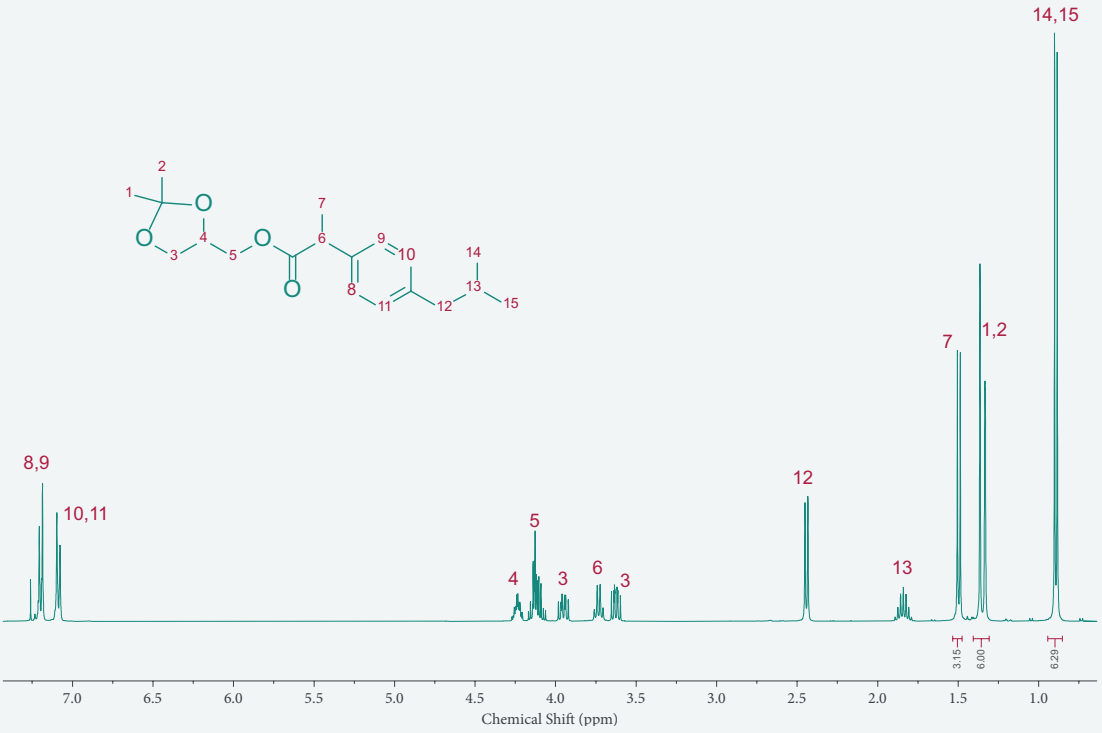

Fig 2.26. ^{1}H-NMR ($CDCl_3$) spectrum of the solketal-ibuprofen ester.

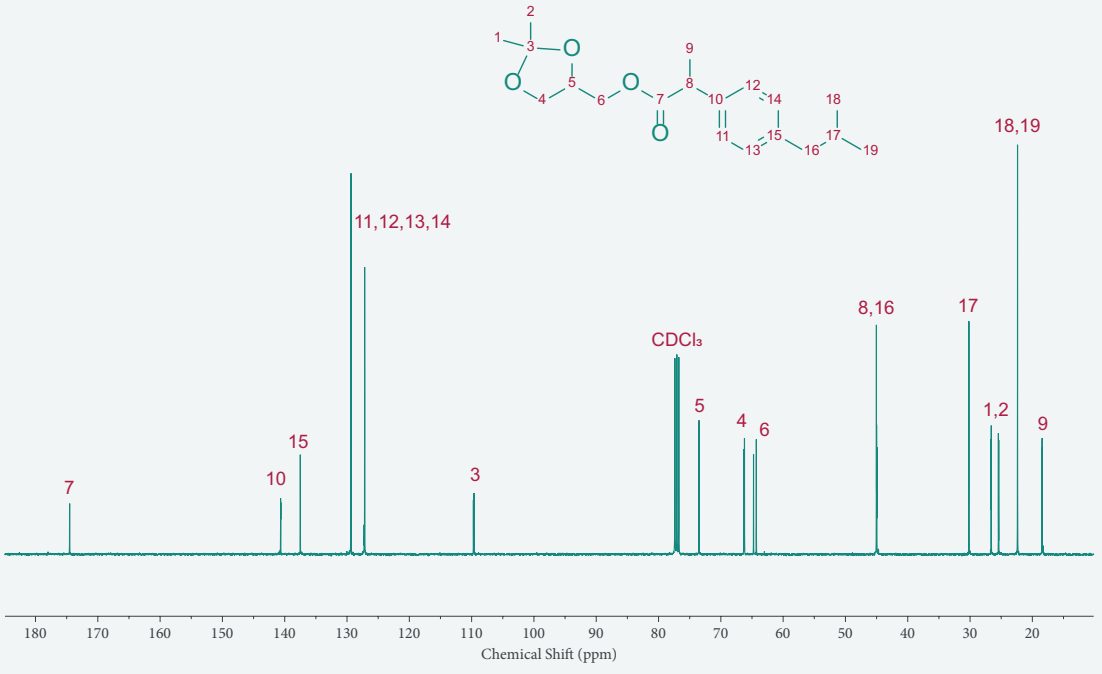

Fig 2.27. ^{13}C-NMR ($CDCl_3$) spectrum of the solketal-ibuprofen ester.

2.2.4.2. Deprotection (glyceryl ibuprofen)

Acid hydrolysis was used to obtain the diol after the esterification of IBU. Different agents in different conditions were investigated to achieve complete deprotection of the hydroxyl groups and

progress was tracked using TLC plates. At first, the compound was stirred at room temperature for a few hours with different concentrations of hydrochloric acid (1, 2, and 3 M) but the deprotection was incomplete in all three cases. Increasing the temperature to 50 °C did not give better results. Fearing that increasing the temperature any further with HCl will cause the hydrolysis of the IBU ester, acetic acid was used instead. At room temperature, mixing the compound with 80% acetic acid yielded barely any noticeable deprotection, but refluxing the mixture at 130 °C for 20-30 minutes resulted in the full deprotection of the diol (Figure 2.28).

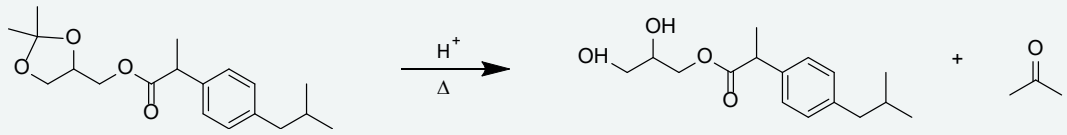

Fig 2.28. Reaction scheme for making the ibuprofen-solketal ester.

^{1}H-NMR analysis of the pure product exhibited the complete disappearance of the peak at 1.35 ppm of the two methyl groups that belonged to the solketal and the emergence of a single peak at 2.51 ppm representing the deprotected hydroxyl groups. The integration of the this peak with the end methyl groups of the ibuprofen was approximately 1:3 indicating the presence of two hydroxyl protons and, therefore, complete deprotection. Figures 2.29 and 2.30 illustrate the ^{1}H-NMR and ^{13}C-NMR spectra of glyceryl ibuprofen, respectively.

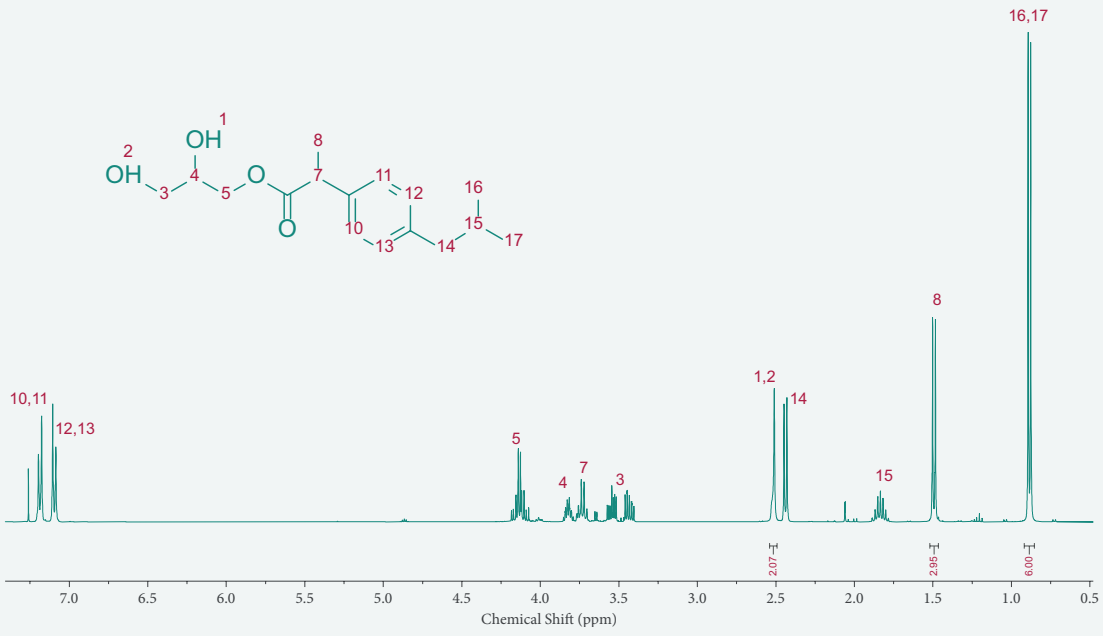

Fig 2.29. ^{1}H-NMR ($CDCl_3$) spectrum of glyceryl ibuprofen.

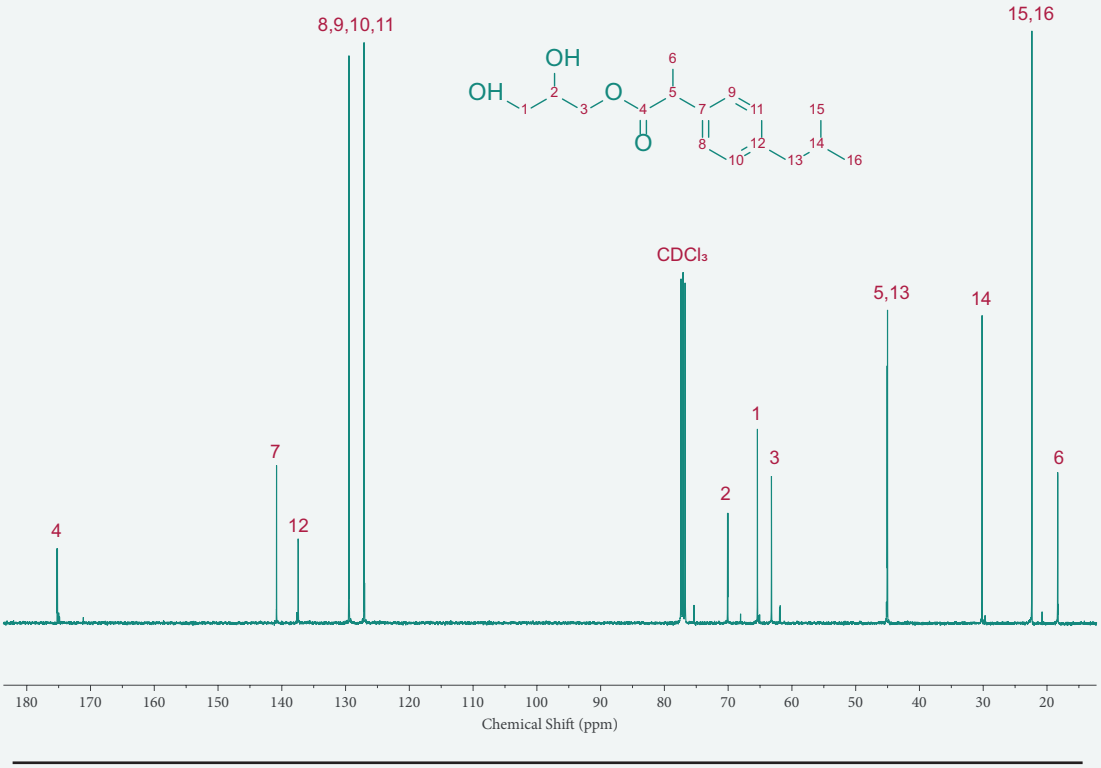

Fig 2.30. ^{13}C-NMR ($CDCl_3$) spectrum of glyceryl ibuprofen.

2.2.4.3. Cyclic phosphoester monomer

The best candidates to use as monomers for ROP when making PPEs are five- and six-member strained cyclic phosphoesters, and although both tri- and pentavalent phosphorus can be used, it is worth noting that trivalent monomers can only be polymerised using cationic initiators while pentavalent ones are polymerisable by a wider array of mechanisms (anionic, cationic, organocatalysis, metallic catalysis).[57]

The cyclic phosphoester polymer (CPM) was synthesised by reacting the glyceryl ibuprofen diol with phosphoryl chloride using equimolar concentrations while slowly adding the two compounds simultaneously at a slow rate to a cold flask to ensure that the end product is a cyclic phosphoester rather than a linear di-phosphoester (Figure 2.31).

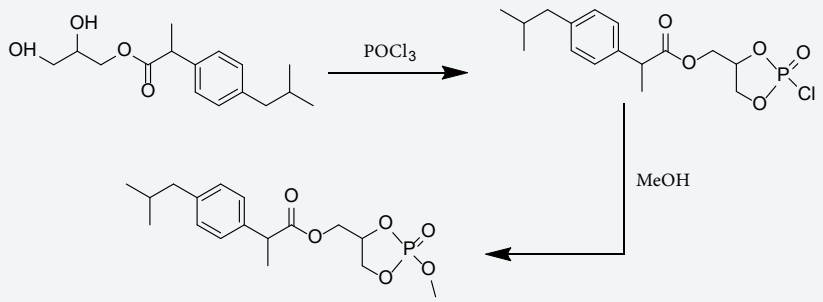

Fig 2.31. Reaction scheme for making the cyclic phospate monomer.

Since the remaining chloride on the cyclic phosphoester was not needed for making pendant groups with any specific function in the final PPE, the pendant arm was capped with a methoxy group that would presumably have a minimal effect on the PPE solubility.[76] A bulkier group would also hinder the accessibility to the ester groups which delays hydrolysis and the subsequent drug release. Typically, this reaction is done using methanol with the presence of a base such as triethylamine or pyridine,[77] but due to the sensitive nature of the ester bond that attaches the IBU to the cyclic phosphoester, the reaction was only quenched with methanol and left to stir for several hours.

^{1}H-NMR analysis of the CPM exhibited the appearance of a new peak around 3.7 ppm corresponding to the methoxy group. Since it was difficult to isolate the methoxy peak from other surrounding peaks, integration was calculated for the whole region between 3.30 and 4.21 ppm which contains, in theory, the peaks of nine protons. Integration value was 8.27 (Figure 2.32). ^{13}C-NMR spectrum exhibited peaks corresponding with the target CPM molecule (Figure 2.33).

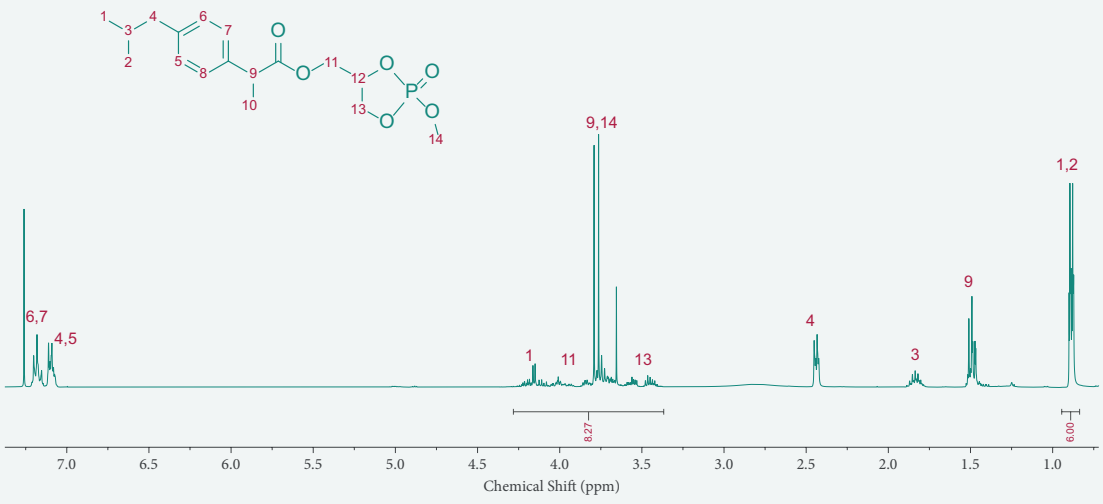

Fig 2.32. ^{1}H-NMR ($CDCl_3$) spectrum of the cyclic phosphate monomer.

$^{31}P\{^{1}H\}$-NMR analysis, on the other hand, was not indicative to any specific phosphate species as the spectrum showed a single peak at 2.48 ppm (Figure 2.34). Compared with the literature, the chemical shift for a cyclic phosphate with a pentavalent phosphorus is around 20 ppm, although these examples are of simple cyclic phosphate molecules.[78,79]

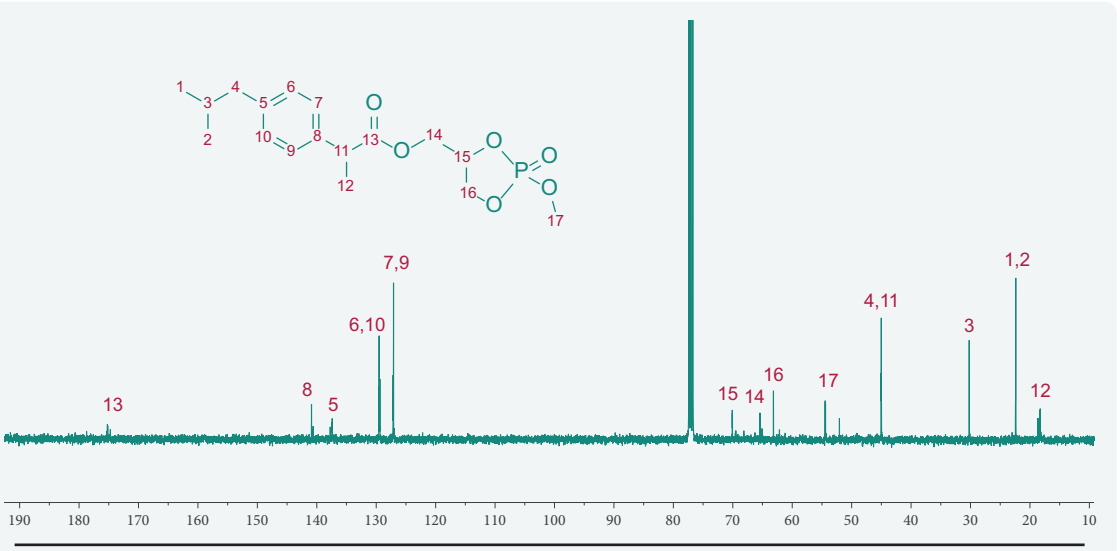

Fig 2.33. ^{13}C-NMR ($CDCl_3$) spectrum of the cyclic phosphate monomer.

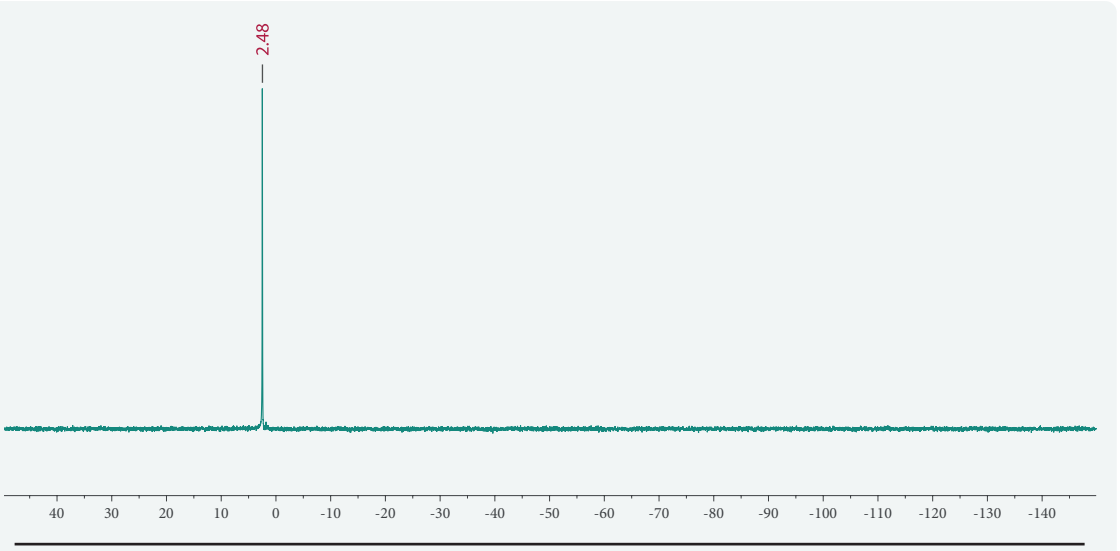

Fig 2.34. $^{31}P\{^{1}H\}$-NMR ($CDCl_3$) spectrum of the cyclic phosphate monomer.

2.2.4.4. Ring-opening polymerisation (ROP)

The synthesis of PPE through ROP was pioneered by Penczek and co-workers in the 1970s through different anionic, cationic, and enzymatic pathways, but it was not until later that well-defined polymers with controlled molecular weights could be achieved through metallic catalysis

and organocatalysis.[77] Since a metal catalyst is not favourable for the synthesis of PPE intended for biomedical applications, an organocatalyst, DBU, is used instead. This kind of catalysis also allows good control over the molecular weight and polydispersity of the polymers.[80]

A simple alcohol is used as an initiator for the ROP. The organocatalyst acts as an acceptor to the hydroxyl proton of the alcohol. The nucleophilic oxygen will, in turn, attack the P=O double bond followed by the breaking of one of the single P-O bonds and the opening of the ring. The newly-formed nucleophilic oxygen at the end of the chain will then propagate the polymerisation reaction on other cyclic monomers and the reaction can be eventually terminated by the addition of an acid.[81]

In this work, benzyl alcohol was used as the initiator, and the reaction was done with the molar ratio of 100/1/1.5 for CPM/DBU/Benzyl alcohol (Figure 2.35). The reaction was monitored using GPC, ^{1}H-NMR, and ^{31}P-NMR.

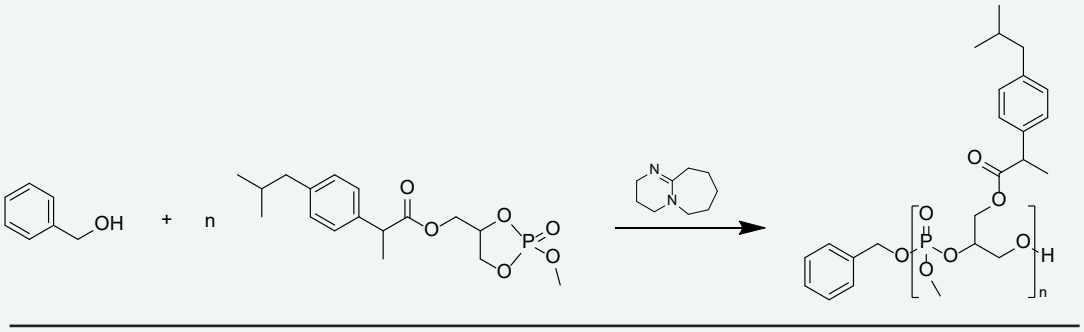

Fig 2.35. Reaction scheme for the ROP.

Even after several hours of running the reaction, no peaks could be detected when analysing the reaction mixture by GPC. NMR spectra did not show any significant changes either. It would be expected, if polymerisation was successful, that the ^{1}H-NMR spectrum would exhibit peak broadening and the ^{31}P-NMR would show new peaks indicative of the presence of PPE as such polymers usually show resonances at $\delta < 0.00$.[77]

The most probable explanation for the failure of the polymerisation is that the synthesised monomer is not a cyclic phosphate. In fact, the ^{31}P-NMR peak of the monomer spectrum falls in a range that could include other phosphorous species of which that is of relevance are dichloro-phosphoester, i.e. $O=P(OR)X_2$, and chloro- diphosophoester, i.e. $O=P(OR_2)X$.

Having low yields and impure cyclic monomers with the method used here (with phosphorus oxychloride) is indeed mentioned in the literature as a common issue. This is why the often used method in making CPMs is via using phosphorus trichloride for ring closure and the subsequent oxidation via heating in benzene with oxygen influx.[57,77] This method was not followed for safety concerns. Another explanation for the possible absence of a CPM is the poor stability of the highly strained five-membered CPMs which requires cautious handling.[79] The time limit of the project did not allow for further attempts to optimise the polymerisation reaction.

2.3. Conclusion

Based on the potential role of salicylic acid as a chemopreventive and chemotherapeutic agent, the synthesis of polymeric prodrugs that have high payloads of the active moiety was investigated. An already existing salicylic acid polymer was re-purposed in a manner that was not tried before.

An amphiphilic BCP (PSA-mPEG) was synthesised and could self-assemble in water to create different morphologies with different sizes. The assembled NPs were within the desired size range for the targeted therapy of solid tumours through the EPR effect. They also possessed a PEG shield that would prolong their circulation half-life and enhance the pharmacokinetic profile of the active drug. The polymeric core proved to be degradable in different biological and non-biological media in accelerated conditions. This suggests that degradation *in vivo* might happen at a much slower rate, which is favourable for the sustained release of the drug in tumours leading to even lower toxicity, less frequent administration, and a better preventive role against metastasis.[83]

The loading capacity of the synthesised NPs for SA could still be possibly improved by using longer homopolymer chains. The main barrier against making BCPs with longer polysalicylate chains was possibly the formation of cyclic chains or double-capped chains that prevented conjugation. It was implied in the patent adopted to make the polymer that temperature was the main parameter that determined the characteristics of the desired polymer, but it appears that the stoichiometry of the reaction might be quite as important.

Nonetheless, the synthesised NPs still possess a potential therapeutic value and some of the structures made, namely vesicles, can be probably exploited to load more of the monomer or in other approaches such as combination therapies and theranostics.

An attempt was also made to synthesise a polyphosphoester loaded with ibuprofen through pendant ester groups. It was believed that such a polymer would make a good delivery vehicle for ibuprofen since PPEs are a promising tool for targeted therapy due to their characteristics that makes them very biocompatible and highly modifiable especially when synthesised via ring-opening polymerisation. The first steps making the monomer for polymerisation were optimised to produce pure products with high yields but, unfortunately, making the cyclic monomer necessary for ROP requires special conditions and cautious handling. Due to time limitations, this part of the project could not be advanced further.

2.4. References

1 J. R. Vane and R. M. Botting, *Thromb. Res.*, 2003, **110**, 255–258.

2 A. Ornelas, N. Zacharias-Millward, D. G. Menter, J. S. Davis, L. Lichtenberger, D. Hawke, E. Hawk, E. Vilar, P. Bhattacharya and S. Millward, *Cancer Metastasis Rev.*, 2017, **36**, 289–303.

3 J. Nagelschmitz, M. Blunck, J. Kraetzschmar, M. Ludwig, G. Wensing and T. Hohlfeld, *Clin. Pharmacol. Adv. Appl.*, 2014, **6**, 51–59.

4 F. M. Williams, *Clin. Pharmacokinet.*, 1985, **10**, 392–403.

5 G. Levy, *Br. J. Clin. Pharmacol.*, 1980, **10**, 285S-290S.

6 R. B. Supernaw, in *Pain Management*, Elsevier, First Edit., 2007, vol. 2, pp. 927–933.

7 M. Uzzaman, M. K. Chowdhury and M. Belal Hossen, *Front. Drug, Chem. Clin. Res.*, 2019, **2**, 1–5.

8 G. Levy, *Arch. Intern. Med.*, 1981, **141**, 279–281.

9 C. J. Needs and P. M. Brooks, *Clin. Pharmacokinet.*, 1985, **10**, 164–177.

10 J. A. Gimenez-Bastida, W. E. Boeglin, O. Boutaud, M. G. Malkowski and C. Schneider, *FASEB J.*, 2019, **33**, 1033–1041.

11 R. Amann and B. A. Peskar, *Eur. J. Pharmacol.*, 2002, **447**, 1–9.

12 J. Paterson, G. Baxter, J. Lawrence and G. Duthie, *Proc. Nutr. Soc.*, 2006, **65**, 93–96.

13 P. C. Elwood, A. M. Gallagher, G. G. Duthie, L. A. Mur and G. Morgan, *Lancet*, 2009, **373**, 1301–1309.

14 L. Erdmann, C. Campo, C. Bedell and K. Uhrich, *ACS Symp. Ser.*, 1998, **709**, 83–91.

15 L. Erdmann, B. Macedo and K. E. Uhrich, *Biomaterials*, 2000, **21**, 2507–2512.

16 L. Erdmann and K. E. Uhrich, *Biomaterials*, 2000, **21**, 1941–1946.

17 R. C. Schmeltzer, M. Johnson, J. Griffin and K. Uhrich, *J. Biomater. Sci. Polym. Ed.*, 2008, **19**, 1295–1306.

18 R. C. Schmeltzer and K. E. Uhrich, *J. Bioact. Compat. Polym.*, 2006, **21**, 123–133.

19 K. Whitaker-Brothers and K. Uhrich, *J. Biomed. Mater. Res. - Part A*, 2006, **76**, 470–479.

20 R. Rosario-Meléndez, M. A. Ouimet and K. E. Uhrich, *Polym. Bull.*, 2013, **70**, 343–351.

21 Y. Chandorkar, R. K. Bhagat, G. Madras and B. Basu, *Biomacromolecules*, 2014, **15**, 863–875.

22 V. Karavelidis, D. Giliopoulos, E. Karavas and D. Bikiaris, *Eur. J. Pharm. Sci.*, 2010, **41**, 636–643.

23 M. O. Omelczuk and J. W. McGinity, *Pharm. Res. An Off. J. Am. Assoc. Pharm. Sci.*, 1992, **9**, 26–32.

24 Y. Chandorkar, N. Bhaskar, G. Madras and B. Basu, *Biomacromolecules*, 2015, **16**, 636–649.

25 Q. Dasgupta, K. Chatterjee and G. Madras, *Mol. Pharm.*, 2015, **12**, 3479–3489.

26 Q. Cai, K. J. Zhu and J. Zhang, *Drug Deliv.*, 2005, **12**, 97–102.

27 S. Tang, S. M. June, B. A. Howell and M. Chai, *Tetrahedron Lett.*, 2006, **47**, 7671–7675.

28 R. Jantas, Z. Draczyński, L. Herczyńska and D. Stawski, *Am. J. Polym. Sci.*, 2012, **2**, 79–84.

29 R. Jabara, N. Chronds and K. Robinson, *Catheter. Cardiovasc. Interv.*, 2008, **72**, 186–194.

30 P. J. Nowatzki, R. R. Koepsel, P. Stoodley, K. Min, A. Harper, H. Murata, J. Donfack, E. R. Hortelano, G. D. Ehrlich and A. J. Russell, *Acta Biomater.*, 2012, **8**, 1869–1880.

31 S. Akkad and C. J. Serpell, *Macromol. Rapid Commun.*, 2018, **39**, 1800182.

32 D. M. White, L. A. Socha, US Patent US4855483, **1989**.

33 I. Manavitehrani, A. Fathi, H. Badr, S. Daly, A. Negahi Shirazi and F. Dehghani, *Polymers (Basel).*, 2016, **8**, 20.

34 M. Chanda, in *Introduction to Polymer Science and Chemistry*, CRC Press, 2013, pp. 159–211.

35 J. U. Izunobi and C. L. Higginbotham, *J. Chem. Educ.*, 2011, **88**, 1098–1104.

36 P. Mishra, B. Nayak and R. K. Dey, *Asian J. Pharm. Sci.*, 2016, **11**, 337–348.

37 J. Milton Harris and R. B. Chess, *Nat. Rev. Drug Discov.*, 2003, **2**, 214–221.

38 H. Parhiz, M. Khoshnejad, J. W. Myerson, E. Hood, P. N. Patel, J. S. Brenner and V. R. Muzykantov, *Adv. Drug Deliv. Rev.*, 2018, **130**, 90–112.

39 P. L. Turecek and J. Siekmann, in *Polymer-Protein Conjugates*, Elsevier, 2020, pp. 61–101.

40 G. Pasut and F. M. Veronese, *J. Control. Release*, 2012, **161**, 461–472.

41 T. Yamaoka, Y. Tabata and Y. Ikada, *J. Pharm. Sci.*, 1994, **83**, 601–606.

42 T. C. Ward, *Molecular weight and molecular weight distributions in synthetic polymers*, 1981, vol. 58.

43 D. W. Shortt, *J. Liq. Chromatogr.*, 1993, **16**, 3371–3391.

44 D. Massella, E. Celasco, F. Salaün, A. Ferri and A. Barresi, *Polymers (Basel).*, 2018, **10**, 1092.

45 Y. Mai and A. Eisenberg, *Chem. Soc. Rev.*, 2012, **41**, 5969–5985.

46 H. Feng, X. Lu, W. Wang, N.-G. Kang and J. Mays, *Polymers (Basel).*, 2017, **9**, 494.

47 D. Kozuch, W. Zhang and S. Milner, *Polymers (Basel).*, 2016, **8**, 241.

48 A. Blanazs, S. P. Armes and A. J. Ryan, *Macromol. Rapid Commun.*, 2009, **30**, 267–277.

49 H. Phan, R. I. Minut, P. McCrorie, C. Vasey, R. R. Larder, E. Krumins, M. Marlow, R. Rahman, C. Alexander, V. Taresco and A. K. Pearce, *J. Polym. Sci. Part A Polym. Chem.*, 2019, **57**, 1801–1810.

50 L. Zhang and A. Eisenberg, *J. Am. Chem. Soc.*, 1996, **118**, 3168–3181.

51 Y. Yu, L. Zhang and A. Eisenberg, *Macromolecules*, 1998, **31**, 1144–1154.

52 K. T. Kim, J. Zhu, S. A. Meeuwissen, J. J. L. M. Cornelissen, D. J. Pochan, R. J. M. Nolte and J. C. M. Van Hest, *J. Am. Chem. Soc.*, 2010, **132**, 12522–12524.

53 T. Azzam and A. Eisenberg, *Langmuir*, 2010, **26**, 10513–10523.

54 A. Kumar and C. K. Dixit, in *Advances in Nanomedicine for the Delivery of Therapeutic Nucleic Acids*, Elsevier, 2017, pp. 43–58.

55 A. Weingand-Ziadé, F. Renault and P. Masson, *Biochim. Biophys. Acta - Protein Struct. Mol. Enzymol.*, 1997, **1340**, 245–252.

56 T. Steinbach and F. R. Wurm, *Angew. Chemie - Int. Ed.*, 2015, **54**, 6098–6108.

57 K. N. Bauer, H. T. Tee, M. M. Velencoso and F. R. Wurm, *Prog. Polym. Sci.*, 2017, **73**, 61–122.

58 F. H. Westheimer, *Science (80-.).*, 1987, **235**, 1173–1178.

59 B. Alberts, A. Johnson and J. Lewis, in *Molecular Biology of the Cell*, New York: Garland Science, 4th editio., 2002.

60 K. M. Botham and P. A. Mayes, in *Harper's Illustrated Biochemistry*, McGraw-Hill, 31st

edn., 2018, pp. 105–110.

61 K. M. Botham and P. A. Mayes, in *Harper's Illustrated Biochemistry*, McGraw-Hill, 31st edn., 2018, pp. 111–116.

62 H. C. Schröder, L. Kurz, W. E. G. Müller and B. Lorenz, *Biochem.*, 2000, **65**, 296–303.

63 J. H. Morrissey, S. H. Choi and S. A. Smith, *Blood*, 2012, **119**, 5972–5979.

64 Y. C. Wang, Y. Y. Yuan, J. Z. Du, X. Z. Yang and J. Wang, *Macromol. Biosci.*, 2009, **9**, 1154–1164.

65 S. Schöttler, G. Becker, S. Winzen, T. Steinbach, K. Mohr, K. Landfester, V. Mailänder and F. R. Wurm, *Nat. Nanotechnol.*, 2016, **11**, 1–6.

66 J. Müller, K. N. Bauer, D. Prozeller, J. Simon, V. Mailänder, F. R. Wurm, S. Winzen and K. Landfester, *Biomaterials*, 2017, **115**, 1–8.

67 A. Bogomilova, M. Höhn, M. Günther, A. Herrmann, K. Troev, E. Wagner and L. Schreiner, *Eur. J. Pharm. Sci.*, 2013, **50**, 410–419.

68 G. Zhang, M. Zhang, J. He and P. Ni, *Polym. Chem.*, 2013, **4**, 4515–4525.

69 C. Y. Sun, S. Dou, J. Z. Du, X. Z. Yang, Y. P. Li and J. Wang, *Adv. Healthc. Mater.*, 2014, **3**, 261–272.

70 C. Q. Mao, J. Z. Du, T. M. Sun, Y. D. Yao, P. Z. Zhang, E. W. Song and J. Wang, *Biomaterials*, 2011, **32**, 3124–3133.

71 T.-M. Sun, J.-Z. Du, Y.-D. Yao, C.-Q. Mao, S. Dou, S.-Y. Huang, P.-Z. Zhang, K. W. Leong, E.-W. Song and J. Wang, *ACS Nano*, 2011, **5**, 1483–1494.

72 S. Zhang, J. Zou, F. Zhang, M. Elsabahy, S. E. Felder, J. Zhu, D. J. Pochan and K. L. Wooley, *J. Am. Chem. Soc.*, 2012, **134**, 18467–18474.

73 J. Bian, M. Zhang, J. He and P. Ni, *React. Funct. Polym.*, 2013, **73**, 579–587.

74 M. Ahmadian, R. E. Duncan, K. Jaworski, E. Sarkadi-Nagy and H. S. Sul, Future Lipidol., 2007, **2**, 229–237.

75 F. Rotondo, A. C. Ho-Palma, X. Remesar, J. A. Fernández-López, M. D. M. Romero and M. Alemany, Sci. Rep., 2017, **7**, 1–14.

76 Y. C. Wang, Y. Li, X. Z. Yang, Y. Y. Yuan, L. F. Yan and J. Wang, Macromolecules, 2009, **42**, 3026–3032.

77 T. Steinbach, R. Schröder, S. Ritz and F. R. Wurm, *Polym. Chem.*, 2013, **4**, 4469.

78 I. E. Nifant'Ev, A. V. Shlyakhtin, V. V. Bagrov, P. D. Komarov, M. A. Kosarev, A. N. Tavtorkin, M. E. Minyaev, V. A. Roznyatovsky and P. V. Ivchenko, *Polym. Chem.*, 2017, **8**, 6806–6816.

79 B. Clément, D. G. Molin, C. Jérôme and P. Lecomte, *J. Polym. Sci. Part A Polym. Chem.*, 2015, **53**, 2642–2648.

80 Y. Iwasaki and E. Yamaguchi, *Macromolecules*, 2010, **43**, 2664–2666.

81 B. C. Clément, B. Grignard, L. Koole, C. J. Jérô, P. Lecomte, B. Clément, B. Grignard, L. Koole, C. Jéroîme and P. Lecomte, *Macromolecules*, 2012, **45**, 4476–4486.

82 T. Dudev and C. Lim, *J. Am. Chem. Soc.*, 1998, **120**, 4450–4458.

83 A. Goyanes, J. Wang, A. Buanz, R. Martínez-Pacheco, R. Telford, S. Gaisford and A. W. Basit, *Mol. Pharm.*, 2015, **12**, 4077–4084.

Chapter 3

Liposomes as salicylic acid nanocarriers

3.1. Introduction

Liposomes are spherical vesicles comprising of one or more concentric lipid bilayers that entrap one or more aqueous compartments. They were first described in the 1960s and have been gaining an increasing interest as drug delivery vehicles, especially in cancer therapy, due to their unique physicochemical characteristics.[1] They can be used for the delivery of hydrophilic and/or lipophilic agents and they can range in size from tens of nanometres to several micrometres. However, only those with sizes within the range of 50-450 nm have an actual medical use, and with over 20 commercialised liposomal formulations and many more in clinical trials they are considered the most successful nano-delivery system to date.[2,3]

The lipid layers of liposomes are comprised of amphiphilic phospholipids. Each phospholipid molecule is composed of a glycerol backbone with one of its hydroxyl groups phosphorylated and the other two esterified with long-chain fatty acids that can be saturated or unsaturated. The phosphate is also esterified on one of its other oxygens with a variety of molecules such as ethanolamine, glycerol, choline, serine, or inositol, to get different phospholipids; phosphatidylethanolamine, phosphatidylglycerol, phosphatidylcholine, phosphatidylserine, and phosphatidylinositol, respectively. The glycerol backbone and the attached phosphoester form the hydrophilic head of the phospholipid, while the fatty acids form the lipophilic tail (Figure 3.1).[4,5]

In aqueous solutions, the phospholipid molecules assemble as bilayer membranes in which the hydrophilic heads are facing outwards while the hydrophobic chains face each other to create the inner compartment of the membrane. These membranes then form closed structures. The architecture is held together and stabilised mainly via two types of interactions; the first is the van der Waals forces between the tail chains, and the second is the hydrogen bonds and polar interactions between the aqueous environment and the hydrophilic heads of the phospholipids.[2,6]

The composition of liposomes, especially when natural lipids are used, makes them non-toxic and biodegradable with a very low chance of inducing immunogenicity, in turn making them among the most biocompatible nano-delivery systems.[7] They are also among the most versatile systems due to their dual nature since they allow the loading of hydrophilic drugs in their aqueous compartment and the embedding of hydrophobic drugs in their lipid membrane. They can also be

loaded with different types of molecules at the same time for combination therapy or theranostic purposes.[8,9] Liposome-NP hybrids have also been developed where other types of NPs such as iron oxide NPs, quantum dots, and polymer-based NPs have been incorporated in liposomes to have further control over their pharmacokinetic and pharmacodynamic profiles and reduce their toxicity.[10]

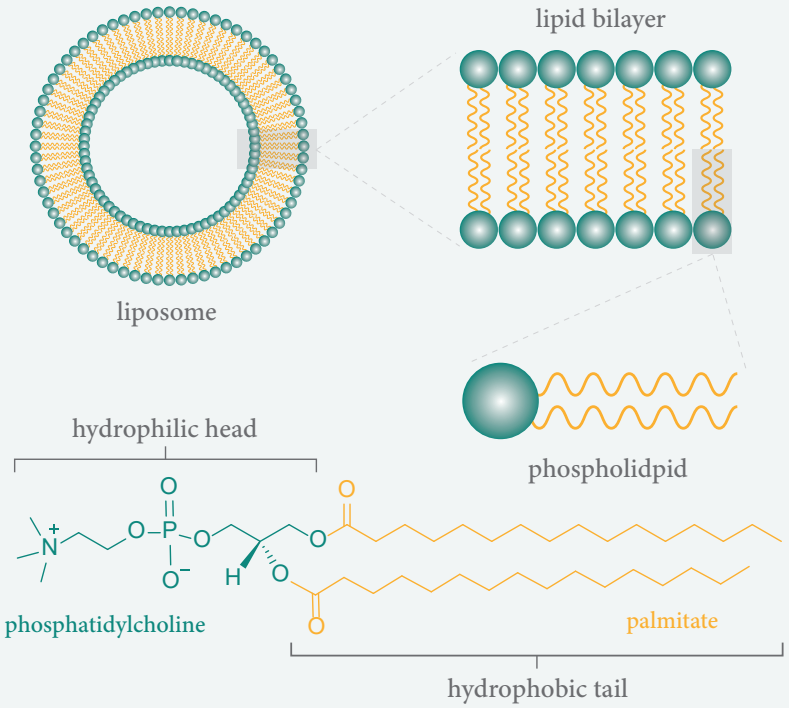

Fig 3.1. The basic anatomy of a liposome. The phospholipid shown, as an example, is dipalmitoylphosphatidylcholine (DPPC) comprising of phosphatidylcholine esterified with two palmitate groups.

Traditional (plain) liposomes are inherently passively-targeted at solid tumours via the EPR effect discussed in Chapter 1 due to their size and they can be used as-is for targeted therapy. However, various modifications have been introduced to liposomes to enhance their bioavailability as well as make them more actively targeted and/or responsive to internal or external stimuli to obtain better therapeutic outcomes. This can be achieved either by modifying the head group of the lipid, using different combinations of lipids, incorporating certain materials in the lipid layer or the aqueous compartment, or a combination of the above.[11]

For example, liposomes can be grafted with PEG to provide a hydration shield against opsonisation proteins and stealth them from the RES to enhance their circulation half-life, which is the case

of many liposomal formulations that are available in the market.[4,12] For more active targeting, transferrin- or folate-coupled liposomes might accumulate more preferentially in tumours where transferrin or folate receptors are overexpressed.[13,14] Antibodies can also be either bound to or anchored into the lipid membrane to create immunoliposomes that have a higher selectivity in targeting towards cells with the corresponding antigen.[11] For an externally-guided approach in targeting, magnetic liposomes (loaded with magnetite in addition to the therapeutic agent) demonstrated better accumulation in tumour tissues where a magnetic field is applied.[15] Finally, stimuli-responsive liposomes have also been developed by incorporating stimuli-sensitive (mainly pH-sensitive) materials in the liposomal formulation.[16] Figure 3.2 illustrated the different types of modifications that can be used with liposomes.

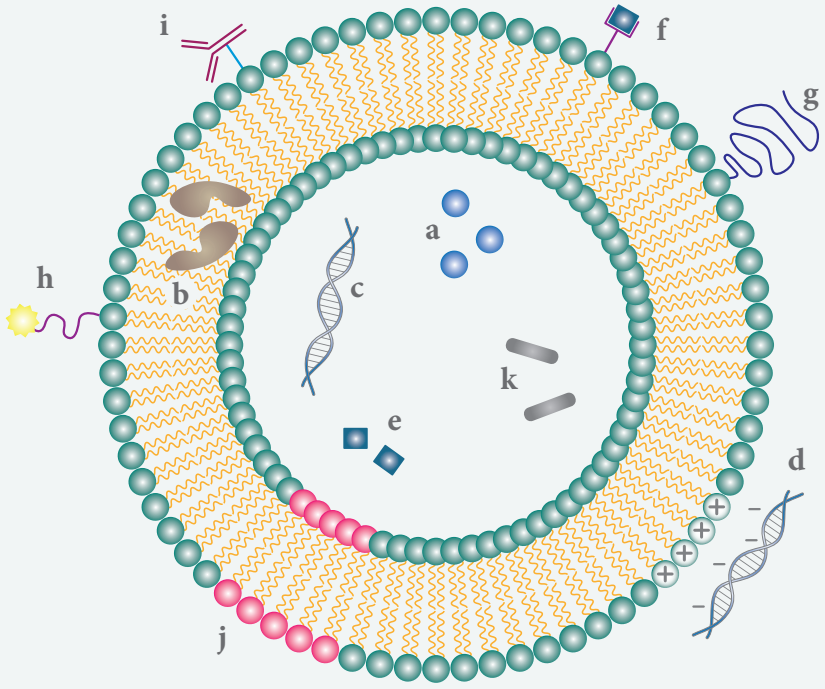

Fig 3.2. Some of the different types of liposomes that has been developed. Water-soluble drugs **(a)** can be loaded in the aqueous phase of the liposome while hydrophobic molecules **(b)** can be embedded in the lipid bilayer. Liposomes can also be used for the delivery of DNA by either entrapping it within the liposome **(c)** or anchoring it to the surface by using positively-charged phospholipids **(d)**. Diagnostic labelling agents can also be either encapsulated within the liposomes **(e)** or conjugated to its surface **(f)**. The circulation half-life of liposomes can be extended by stealthing them with a polymer like PEG **(g)** and they be more actively targeted by conjugating specific ligands **(h)** like folate or transferrin, or by attaching specific antibodies to the liposome **(i)**. Further control on the behaviour of liposomes can be exerted by the incorporation of stimuli-responsive materials such as thermoresponsive lipids or polymers **(j)** or the addition of encapsulation of magnetic particles **(k)**. Adapted from [11].

The versatility and biocompatibility of liposomal formulations attracted much attention as excellent candidates to increase the bioavailability of poorly soluble drugs, reduce the toxicity of drugs with a narrow therapeutic index, and develop a targeted approach in therapy, especially in cancer. The very first NP-based formulation approved by the FDA for clinical use was Doxil®, a PEGylated liposomal intravenous formulation of the cytotoxic drug, doxorubicin, for the treatment of Kaposi's sarcoma and ovarian and breast cancers. This formulation was associated with a significant increase in the accumulation of doxorubicin in tumour tissues compared to the conventional free drug as well as a decrease in cardiotoxicity, the main adverse effect of doxorubicin.[17]

Cytotoxic drugs are not the only class of drugs that have been incorporated into liposomes and neither is the intravenous route the only method by which liposomes can be used. For example, AmBisome® is a liposomal amphotericin B that is used for the treatment of invasive fungal infection while reducing the renal toxicity of the drug.[18] Epaxal® and Inflexal® are two intramuscular 'virosomal' formulations in which liposomes are used as more tolerable adjuvants than aluminium hydroxide that is used in their conventional counterparts for the vaccination against hepatitis A and influenza, respectively.[19,20] Depodur™ is a third example where liposomes loaded with morphine sulphate are injected epidurally providing an extended release of the drug for a more controlled approach to pain management.[21]

Nonetheless, with all the advantages that liposomal formulations have, there are a few drawbacks. These include the low colloidal stability of such formulations, especially on long-term storage, causing the leakage of the active materials or the fusion of liposomes to form larger vesicles, the oxidative damage that phospholipids might undergo under certain conditions, the high cost of production, and the challenging large-scale manufacturing of such formulations.[22,23]

There is a multitude of methods by which liposomes are prepared. What follows is a brief outline of the most common preparation methods:[2,5,22–24]

1. The film hydration method. Also known as "Bangham method" which is the first and one of the still widely used methods for the preparation of liposomes. It involves the hydration of a thin lipid film with aqueous media. However, it produces large and nonhomogeneous multilamellar vesicles (MLVs) that require post-processing to obtain liposomes with the desired attributes.

2. The reverse-phase evaporation. This method involves two steps; first, the aqueous medium is slowly introduced to an excess of an organic solvent that contains the lipid followed by sonication to produce inverted micelles. In the second phase, the organic solvent is removed under vacuum and the micelles come together to form a gel-like matrix that, at a critical point, collapses as some of the micelles are disrupted and their components rearrange around the intact micelles to form liposomes. This method yields a better encapsulation efficacy than the film-hydration method, but it is not suitable for organic solvent-sensitive materials, such as peptides.
3. The solvent-injection method. In this method, the organic phase which contains the lipid is injected in excess of the aqueous phase, then the solvent is removed via evaporation. This method has similar advantages and disadvantages to the reverse-phase evaporation method.

4. The detergent-depletion method. In this method, a lipid film is hydrated with a detergent to form micelles. The detergent is then removed, and at a critical lipid-to-detergent ratio, liposomes are formed. This method effectively produces unilamellar liposomes, but it is rarely used because of its low encapsulation efficacy.

5. The microfluidic-based method. Which is a relatively new method that uses microfluidic channels to allow a highly controlled mixing of phases to obtain the desired vesicles.

It should be noted that most of the methods mentioned above produce vesicles with different sizes and lamellarity, such as large unilamellar vesicles (LUVs) and multilamellar vesicles (MLVs) and post-formation processing, such as sonication and membrane extrusion, is required to obtain liposomes with specific size, homogeneity, and lamellarity.[2] It is also worth noting that although that the most common technique to load drugs into liposomes involves dissolving them in either phase prior to preparation (i.e. direct loading), empty liposomes can also be prepared with drugs then being remotely loaded into them.[25,26]

There are plenty of examples in literature in which liposomes are used for the encapsulation of NSAIDs. However, the purpose of most of these formulations is either to enhance the penetration of the drug through the skin when used topically, or to enhance the bioavailability and provide a sustained release of the drug when given orally or injected locally, such as the formulations intended for intra-articular injection for the management of osteoarthritis.[27–30] Fewer formulations

that are intended for systemic application to take advantage of the EPR effect could be identified. These included liposomal formulation of diclofenac, flurbiprofen, and celecoxib.[31–33]

Regarding the salicylates group of NSAIDs, there exist in the literature multiple liposomal formulations for various purposes. For example, Bhalerao *et al.* made SA-containing liposomes to enhance SA penetration of the skin for the treatment of acne and dry skin conditions.[34] Kwon *et al.* synthesised aspirin-containing liposomes to enhance skin penetration for the treatment of inflammatory conditions.[35] They failed, however, to provide information regarding encapsulation efficacy or the release profile of the liposomes but instead used the liposomal suspension as-is after encapsulation for the *in vitro* studies. For cancer-targeting purposes, Park *et al.* developed liposomes loaded with metformin and sodium salicylate as a combination therapy. However, their work also was lacking in terms of liposome characterisation and stability studies and the focus was mainly on *in vitro* studies.[36]

Lichtenberger *et al.* recently made a formulation of aspirin (and another of indomethacin) with phosphatidylcholine (PC) and tested their anti-tumour activity.[37,38] Interestingly, even though those formulations were prepared using the traditional film-hydration method, they were not deemed as liposomal, or at least lipid-based vesicular, nanocarriers. Instead, they were only named PC-NSAID preparations (and were even patented as such), and the anti-tumour activity was investigated directly after preparation (with no characterisation, release profile, etc.) *in vitro* and *in vivo* (orally) against colorectal cancer.

Since salicylic acid was the focus in making a polymeric anti-cancer prodrug in Chapter 2, a conventional liposomal salicylic acid formulation was attempted in this chapter as another form of nano-delivery systems of the NSAID for comparison with the polymeric vesicles.

3.2. Materials and methods

Salicylic acid (SA) and aspirin, were obtained from Acros Organics. Phosphatidylcholine (PC), cholesterol, and calcium acetate were obtained from Sigma Aldrich. 1,2-dipalmitoyl-sn-glycero-3-phosphocholine (DPPC) was obtained from Avanti Lipids. Gibco® phosphate-buffered saline (PBS) and sodium sulphate were obtained from Fisher Scientific. Visking dialysis tubing was obtained from Medicell Membranes Ltd.

Avestin Liposofast Extruder was used for vesicle extrusion. The polycarbonate membranes (pore size 100 nm) used in the device were obtained from Sigma Aldrich.

Dynamic light scattering (DLS) measurement were performed using Zeta Sizer Nano-ZS by Malvern Instruments Limited. Measurements were conducted using a glass cuvette at 25 °C. The refractive index (RI) of the dispersant (water) was set to 1.33 with the viscosity of 0.8872 cP while the RI for the material measured was set to 1.45.

Zeta-potential (ζ-potential) measurement for the vesicle preparation with the final concentration of 1 wt% was conducted at 25 °C.

High-performance liquid chromatography (HPLC) measurements were conducted on a Dionex UltiMate 3000 system equipped with a C18 column in a 30 °C oven. The mobile phase was composed of 75% water, 25% acetonitrile, and 0.1% formic acid. The flow rate was set to 4 mL/min and the injection volume was 10 µL. UV detection was used at a wavelength of 234 nm.

3.3. Experimental

3.3.1. PC liposomes by direct loading (freeze/thawing)

A solution of the lipid in chloroform was added to a round-bottom flask and then dried using the rotary evaporator to create a thin film of the lipid. The film was further dried *in vacuo* for 24 hours. The film was then hydrated with a 2-3 mg/mL solution of SA in PBS to get a final concentration of about 25 mM of the lipid. The flask was then subjected to 5-7 cycles of freeze-thawing by moving it between a dry ice/acetone bath and warm water. The resulting suspension was passed back and forth an odd number of times (between 19-23) through two stacked polycarbonate membranes with a pore size of 100 nm using the extruding device. The suspension was dialysed using a Visking dialysis membrane with PBS as the dialysis medium. The medium was changed after 2 hours, 8 hours, and 24 hours.

3.3.2. PC liposomes by direct loading (sonication)

The same procedure mentioned above was used to make the liposomes except that the hydration technique used was sonication for 30 minutes in an ultrasonic water bath instead of freeze/thawing.

For the lipid:cholesterol (PC:chol) preparations, the film was prepared from a mixture of PC and cholesterol at a molar ratio of 70:30%.

3.3.3. DPPC liposomes by direct loading

A solution of the lipid in chloroform was added to a round-bottom flask and then dried using the rotary evaporator to create a thin film of the lipid. The film was further dried *in vacuo* for 24 hours. The film was then hydrated with a 2-3 mg/mL solution of SA in PBS to get a final concentration of 15 mM of the lipid. The content of the flask was sonicated for 30 minutes in an ultrasonic water bath set at 50 °C. The resulting suspension was passed back and forth an odd number of times (between 19-23) through two stacked polycarbonate membranes with a pore size of 100 nm using the extruding device submerged in a water bath set at 50 °C. The suspension was dialysed using a Visking dialysis membrane with PBS as the dialysis medium at room temperature. The medium was changed after 2 hours, 8 hours, and 24 hours.

For the lipid:cholesterol (DPPC:chol) preparations, the film was prepared from a mixture of DPPC and cholesterol at a molar ratio of 70:30%.

3.3.4. DPPC liposomes by remote loading

A solution of the lipid in chloroform was added to a round-bottom flask and then dried using the rotary evaporator to create a thin film of the lipid. The film was further dried *in vacuo* for 24 hours. The film was then hydrated with 5 mL of a 120 mM solution of calcium acetate (pH = 7.47) to get a final concentration of 10 mM of the lipid. The content of the flask was sonicated for 30 minutes in an ultrasonic water bath set at 50 °C. The resulting suspension was then passed back and forth an odd number of times (between 19-23) through a stack of two polycarbonate membranes with a pore size of 100 nm using the extruding device submerged in a water bath set at 50 °C. The suspension was then brought to room temperature and then filtered using centrifugal filters. The filtrate was washed three times with a 120 mM solution of sodium sulphate (pH = 6) and then extracted from the filters. The filtrate was then resuspended in a 3 mg/mL solution of SA in 120 mM sodium sulphate and was left stirring in a water bath at around 50 °C for 7 hours. Liposome were then washed with PBS using centrifugal filters.

For the lipid:cholesterol preparations, the film was prepared from a mixture of PC and cholesterol at a molar ratio of 70:30%.

3.3.5. Sample preparation for HPLC analysis

To measure the liposomes' content of SA, the samples were mixed with either a solution of 5% SDS or 10% triton-X then run through the centrifugal filters and the filtrate was used for the measurement. All other samples did not require further processing.

3.4. Results and discussion

The aim of this part of the project was to synthesise SA-loaded liposomes with the highest loading capacity possible while, at the same time, achieve maximum retention of the drug inside the liposomes in storage conditions, only to get a controlled release in biological conditions.

The hydration method, first described by Bangham *et al.* in 1965, was used for making the lipid vesicles since it is the most common and most straightforward method for entrapping drugs that are stable during the post-formation processing, i.e. sonication, freeze-thawing, and extrusion.[39]

The size of the round-bottom flask (i.e. the glass support) was proportional to the amount of the lipid used in a way that guarantees the formation of the thin phospholipid (PL) film upon drying from the organic solvent under nitrogen. Drying the lipid film under high vacuum for at least 24 hours was also crucial since the presence of any residual organic solvent is not only a health hazard were these liposomes to be used in a clinical setting (and would affect prospective biological studies at the very least), but it can also affect the stability and permeability of the liposomes after formation.

Upon hydration, the PL film swells and flakes start peeling off from the glass support (i.e., the round-bottom flask). To avoid the exposure of the lipid chains to the aqueous medium at the edges, the flakes tend to curve and seal themselves to create vesicles.[6] Since the glass support is very smooth, surface properties would have no effect on the size and homogeneity of the resulting flakes. Instead, they are mainly determined by the crystal defects in the PL film. Nonetheless, Large flakes would result in the formation of multilamellar vesicles (MLVs), while smaller flakes would form large unilamellar vesicles (LUVs) and small unilamellar (SUVs).[40]

To achieve a higher degree of homogeneity, agitation is used to disrupt and break the MLVs

which then re-assemble to form SUVs.[40] Two different methods were used to produce such effects; sonication and repeated freeze-thawing. While sonication directly dissipates the energy required for the disruption of vesicles, freeze-thawing is believed to cause destabilisation and breaking of the lipid bilayers due to the expansion of the aqueous phase and the dehydration of the head groups during freezing, followed by the re-exposure of the hydrophobic chains to water during thawing causing them to fuse again, forming new vesicles.[41]

Further homogenisation and size control could be achieved by extruding the vesicles from the previous step through a polycarbonate membrane with specific pore size. Since the desirable size range for particles used in nanotherapy is 100-200 nm, as discussed in Chapter 1, the chosen pore size was 100 nm.

Membrane extrusion was performed in an air-tight, hand-driven device developed by MacDonald *et al.* in 1990 as a method for small-volume extrusion using low pressure (Figure 3.3). One or two polycarbonate membranes are fitted between two membrane supports and the vesicle suspension is pushed back and forth through the membrane with two 500 µL Hamilton syringes equipped with Luer locks. A nylon mesh on both sides of the membrane support distributes the injected sample over the surface of the membrane. This back and forth movement maximises homogeneity while reducing the blockage of the membrane and the need to replace it while processing each patch.[42]

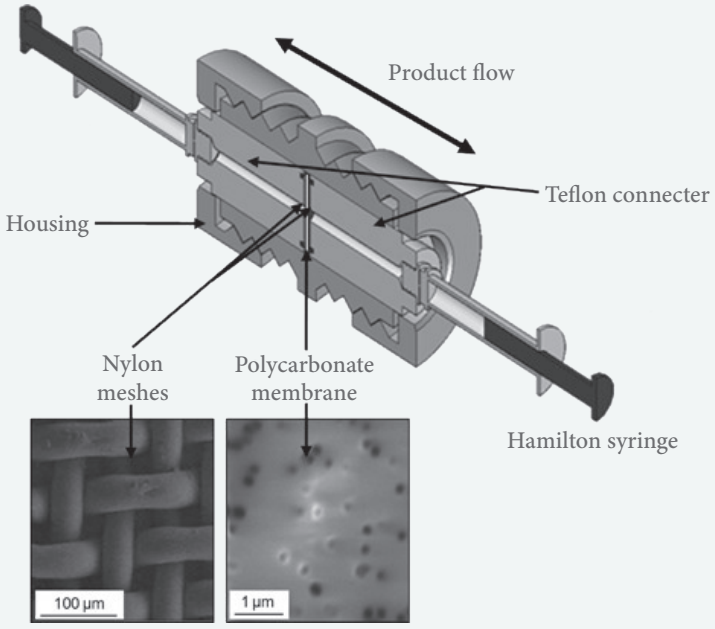

Fig 3.3. Layout of Liposofast, the small-volume extruder used to homogenise liposomes. Reproduced from [44].

In addition to the pore size of the membrane, the particle size distribution of the extruded particles is determined by the external pressure applied to the device and the viscosity of the formulation which is primarily controlled by temperature, namely the phase transition temperature (T_m).[42] At T_m, the hydrocarbon chains of the phospholipids transform from their extended and tightly-packed form, that gives phospholipids their rigid gel-like structure, to a randomly-oriented form, that causes phospholipids to have a liquid crystalline structure with more empty spaces between the phospholipids.[43] For this reason, extrusion (and sonication where applicable) was performed above the T_m of the phospholipid.

While vesicles with a size close to or below the pore size pass the membrane uninterrupted during extrusion, larger vesicles undergo expansion and shear forces that, in addition to interfacial tension effects and the steric hindrance between vesicles, cause them to break up and form smaller liposomes. After multiple cycles of extrusion, suspensions with a particle size distribution around the membrane pore size and with low polydispersity are achieved.[44]

Two different approaches were investigated to load the therapeutic agent, SA, into liposomes; the direct loading and the remote loading methods.

3.4.1. Liposomes prepared via the direct (passive) loading method

In this method, SA was dissolved at the highest concentration possible (2-3 mg/mL) (water solubility of SA is 2.48 g/L at 25 °C)[45] in the aqueous phase used to hydrate the lipid film.

Egg L-α-phosphatidylcholine (PC, also called L-α-Lecithin) was first used for the lipid phase. Egg PC is a mixture of phosphoesters of saturated and unsaturated fatty acids, mainly palmitic (16:0), stearic (18:0), oleic (18:1), and linoleic (18:2) acids, and has a phase transition temperature that is below 0 °C (-5 to -15).[46] Because of the low T_m of the phospholipid, synthesis processes like sonication and extrusion were performed at room temperature.

After film hydration with the SA solution, one of two homogenisation methods (sonication or freeze-thawing) was performed and then the suspension was extruded through the 100 nm membrane. DLS was used to determine particle size which ranged between 135-145 nm with PdI values ranging between 0.07 and 0.120. Figure 3.4 illustrates particle size distribution as determined by DLS.

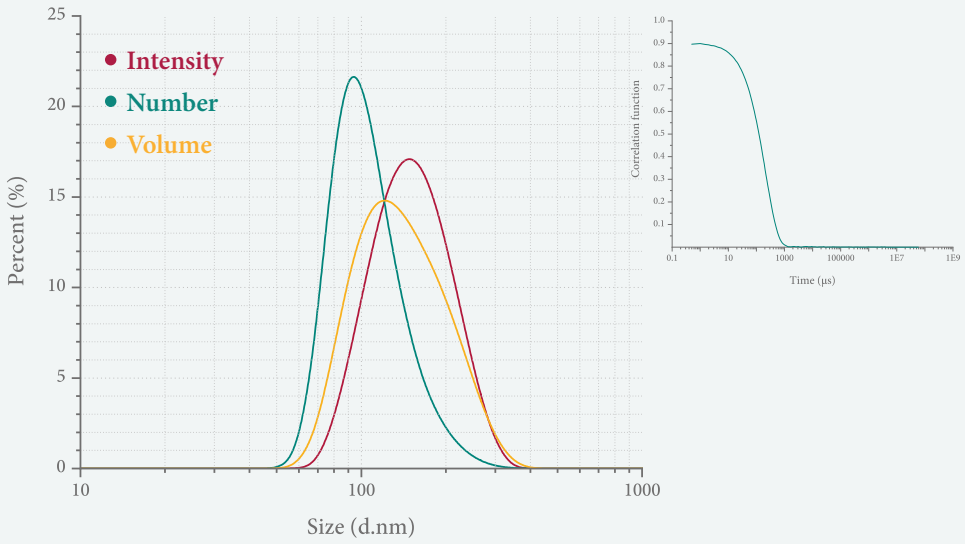

Fig 3.4. Size distribution of liposomes after extrusion as determined by DLS.

Drug entrapment could be quantified via the encapsulation efficiency (EE%) which represents the per cent fraction of the input drug that is loaded in the liposomes at a particular phospholipid concentration and can be expressed by the following equation:[47,48]

$$EE(\%) = \frac{C_{tot} - C_f}{C_{tot}} \times 100$$

Where C_{tot} is the total concentration used of the drug and C_f is the concentration of the free drug after encapsulation. Free (unentrapped) drug concentration was measured in the suspension medium after separating it from the liposomes using centrifugal filters (Figure 3.9).

The average EE was 47% for liposomes prepared via freeze-thawing and 60% for those prepared via sonication.

Although the mechanism by which sonication reduces the size of the vesicles is not fully understood, it is speculated that the gas bubbles within the suspension oscillate in response to sonication creating localised pressure forces that draw towards the bubbles any particles that have densities higher than the surrounding liquid. The radii of the oscillating gas bubbles also expand and contract on the microsecond scale, creating a convective flow near the surface of the bubbles. It is believed that this convective flow subjects the liposomes that are attracted towards the bubble's

surface, due to the aforementioned pressure, to high shear forces causing their division.[49] On the other hand, the mechanism of size reduction in the freeze-thawing method, as discussed earlier, is thought to be due to the breaking of the lipid bilayer due to dehydration and the mechanical pressure caused by the growth of ice crystals during freezing followed by rehydration and the reassembly of vesicles upon thawing.[50] In other words, freeze-thawing induces a system-wide breaking and reassembly of the lipid bilayer, causing SA to be released and re-entrapped. In contrast, sonication causes vesicles to divide and split with less pronounced loss of their content. It could be the more disruptive nature of the freeze-thawing method that causes it to result in lower EE than the sonication method.

It is worth noting that EE expresses the efficiency by which a specific method and/or phospholipid can entrap the input drug regardless of the amount of the drug used. This means that EE can be high even when low concentrations of the drug are used and *vice versa*. This is distinguishable from loading capacity (LC) which represents the maximum amount of the drug at a particular phospholipid concentration and is expressed as a per cent molar ratio of the entrapped drug to the lipid by the equation:[33,48]

$$LC(\%) = \frac{Mol\ of\ encapsulated\ drug}{Mol\ of\ lipid\ used} \times 100$$

It is also referred to as a molar ratio (moles of drug per moles of lipid) which is called the drug-to-lipid ratio, or D/L ratio.[48]

The LCs for the synthesised SA liposomes were 34% and 53% for the sonicated and the freeze-thawed samples, respectively.

It is also worth noting that, assuming the resulting vesicles are unilamellar, the number of liposomes per mL of solution and their content of SA can be estimated. This depends on the type of lipid used, its final concentration, and the amount of the entrapped drug. The number of liposomes per mL of the solution can be then calculated using the equation:[51]

$$N_{liposomes} = \frac{M_{lipid} \times N_A}{N_{tot} \times 1000}$$

Where N_A is the Avogadro number, M_{lipid} is the molar concentration of the lipid, and N_{tot} is the total number of lipids per liposome. N_{tot} can be calculated from the following equation:

$$N_{tot} = \frac{4\pi\left(\frac{d}{2}\right)^2 + 4\pi\left(\frac{d}{2} - h\right)^2}{a}$$

Where $4\pi\left(\frac{d}{2}\right)^2$ is the surface area of a single liposome that has the diameter d, *h* is the thickness of the bilayer (5 nm in the case of egg PC), and *a* is the area of the lipid head group (0.71 nm^2 for egg PC).[51]

By applying the previous formulae to the sonicated preparation, for example, the number of liposomes can be estimated to be around 86.7 x 10^{12} liposomes/mL. By dividing the concentration of entrapped SA on the number of liposomes per mL, it can be speculated that each liposome contains about 21.9 femtograms of SA.

The following step involved washing the liposome suspension to remove the unentrapped drug from the suspension. This was carried out via dialysing the suspension using Visking dialysis tubing with a molecular weight cut-off of 12-14 kDa. After 24 hours of dialysis, during which the dialysis medium was changed three times, the liposome suspension was investigated again for the free drug, and only a trace amount was detected by HPLC.

To investigate whether the liposomes' content of SA corresponds with the entrapped amount, the liposomes suspensions were mixed with a known amount of a surfactant to lyse the liposomes and release the entrapped drug for measurement. Either a 10% solution of Triton-X or a 5% solution of sodium dodecyl sulphate (SDS) was used for lysis. However, only trace (negligible) amounts of SA was detected from any of the preparations. Figure 3.5 shows the chromatograms of SA during the different stages of the preparation process.

Upon further investigation, it was found that the whole amount of SA used to load the liposomes (i.e. both entrapped and free) was being lost in the dialysis medium during the first two hours of the dialysis process. The most probable explanation for this issue is that the lipid used to make the liposomes has a very low T_m (-5 to -15 °C) at which the lipid exists in its liquid crystalline phase making liposomes more prone to leakage.[52]

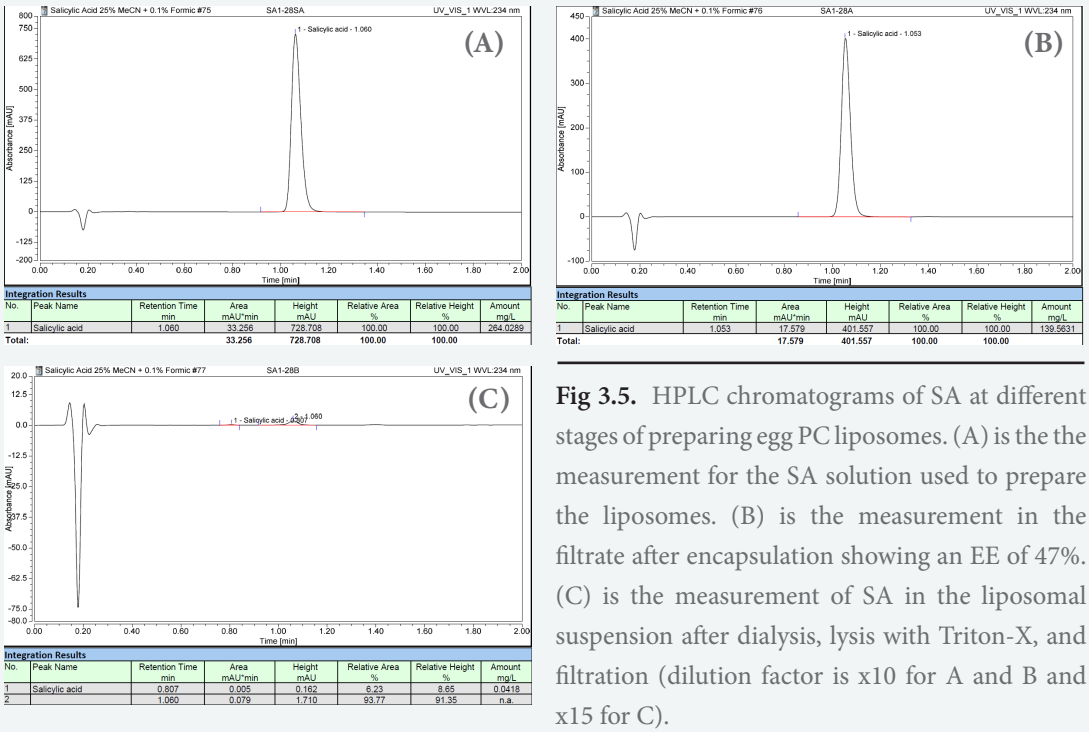

Fig 3.5. HPLC chromatograms of SA at different stages of preparing egg PC liposomes. (A) is the the measurement for the SA solution used to prepare the liposomes. (B) is the measurement in the filtrate after encapsulation showing an EE of 47%. (C) is the measurement of SA in the liposomal suspension after dialysis, lysis with Triton-X, and filtration (dilution factor is x10 for A and B and x15 for C).

The first approach that was explored to overcome this issue is by incorporating cholesterol in the lipid phase of the liposomes. Cholesterol, which is also an essential component of the membrane of biological cells, is known to decrease the permeability of the lipid bilayer and increase its rigidity possibly by increasing the packing of the phospholipid molecules and increasing the hydrophobicity of the membrane.[53,54]

The preferred molar ratio of lipid to cholesterol is about 2:1 (or 70:30%).[53] Hence a new preparation of liposomes was synthesised from egg PC and cholesterol with that ratio. Film hydration followed by sonication and extrusion was henceforth used for liposome preparation since it yielded better encapsulation and was more straightforward than freeze-thawing. The addition of cholesterol had no effect on the size of the liposomes. EE was 66% and LC was 38%. Nonetheless, dialysing the suspension resulted in the same issue of leakage, and the liposomes lost their load of SA during the first two hours of dialysis.

The lipid was changed to DPPC, a phosphatidylcholine ester with two palmitoyl saturated chains. The homogeneity of the lipid and the stronger van der Waals interactions observed with long acyl chains, as opposed to shorter ones, and the absence of kinks associated with the *cis*-double bonds in unsaturated chains raise the T_m of DPPC to 41 °C which makes it one of the preferable lipids in drug delivery since it is only a few degrees above the body temperature.[46,55]

The same method, film hydration followed by sonication then extrusion, was used to prepare the DPPC liposomes with the exception that all synthesis processes, i.e. hydration, sonication, and extrusion, were conducted above the T_m of DPPC.

The average EE was about 59% and LC of up to 71% could be achieved (depending on the concentration of DPPC used). However, the same leakage issue was encountered with the new lipid, and most of the SA load was being lost during the first two hours of washing even after incorporating cholesterol at a 70:30% molar ratio. Figure 3.6 shows the chromatograms of SA during the different stages of the preparation process of DPPC:Chol (2:1) liposomes.

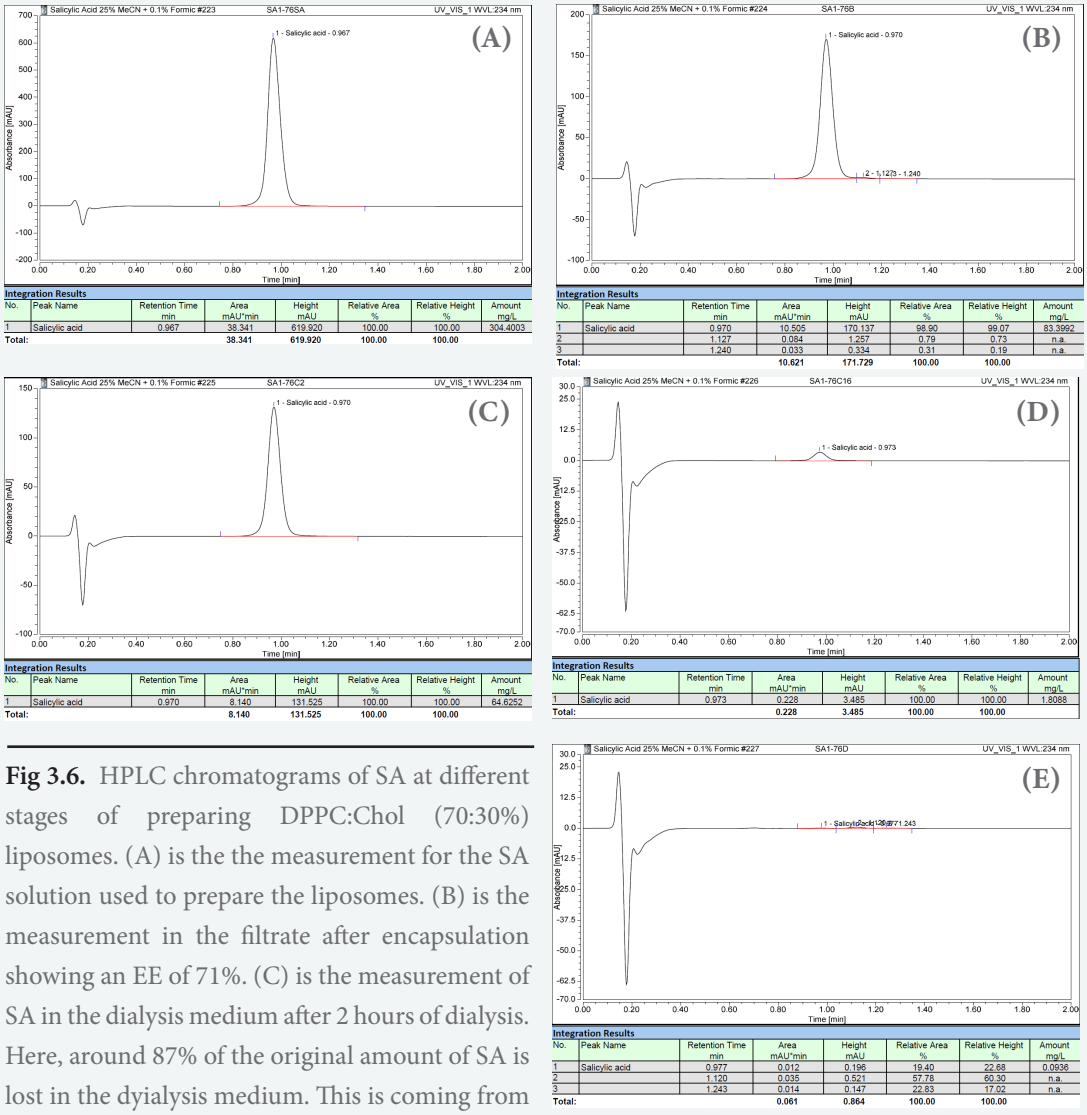

Fig 3.6. HPLC chromatograms of SA at different stages of preparing DPPC:Chol (70:30%) liposomes. (A) is the the measurement for the SA solution used to prepare the liposomes. (B) is the measurement in the filtrate after encapsulation showing an EE of 71%. (C) is the measurement of SA in the dialysis medium after 2 hours of dialysis. Here, around 87% of the original amount of SA is lost in the dyialysis medium. This is coming from both the unentrapped SA and the portion that is being released from the liposomes. (D) is the measurement of SA in the dialysis medium after 12 hours of dialysis. All of SA has been practically washed away at this stage. (E)is the measurement of SA in the liposomal suspension after dialysis, lysis with Triton-X, and filtration (dilution factors are x10 for A and B, approximately x41 for C and D, and x15 for C).

This is comparable to what is found in the literature. For example, Bhalerao *et al.* synthesised SA liposomes for skin application via film hydration using soy lecithin which has a transition temperature of 40-50 °C. The liposomes were not washed to remove the unentrapped but rather just separated from the hydration medium via centrifugation, resuspended in fresh medium, and then immediately stored at 4 °C. The preparation suffered leakage even during the first hours of storage and it increased significantly when the temperature increased.[34]

Hagiwara *et al.* encountered a similar issue with their liposomal preparations of SA where they measured EE after dialysis and found it to be less than 1%. However, the focus of their study was not SA per se but rather the use of γ-Cyclodextrin to enhance entrapment, and SA was used as a model drug for the system.[56] Nonetheless, the SA-γ-Cyclodextrin conjugate had an EE of about 8% which is still considered to be very low.

The loss of drug from liposomes could be explained by the fact that SA is a weak acid and it exists in aqueous solutions in equilibrium between the ionised (deprotonated) and neutral (protonated) states. Lipid bilayers are typically permeable to the non-ionised species, and after encapsulation, an osmotic equilibrium is reached between the inner and outer phases of the liposomes. When an osmotic perturbation occurs (in this case, dialysis), the permeant species of the acid (i.e., the neutral form) and water move across the membrane to establish diffusion equilibrium.[57] Since SA is being depleted continuously from the outer phase via dialysis, the weak acid equilibrium shifts towards the formation of the neutral form of the acid which in turn permeates across the membrane until very little SA remains inside the liposomes.

The permeation of a molecule can be estimated from its lipophilicity expressed as partition coefficient (*P*), or its decimal logarithm Log*P*, which is determined experimentally in a polar/non-polar system (usually octanol-water) where a higher value means higher lipophilicity and, subsequently, higher membrane permeability.[58]

Because aspirin is less lipophilic than SA (Log*P* is 2.35 for SA and 1.14 for aspirin),[59] an attempt was made to entrap aspirin instead of SA using the same direct loading method discussed above. However, the hydrolysis of aspirin to SA in the aqueous solution was very fast making the process inefficient. The rapid hydrolysis was identified by the appearance of two peaks in the HPLC chromatogram (Figure 3.7) of freshly prepared standard samples of aspirin.

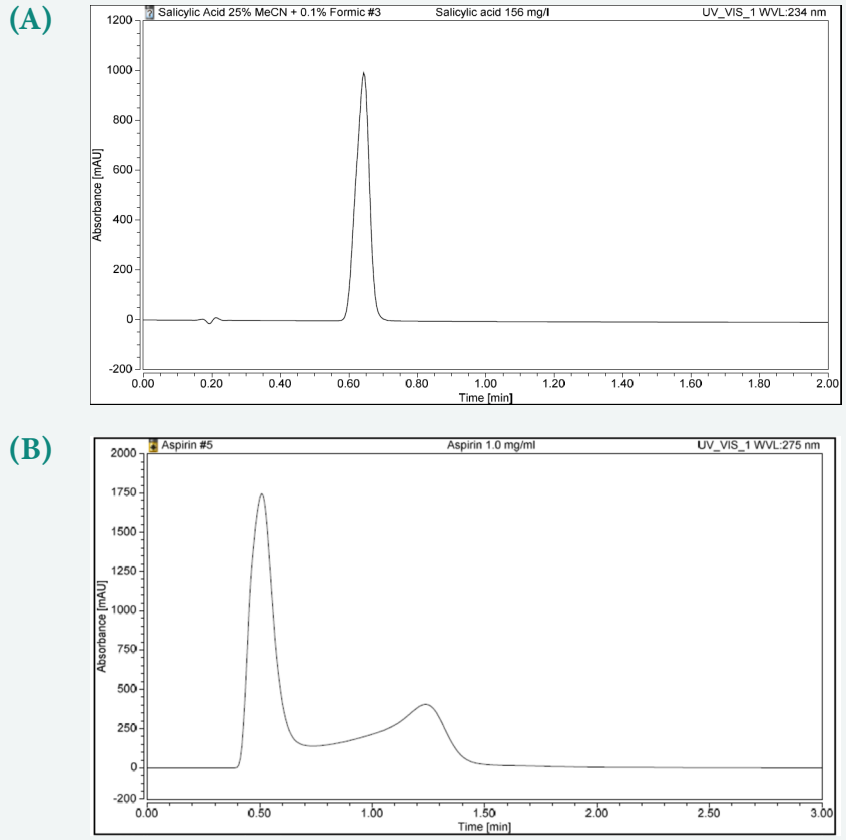

Fig 3.7. HPLC chromatograms of freshly prepared standard samples of salicylcic acid (**A**) and aspirin (**B**).

3.4.2. Liposomes prepared via the remote (active) loading method

To overcome the problems related to the retention of weak acids or basis inside lipid vesicles, a pH gradient approach has been successfully employed for the active loading of drugs. In this method, the difference in permeability between ionised and neutral forms of a drug is exploited via a transmembrane pH gradient. Empty liposomes are first prepared in a suspension that provides a difference in pH between the inside and the outside of liposomes. When the drug is added to the suspension, the neutral form permeates through the lipid membrane into the liposomes. The pH in the inner phase causes the drug to ionise and stay entrapped in the liposomes since the ionised form is impermeable through the membrane.[26] A gradient of ammonium sulphate, for example, has been established as an effective method for the remote loading of weak bases, such as the anti-tumour drug doxorubicin.[60]

For the remote loading of SA, calcium acetate was considered for the pH gradient method. This method (known in this case as the acetate gradient method) has been successfully used to entrap other weak acids, such as the antibacterial nalidixic acid and the NSAID diclofenac.[61,62]

Calcium acetate is preferably used for the remote loading of weak acids because it has the following characteristics: (1) it is the water-soluble salt of an amphipathic weak acid at high concentrations, (2) the permeability coefficient of the weak acid is high enough to ensure a rapid transmembrane movement (on the scale of 10 milliseconds), (3) the cation (calcium) is practically impermeable, and (4) the cation, being divalent, facilitate the formation of intraliposomal salts of the loaded drug that could probably be insoluble, which enhances drug retention.[62]

Empty liposomes were prepared via the film hydration method. Two different preparations were made; one contained only the lipid DPPC, while the other was prepared from a mixture of DPPC and cholesterol (70:30 mol%). The lipid film was hydrated with a solution of calcium acetate and then washed with sodium sulphate to remove the calcium acetate from the outer phase and create the acetate gradient. Sodium sulphate was used as the external phase because of the poor permeability of both the sodium and sulphate ions.[62] The external phase was prepared at the same concentration of the internal phase to preserve osmolarity.

After removing the calcium acetate from the external medium, internal acetic acid would permeate until an equilibrium of acetate concentration is reached between the inside and the outside. Through this movement, acetate acts as a proton shuttle and it causes the pH of the internal phase to rise with minimum effect on the pH of the external phase (since the volume of the external phase is much larger than the internal phase), thus a gradient in pH is created between the inside and outside of the liposomes. When another weak acid is added, SA in this case, the neutral form also starts to permeate through the lipid membrane, but with the higher pH inside the liposomes, SA would ionise and get trapped. This ionisation would also disturb the equilibrium of neutral SA between the two phases causing more SA to permeate through to the inner phase. Inside the liposomes, the salicylate ion possibly binds to the calcium ion and form salt complexes that might further precipitate providing even better retention and a slower release of the drug.[62-64] Figure 3.8 summarises the process of remote loading of a weak acid.

The EE of the preparations were 18% and 13% for the DPPC and the DPPC:chol liposomes, respectively. These results are much lower than expected EE values via the remote loading method which is considered much more effective than the direct loading method for ionisable drugs (efficiency is usually above 90%).[63,64]

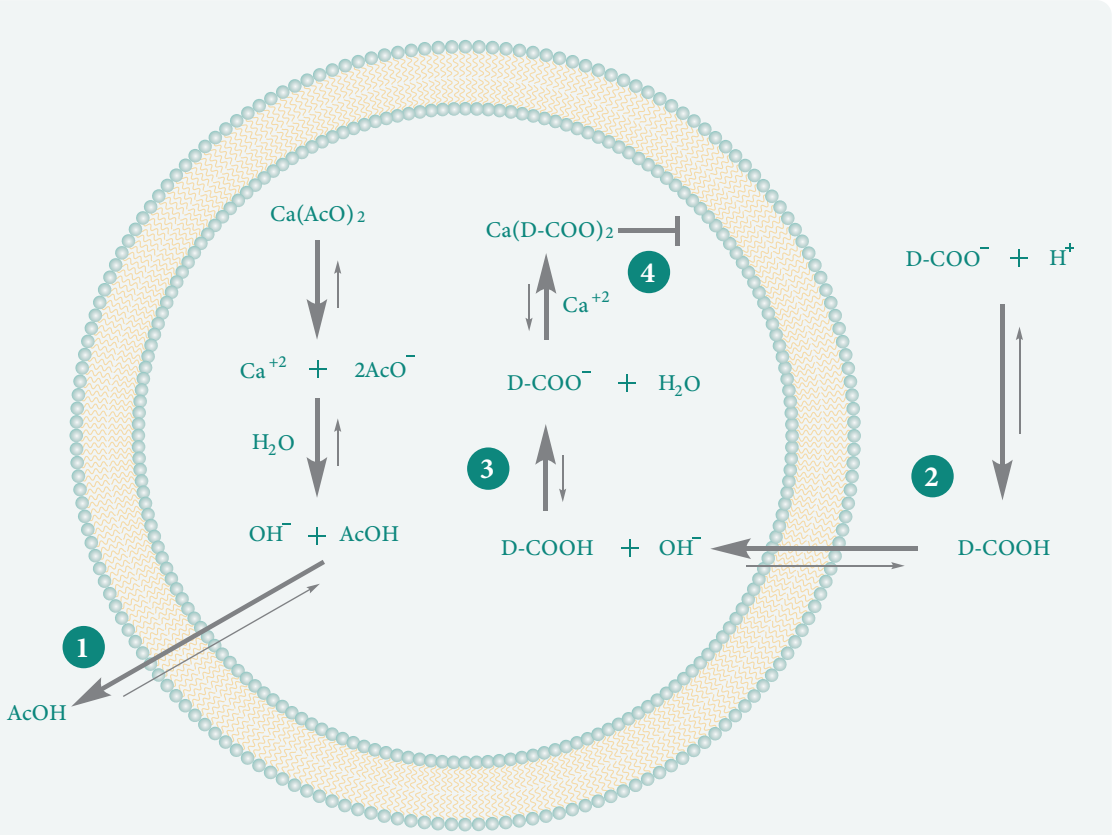

Fig 3.8. A summary of the remote loading (acetate gradient) method. **(1)** after loading the liposomes with calcium acetate and removing it from the outer phase, the acetate readily permeates to the outside of the liposome which raises the pH inside creating a transmembrane gradient. **(2)** When the weakly acidic drug (D-COOH) intended for loading is added, the neutral form permeates to the inside of the liposome. **(3)** because of the higher pH inside, the drug ionises and becomes entrapped due to the decreased permeability of the ionised form. **(4)** the calcium ion might form salts with the drug that have low solubility which could cause precipitation and further enhance drug retention. The depletion of the neutral form of the drug inside the liposome causes the transmembrane equilibrium of the drug to shifts more towards the inside which helps boost the loading process. Adapted from [64].

Nonetheless, after washing the liposomal preparations and then lysing them using Triton-X 100, no SA was detected, indicating that again SA leaked out of the liposomes during washing even though washing was performed on a small scale using the centrifugal vials (by a few cycles of removing the washing medium, resuspension, and washing again) rather than dialysing the liposomal suspension for prolonged periods of time, as illustrated in Figure 3.9.

Supposing encapsulation was successful with the aforementioned efficiency, the most likely explanation for the poor EE and the leakage of SA during washing is that the lipid bilayer was compromised causing the liposomes to be unstable and leaky. This could be due to the possible

hydrolysis of the lipids constituting the bilayer membrane. Hydrolytic degeneration is a common stability issue with liposomes made from phospholipids with saturated hydrocarbon chains.[65]

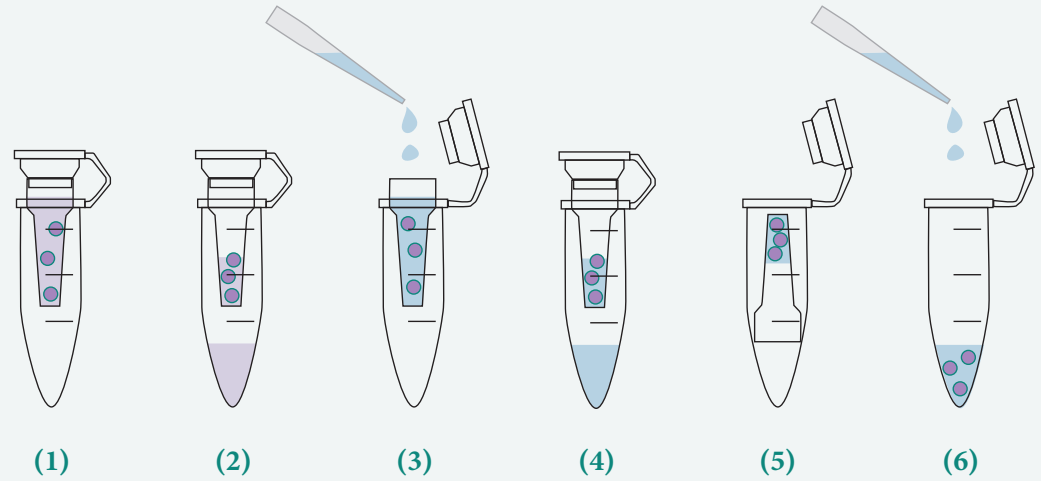

Fig 3.9. Washing liposomes with centrifugal filters. (1) the freshly prepared Liposomal suspension is added in the filter compartment and centrifuged. (2) the solution containing the unentrapped drug passes through the membrane while the liposomes stay in the upper compartment. (3) the washing medium is added to the filter compartment and the liposomes are resuspended. (4) the sample is centrifuged again to remove the washing medium and the process is repeated a few times. (5) to recover the liposomes, the filter compartment is inverted and the sample is centrifuged. (6) after their recovery in the vial, the liposomes are suspended in fresh medium.

The first stages of DPPC hydrolysis produce the lysophospholipid (a phospholipid with one fatty acyl chain) MPPC and the free fatty acid, palmitic acid. Further, slower hydrolysis of the lysolipid produces glycerol-3-phosphatidylcholine and glycerol-3-phosphoric acid, while the complete hydrolysis to glycerol and phosphoric acid is very slow and practically absent in pharmaceutically-relevant conditions.[65,66] Figure 3.10 shows the hydrolysis products of the phospholipid DPPC.

It has been determined that the presence of lysolipids and free fatty acids in the lipid bilayer could compromise its integrity and induce leakage, probably through the alteration of the pure lipid's T_m.[67–69] This causes a collapse in the acetate gradient and the leakage of the calcium ions resulting in the failure of SA encapsulation.

Although hydrolysis usually occurs during the long-term storage of liposomes in their aqueous suspensions or at extreme pH levels or high temperatures, it is possible that such impurities already existed in the DPPC batch used to prepare the liposomes since it had already been in storage for almost two years at the time of the experiment. Furthermore, it has been suggested

that bubble cavitation during sonication could produce free radicals leading to the oxidation and hydrolysis of phospholipids. For this reason, it might be necessary to exert more control over mixture temperature during sonication and limit sonication time.[70,71]

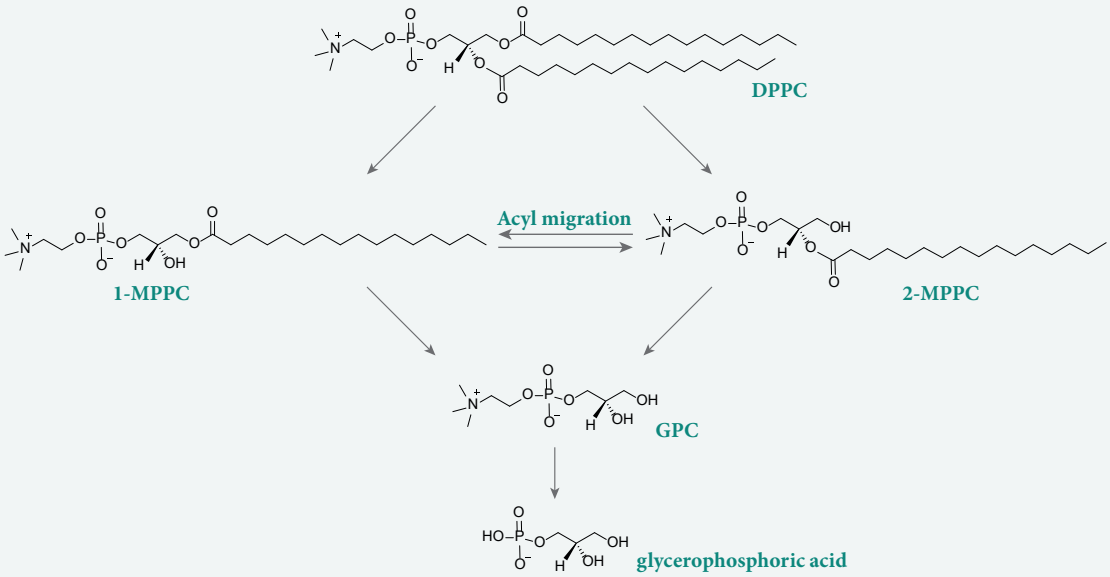

Fig 3.10. The hydrolysis products of DPPC. The lysophospholipids 1-MPPC and 2-MPPC result from the hydrolysis of the carboxy esters at *sn*-2 and *sn*-1, respectively. In certain pH and buffer conditions, 2-MPPC is rapidly converted to the more stable 1-MPPC. The end product of hydrolysis is glycerophosphoric acid, while further hydrolysis to phosphoric acid and glycerol is not observed in pharmaceutically-relevant condition. The presence of any of these species in the phospholipid bilayer compromises its stability. [65]
DPPC: 1,2-dipalmitoyl-sn-glycero-3-phosphocholine. **1-MPPC:** 1-palmitoyl-2-hydroxy-*sn*-glycerol-3-phosphatidylcholine, **2-MPPC:** 2-palmitoyl-1-hydroxy-*sn*-glycerol-3-phosphatidylcholine. **GPC:** *sn*-glycerol-3-pbosphorylclaoline. Adapted from [65].

The time limitation of the project did not allow for further investigation of the presence of lysolipids or any other possible changes in the structure of the phospholipid, nor did it allow to study the effect of sonication and other methods on the structure of the phospholipid during the preparation of liposomes.

It is also worth noting that the zeta potential values of liposomes prepared from DPPC are close to zero (between -0.03 and 0.69 mv), which is in agreement with the literature under similar experimental conditions (PBS).[72] This might be due to the overall neutral charge of the head group at a pH of 7.4.[73] These low values of zeta potential are of concern when it comes to the long-term stability since liposomes with such values tend to aggregate.[74] This could be improved

by incorporating other charged lipids in the bilayer or decorating the surface with various polymers.[75,76] However, the main priority was to achieve better retention of salicylic acid before investigating the long-term stability of the preparations.

Table 3.1 summarises the different SA liposomal preparations. As discussed above, egg PC was first used for the lipid membrane and one of two homogenisation methods, in addition to extrusion, was used. As preparation 2 shows, sonication yielded better EE than freeze/thawing probably due to the less aggressive splitting of vesicles associated with sonication. It was therefore used with all the subsequent preparations. Preparation 3 showed that the addition of cholesterol had a mild effect on EE but LC decreased due to the decrease in drug/lipid ratio after the addition of cholesterol. In preparation 4, DPPC was used instead of egg PC and yielded similar EE to the previous lipid. Adding cholesterol in preparation 5, however, increased EE probably via stabilising the liposomes and making them less leaking during the preparation process. Preparations 6 and 7 were done using the remote loading method without and with the addition of cholesterol, respectively. Low EE values are probably due to the collapse of the pH gradient that resulted from the compromised lipid membrane, most likely due to sonication. LC values follow EE values, again, due to a decrease in the drug/lipid ratio.

	Phospholipid	Lipid:chol molar ratio	Loading method	Homogenisation methods		EE (%)	LC (%)
				1st	2nd		
1	Egg PC	1:0	direct	freeze/thawing	extrusion	47%	34%
2	Egg PC	1:0	direct	sonication	extrusion	60%	53%
3	Egg PC	2:1	direct	sonication	extrusion	66%	38%
4	DPPC	1:0	direct	sonication	extrusion	46%	71%
5	DPPC	2:1	direct	sonication	extrusion	59%	67%
6	DPPC	1:0	remote	sonication	extrusion	18%	26%
7	DPPC	2:1	remote	sonication	extrusion	13%	19%

Table 3.1. Summary of the different salicylic acid liposomal preperations.
PC: phosphatidylcholine. **DPPC:** Dipalmitoylphosphatidylcholine. **Chol:** cholesterol. **EE:** encapsulation efficiency. **LC:** loading capacity.

3.5. Conclusion

Attempt were made to synthesise SA-loaded liposomes as another nanodelivery medium for SA to compare it with the polymeric vesicles presented in Chapter 2. In early experiments, egg PC for the synthesis of the lipid vesicles which lead, inevitably, to the end product being leaky due to low gel

transition temperature of the lipid. The addition of cholesterol to the formulation did not influence the permeability of the liposomes.

DPPC was then used instead of egg PC. Being a favourite when it comes to the synthesis of lipid vesicles for drug delivery due to its transition temperature that is only a few degrees above normal body temperature, DPPC was expected to yield better results than its predecessor. However, the DPPC liposomes prepared with the conventional method of synthesising liposomes, i.e. the direct (passive) loading via film hydration, still lost their load of SA during purification, even with the integration of cholesterol, at a rate unsuitable for the purposes of targeted therapy. For this reason, another method that has been successfully used to load liposomes with weak acids and bases was investigated.

Theoretically, the remote (active) loading method was expected to increase the loading capacity of the liposomes and enhances the retention of SA via a transmembrane calcium acetate gradient that causes a difference in pH between the inner and outer phases of the liposomes. This difference in pH could drive the loading process by allowing the permeable species of SA to enter the empty liposomes, become ionised, and stay entrapped.

Unfortunately, the liposomes synthesised by this method still failed the give satisfactory results. This might be attributed either to the degraded quality of the starting materials over time, or to ultrasonication that was used to homogenise the lipid vesicles since it has been found to compromise the integrity of the lipid bilayer via inducing hydrolysis. Nonetheless, it was not possible to further investigate these issues within the time frame of the project.

However, these findings raise some questions about similar formulations in the literature, since the stability and release profile of some of these formulations were not appropriately addressed. Even though this could be tolerated to a certain degree for topical application in semi-solid preparations, the issue of poor retention or leakage represents a major challenge if those liposomes were to be used systemically for targeted therapy. Some formulations made for this purpose were presented as novel lipid-associated NSAIDs even though their preparation method is identical to that used for the synthesis of conventional lipid vesicles. These formulations were used as-is and the focus was on the study of their pharmacological effects rather than their physicochemical properties.

Creating liposomes with good encapsulation efficiencies and loading capacities for the purposes of targeted therapy via systemic administration represents a major challenge that is encountered throughout literature. This is especially the case with amphiphilic weak acids and bases, which is the case in the vast majority of drugs. Since the direct loading method has proven ineffective in many cases, as in the work discussed above, the remote loading method shows some promise, at least theoretically, in improving the retention of small-molecule weak acids, such as salicylic acid. Further examination of the quality of the lipid used and making sure that the storage conditions and the preparation method do not produce lysolipids that compromise the integrity of the lipid bilayer might prove useful in attaining liposomes that are stable enough to hold their load of salicylic acid in relevant biological conditions until they reach their target tissue.

3.6. References

1 T. M. Allen, *Liposomes Opportunities in Drug Delivery*, 1997, vol. 4.

2 G. Bozzuto and A. Molinari, *Int. J. Nanomedicine*, 2015, **10**, 975–999.

3 B. Felice, M. P. Prabhakaran, A. P. Rodríguez and S. Ramakrishna, *Mater. Sci. Eng. C*, 2014, **41**, 178–195.

4 E. Beltrán-Gracia, A. López-Camacho, I. Higuera-Ciapara, J. B. Velázquez-Fernández and A. A. Vallejo-Cardona, *Cancer Nanotechnol.*, 2019, **10**, 11.

5 S. Vemuri and C. T. Rhodes, *Pharm. Acta Helv.*, 1995, **70**, 95–111.

6 V. A. Frolov, A. V. Shnyrova and J. Zimmerberg, *Cold Spring Harb. Perspect. Biol.*, 2011, **3**, a004747–a004747.

7 S. Hua and S. Y. Wu, *Front. Pharmacol.*, 2013, **4**, 1–7.

8 J. Lao, J. Madani, T. Puértolas, M. Álvarez, A. Hernández, R. Pazo-Cid, Á. Artal and A. A. Torres, *J. Drug Deliv.*, 2013, **2013**, 12.

9 S. Li, B. Goins, L. Zhang and A. Bao, *Bioconjug. Chem.*, 2012, **23**, 1322–1332.

10 W. T. Al-Jamal and K. Kostarelos, *Nanomedicine*, 2007, **2**, 85–98.

11 V. P. Torchilin, *Nat. Rev. Drug Discov.*, 2005, **4**, 145–160.

12 A. L. Klibanov, K. Maruyama, V. P. Torchilin and L. Huang, *FEBS Lett.*, 1990, **268**, 235–237.

13 H. Hatakeyama, H. Akita, K. Maruyama, T. Suhara and H. Harashima, *Int. J. Pharm.*, 2004, **281**, 25–33.

14 R. J. Lee and P. S. Low, *J. Biol. Chem.*, 1994, **269**, 3198–204.

15 H. Nobuto, T. Sugita, T. Kubo, S. Shimose, Y. Yasunaga, T. Murakami and M. Ochi, *Int. J. Cancer*, 2004, **109**, 627–635.

16 S. Simões, J. Nuno Moreira, C. Fonseca, N. Düzgüneş and M. C. Pedroso De Lima, *Adv. Drug Deliv. Rev.*, 2004, **56**, 947–965.

17 Y. Barenholz, *J. Control. Release*, 2012, **160**, 117–134.

18 V. Wagner, A. Dullaart, A. K. Bock and A. Zweck, *Nat. Biotechnol.*, 2006, **24**, 1211–1217.

19 P. A. Bovier, *Expert Rev. Vaccines*, 2008, **7**, 1141–1150.

20 R. Mischler and I. C. Metcalfe, *Vaccine*, 2002, **20**, B17–B23.

21 M. Alam and C. T. Hartrick, *Pain Pract.*, 2005, **5**, 349–353.

22 A. Akbarzadeh, R. Rezaei-Sadabady, S. Davaran, S. W. Joo, N. Zarghami, Y. Hanifehpour, M. Samiei, M. Kouhi and K. Nejati-Koshki, *Nanoscale Res. Lett.*, 2013, **8**, 102.

23 B. Maherani, E. Arab-Tehrany, M. R. Mozafari, C. Gaiani and M. Linder, *Curr. Nanosci.*, 2011, **7**, 436–452.

24 D. Powers and N. Nosoudi, *Biomed. Res.*, 2019, **30**, 288–295.

25 D. D. Lasic, B. Čeh, M. C. A. Stuart, L. Guo, P. M. Frederik and Y. Barenholz, *BBA - Biomembr.*, 1995, **1239**, 145–156.

26 S. Sur, A. C. Fries, K. W. Kinzler, S. Zhou and B. Vogelstein, *Proc. Natl. Acad. Sci. U. S. A.*, 2014, **111**, 2283–2288.

27 I. Elron-Gross, Y. Glucksam and R. Margalit, *Int. J. Pharm.*, 2009, **376**, 84–91.

28 L. Tarţău, A. Cazacu and V. Melnig, *J. Mater. Sci. Mater. Med.*, 2012, **23**, 2499–2507.

29 C. Puglia, D. Trombetta, V. Venuti, A. Saija and F. Bonina, *J. Pharm. Pharmacol.*, 2004, **56**, 1225–1232.

30 J. Dong, D. Jiang, Z. Wang, G. Wu, L. Miao and L. Huang, *Int. J. Pharm.*, 2013, **441**, 285–290.

31 R. Jukanti, G. Devaraj, R. Devaraj and S. Apte, *Int. J. Pharm.*, 2011, **414**, 179–185.

32 M. Y. Begum, K. Abbulu and M. Sudhakar, *J. Young Pharm.*, 2012, **4**, 209–219.

33 Y. D. P. Limasale, A. Tezcaner, C. Özen, D. Keskin and S. Banerjee, *Int. J. Pharm.*, 2015, **479**, 364–373.

34 S. S. Bhalerao and a Raje Harshal, *Drug Dev. Ind. Pharm.*, 2003, **29**, 451–467.

35 K. Kwon and J.-C. Kim, *Biotechnol. Bioprocess Eng.*, 2016, **21**, 659–666.

36 H.-B. Park, Y.-J. Kim, S.-M. Lee, J. S. Park and K.-S. Kim, *Biomed. Sci. Lett.*, 2019, **25**, 159–169.

37 L. M. Lichtenberger, T. Phan, D. Fang and E. J. Dial, *Oncol. Lett.*, 2018, **15**, 6688–6694.

38 S. Burge and L. M. Lichtenberger, *Oncol. Lett.*, 2019, **18**, 6243–6248.

39 A. D. Bangham, M. M. Standish and J. C. Watkins, *J. Mol. Biol.*, 1965, **13**, 238–252.

40 D. D. Lasic, *J. Colloid Interface Sci.*, 1988, **124**, 428–435.

41 S. Supaporn, *Open Colloid Sci. J.*, 2011, **4**, 1–8.

42 R. C. MacDonald, R. I. MacDonald, B. P. M. Menco, K. Takeshita, N. K. Subbarao and L. Hu, *Biochim. Biophys. Acta - Biomembr.*, 1991, **1061**, 297–303.

43 W. Chen, F. Duša, J. Witos, S. K. Ruokonen and S. K. Wiedmer, *Sci. Rep.*, 2018, **8**, 14815.

44 S. Joseph and H. Bunjes, *J. Pharm. Sci.*, 2012, **101**, 2479–2489.

45 F. L. Nordström and Å. C. Rasmuson, *J. Chem. Eng. Data*, 2006, **51**, 1668–1671.

46 J. Li, X. Wang, T. Zhang, C. Wang, Z. Huang, X. Luo and Y. Deng, *Asian J. Pharm. Sci.*, 2014, **10**, 81–98.

47 A. Gonzalez Gomez, S. Syed, K. Marshall and Z. Hosseinidoust, *ACS Omega*, 2019, **4**, 10866–10876.

48 M. Chountoulesi, N. Naziris, N. Pippa and C. Demetzos, *J. Liposome Res.*, 2018, **28**, 249–258.

49 E. S. Richardson, W. G. Pitt and D. J. Woodbury, *Biophys. J.*, 2007, **93**, 4100–4107.

50 K. Sou, Y. Naito, T. Endo, S. Takeoka and E. Tsuchida, *Biotechnol. Prog.*, 2003, **19**, 1547–1552.

51 M. Sardan, M. Kilinc, R. Genc, A. B. Tekinay and M. O. Guler, *Faraday Discuss.*, 2013, **166**, 269–283.

52 T. Ta and T. M. Porter, *J. Control. Release*, 2013, **169**, 112–125.

53 M.-L. L. Briuglia, C. Rotella, A. Mcfarlane and D. A. Lamprou, *Drug Deliv. Transl. Res.*, 2015, **5**, 231–242.

54 S. Kaddah, N. Khreich, F. Kaddah, C. Charcosset and H. Greige-Gerges, *Food Chem. Toxicol.*, 2018, **113**, 40–48.

55 B. Alberts, A. Johnson, J. Lewis, D. Morgan, M. Raff, K. Roberts and P. Walter, *Molecular Biology of the Cell*, Garland Science, 6th Editio., 2014.

56 Y. Hagiwara, H. Arima, Y. Miyamoto, F. Hirayama and K. Uekama, *Chem. Pharm. Bull. (Tokyo).*, 2006, **54**, 26–32.

57 M. Gabba, J. Fralliccardi, J. van 't Klooster, R. Henderson, Ł. Syga, R. Mans, A. J. A. van Maris and B. Poolman, *Biophys. J.*, 2020, **118**, 422–434.

58 C. Giaginis and A. Tsantili-Kakoulidou, *J. Pharm. Sci.*, 2008, **97**, 2984–3004.

59 M. Dołowy and A. Pyka, *J. Liq. Chromatogr. Relat. Technol.*, 2015, **38**, 485–491.

60 E. M. Bolotin, R. Cohen, L. K. Bar, N. Emanuel, S. Ninio, Y. Barenholz and D. D. Lasic, *J. Liposome Res.*, 1994, **4**, 455–479.

61 S. Hwang, Y. Maitani, X.-R. Qi, K. Takayama and T. Nagai, *Int. J. Pharm.*, 1999, **179**, 85–95.

62 S. Clerc and Y. Barenholz, *Biochim. Biophys. Acta - Biomembr.*, 1995, **1240**, 257–265.

63 Y. Avnir, K. Turjeman, D. Tulchinsky, A. Sigal, P. Kizelsztein, D. Tzemach, A. Gabizon and Y. Barenholz, *PLoS One*, 2011, **6**, e25721.

64 J. Gubernator, *Expert Opin. Drug Deliv.*, 2011, **8**, 565–580.

65 M. Grit and D. J. A. Crommelin, *Chem. Phys. Lipids*, 1993, **64**, 3–18.

66 L. M. Ickenstein, M. C. Sandström, L. D. Mayer and K. Edwards, *Biochim. Biophys. Acta - Biomembr.*, 2006, **1758**, 171–180.

67 N. J. Zuidam, H. K. M. E. Gouw, Y. Barenholz and D. J. A. Crommelin, *BBA - Biomembr.*, 1995, **1240**, 101–110.

68 M. Grit and D. J. A. Crommelin, *Chem. Phys. Lipids*, 1992, **62**, 113–122.

69 J. Davidsen, O. G. Mouritsen and K. Jorgensen, *Biochim. Biophys. Acta - Biomembr.*, 2002, **1564**, 256–262.

70 R. Silva, H. Ferreira, C. Little and A. Cavaco-Paulo, *Ultrason. Sonochem.*, 2010, **17**, 628–632.

71 R. Almog, R. Forward and C. Samsonoff, *Chem. Phys. Lipids*, 1991, **60**, 93–99.

72 E. Chibowski and A. Szcześ, Adsorption, 2016, 22, 755–765.

73 M. S. Fernández, Berichte der Bunsengesellschaft für Phys. Chemie, 1995, 99, 965–968.

74 A. J. Shnoudeh, I. Hamad, R. W. Abdo, L. Qadumii, A. Y. Jaber, H. S. Surchi and S. Z. Alkelany, in Biomaterials and Bionanotechnology, Elsevier, 2019, pp. 527–612.

75 P. Maity, B. Saha, G. S. Kumar and S. Karmakar, Biochim. Biophys. Acta - Biomembr., 2016, 1858, 706–714.

76 H. G. Meland, A. Røv-Johnsen, G. Smistad and M. Hiorth, Colloids Surfaces B Biointerfaces, 2014, 114, 45–52.

Chapter 4

Preliminary *in vitro* studies

4.1. Introduction

No matter how meticulously engineered, the biological response obtained from any given nano-delivery system can be very hard to predict, and how nanoparticles interact with biological systems is still not fully understood.[1]

The pharmacokinetics and biodistribution of nanoparticles are different from their small-molecule counterparts. The drug delivery process using intravenously-injected nanocarriers can be divided into three phases: (1) systemic circulation and the interaction with the reticuloendothelial system (RES), (2) extravasation and tumour penetration, and (3) interaction with the target cells (i.e. uptake and intracellular trafficking) and drug release.[2]

Immediately after their systemic administration, injected nanoparticles encounter a wide array of blood proteins (e.g. immunoglobulin G, serum albumin, fibrinogen, apolipoproteins, complement components, etc.) that adsorb onto the surface of the particle, creating a "protein corona" that alters the physicochemical characteristics of the nanoparticle by changing its surface properties and helps shape its biological identity.[3,4] Some of these proteins (especially the immunoglobulins and complement components), called "opsonins", help the immune system identify the nanoparticles as foreign intruders and make them visible to the macrophages of the reticuloendothelial system (RES), especially in the liver and spleen, which in turn clear the particles from circulation via the endocytic process of phagocytosis.[5]

In addition to being phagocytised by Kupffer cells (the liver's macrophages), particles smaller than 50 nm entering hepatic circulation might extravasate through the vascular fenestration of the liver's endothelium, causing them to accumulate in and interact with hepatocytes.[6] As the size of the particles increases, hepatic clearance appears to decrease while the splenic capture increases.[7] It has been demonstrated that particles with a size of about 300 nm and above start to accumulate in the spleen in a size-dependant manner unrelated to the spleen's phagocytic system.[7,8] On the other hand, very small NPs that have the size of about 5 nm (or a molecular weight of about 40 kDa) are rapidly cleared out by the kidneys via glomerular filtration.[9,10]

NPs can still reach the target tissues before encountering macrophages or can evade phagocytosis altogether either because of being PEGylated or due to the saturation of the endocytic capacity of the macrophages and/or the depletion of opsonins.[11–13] When those NPs reach the microvessels of a solid tumour (in the case of its presence) they diffuse throughout the tissue after extravasating through the fenestrations in the walls of the blood vessels supplying the tumour to be taken up after that by cells via various forms of endocytosis.[14]

While the first form of endocytosis, phagocytosis "cellular eating", is exclusive to phagocytes (i.e. macrophages, monocytes, and dendritic cells) and is observed to take place with large particles (>500 nm), the uptake of most of NPs that have a size range between a few nanometres and a few hundred nanometres happen via pinocytosis "cellular drinking" which is the primary mechanism of uptake in all kinds of cells, including tumorous ones.[15,16] Both types of endocytosis involve engulfing NPs in membrane invaginations, followed by their budding and pinching off on the intracellular side of the membrane. In phagocytosis, however, the phagocytic membrane is tightly apposed to the solid particle itself in contrast with pinocytosis where the cell engulfs a volume of the interstitial fluid that contains the NPs, hence the distinction between the 'eating' and 'drinking' processes.[17]

Pinocytosis can be further divided into four subtypes:[1,15,18,19]

1- Clathrin-mediated endocytosis (CME), which is the primary mechanism by which cells obtain their main nutrients and plasma membrane components such as iron and cholesterol. CME happens either via receptor-specific uptake or by nonspecific adsorptive uptake through the hydrophobic or electrostatic interactions between the NPs and the membrane of the cell. Clathrin is the protein that is considered the assembly unit that causes curvatures in the cellular wall forming pits that are about 100-150 nm in size that engulf the NPs then bud and pinch off to form the endocytic vesicles. Those vesicles usually end up fusing with the degradative lysosomes in the cytoplasm.
2- Caveolae-mediated endocytosis (CvME), which occurs in cells that contain caveolin, a protein that plays a role in cell signalling and the regulation of membrane proteins. The invaginations formed in this pathway are characterised by their flask-like shape that is around 50-80 nm in size. Since the resulting vesicles do not usually fuse with lysosomes, their content does

not typically undergo enzymatic degradation. Hence, this pathway is usually exploited by pathogens to avoid lysosomal enzymes and, for the same reason, there has been a growing interest in this pathway as a potential means to deliver NPs loaded with enzyme-sensitive materials such as proteins and peptides.

3- Clathrin- and caveolae- independent endocytosis, which happens in cells that lack both proteins. Cellular uptake of extracellular fluids, growth hormones, and interleukin-2 takes place via this pathway. Because folic acid is also internalised via this route, NPs that are functionalised with folate are usually taken up into cells through this route. Folate-conjugated particles are also not usually delivered to lysosomes, but instead are either retained in the endocytic compartments or released into the cytoplasm.

4- Macropinocytosis, which is a nonspecific uptake pathway in which the cytoskeleton rearranges to form large membrane extensions that engulf a large extracellular volume and then fuses back with the membrane forming large vesicles (0.2-5 μm), making it a good candidate for the uptake of large NPs.

Other entry mechanisms have been reported, such as passive diffusion and nanoscale hole formation via disruption of the lipid bilayer, as well as artificially-induced mechanisms, such as direct cytoplasmic microinjection and electroporation (inducing the formation of transient pores in the lipid bilayer through the application of external high-voltage electrical impulses).[1]

It is worth noting that the uptake mechanism depends on the type of target cells as well as the physicochemical characteristics of the NPs, such as the composition, shape, size, and surface charge.[2,5]

After pinching off from the cell membrane, the internalised vesicles go through the process of intracellular trafficking that determines the final fate of the cargo. For vesicles destined for enzymatic degradation, they fuse with the membrane-bound “early endosomes” that act as temporary storage for the cargo before being sorted via the differentiation of the early liposomes to either “recycling endosomes”, that carry part of the cargo back to the cellular membrane and out to the exterior of the cell, or to “late endosomes” that fuse with lysosomes to form endolysosomes where the hydrolytic enzymes degrade its content, mediated by the acidic pH in the lysosomes.[20,21]

Other vesicles, such as those formed via caveolae-dependent endocytosis, are delivered to other cellular components, such as the Golgi apparatus and the endoplasmic reticulum in order for their content to be utilised by the cell.[22]

It should be noted, however, that even if particles escape being delivered into lysosomes, they still might be cleared sometimes from the cytoplasm through autophagy, a process in which special endosomes (autophagosomes) appear around objects in the cytoplasm, engulf them, and deliver them to lysosomes.[23] Figure 4.1 illustrates the different pathways of the cellular uptake of NPs.

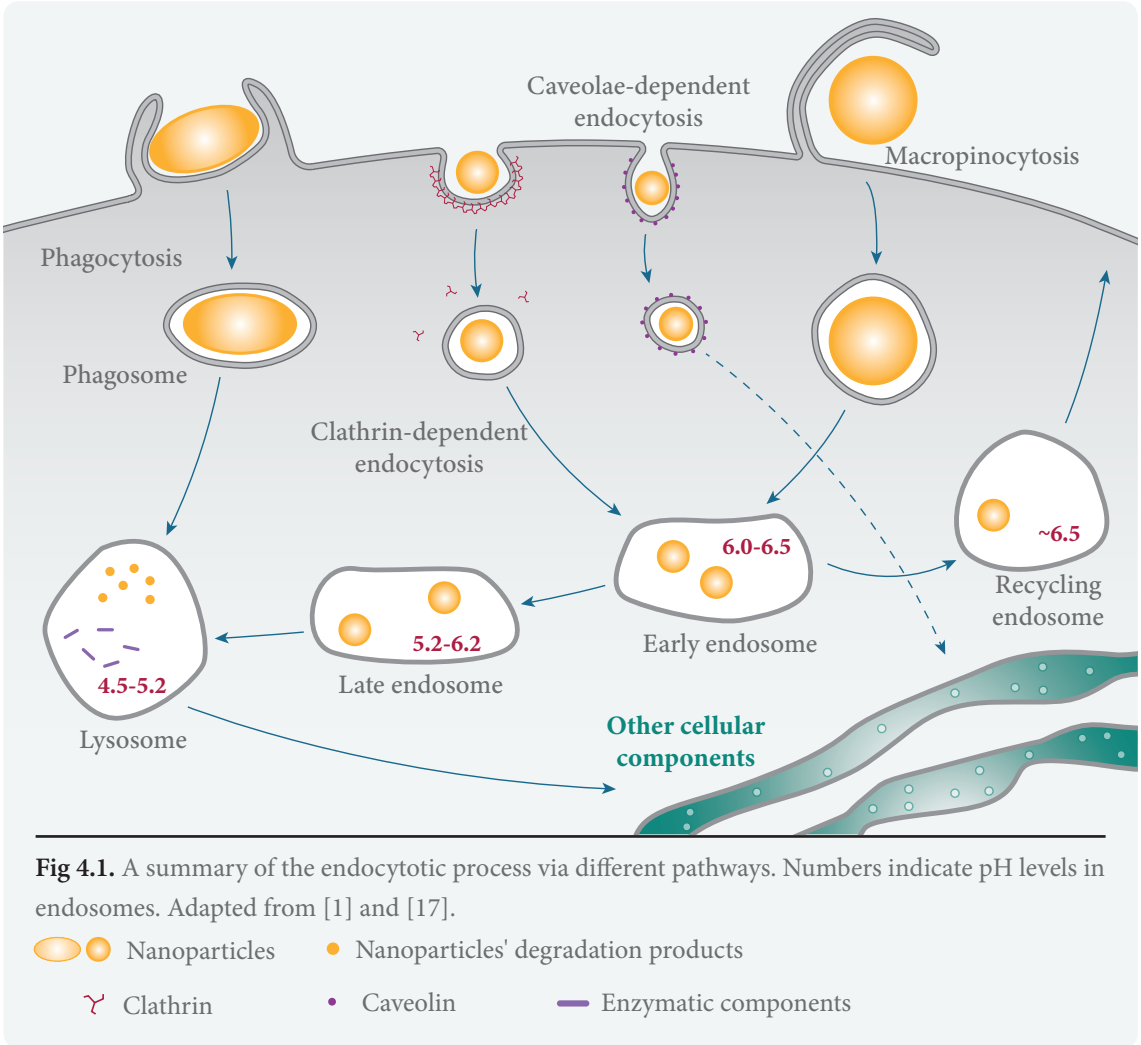

Fig 4.1. A summary of the endocytotic process via different pathways. Numbers indicate pH levels in endosomes. Adapted from [1] and [17].

Finally, it should be noted that it is of great importance to factor the uptake mechanism and the biofate of nanomaterials engineered for therapeutic purposes into their design. To obtain effective nanodelivery system, it would be important, for example, to determine whether the delivered NPs are needed to be hydrolysed in the lysosome to release the active drug, or whether the cargo is sensitive to enzymatic degradation and should be designed to avoid meeting lysosomes altogether.[2]

Attaining this kind of understanding of the possible biofate of the salicylic-acid-based NPs developed in work requires extensive research and is out of the scope of this project. However, *in vitro* work has been carried out to gauge how certain cancer cell lines react to being exposed to these particles and how that compares to their single-molecule counterparts.

4.2. Materials and instrumentation

The HCC1806 human breast cancer cell lines and the UKF-NB-3 human neuroblastoma cell line were provided by the Resistant Cancer Cell Line (RCCL) Collection established by the laboratories of Dr Jindrich Cinatl (Goethe University Frankfurt, Germany) and Dr Martin Michaelis (University of Kent, UK).

Iscove Modified Dulbecco Medium (IMDM) and foetal bovine serum (FBS) were obtained from Gibco. Phosphate-buffered saline (PBS) was obtained from Oxoid. Trypsin-EDTA and penicillin-streptomycin (Pen Strep) were obtained from Invitrogen. Trypan Blue was obtained from Sigma-Aldrich.

3-(4,5-dimethylthiazol-2-yl)-2,5-diphenyltetrazolium bromide (MTT), sodium dodecyl sulphate (SDS), and dimethylformamide (DMF) were obtained from Fisher scientific.

Paclitaxel, bleomycin, mitomycin, and temozolomide, and zeocin were sourced from Cayman Chemicals. Salicylic acid and aspirin were obtained from Acros Organics.

Cellstar® 96-well cell culture microplates were obtained from Greiner Bio-One. Dye intensity in the microplates was measured in PerkinElmer's Victor X4 Multilabel Plate Reader at a wavelength of 600 nm.

4.3. Experimental

4.3.1. Maintenance of cell lines

All consumables used for cell culture such as cell culture flasks, pipette tips, and serological pipettes were either sterile as purchased or were sterilised in-house via autoclaving. All surfaces and implements were sprayed with 70% ethanol before being placed in class II biological safety cabinet in which all handling of cell cultures was carried out.

Cells were typically grown in Iscove's Modified Dulbecco Medium supplemented with foetal bovine serum 10% v/v and penicillin/streptomycin 1% v/v. Cells were maintained in a humidified incubator at 37 °C under 5% CO_2 at physiological pH (7.2-7.4).

At about 80% confluence, the culture's medium was removed, and the cells were washed with 3 mL of PBS. The cells were detached following incubation with 1 mL of trypsin/EDTA solution for 5 minutes at 37 °C. The trypsin enzymatic reaction was terminated by the addition of 9 mL of complete medium to the cell culture flask. Cell passaging was usually done at a ratio of 1:10 by adding 1 mL of the newly suspended cell culture to 9 mL of complete medium in a new T25 flask.

For the paclitaxel-resistant cell line, 10 µL of paclitaxel in DMSO (20 µg/mL) was added to the new 10-mL T25 flask to achieve a final concentration of 20 ng/mL of paclitaxel.

All solid waste was autoclaved, whilst liquid waste was aspirated into a flask containing a working concentration (1%) of Virkon disinfectant solution.

4.3.2. Cell counting

A haemocytometer was used to determine the number of cells per mL. Briefly, a small volume of the cell suspension was mixed with Trypan Blue at a known ratio (the dilution factor), then about 10 µL of that mixture was deposited between the haemocytometer counting chamber and a coverslip. The haemocytometer was placed under an inverted microscope and cells were counted in the four outer quadrants of the chamber (each quadrant has a volume of 10^{-4} mL) and then the number was averaged. The number of cells per mL was then calculated as follows:

$$\text{Number of cells per mL} = \text{average number of counted cells} \times \text{dilution factor} \times 10^4$$

4.3.3. Cell viability assay

4.3.3.1. Determination of the half-maximal inhibitory concentrations (IC_{50})

After determining the number of cells per mL, about 5000 cells were seeded in each well of a 96-well culture plate (in a volume of 50 µL of the medium in each well).

Drug solutions were prepared in 8-point serial dilution sets at a ratio of 1:4 then aliquots of 50 µL of the drug solutions were added to the cell plates. Each set was repeated on the plate in triplicate. The plates were then incubated for five days in the cell culture incubator at 37°C with 5% CO_2.

After the incubation period, 25 μL of MTT was added to each well, and then the plates were incubated for a further 4 hours. 100 μL solution of SDS 20% (w/v) in a 1:1 mixture of DMF and de-ionised water (pH = 3.5-4.5) was added to each well, and the plates were left in the incubator overnight. The plates were read the next day in the plate reader at 600 nm. Viability changes upon treatment were determined as intensity percentages against control wells (untreated cells) after subtracting background values (blanks, medium only). Readings were normalised when possible and were then fit in a log(dose)-response model (in Prism GraphPad software) from which IC_{50}, the concentration of the compound that caused a 50% loss of metabolic activity, was calculated.

4.3.3.2. Drug comparison against different cell lines

After determining the IC_{50} for the different drugs, plates for different cell lines were prepared with around 5000 cells per well for each plate. Drugs, either individually or combinations, were added to the wells at their respective IC_{50}s in triplicates. The same MTT assay procedure mentioned above was followed.

4.3.4. Preparation of self-assembled PSA-b-mPEG NPs for the *in vitro* study

The co-solvent method discussed in Chapter 2 was used to prepare PSA-*b*-mPEG NPs for the cell viability assay with the exception of using autoclaved PBS for the aqueous medium instead of de-ionised water. Briefly, 10 mg of the block co-polymer was dissolved in 1 mL of THF. As the solution was stirring in a round-bottom flask, autoclaved PBS solution was added dropwise in a uniform manner using a micropipette until a tenfold dilution was achieved. The suspension was then loaded in a Visking dialysis membrane and was dialysed using autoclaved PBS. The volume was measured before and after removing the solvent to keep track of and adjust the concentration accordingly. Implements were washed, when possible, with 70% ethanol prior to their use.

4.4. Results and discussion

The MTT assay was used to evaluate the response of selected cancer cells to PSA-PEG NPs, their active molecule, salicylic acid (SA), and its therapeutically-related molecule aspirin (acetylsalicylic acid, ASA). This assay is a sensitive indicator that can be used to quantitatively measure the effect of treatment on the metabolic activity on cells *in vitro*. After treating cells with a proposed treatment, the yellow water-soluble tetrazolium dye, MTT, is added to the cell culture. Depending on the

viability of the cells in the culture, MTT is converted to the purple-coloured formazan crystals, primarily by the mitochondrial dehydrogenases. After dissolving the crystals, in DMF or DMSO for example, the concentration of the formazan product is analysed spectrophotometrically and is compared against untreated cells to determine the viability of the treated ones.[24] Figure 4.2 shows the structure of the MTT dye and its reduced version.

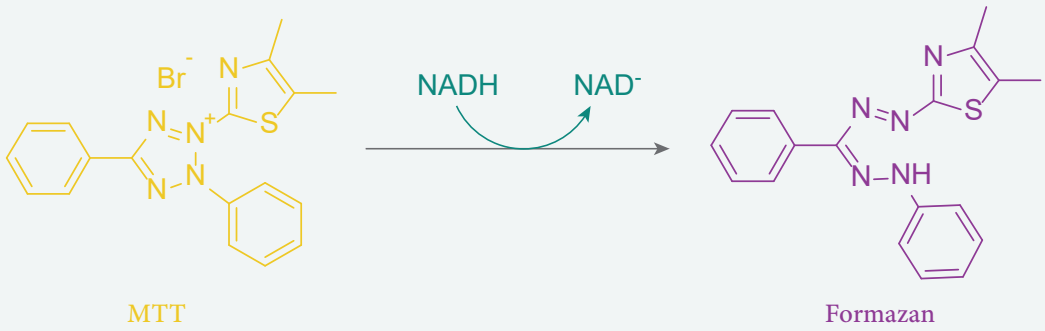

Fig 4.2. Reduction of MTT dye. The mitochondrial dehydrogenase converts the water-soluble yellow MTT dye to the insoluble formazan crystals.

Experiments were mainly conducted on two breast cancer cell lines, the chemo-naïve (parental) HCC1806 and its paclitaxel-resistant subline, HCC1806rPCL20 (i.e. HCC1806 cell line adapted to 20 ng/mL of paclitaxel, PCL). HCC1806 is a triple-negative breast cancer (TNBC) cell line, meaning that it lakes tumour cells lack oestrogen and progesterone receptors as well as the absence of the overexpression of human epidermal growth factor receptor-2 (HER-2).[25] Compared to the subtypes of breast cancer that express those receptors and respond well to hormonal and/or anti-HER-2 antibodies, TNBCs are resistant to many treatments and is associated with poor prognosis.[26] Even though TNBCs usually respond to cytotoxic chemotherapy, they have high relapse rates and a poor overall clinical outcome.[27] It was hypothesised that, if SA and its NP formulation could produce cell death in these cell lines, then this formulation would be a good candidate for the safe and effective management and prevention of TNBCs that would enhance patients' survival rate and their overall quality of life.

The first step was to evaluate the cytotoxicity of SA and ASA against the chosen cell lines in order to compare their effects as molecules with their NP counterparts and with other anti-tumour drugs.

For the sake of simplicity, the parental cell line will henceforth be called HCC180 PTL and the paclitaxel-resistant one will be called HCC1806 PAX.

Different sets of serial dilutions of SA and ASA were tried on the two cell lines. Concentrations with a micromolar order of magnitude (which is usually used with anti-tumour drugs) did not give any cytotoxic effects. Hence, concentrations within the millimolar order of magnitude were used instead until a response was achieved. Data was normalised and then plotted on a log(dose)-response graph to give a sigmoidal dose-response relationship to determine the IC_{50} values. The experiments were repeated in triplicates.

The IC_{50} of ASA for HCC1806 PTL was 0.65 mM (95% CI: 0.46-0.90, $r^2 = 0.94$) and 0.7 mM for HCC1806 PAX (95% CI: 0.58-0.86, $r^2 = 0.97$). The two cell lines were less sensitive to SA as its IC_{50} values were 0.99 mM (95% CI: 0.79-1.25, $r^2 = 0.97$) and 2.02 mM (95% CI: 1.60-2.56, $r^2 = 0.96$) for HCC1806 PTL and HCC1806 PAX, respectively. These concentrations are still within the clinically-relevant range as the therapeutic concentration after the administration of salicylates is typically between 1-2 mM.[28,29] Figure 4.3 illustrates the normalised log(dose)-response curves of ASA and SA for both cell lines.

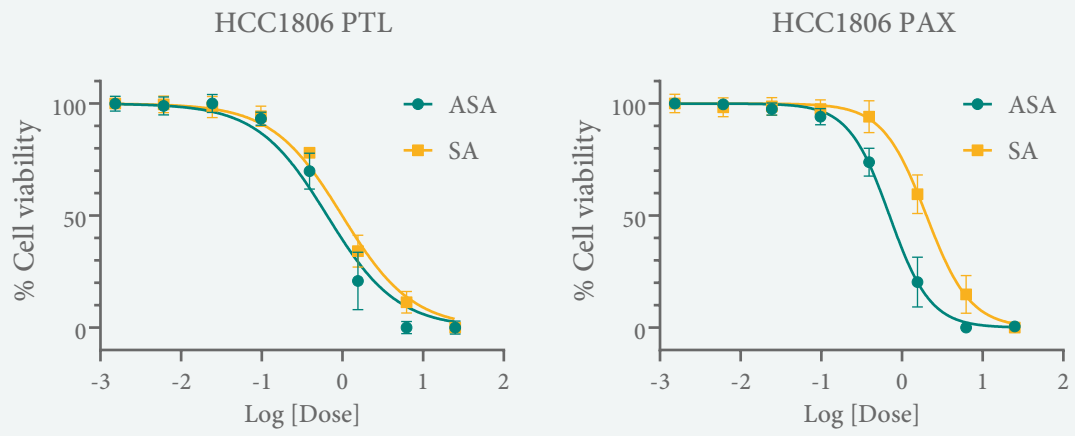

Fig 4.3. Normalised log(dose)-response curves of aspirin (ASA) and salicylic acid (SA) against the chemo-naïve (HCC1806 PTL) and the paclitaxil-resistant (HCC1806 PAX) breast cancer cell lines.

These values are comparable to the findings of Bashir *et al.* who tested ASA and SA on a colorectal cancer cell line and found that the IC_{50} values were 1.8 mM for ASA and 2.6 mM for SA.[30] Castaño[31] et al. identified the IC_{50} for ASA at 5 mM for a human colon adenocarcinoma cell line while

Vejselova et al[32] found the IC_{50} of SA to be 6 mM for a human lung adenocarcinoma cell line. Raza *et al.* also tested the inhibitory effect of ASA on a hepatoma cell but needed higher concentrations (5-10 mM).[33] The IC_{50} was not calculated, however, and these concentrations were used to induce maximum inhibition.

Results from the in vitro studies in this project and from the work of others, such as Bashir et al. discussed above,[30] show that the tested cancer cell lines are more sensitive to ASA than SA. From this, it could be inferred that the conversion of ASA to SA might not be as quick in vitro as it is in vivo, and that the two drugs might be interacting differently with cancer cells based on their lipophilicity.

As discussed in Chapter 2, the maximum circulation half-life of ASA in the body is about 20 minutes since it is rapidly hydrolysed to salicylic acid.[29] However, this hydrolysis might be happening at a much slower rate in the *in vitro* experiments. ASA is thought to be mainly hydrolysed via butyrylcholinesterase, paraoxonase, and albumin in the plasma as well as the platelet-activating Factor Acetylhydrolase 1b2 (PAFAH1b2) in the platelets.[34,35] However, the concentration of these hydrolases in the *in vitro* experiment would be very small, especially that the component of the growth medium that might contain these enzyme, i.e. FBS, is only used at a concentration of 10%. These hydrolases, if existent in the growth medium, would be easily saturated with the concentration of ASA used. The non-enzymatic hydrolysis of ASA happens at a slower rate. For instance, Bakar *et al.* found that the hydrolysis half-life of aspirin at 37 °C increased from 0.21 hours in complete blood, to 2.8 hours in plasma, to 15.4 hours in a phosphate buffer.[36]

It is well established that the more lipophilic a drug is the more rapidly it moves across the cell membrane during passive transcellular transport, but it could also undergo higher retention in the membrane which might limit its internalisation.[37,38] It could therefore be argued that, since SA is more lipophilic than ASA (Log*P* = 1.14 and 2.35 for ASA and SA, respectively),[39] SA is retained in the cell membrane at a greater extent than ASA while the later gets internalised more easily leading to a greater pharmacological response.

Determination of IC_{50} for polysalicylate (PSA) was not as straightforward. Because of its hydrophobic nature, the addition of PSA (dissolved in DMSO) to the culture medium caused it to precipitate immediately. The small volume of PSA (5 µL) added to the 995 µL of culture medium caused the formation of a rigid pellet that could not be dissolved upon agitation with the pipette, but instead broke down to small flakes. For this reason, the flake suspension was used as it is for seeding the polymer in the well plate with reconstitution upon each addition. Thus, the serial dilutions were of the flakes rather than PSA itself, making estimating the concentration of the polymer less accurate. Furthermore, The insoluble state of the polymer complicates interaction with the seeded cells. Nonetheless, Dasgupta et al. and Chandorkar et al. used discoid implants of their respective salicylic-acid-based polymers (discussed in Chapter 2) for their cytocompatibility studies, possibly due to similar solubility issues.[40,41]

Results were fitted in the same model as the small-molecule drugs (SA and ASA), but normalising data did not provide an accurate estimation of the IC_{50} of PSA (as could be inferred from the coefficient of determination, r^2) since none of the concentrations produced full inhibition of cell growth. Figure 4.4 illustrates both, the normalised and non-normalised log(dose)-response curves of PSA for both cell lines. The trend is the same in both cases, and although it is difficult to determine the IC 50 with a good degree of confidence from the normalised curve in this case, the non-normalised curve provides better information about how much inhibition each concentration produced. For example, The highest concentration of the PSA suspension produced 75% and 69% inhibition for the HCC1806 PTL and HCC1806 PAX respectively, while the lowest concentration produced only 9% and 14% inhibition for the parental and the paclitaxel-resistant cell lines, respectively.

Calculated IC_{50} values for the PSA suspensions as determined from the normalised curves were 0.58 mM (95% CI: 0.45-0.72, $r^2 = 0.84$) [equivalent to 3.48 mM SA] and 0.49 mM (95% CI: 0.36-0.66, $r^2 = 0.78$) [equivalent to 2.94 mM SA] for HCC1806 PTL and HCC1806 PAX, respectively.

Although expressing the inhibitory effect of PSA in this case by concentration is not truly representative both because of the solubility issue and the poorly-fitted graph, the data shows that PSA still exhibited some cytotoxic activity even in its non-dissolved state. Since both cell lines

are of the adherent type, cells were seeded and were left in the incubator for 24 hours before the addition of the PSA suspension, as opposed to seeding the cells and the drug flakes in the same settings. This was done to exclude the physical interference of the flakes with the adhesion of the cells. The results, however, were similar in both cases.

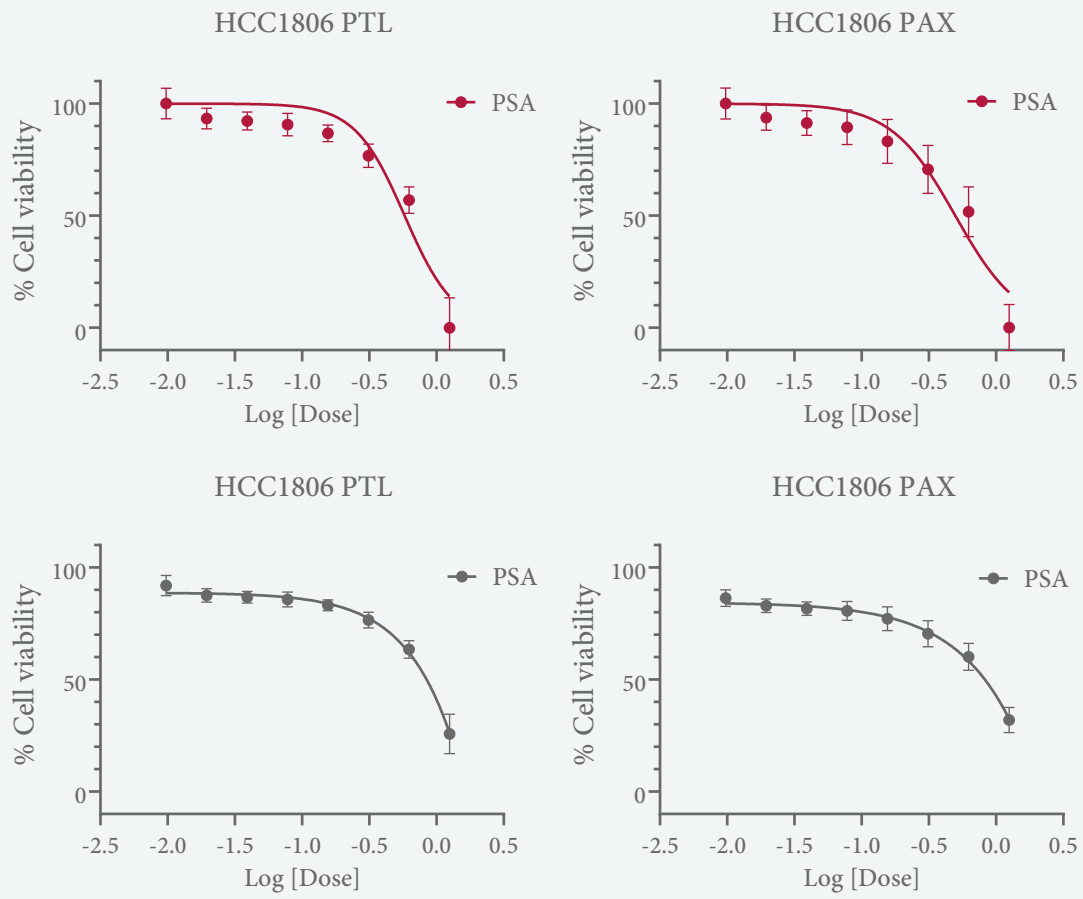

Fig 4.4. Normalised (top) and non-normalised (bottom) log(dose)-response curves of polysalicylate (PSA) against the chemo-naïve (HCC1806 PTL) and the paclitaxil-resistant (HCC1806 PAX) breast cancer cell lines.

Whether there is some sort of physical inhibition to cellular growth, or whether the PSA has inherent cytotoxic properties, or whether there is simply a slow release of SA from the polymer that induced some inhibition of cell growth over the incubation period of 5 days warrants further investigation.

Self-assembled PSA-PEG vesicles like those discussed in Chapter 2 were also prepared in autoclaved PBS and tested for their cytotoxic effect. The tested vesicles had a z-average diameter of 364 nm as determined by DLS (Figure 4.5). Because the synthesis method did not allow for

the use of high concentrations of the NPs without resulting in non-uniform precipitations during self-assembly, and because only a reasonable amount of the NP suspension could be added to the cell cultures without diluting the growth medium to the extent that would interfere in cell growth, the maximum concentration of the NP suspension that could be used was 0.25 mg/mL and, consequently, the serial dilutions for the cell viability assay were only performed at a ratio of 1:2 to avoid exaggerated dilution.

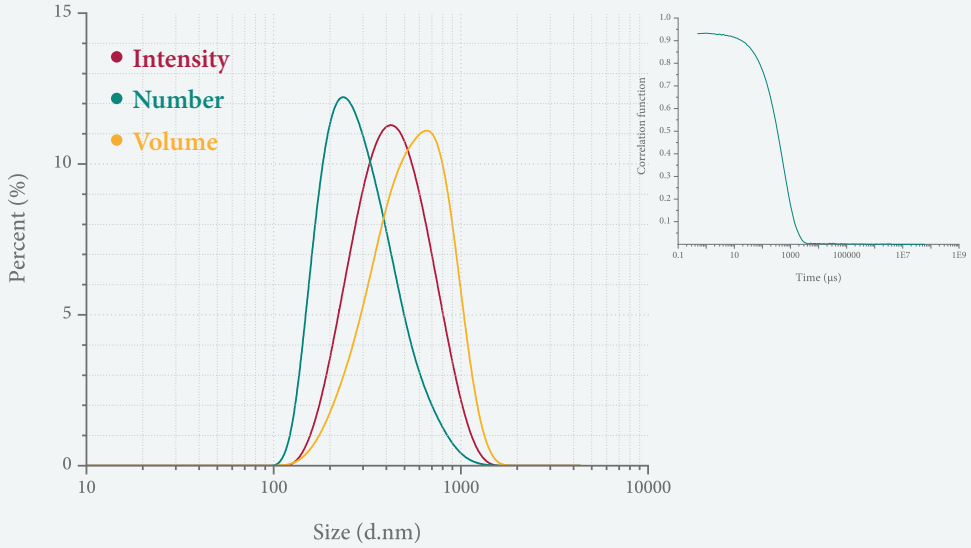

Fig 4.5. Size distribution of the PSA-PEG NPs used for the cell viability assay.

Nonetheless, the highest concentrations still exhibited some cytotoxic activity for both cell lines. However, fitting and normalising data in the familiar log(dose)-response model to extrapolate the IC_{50} did not yield accurate results because, as in the case with PSA, none of the concentrations used fully inhibited cell growth. The calculated IC_{50} values were 0.07 mg/mL (95% CI: 0.04-0.12, $r^2 = 0.65$) and 0.03 mg/mL (95% CI: 0.02-0.14, $r^2 = 0.83$) for HCC1806 PTL and HCC1806 PAX, respectively (Figure 4.6).

Although IC_{50} values could not be inferred from the normalised data, the raw data shows that the highest concentration of the NP suspension still managed to kill about 45% and 30% of the culture for the HCC1806 PTL and HCC1806 PAX cell lines, respectively.

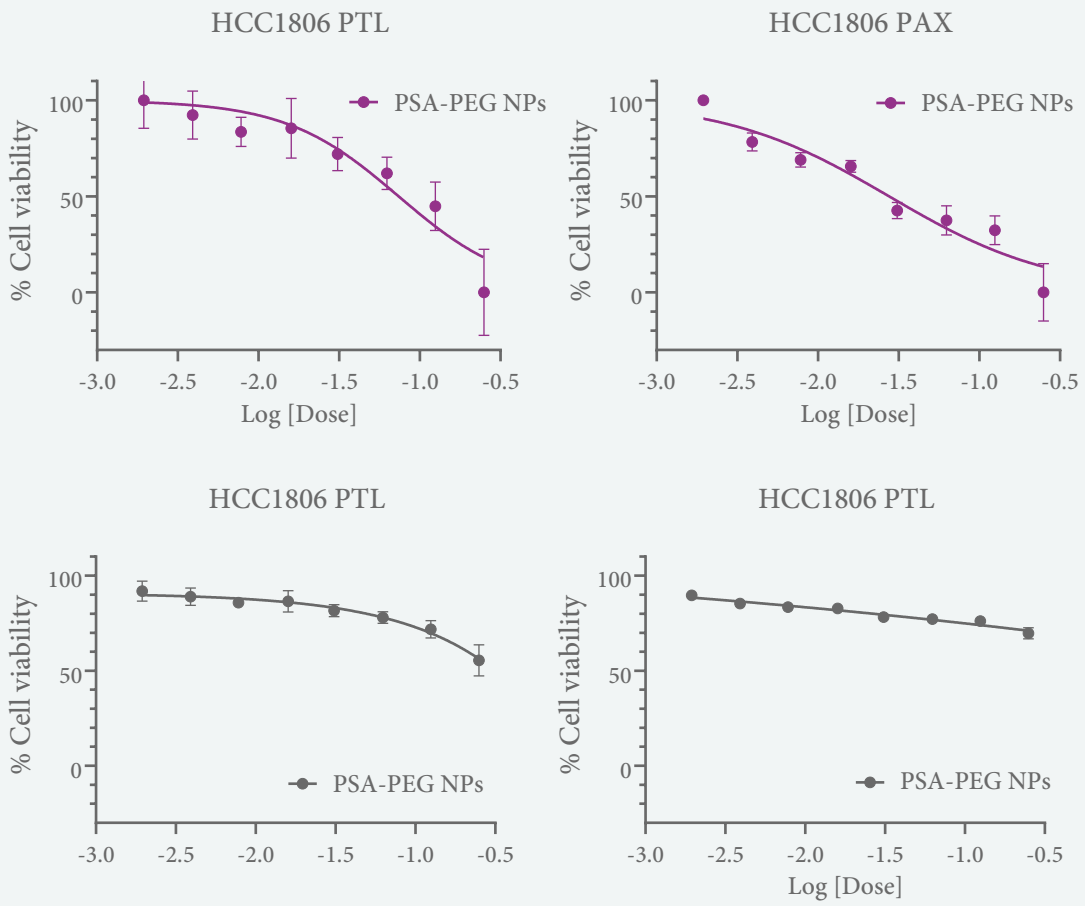

Fig 4.6. Normalised (top) and non-normalised (bottom) log(dose)-response curves of PSA-PEG nanoparticles against the chemo-naïve (HCC1806 PTL) and the paclitaxil-resistant (HCC1806 PAX) breast cancer cell lines.

To investigate whether PEG had an active role in the cytotoxicity of NPs, the MTT assay was also performed on the cells using PEG. However, it failed to produce any notable toxicity even at high concentrations (20 mM). Figure 4.7 shows the log(dose)-response curves of mPEG for the two cell lines.

Without proper visualisation methods backed by genetic manipulation and/or pharmacological manipulation studies (to inhibit specific uptake routes to examine others),[42] it would not be possible to determine the pathway by which the PSA-PEG NPs are taken up by the cells. However, judging by the relatively large size of the vesicles and the lack of targeting ligands on the NPs, it can be speculated that the uptake most likely happened via macropinocytosis.[1,43] This pathway was observed to be the main entry route for a wide array of nanoparticles, including polymeric ones, and of different shapes and sizes.[44] However, large particles appear to only be able to enter

cells either by micropinocytosis or phagocytosis.[44,45] The endosomes containing the particles would then possibly fuse with the lysosomes where there is an abundance of hydrolytic enzymes (about 60 in some cells) and an acidic pH or about 4.0-5.5.[46–48] It could be speculated that, after the degradation of the ester bonds on the PSA, some of the released SA becomes protonated at that pH and is able to permeate through the phospholipid membrane of the lysosome and into the cytoplasm of the cell.

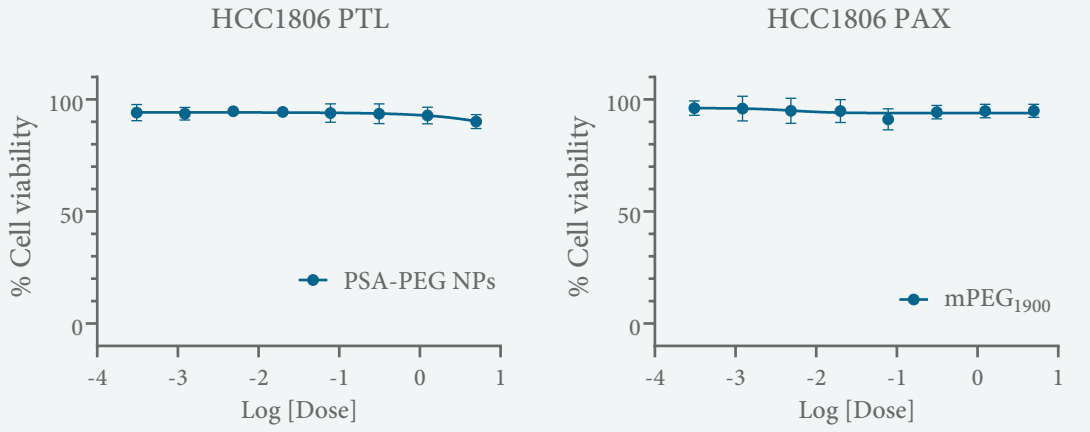

Fig 4.7. Log(dose)-response curves of methoxy polyethylene glycol ($mPEG_{1900}$) against the chemo-naïve (HCC1806 PTL) and the paclitaxil-resistant (HCC1806 PAX) breast cancer cell lines.

The NPs were also investigated for a potential synergetic effect with other cytotoxic drugs. Firstly, four drugs, bleomycin, mitomycin, and temozolomide, and zeocin were screened for their cytotoxic effect on both cell lines. Of the four, only bleomycin and mitomycin exhibited inhibitory effects. The cytotoxic effect of these agents is mainly due to their ability to bind to and damage cellular DNA.[49,50]

The IC_{50} values for these two drugs were then determined for the two cancer cell lines. For bleomycin, IC_{50} was 0.10 μM (95% CI: 0.07-0.14, $r^2 = 0.99$) and 0.14 μM (95% CI: 0.04-0.41, $r^2 = 0.88$) for HCC1806 PTL and HCC1806 PAX, respectively. For mitomycin, the values were 0.04 μM (95% CI: 0.03-0.05, $r^2 = 0.99$) and 0.12 μM (95% CI: 0.09-0.16, $r^2 = 0.99$) for HCC1806 PTL and HCC1806 PAX, respectively. These results are comparable to the values provided by The Genomics of Drug Sensitivity in Cancer Project for the HCC1806 cell line where the IC_{50} values are 0.23 μM for bleomycin and 0.14 μM for mitomycin.[51,52] Figure 4.8 shows the normalised log(dose)response curves of bleomycin and mitomycin for the two cell lines.

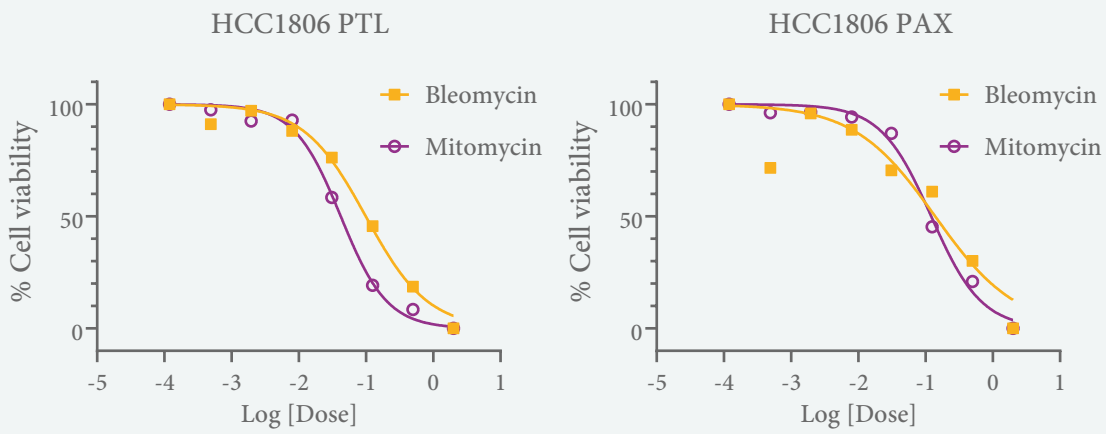

Fig 4.8. Normalised log(dose)-response curves of bleomycin and mitomycin against the chemo-naïve (HCC1806 PTL) and the paclitaxil-resistant (HCC1806 PAX) breast cancer cell lines.

The individual drugs (ASA, SA, bleomycin and mitomycin), PSA-PEG NPs, and different combinations were tested against the cell lines using their respective IC_{50}s under the same experimental conditions.

Figure 4.9 shows a comparison of the effect of different treatments, either individually or in combinations, on the two cancer cell lines. Generally, the parental cell line was more sensitive to almost all treatments than the paclitaxel-resistant cell line. Aspirin showed efficacy comparable to that of bleomycin and mitomycin by suppressing cell growth by 80% for the parental cell line and 70% for the paclitaxel-resistant one. Salicylic acid exhibited almost half of the efficacy of aspirin. PSA-PEG vesicles showed minimal inhibition of both cell lines with inhibition of only about 22% for HCC1806 PTL and about 15% for HCC1806 PAX.

Combining aspirin with the cytotoxic drugs bleomycin and mitomycin increased their efficacy by about 10%, while the increase was marginal or non-existent in the case of combining salicylic acid or the PSA-PEG nanoparticles with either drug. The increase of cytotoxicity might be due to the different mechanisms by which bleomycin and mitomycin, on one hand, and ASA (and possibly SA and its NP formulation at higher doses), on the other, exert their effects on cancer cells. While the cytotoxic drugs used affect cancer cells by damaging their DNA, aspirin might induce cell apoptosis by increasing the expression of pro-apoptotic proteins (such as Bcl2) and reduce the expression of anti-apoptotic proteins (such as Bax), possibly through COX-independent pathways.[53]

Fig 4.9. A comparison of cytotoxicity of different treatments, individually and in combinations, against the two breast cancer cell lines. Data is represented by mean ± SD from a representative experiment with treplicate wells per treatment.

If this is the case, then it would be advantageous to combine both classes, firstly to minimise the gruesome side effects of the cytotoxic drugs, and secondly to have a better therapeutic response with drug-resistant cancers. Resistance to chemotherapy has been attributed to the to the upregulation of anti-apoptotic proteins and the downregulation of the pro-apoptotic ones.[54] It has also been linked to mutations in the p53 gene, impairing the connection between DNA damage (caused by the cytotoxic drugs) and the activation of apoptosis.[55] Combining NSAIDs with chemotherapy could enhance the therapeutic outcome.

It should be noted, nonetheless, that this was a preliminary experiment that was performed towards the end of the project to form a basic idea about how the PSA-PEG NPs compare to their small-molecule counterparts and in combination with other cytotoxic drugs. The experiment should be repeated at least in triplicate before any significance could be drawn from it through analysis of variance (ANOVA), for instance. Perhaps the biggest drawback of this experiment was the limit on the concentration of the NPs that could be used, but the inhibitory response that the NP suspensions exhibited either alone or in combination with other established cytotoxic drug, albeit modest, shows that the polysalicylate nanoparticles might have a potentially useful application in targeted therapy even when used at low concentrations.

Towards the end of the project, more *in vitro* studies were initiated for another cancer cell line, that being the neuroblastoma cell line; UKF-NB-3. Neuroblastoma is the most common and deadly solid tumour of childhood with cases ranging from spontaneous regression in some patients to very bad prognosis and metastasis, even with aggressive treatment, in others.[56] This heterogeneity in prognosis and the general trend towards minimising therapy[57] make a targeted approach to therapy a favourable option. Moreover, aspirin and its derivatives are contraindicated in children due to the high risk of developing Reye's syndrome. Although not fully understood yet, the disease that causes deadly injuries to the brain and liver is believed to develop in children under 16 years of age when they are treated with salicylates during or around an incidence of viral infection.[58] If aspirin was proved to be effective in the management of neuroblastoma in children, a targeted approach in therapy that concentrates the drug in the solid tumour would help mitigate, or even eliminate, the risk of developing Reye's syndrome.

MTT assay showed a similar trend in response to treatments to those observed in the HCC1806 cell lines, although the neuroblastoma cell line appeared to be slightly more sensitive that the breast cancer cell line. IC_{50} values were 0.31 mM (95% CI: 0.18-0.52, $r^2 = 0.97$) for ASA and 0.48 mM (95% CI: 0.35-0.66, $r^2 = 0.99$) for SA (Figure 4.10).

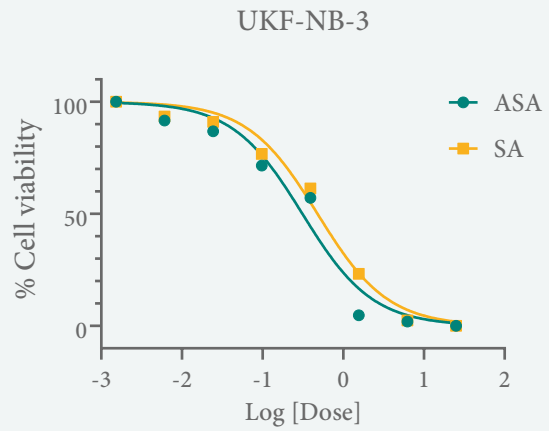

Fig 4.10. Normalised log(dose)-response curves of aspirin (ASA) and salicylic acid (SA) against the UKF-NB-3 neuroblastoma cell line.

Sensitivity to PSA (Figure 4.11) also showed a similar trend with the exception that the highest concentration of the PSA suspension (1.25 mM, equivalent to 7.5 mM SA) killed 96% of the cell

culture. However, given the fact that the experiment was only carried out once and that PSA was used as a suspension rather than a solution, this result should be interpreted cautiously and requires further investigation.

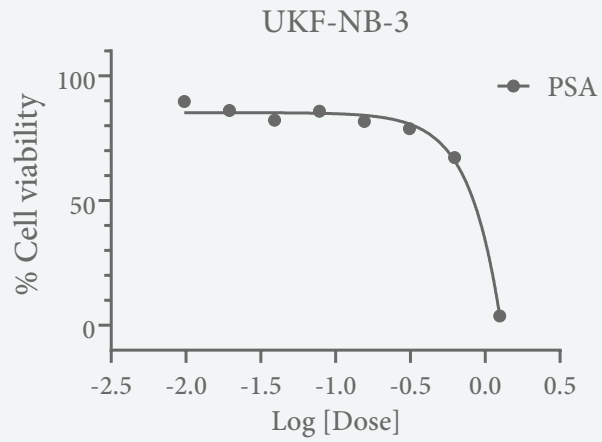

Fig 4.11. Log(dose)-response curve of PSA against the UKF-NB-3 neuroblastoma cell line.

The UKF-NB-3 cell line also showed a response to PSA-PEG NPs similar to that of the other cell lines. IC_{50} was found to be 0.05 mg/mL (95% CI: 0.03-0.08, r^2 = 0.94). Figure 4.12 shows the normalised and non-normalised log(dose)-response curves for the PSA-PEG NPs against the neuroblastoma cell line.

Although this value might not be representative of a true IC_{50} due to the lack of a good distribution of points between 0% and 100% in the original (non-normalised) data, it still can be noted that the NPs induced an inhibitory response that is comparable across all three cell lines.

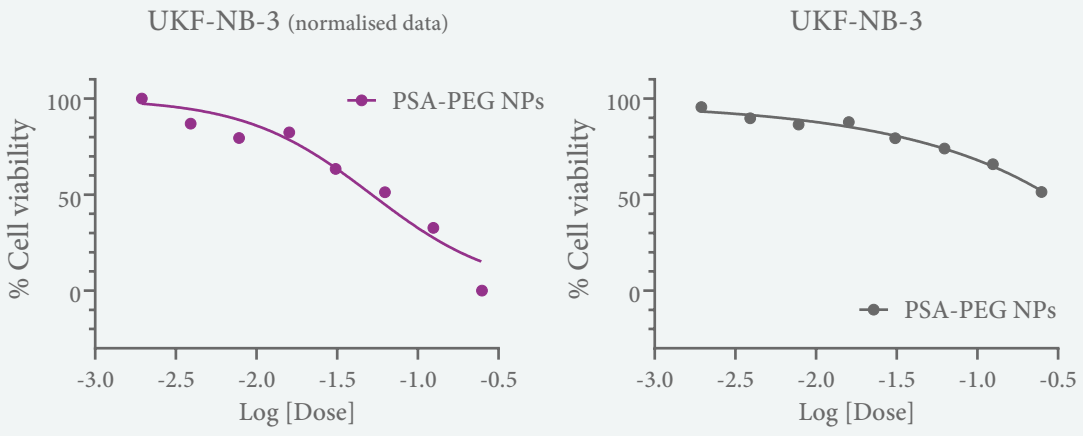

Fig 4.12. The normalised (left) and non-normalised (right) log(dose)-response curves of PSA-PEG NPs against the UKF-NB-3 cell line.

In anticipation of the successful synthesis of the ibuprofen-loaded polyphosphoesters, the three cell lines were inspected for sensitivity against ibuprofen. The drug induced a cytotoxic response in all three cell lines similar to that observed with ASA and SA.

IC_{50} values were 0.30 mM (95% CI: 0.18-0.49, $r^2 = 0.97$), 0.22 mM (95% CI: 0.14-0.34, $r^2 = 0.98$), and 0.13 mM (95% CI: 0.09-0.18, $r^2 = 0.98$) for HCC1806 PTL, HCC1806 PAX, and UKF-NB-3, respectively. Figure 4.13 illustrates the normalised log(dose)-response curve of ibuprofen against the three cell lines.

Like the case of ASA and SA, These values fall within the range of plasma concentrations of ibuprofen after a normal therapeutic dose.[59] This might be another indication of the potential value of NSAIDs in the fight against cancer.

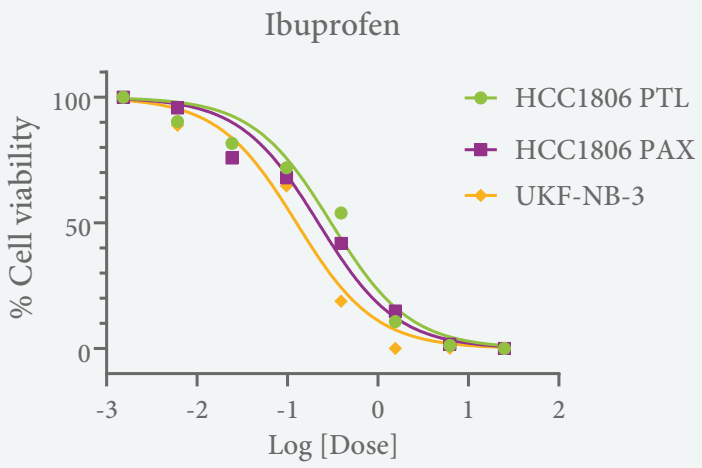

Fig 4.13. Normalised log(dose)-response curve of ibuprofen against HCC1806 PTL, HCC1806 PAX, and UKF-NB-3.

4.5. Conclusion

The first *in vitro* study of the developed PSA-PEG NPs showed that they are able to induce cytotoxicity, albeit modest at low concentrations, in at least three cell lines; two breast cancer cell lines, one of which is chemo-resistant, and one neuroblastoma cell line. The study also confirmed that aspirin and its anti-inflammatory hydrolysis product, salicylic acid, do induce cytotoxicity in the same cell lines at clinically relevant concentrations. This proves that designing nano-vehicles

that can effectively deliver the anti-inflammatory salicylic acid to solid tumours might indeed prove to be useful in maximising the potential chemotherapeutic value of this drug.

However, biological systems are much more complicated than a small cell culture and the MTT assay, despite being a good basis to evaluate the biological response, has many shortcomings when it comes to testing NPs. For example, not only does not account for the immunological response of the RES system towards NPs and other barriers that particles have to overcome before reaching cancer cells (e.g. the interstitial fluid pressure), but it can also be affected by other factors not encountered with conventional drugs, such as the fact that the adsorption of the medium's proteins on the tested nanoparticles might possibly change the composition of the medium and deprive the cell culture of vital nutrients, complicating the results of the test.[60] Moreover, one of the proposed mechanisms by which the NSAID-mediated suppression of PGE_2 leads to curbing tumour growth is via the suppression of angiogenesis, cell adhesion and metastasis,[61] all of which cannot be observed in simple cell cultures.

Nonetheless, this assay still serves as a good starting point for more sophisticated testing such as those carried out *in vitro* in 3D cell culture models or *in vivo*.[62]

4.6. References

1 S. Behzadi, V. Serpooshan, W. Tao, M. A. Hamaly, M. Y. Alkawareek, E. C. Dreaden, D. Brown, A. M. Alkilany, O. C. Farokhzad and M. Mahmoudi, *Chem. Soc. Rev.*, 2017, **46**, 4218–4244.

2 M. J. Ernsting, M. Murakami, A. Roy and S. D. Li, *J. Control. Release*, 2013, **172**, 782–794.

3 C. Auría-Soro, T. Nesma, P. Juanes-Velasco, A. Landeira-Viñuela, H. Fidalgo-Gomez, V. Acebes-Fernandez, R. Gongora, M. J. Almendral Parra, R. Manzano-Roman and M. Fuentes, *Nanomaterials*, 2019, **9**, 1365.

4 S. Zanganeh, R. Spitler, M. Erfanzadeh, A. M. Alkilany and M. Mahmoudi, *Int. J. Biochem. Cell Biol.*, 2016, **75**, 143–147.

5 H. Hillaireau and P. Couvreur, *Cell. Mol. Life Sci.*, 2009, **66**, 2873–2896.

6 S. M. Moghimi, A. C. Hunter and J. C. Murray, *Pharmacol. Rev.*, 2001, **53**, 283–318.

7 M. Cataldi, C. Vigliotti, T. Mosca, M. Cammarota and D. Capone, *Int. J. Mol. Sci.*, 2017, **18**, 1249.

8 M. Demoy, J. P. Andreux, C. Weingarten, B. Gouritin, V. Guilloux and P. Couvreur, *Pharm. Res.*, 1999, **16**, 37–41.

9 H. Soo Choi, W. Liu, P. Misra, E. Tanaka, J. P. Zimmer, B. Itty Ipe, M. G. Bawendi and J. V. Frangioni, *Nat. Biotechnol.*, 2007, **25**, 1165–1170.

10 J. Fang, H. Nakamura and H. Maeda, *Adv. Drug Deliv. Rev.*, 2011, **63**, 136–151.

11 A. Vonarbourg, C. Passirani, P. Saulnier and J. P. Benoit, *Biomaterials*, 2006, **27**, 4356–4373.

12 J. V. Jokerst, T. Lobovkina, R. N. Zare and S. S. Gambhir, *Nanomedicine*, 2011, **6**, 715–728.

13 A. Gabizon, R. Isacson, O. Rosengarten, D. Tzemach, H. Shmeeda and R. Sapir, *Cancer Chemother. Pharmacol.*, 2008, **61**, 695–702.

14 J. W. Nichols and Y. H. Bae, *Nano Today*, 2012, **7**, 606–618.

15 P. Foroozandeh and A. A. Aziz, *Nanoscale Res. Lett.*, 2018, **13**, 339.

16 F. Zhao, Y. Zhao, Y. Liu, X. Chang, C. Chen and Y. Zhao, *Small*, 2011, **7**, 1322–1337.

17 M. C. Kerr and R. D. Teasdale, *Traffic*, 2009, **10**, 364–371.

18 B. Yameen, W. Il Choi, C. Vilos, A. Swami, J. Shi and O. C. Farokhzad, *J. Control. Release*, 2014, **190**, 485–499.

19 A. E. Nel, L. Mädler, D. Velegol, T. Xia, E. M. V Hoek, P. Somasundaran, F. Klaessig, V. Castranova and M. Thompson, *Nat. Mater.*, 2009, **8**, 543–557.

20 J. P. Luzio, P. R. Pryor and N. A. Bright, *Nat. Rev. Mol. Cell Biol.*, 2007, **8**, 622–632.

21 J. E. DiCiccio and B. E. Steinberg, *J. Gen. Physiol.*, 2011, **137**, 385–390.

22 I. R. Nabi and P. U. Le, *J. Cell Biol.*, 2003, **161**, 673–677.

23 N. Mizushima, *Genes Dev.*, 2007, **21**, 2861–2873.

24 V. Patravale, P. Dandekar and R. Jain, in *Nanoparticulate Drug Delivery*, Elsevier, 2012, pp. 123–155.

25 K. J. Chavez, S. V. Garimella and S. Lipkowitz, *Breast Dis.*, 2010, **32**, 35–48.

26 S. Boichuk, A. Galembikova, A. Sitenkov, R. Khusnutdinov, P. Dunaev, E. Valeeva and N. Usolova, *Oncol. Lett.*, 2017, **14**, 5039–5045.

27 A. Bosch, P. Eroles, R. Zaragoza, J. R. Viña and A. Lluch, *Cancer Treat. Rev.*, 2010, **36**, 206–215.

28 B. Frantz, E. A. O'Neill;, S. Ghosh and E. Kopp, *Science (80-.).*, 1995, **270**, 2017–2019.

29 R. Amann and B. A. Peskar, *Eur. J. Pharmacol.*, 2002, **447**, 1–9.

30 A. I. J. Bashir, C. S. Kankipati, S. Jones, R. M. Newman, S. T. Safrany, C. J. Perry and I. D. Nicholl, *Int. J. Oncol.*, 2019, **54**, 1256–1270.

31 E. Castaño, M. Dalmau, M. Barragán, G. Pueyo, R. Bartrons and J. Gil, *Br. J. Cancer*, 1999, **81**, 294–299.

32 D. Vejselova and H. M. Kutlu, *Turkish J. Biol.*, 2015, **39**, 1–5.

33 H. Raza, A. John and S. Benedict, *Eur. J. Pharmacol.*, 2011, **668**, 15–24.

34 G. Zhou, G. K. Marathe, J. Hartiala, S. L. Hazen, H. Allayee, W. H. Wilson Tang and T. M. McIntyre, *J. Biol. Chem.*, 2013, **288**, 11940–11948.

35 F. G. Bahar and T. Imai, *Drug Metab. Dispos.*, 2013, **41**, 1450–1456.

36 S. K. Bakar and S. Niazi, *J. Pharm. Sci.*, 1983, **72**, 1024–1026.

37 Y. Lee and S. Q. Choi, Eur. J. Pharm. Sci., 2019, **134**, 176–184.

38 M. R. Naylor, A. M. Ly, M. J. Handford, D. P. Ramos, C. R. Pye, A. Furukawa, V. G. Klein, R. P. Noland, Q. Edmondson, A. C. Turmon, W. M. Hewitt, J. Schwochert, C. E. Townsend, C. N. Kelly, M. J. Blanco and R. S. Lokey, J. Med. Chem., 2018, **61**, 11169–11182.

39 M. Dołowy and A. Pyka, J. Liq. Chromatogr. Relat. Technol., 2015, **38**, 485–491.

40 Q. Dasgupta, K. Chatterjee and G. Madras, *Mol. Pharm.*, 2015, **12**, 3479–3489.

41 Y. Chandorkar, R. K. Bhagat, G. Madras and B. Basu, *Biomacromolecules*, 2014, **15**, 863–875.

42 D. Vercauteren, R. E. Vandenbroucke, A. T. Jones, J. Rejman, J. Demeester, S. C. De Smedt, N. N. Sanders and K. Braeckmans, *Mol. Ther.*, 2010, **18**, 561–569.

43 M. Walsh, M. Tangney, M. J. O'Neill, J. O. Larkin, D. M. Soden, S. L. McKenna, R. Darcy, G. C. O'Sullivan and C. M. O'Driscoll, *Mol. Pharm.*, 2006, **3**, 644–653.

44 A. S. Desai, M. R. Hunter and A. N. Kapustin, *Philos. Trans. R. Soc. Lond. B. Biol. Sci.*, 2019, **374**, 20180156.

45 D. A. Kuhn, D. Vanhecke, B. Michen, F. Blank, P. Gehr, A. Petri-Fink and B. Rothen-Rutishauser, *Beilstein J. Nanotechnol.*, 2014, **5**, 1625–1636.

46 G. Bloomfield and R. R. Kay, *J. Cell Sci.*, 2016, **129**, 2697–2705.

47 A. M. Cataldo, P. A. Paskevich, E. Kominami and R. A. Nixon, *Proc. Natl. Acad. Sci.*, 1991, **88**, 10998–11002.

48 B. Rathore, K. Sunwoo, P. Jangili, J. Kim, J. H. Kim, M. Huang, J. Xiong, A. Sharma, Z. Yang, J. Qu and J. S. Kim, *Biomaterials*, 2019, **211**, 25–47.

49 J. Chen, M. K. Ghorai, G. Kenney and J. Stubbe, 2008, **36**, 3781–3790.

50 M. M. Paz, X. Zhang, J. Lu and A. Holmgren, *Chem. Res. Toxicol.*, 2012, **25**, 1502–1511.

51 Genomics of Drug Sensitivity in Cancer, Bleomycin, https://www.cancerrxgene.org/compound/Bleomycin/190/overview/ic50, (accessed 30 September 2020).

52 Genomics of Drug Sensitivity in Cancer, Mitomycin-C, https://www.cancerrxgene.org/compound/Mitomycin-C/136/overview/ic50, (accessed 30 September 2020).

53 Z. Zhang, F. Chen and L. Shang, *Cancer Manag. Res.*, 2018, **Volume 10**, 4631–4640.

54 B. Mansoori, A. Mohammadi, S. Davudian, S. Shirjang and B. Baradaran, *Adv. Pharm. Bull.*, 2017, **7**, 339–348.

55 J. M. L. De Vree, E. Jacquemin, E. Sturm, D. Cresteil, P. J. Bosma, J. Aten, J. F. Deleuze, M. Desrochers, M. Burdelski, O. Bernard, R. P. J. Oude Elferink and M. Hadchouel, *Proc. Natl. Acad. Sci. U. S. A.*, 1998, **95**, 282–287.

56 G. M. Brodeur, *Nat. Rev. Cancer*, 2003, **3**, 203–216.

57 J. R. Park, A. Eggert and H. Caron, *Pediatr. Clin. North Am.*, 2008, **55**, 97–120, x.

58 A. Pugliese, T. Beltramo and D. Torre, *Cell Biochem. Funct.*, 2008, **26**, 741–746.

59 N. M. Davies, *Clin. Pharmacokinet.*, 1998, **34**, 101–154.

60 M. Mahmoudi, A. Simchi, M. Imani, M. A. Shokrgozar, A. S. Milani, U. O. Häfeli and P. Stroeve, Colloids Surfaces B Biointerfaces, 2010, **75**, 300–309.

61 D. G. Menter and R. N. DuBois, *Int. J. Cell Biol.*, 2012, **2012**, 1–21.

62 L. B. Sims, M. K. Huss, H. B. Frieboes and J. M. Steinbach-Rankins, *J. Nanobiotechnology*, 2017, **15**, 1–15.

Chapter 5

Summary and future outlook

Summary of work

The race against cancer calls for innovative treatments that are not only efficacious against the vicious disease, but that also mitigate its devastating effects on all levels. Treatments that could enhance the patient's quality of life effectively and safely or be used as prevention, all while reducing costs both during development and hospitalisation are the holy grail of cancer therapy.

This project stemmed from the concept that aspirin and other NSAIDs have shown promise in reducing cancer risk in susceptible patients. Being a class of drugs that is cheap, widely available, and with a wide therapeutic window that makes them safer to use and handle than conventional cytotoxic drugs, NSAIDs provided good candidates to be employed in a nanodelivery systems. These systems can be loaded with drugs and exclusively deliver them to tumour foci in concentrations much higher than conventional therapy and with much reduced adverse effects thanks to their unique physicochemical characteristics that help them exploit the uniqueness of the tumour microenvironment (TME).

1

The first part of Chapter 1 of this thesis explored the evidence of the efficacy of various NSAIDs in reducing the risk, recurrence, and metastases of different types of cancer. The strength of this evidence was investigated based on the types of trials and their results. Unsurprisingly, aspirin was the most studied NSAID since it has been the most popular of its class for decades. The strongest evidence came from trials that investigated the effects of aspirin on the incidence and mortality of colorectal cancer since those trials included a very large number of patients and for long periods of time. Nonetheless, aspirin and other NSAIDs have shown a positive role in different types of cancer as well, such as prostate, breast and kidney malignancies.

The possible mechanisms by which NSAIDs exert their anti-tumour effects were examined in the second part of Chapter 1. The most prominent hypothesis argues that NSAIDs suppress tumour growth through their inhibition of cyclooxygenases 1 and 2 (COX-1,-2) and the subsequent interruption in the production of prostaglandin E_2 (PGE_2), an eicosanoid responsible for inducing inflammation and the proliferation and growth of cancer cells. COX-independent mechanisms that lead to the induction of apoptosis have also been suggested.

The third part of the chapter looked into the main concepts behind nanotherapy via examining the pathophysiological characteristics that distinguish the tumour microenvironment from healthy tissues and how they can be exploited. The main pathophysiological feature of TME was the leaky vasculature and the poor lymphatic drainage that lead to the enhanced permeability and retention (EPR) effect which allows nanoparticles of a certain size (ideally 100-200 nm) to penetrate the TME and accumulate in it. The text examined other features as well, such as the overexpression of certain receptors that can be used for a more targeted approach in nanomedicine. Barriers to nanotherapy were also discussed; phagocytosis by the reticuloendothelial system (RES), and the elevated interstitial fluid pressure (IFP) were among the primary concerns.

A summary followed of the relationship between the nanoparticles' physicochemical characteristics like shape, size and surface charge with the biological response. The chapter concluded with an overview of the mainstream types of nanoparticles that are either in clinical use or under development and some of the examples of how different nano-systems has been developed for the delivery of NSAIDs, some of which were intended for cancer targeting.

2

Chapter 2 presented the work done to develop NSAID-based polymeric NPs. Since the anti-inflammatory effect of aspirin is mainly attributed to its hydrolysis product, salicylic acid, the latter was the main building block of the polymer. Because the molecule possesses one hydroxyl and one carboxyl groups, linear polymers (polysalicylate, or PSA) were achievable by the polycondensation of the monomer at high temperatures. This method yielded polymeric chains comprising solely of repeating units (between 5-30) of salicylate linked by ester bonds with an acetyl group on one end and a carboxyl group on the other. Factors affecting the degree of polymerisation were discussed as well as the possibility of the formation of unwanted products that would limit the ability to modify further the polymer, such as cyclic and capped polymers.

An amphiphilic block copolymer (BCP) was then created by the conjugation of polysalicylate with polyethylene glycol, a biocompatible polymer that would not only form the hydrophilic part of the BCP but that would also create a stealthing shell upon self-assembly that would prolong the circulation half-life of the nanoparticles by rendering them invisible to macrophages. The BCP had a loading capacity of around 40% of the active moiety.

Self-assembly was then carried out using the co-solvent method and yielded interesting morphologies depending on the organic solvent used. While an acetone/water system produced spherical micelles with an average hydrodynamic diameter of 25 nm, a THF/water system yielded vesicles with an average hydrodynamic diameter of about ten times the size of the previous ones, making the latter more suitable for targeted therapy purposes. Factors controlling the self-assembly of the BCP, such as the solvent-polymer interactions and the length of the polymer chains, were discussed in detail.

Degradation studies on the PSA were also conducted in biological and nonbiological media with varying hydrolytic potencies to estimate the amount of the drug that could be under different condition. At a temperature close to that of the human body, release of the active drug was observed only in the basic medium while the polymer showed good stability in the presence of some blood components and some esterases. Accelerated conditions, on the other hand, induced drug release in biological media. PSA-mPEG NPs exhibited similar release trends.

These studies indicate that the synthesised NPs could be stable during circulation until they accumulate in solid tumours and are taken up by cancer cells where they could be broken down by a multitude of hydrolytic enzymes.

Several steps towards the making of another NSAID-based polymer were also accomplished. The intention was to create a polyphosphoester with ibuprofen linked as the pendant via ester groups. This polymer would then self-assemble into NPs with high biocompatibility. This biocompatibility stems from the fact that phosphate and its polymers are abundant in nature and make up the key components in the human biology from DNA to buffers and enzymes. Upon delivery to the TME, the polymer would supposedly break down to its basic components; phosphate, glycerol (another molecule that is natural to the body), and ibuprofen.

The monomer necessary for making the polymer was synthesised successfully with high purity, but time did not allow for the optimisation of the ring-opening polymerisation reaction, which is known for its sensitivity.

In Chapter 3, another type of SA-loaded nanocarriers were prepared. Liposomes are considered among the safest nanodelivery systems and almost all of nano-systems approved for clinical use are liposomal formulations. Their phospholipid shell resembles biological membranes they induce little to no immunological response. For this reason, they were explored as potential carriers for SA.

The egg phosphatidylcholine that was fist used to make the liposomes yielded good encapsulation efficacy (EE) with a desirable size range but resulted in bad retention of the drug due to its low transition temperature. DPPC was believed to be a better alternative since it had a transition temperature just a few degrees above average normal body temperature. The use of DPPC yielded liposomes with even a higher EE that reached about 71%. However, the poor retention issue persisted even with the incorporation of cholesterol with the lipid to increase the rigidity of the phospholipid bilayer.

It was then concluded that the poor retention was due to the amphiphilic nature of SA based on its protonation state. Being a weak acid, it is believed that the protonated form of the acid is able to permeate through the membrane while the ionised version is trapped in the aqueous phase. For this reason, another method of loading the liposomes with SA was tested.

In contrast to the direct (passive) loading method used earlier, the remote (active) loading method depended on creating a difference in pH between the inner and the outer phases of the lipid bilayer in order to drive the protonated form of salicylic acid through the membrane of pre-made empty liposomes. However, the EE of liposomes using this method was poor, with and without the incorporation of cholesterol. It was speculated that the presence of lysophospholipid, either due to the sonication method used for homogenisation or from the outdate patch of the lipid used, compromised the integrity of the lipid membrane and lead to leakage and poor retention.

Nonetheless, the results of these experiments raised questions about some liposomal preparations of SA that exist in the literature, warranting some scrutiny.

The final chapter investigated the basic biological effects of the prepared PSA-PEG NPs against a triple-negative breast cancer cell line and its paclitaxel-resistant subline. MTT assay was the method of choice for the determination cell viability.

The half-maximal inhibitory concentrations (IC_{50}s) for SA and ASA were first established as a point of reference and were found to be in agreement with literature in regards to cancer cell line testing. These values were also within the range of plasma concentration after therapeutic doses of these drugs which emphasises the potential anti-tumour role of NSAIDs derived from clinical data.

The IC_{50} values for PSA and the PSA-PEG NPs could not be accurately determined due solubility issues with the former and the inability to use high concentrations of the latter. Nonetheless, they both exhibited a consistent cytotoxic effect on both cell lines.

A comparison of the cytotoxicity of the monomers and the NPs was carried out using their respective IC_{50}s. The comparison also included conventional cytotoxic drugs as well as different combinations of the above. The response from the NPs was modest compared to the other drugs, but that was expected due to the low concentration of the NPs that could be used. Nonetheless, it can be speculated from the observed response and the cytotoxicity of the monomer that is comparable to that of conventional chemotherapeutics that SA-loaded NPs might indeed have a positive role in limiting the growth and metastasis of cancer upon accumulating in cancer tissue.

Future outlook

The degradability and cytotoxicity of the SA-based polymer and polymeric nanoparticles suggest that such nanocarriers might be of use in the fight against cancer and in boosting the patients' quality of life. This calls for fine-tuning the nanocarriers to maximise their benefits.

One suggestion would be to separate the polymeric chains based on molecular weight which not only would be necessary to improve the dispersity profile of the polymer and consequently have more control over dosage, but that would also remove cyclic and capped polymers that hinder the synthesis of pure block co-polymers.

As was shown in the work, different solvent systems produced different morphologies. These morphologies might be re-purposed in a variety of ways. For instance, even though spherical micelles produced from the acetone/water system might not be very effective in targeting cancer since they would be rapidly cleared by the kidneys, they might be useful in an intra-articular formulation, for example, where they would produce a sustained release of the NSAID. The inner phase of the vesicles produced by the THF/water system, on the other hand, could be exploited to load other molecules. For example, they could be loaded with either the monomer, another therapeutic molecule, a diagnostic agent, or a combination of all the above.

The initial biological studies showed that the synthesised particles exhibit a cytotoxic activity but further in-depth studies are required. The mechanism by which particles are taken up by the cells ought to be established in order to understand how particles are inducing their cytotoxicity. This would also help in determining the cellular components that the particles encounter which would be useful in adjusting their drug release profile. The use of systems more sophisticated that conventional cell cultures, such as 3D cell cultures and animal models, would give a better understanding about how these nanoparticles interact with the tumour as a whole and how they affect components other than the cells, which are just as important for the growth and survival of tumours.